

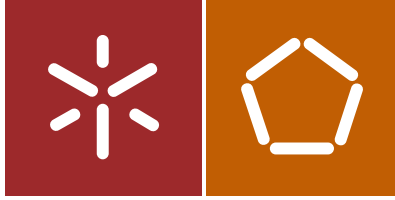


Iran Gomes da Rocha Segundo

ECOLOGICAL, PHOTOCATALYTIC,
SUPERHYDROPHOBIC AND SELF-CLEANING
ASPHALT PAVEMENT SURFACES

Universidade do Minho
Escola de Engenharia





Universidade do Minho
Escola de Engenharia

Iran Gomes da Rocha Segundo

ECOLOGICAL, PHOTOCATALYTIC,
SUPERHYDROPHOBIC AND SELF-CLEANING
ASPHALT PAVEMENT SURFACES

Tese de Doutoramento
Programa Doutoral em Engenharia Civil

Trabalho realizado sob a orientação de:
Professora Doutora Elisabete Fraga de Freitas
Professor Doutor Joaquim A. dos S. A. de Oliveira
Carneiro

Julho de 2021

DIREITOS DE AUTOR E CONDIÇÕES DE UTILIZAÇÃO DO TRABALHO POR TERCEIROS

Este é um trabalho académico que pode ser utilizado por terceiros desde que respeitadas as regras e boas práticas internacionalmente aceites, no que concerne aos direitos de autor e direitos conexos.

Assim, o presente trabalho pode ser utilizado nos termos previstos na licença abaixo indicada.

Caso o utilizador necessite de permissão para poder fazer um uso do trabalho em condições não previstas no licenciamento indicado, deverá contactar o autor, através do RepositóriUM da Universidade do Minho.

Licença concedida aos utilizadores deste trabalho



Atribuição-SemDerivações

CC BY-ND

<https://creativecommons.org/licenses/by/4.0/>

ACKNOWLEDGMENT

The space was dedicated to those who contributed to this thesis, who contributed academically and/or in a particular way in my life, leaving the sincerest thanks to: My parents, Iran and Ciara. I love you and thank you so much for all backing during this very long journey. This achievement only shows what you have planted; My brothers, Tallyta, Lohana, Neto, Terceiro, and Alexandre for the immense mutual love; My whole family, especially my aunt and godmother Tindarena, who fed my dreams from the beginning; My eternal aunts Rozilda and Rosimeire (in memoriam); My niece Alice; My advisors, profs. Elisabete Freitas and Joaquim Carneiro, they never gave up on me, showing enormous support (from beginning - PhD scholarship, middle - supervision, mobilities, conference presentations, and papers, end - pandemic, and future - concern for a new position), presenting brilliant ideas. Joining areas is undoubtedly a huge challenge; FCT (SFRH/BD/137421/2018) and TECMINHO for the scholarships; My previous supervisors, Verônica Castelo Branco and Jorge Soares, who contributed to my base knowledge; The technicians and engineers from UM, Hélder Torres and Carlos Palha, who are high-quality professionals worldwide; The profs. from UM, especially Joel Oliveira, Hugo Silva, Rui Ramos, Manuel Costa, and Carlos Tavares for their huge support; Profs. Graça Soares and Jorge Santos and technicians Ângela and Anabela from Textile Engineering; Prof. Sandra Soares and technicians Wesley and Rômulo for their help during the mobility period in Brazil; The Belgian professors and friends, especially Prof. Cedric Vuye, Alex, George, Ben, Myrthe, and Jelle. All my Portuguese friends that I made during my PhD, especially Francisco; The students who worked with me, Cristiano, Sérgio, Leonel, Jaffer; Amanda; Salmon, Filipa and Behzad, who much contributed to this research. Students from prof. Tavares' lab (specially Filipe and Juliana). All my colleagues from UM who helped me, and all the friends made at the Civil Eng. Lab., mainly César, Gonçalves, Pokee, and Marco; Laura Soares for listening and encouraging me during the most challenging work period; My Brazilian friends who made me feel home, especially Doctor Natália Homem, Caio, Sarah, Hogana, Wagner, Zê, Orlando, Marlon, Ylan, Toinho, Alê, and Edu and the foreign friends who made me culturally grow, especially Alberto Mexicano, Matthias and his family, Leidy, and Kamel. All friends from Fortaleza, especially Claver, Natália, Talita, Núbio, Jeffin, Wallace, Larissa, Kátia, Gui, Iuri, Edu, both Hugos; A Elite; Grammy III; LMP and CAMP; My BJJ coach Paulo Sérgio, David Santos and my training friends, who made me feel more Brazilian here in Portugal; Portuas and FEC.

STATEMENT OF INTEGRITY

I hereby declare having conducted this academic work with integrity. I confirm that I have not used plagiarism or any form of undue use of information or falsification of results along the process leading to its elaboration.

I further declare that I have fully acknowledged the Code of Ethical Conduct of the University of Minho.

SUPERFÍCIES DE PAVIMENTOS ASFÁLTICOS ECOLÓGICAS, FOTOCATALÍTICAS, SUPERHIDROFÓBICAS E AUTOLIMPANTES

RESUMO

Atualmente, é crescente a preocupação com a poluição do ar, o esgotamento dos recursos naturais e, conseqüentemente com os danos impostos ao meio ambiente. Os pavimentos asfálticos precisam ser tecnicamente viáveis do ponto de vista mecânico, apresentar características funcionais adequadas em termos de conforto e segurança rodoviária e ser sustentáveis e de custo aceitável. Nesse contexto, o objetivo desta tese é desenvolver misturas asfálticas recicladas (ecológicas pela substituição parcial de material virgem) e com novas funções através da integração de nano/micropartículas para a camada superficial dos pavimentos. A integração de nano/micropartículas proporciona novas capacidades (funcionalização) às misturas asfálticas, nomeadamente fotocatalíticas, superhidrofóbicas e autolimpantes com um efeito adicional de antienvelhecimento dos ligantes asfálticos. Com o desenvolvimento da capacidade fotocatalítica, as misturas asfálticas são capazes de fotodegradar poluentes, melhorando assim a qualidade do ar. Sobre a capacidade superhidrofóbica, as misturas asfálticas funcionalizadas passam a repelir a água, proporcionando maior segurança rodoviária, principalmente em períodos de chuva e temperatura ambiental negativa. Com o efeito autolimpante, as misturas asfálticas funcionalizadas conseguem limpar poluentes, como partículas de sujeira, óleo e gordura, mitigando a diminuição do atrito devido à presença desses materiais na sua superfície. Para tanto, foi realizada uma extensa revisão bibliográfica para fundamentar esta tese de doutoramento. Em seguida, as misturas asfálticas foram funcionalizadas através de diferentes métodos de aplicação (incorporação em volume, modificação de ligante e revestimento por pulverização) e usando diferentes materiais (TiO_2 , ZnO e Politetrafluoroetileno). As novas propriedades e seus impactos foram analisados sob o ponto de vista mecânico, funcional e de funcionalização. As principais conclusões indicam que as misturas asfálticas podem ser funcionalizadas por esses materiais a fim de apresentarem novas capacidades, apresentando benefícios para o meio ambiente, sociedade, economia e também para o desempenho das misturas asfálticas.

Palavras chave: anti-envelhecimento, efeito autolimpante, mistura asfáltica fotocatalítica, mistura asfáltica inteligente, mistura asfáltica superhidrofóbica.

ECOLOGICAL, PHOTOCATALYTIC, SUPERHYDROPHOBIC AND SELF-CLEANING ASPHALT PAVEMENT SURFACES

ABSTRACT

Currently, there is a growing concern with air pollution, the depletion of natural resources, and, consequently, with the damage imposed on the environment. Asphalt pavements need to be technically viable from a mechanical point of view, present adequate functional characteristics in terms of comfort and road safety, be sustainable and at an acceptable cost. In this context, this thesis aims to develop recycled asphalt mixtures (ecological through the partial replacement of virgin material) and with new functions through the integration of nano/microparticles for the surface layer of asphalt pavements. The integration of nano/microparticles provides new capabilities (functionalization) to asphalt mixtures, namely photocatalytic, superhydrophobic, and self-cleaning with the additional anti-aging effect of asphalt binders. With the development of the photocatalytic capability, the asphalt mixtures are able to photodegrade pollutants, and therefore improving the air quality. Regarding the superhydrophobic capability, the functionalized asphalt mixtures start to repel the water, providing higher road safety, especially in periods of rain and negative environmental temperature. With the self-cleaning effect, the functionalized asphalt mixtures are able to clean pollutants, such as dirt particles, oil, and grease, over their surface, mitigating the decrease of friction due to the presence of these materials over their surface. Therefore, an extensive bibliographic review was carried out to support this doctoral thesis. Then, the asphalt mixtures were functionalized using different application methods (volume incorporation, modification of binder, and spraying coating) and using different materials (TiO_2 , ZnO , and Polytetrafluoroethylene). The new properties and their impacts were analyzed from mechanical, functional, and functionalization point of views. The main conclusions indicate that these materials can functionalize the asphalt mixtures to provide them with new capabilities, presenting benefits for the environment, society, economy, and for the performance of the asphalt mixtures.

Keywords: anti-aging, photocatalytic asphalt mixture, self-cleaning effect, smart asphalt mixture, superhydrophobic asphalt mixture.

OUTLINE

CHAPTER 1 – INTRODUCTION	1
1.1. OBJECTIVES.....	2
1.2. THESIS ORGANIZATION.....	4
CHAPTER 2 – LITERATURE REVIEW: PHOTOCATALYTIC ASPHALT MIXTURES	9
2.1. INTRODUCTION.....	10
2.2. GENERAL ASPECTS AND CHARACTERISTICS OF TITANIUM DIOXIDE.....	11
2.3. BASIC PRINCIPLES OF PHOTOCATALYSIS.....	13
2.4. GENERAL APPLICATION FOR CIVIL ENGINEERING MATERIALS.....	18
2.5. PHOTOCATALYTIC ASPHALT PAVEMENTS.....	20
2.5.1. Materials and techniques for application of photocatalytic effect on asphalt mixtures.....	21
2.5.2. Testing, results analysis of photocatalytic asphalt mixtures.....	24
2.5.3. Photocatalytic asphalt mixtures modeling.....	28
2.5.4. Mechanical and surface impacts and design of photocatalytic asphalt mixtures.....	29
2.5.5. Photocatalytic applications in real context or small road sections.....	30
2.5.6. Cost analysis.....	32
2.6. CONCLUSIONS.....	33
CHAPTER 3 – LITERATURE REVIEW: SUPERHYDROPHOBIC ASPHALT MIXTURES	35
3.1. INTRODUCTION.....	36
3.2. SUPERHYDROPHOBIC ASPHALT MIXTURES USING NANO/MICROPARTICLES.....	36
3.3. APPLICATION METHOD.....	37
3.4. ANALYSIS.....	37
3.5. RESULTS ON LITERATURE.....	38
3.6. CONCLUSIONS.....	39
CHAPTER 4 – LITERATURE REVIEW: SMART ASPHALT MIXTURES	40
4.1. INTRODUCTION.....	41
4.2. DEICING AND SELF ICE-MELTING CAPABILITIES.....	42
4.2.1. Self-ice-melting pavements using anti-icing additives.....	42
4.2.2. Deicing pavements using conductive materials.....	43
4.3. SELF-HEALING CAPABILITY.....	45
4.3.1. Self-healing capability by heating.....	45
4.3.2. Self-healing capability by adding nanomaterials or healing agents.....	47
4.4. THERMOCHROMIC CAPABILITY.....	50
4.5. LATENT HEAT THERMAL ENERGY STORAGE (LHTS) CAPABILITY.....	53
4.6. SUMMARY.....	56

4.7. CRITICAL ANALYSIS AND CONCLUSIONS	58
CHAPTER 5 – DEVELOPMENT OF PHOTOCATALYTIC AND SUPERHYDROPHOBIC ASPHALT MIXTURES.....	61
5.1. INTRODUCTION.....	62
5.2. MATERIALS AND METHODS	62
5.2.1 Materials.....	62
5.2.2. Sample preparation.....	63
5.2.3. Methods.....	65
5.3. RESULTS.....	67
5.3.1. Atomic force microscopy (AFM).....	67
5.3.2. Fourier transform infrared spectroscopy (FTIR)	69
5.3.3. Water contact angle analysis.....	69
5.3.4. Photocatalytic efficiency.....	73
5.3.5. Mechanic impact of semiconductors.....	76
5.4. CONCLUSIONS.....	77
CHAPTER 6 – MECHANICAL IMPACTS AND PHOTOCATALYTIC EFFICIENCY OF ASPHALT MIXTURES.....	79
6.1. INTRODUCTION.....	80
6.2. MATERIALS AND SAMPLES PREPARATION	80
6.3. METHODS	82
6.3.1. Water sensitivity.....	82
6.3.2. Permanent deformation.....	82
6.3.3. Stiffness modulus	83
6.3.4. Fatigue test	83
6.3.5. Photocatalytic efficiency.....	83
6.3.6. Traffic simulation	84
6.3.7. Rain simulation.....	84
6.4. RESULTS AND DISCUSSIONS	84
6.4.1. Performance of the asphalt mixtures	84
6.4.2. Photocatalytic efficiency	86
6.5. CONCLUSIONS.....	91
CHAPTER 7 – FUNCTIONAL IMPACTS OF FUNCTIONALIZED ASPHALT MIXTURES.....	94
7.1. INTRODUCTION.....	95
7.2. MATERIALS AND METHODS	95
7.2.1. Materials.....	95
7.2.2. Methods	96
7.2.3. Testing set up and analysis.....	97
7.3. RESULTS.....	99
7.3.1. Macrotexture	99
7.3.2. Skid resistance	100

7.3.3. Microtexture.....	102
7.4. CONCLUSIONS.....	104
CHAPTER 8 – EFFECTS AND POTENTIALITIES OF MODIFICATION OF ASPHALT BINDERS WITH TiO₂.....	106
8.1. CONTEXTUALIZATION.....	106
8.2. STUDY OF ANTI-AGING EFFECT OF TiO ₂ ON ASPHALT BINDER.....	107
8.2.1. Introduction.....	107
8.2.2. Materials and methods.....	107
8.2.3. Results and discussion.....	109
8.2.4. Conclusions	113
8.3. STUDY OF COLOR-LESS ASPHALT BINDER MODIFIED WITH TiO ₂	114
8.3.1. Introduction.....	114
8.3.2. Materials.....	115
8.3.3. Methods	116
8.3.4. Results and discussions	121
8.2.5. Conclusions	133
CHAPTER 9 –RECYCLED ASPHALT MIXTURE USING STEEL SLAGS AND RECLAIMED ASPHALT	135
9.1. INTRODUCTION.....	136
9.2. MATERIALS	137
9.2.1. Aggregates and bitumen.....	137
9.2.2. Asphalt mixtures.....	138
9.3. METHODS	139
9.3.1. Mechanical characterization	139
9.3.2. Superficial characterization.....	139
9.4. RESULTS.....	140
9.5. CONCLUSIONS.....	142
CHAPTER 10 – ECOLOGICAL, PHOTOCATALYTIC, SUPERHYDROPHOBIC AND SELF-CLEANING ASPHALT MIXTURES	144
10.1. INTRODUCTION.....	144
10.2. MATERIALS AND METHODS	145
10.2.1. Materials	145
10.3. Results and discussions.....	148
10.4. CONCLUSIONS.....	156
CHAPTER 11 – CONCLUSIONS AND PARALLEL AND FUTURE WORKS.....	159
11.1. CONCLUSIONS.....	159
11.2. PARALLEL WORKS.....	162
11.3. FUTURE WORKS.....	166
REFERENCES	168

LIST OF FIGURES

Figure 1: Schematic representation of this thesis: part 1	7
Figure 2: Schematic representation of this thesis: part 2	8
Figure 3: First page of the research work published in Coatings [1]	9
Figure 4: Schematic representation of the photo-excitation in a semiconductor material. Adapted from [36].....	15
Figure 5: Diffuse reflectance spectroscopy of TiO ₂ nanoparticles (a) and calculation of the TiO ₂ energy band gap by the Kubelka–Munk theory (b) [43]	17
Figure 6: Photocatalytic asphalt mixture from [9]	20
Figure 7: Experimental tests to measure the photocatalytic activity: (a) NO _x degradation efficiency (1: lamp for light irradiation, 2: quartz window, 3: test specimen, and 4: temperature stabilizer); (b) degradation of an organic dye; (c) aqueous solution of an organic dye of different color intensity over time, thus indicating its degradation.....	24
Figure 8: Results of photocatalytic tests: (a) variation (over time) of gas concentration, indicating its photodegradation from [61] (b) absorbance variation (over time) of the dye's aqueous solution, indicating its photodegradation from [7]	25
Figure 9: Photocatalytic test sections: (a) by Hassan et al. [10]; (b) by Wang et al. [78] , and (c) by Bocci et al. [74].....	31
Figure 10: First page of the research work published in EPJ Web of Conferences [92]	35
Figure 11: Microtopography of an asphalt mixture	37
Figure 12: a) Water drop carrying dirt. Adapted from [99]	38
Figure 13: Manuscript first page submitted to a prestigious scientific journal	40
Figure 14: Fatigue life of porous asphalt mixture with 8% steel wool [127]	47
Figure 15: a) Asphalt with microencapsulation, b) microcapsules are broken by the crack, and c) release of the healing agents [130]	48
Figure 16: Detail of the sunflower oil coming out [131]	48
Figure 17: Mechanism of the healing effect due to: a) ionomers and b) nanomaterials [133]	50
Figure 18: Thermochromic powders (blue, black and red) disactivated under 31 °C (left) and activated above 31 °C (right) [144].....	52
Figure 19: a) Different types of PCM [152] and b) Melting enthalpy versus melting temperature [153]	55
Figure 20: First page of the research work published in Construction and Building Materials [8]	61
Figure 21: Sample preparation for AFM, FTIR, mechanical impact, water contact angle and photocatalytic efficiency measurements.....	65

Figure 22: AFM Results: a) Cepsa 35/50; b) Cepsa 35/50 + TiO ₂ ; c) Cepsa 35/50 + ZnO; d) Cepsa 35/50 + TiO ₂ + ZnO; e) Elaster 13/60; f) Elaster 13/60 + TiO ₂ ; g) Elaster 13/60 + ZnO; h) Elaster 13/60 + TiO ₂ + ZnO	68
Figure 23: FTIR of 35/50 and Elaster (E) before and after the application of semiconductors.....	69
Figure 24: Water Contact Angle: a) AC 14; b) AC 6; c) AC 14 TiO ₂ ; d) AC 6 TiO ₂ ; e) AC 14 ZnO; f) AC 6 ZnO; g) AC 14 TiO ₂ ZnO; h) AC 6 TiO ₂ ZnO	71
Figure 25: Photocatalytic Efficiency: a) AC 14; b) AC 6; c) AC 14 TiO ₂ ; d) AC 6 TiO ₂ ; e) AC 14 ZnO; f) AC 6 ZnO; g) AC 14 TiO ₂ ZnO; h) AC 6 TiO ₂ ZnO	74
Figure 26: First page of the research work published in Catalysis Today [9].....	79
Figure 27: Graphical Abstract of the paper [9].....	80
Figure 28: a) Water Sensitivity; b) Permanent Deformation Results [9].....	85
Figure 29: a) Stiffness Modulus; b) Fatigue Resistance [9].....	86
Figure 30: Photocatalytic Efficiency for Different Temperatures: a) before abrasion and without lateral covering; b) before abrasion and with lateral covering; c) after 1% superficial abrasion and rain simulation [9].....	87
Figure 31: Photocatalytic Efficiency for Different Spraying Rates: a) before abrasion; b) after 0.125% of a superficial abrasion; c) after rain simulation [9].....	89
Figure 32: Photocatalytic Efficiency: a) before abrasion; b) after rain simulation; c) after 0.5% of a superficial abrasion; d) after 0.5% of a superficial abrasion and rain simulation; e) after 2% of superficial abrasion; f) after 2% of superficial abrasion and rain simulation [9].....	91
Figure 33: First page of the research work published in Catalysis Today	94
Figure 34: The MICROTOP.06.MFC [170].....	97
Figure 35: Flow Chart of this Study	99
Figure 36: Results of Pendulum Test: a) Dry Condition and b) Wet Condition	100
Figure 37: Microtexture Results: a) Sa, b) Sq, c) St, d) Sp, e) Sv and f) Sz	103
Figure 38: Microtexture Results: a) Ssk and b) Sku	104
Figure 39: Publications in a) Portuguese Road Congress and b) Nanomaterials	107
Figure 40: Schematic Representation of the Methodology of this section.....	108
Figure 41: Penetration Results before and after aging by RTFOT.....	109
Figure 42: Softening point results before and after aging by RTFOT	110
Figure 43: Results of mass loss after aging by RTFOT	111
Figure 44: Viscosity results: before RTFOT (left) and after RTFOT (right).....	112
Figure 45: Complex modulus results before RTFOT (left) and after RTFOT (right)	113
Figure 46: Results of complex modulus after PAV (left) and with the enlarged image of all situations evaluated (right).....	113

Figure 47: Schematic representation of this research	117
Figure 48: Penetration results of the binders of this study	122
Figure 49: Softening point results of the binders of this study	122
Figure 50: Dynamic viscosity results of the binders of this study.....	123
Figure 51: (a) Complex modulus and (b) phase angle master curves of the binders of this study.....	124
Figure 52: Black diagram of the evaluated reference and transparent binders.....	126
Figure 53: LAS Test: N_f versus applied strain	127
Figure 54: FTIR spectra of the binders of this study.....	130
Figure 55: Correlation of the nano-TiO ₂ modification level with the increase of the TiO ₂ -related index.....	131
Figure 56: FTIR indices of the nano-TiO ₂ -modified, base and reference binders	132
Figure 57: First page of the research work published in Wastes [51]	135
Figure 58: a) Permanent Deformation, b) Dynamic Modulus, c) Fatigue and d) Absorption and Damping	142
Figure 59: a) Photocatalytic Efficiency of all the samples from the first step (selection of best solution)	149
Figure 60: Photocatalytic Efficiency of the samples comparing the: a) particles with ketone; b) particles with ethyl alcohol; c) solvent with TiO ₂ ; d) solvent with TiO ₂ and PTFE from the first step (selection of best solution).....	150
Figure 61: Results of Water Contact Angle of all the samples from the first step (selection of best solution)	151
Figure 62: Results of Water Contact Angle comparing the: a) best solvent with TiO ₂ ; b) best solvent with PTFE; c) best solvent with TiO ₂ and PTFE.....	152
Figure 63: Results of Water Contact Angle (analysis of the particles) comparing the: a) best particles with acetone, and b) best particles with ethyl alcohol.	152
Figure 64: Results of Photocatalytic Efficiency of the mixture R with resin and BS	153
Figure 65: Results of Photocatalytic Efficiency of the mixture F with resin and BS	154
Figure 66: Results of Photocatalytic Efficiency of the mixture A with resin and BS	154
Figure 67: Results of Water Contact Angle for the mixtures without treatment (R – Reference, F – with 30% of RAP, and A – with 30% of SS).....	155
Figure 68: Results of Water Contact Angle for mixture R: a) with resin, and b) resin+BS.....	155
Figure 69: Results of Water Contact Angle for mixture F: a) with resin, and b) resin+BS.....	156
Figure 70: Results of Water Contact Angle for mixture A: a) with resin, and b) resin+BS.....	156
Figure 71: The first page of the research work published in: a) Road Materials and Pavement Design [80], and b) Applied Acoustics [227].....	163
Figure 72: First page of the research work published in Construction and Building Materials [228]	164

LIST OF TABLES

Table 1: Superhydrophobic Asphalt Mixtures.....	38
Table 2: Influences, Benefits, Materials and Mains Applications of the Multifunctional Capabilities	57
Table 3: Properties of the Bitumens	62
Table 4: Properties of Asphalt Mix Slabs	63
Table 5: Maximum and Minimum Results for Water Contact Angle	72
Table 6: Results of ANOVA for Contact Angle.....	72
Table 7: Results of ANOVA for Photocatalytic Efficiency	76
Table 8: Properties of Asphalt Mixes	96
Table 9: Macrotexture Results.....	99
Table 10: Linear Trend Equations for Skid Resistance	101
Table 11: Results of penetration, softening point, and mass loss	109
Table 12: LAS test results.....	127
Table 13: MSCR test results	128
Table 14: Main properties of the natural and recycled aggregates.....	137
Table 15: Form, sphericity, angularity and texture characterization.....	138
Table 16: Asphalt mix composition and volumetric properties.....	139
Table 17: Water sensitivity results.....	141
Table 18: Macrotexture and friction results	142
Table 19: Mixture AC 10 (R) sprayed with different solutions.	146
Table 20: Name of the samples for the immobilization of BS.....	147

CHAPTER 1 – INTRODUCTION

The functionalization of materials consists of developing and applying a technique that aims to provide them new capabilities or functions. Currently, some methods are being studied from the incorporation of nano/microparticles in asphalt mixtures to achieve this goal. Such characteristics are mainly related to the surface of the pavements.

Some application methods and nano/micromaterials were applied to asphalt mixtures as reported in the literature to obtain a smart material. However, the functionalization processes need improvements. The combination of (nano or micro) materials is rare. The available application methods should be compared and evaluated. Mostly, nano/microparticles are applied to provide just one new functionality. The essential characteristics are not commonly evaluated. Also, the immobilization of the particles is crucial to keep the new functionality working. Other perspectives regarding the use of these techniques may be also explored, for example, the (transparent) asphalt binder modification with nanomaterials. Finally, the application of new capabilities on recycled asphalt mixtures is uncommon. In this case, the functionalization process may provide an ecological and smart material from the beginning of the lifetime. Thus, the objective of this doctoral thesis is to develop multifunctional and ecological asphalt mixtures fulfilling the technical (mechanical and functional) requirements.

Asphalt mixtures with photocatalytic properties promotes air purification through the application of semiconductor materials. The photocatalytic asphalt pavements degrade organic pollutants, SO_2 , and NO_x in the presence of water and oxygen when irradiated by sunlight. Such an effect contributes to air cleaning and surface cleaning when adsorbed oils and greases contaminate the pavements. Another functionalization process is the development of the superhydrophobic capacity. A superhydrophobic asphalt mixture has the ability to repel water and prevent the formation of ice on the surface, which might improve road safety. The self-cleaning capacity, associated with the superhydrophobic property, is based on the fact that the water drops present a sphere form that can easily roll over the surface carrying dirt particles. For road safety, this effect will help removing dirt particles from the surface, avoiding skidding problems. The self-cleaning effect also occurs with the photocatalytic capability. In this case, oil and greases are photodegraded, cleaning the surface.

There is also a demand for techniques that are less harmful to the environment worldwide, through the signing of the Kyoto Protocol and the holding of the 2015 UN Climate Change Conference (COP21), which aimed to limit the increase in global temperature below 2 °C, revised every 5 years from 2020. In

the Transport Infrastructure area, it is necessary to appeal to techniques such as recycling to optimize resources, avoid the use of natural resources and decrease emissions due to the reduction of raw material pre-processing.

The pavement deterioration is directly related to the ageing of the asphalt bitumen (the binder) that occurs due to the combined action of UV and oxidation in the presence of oxygen and high temperatures. To mitigate this problem, semiconductors, which absorb and reflect UV light during photocatalysis, can be applied to asphalt mixtures.

The functionalization of asphalt pavements may improve functional characteristics (texture, longitudinal and transversal irregularities, friction, noise level, resistance to rolling, light reflection, and surface drainage), which are related to safety, comfort, and, more recently, environmental parameters. In this context, the functionalization of ecological surface layers of asphalt pavements will bring environmental, social, and economic benefits.

In this doctoral thesis, in order to obtain a multifunctional asphalt mixture, some research problems and advances are aimed concerning the combination of nano/micromaterials, comparison between application methods, assessment of the essential characteristics and the particles immobilization, new potentialities of use of TiO_2 , and application of new capabilities on recycled asphalt mixtures. To fulfil these objectives, first, an extensive literature review was carried out. Then, two types of asphalt mixtures were functionalized with TiO_2 and ZnO semiconductors (by spraying coating and volume incorporation), their new capabilities were analyzed, and their mechanical and functional characteristics were also assessed. Furthermore, the semiconductors were applied by asphalt binder modification to analyze their impacts on their physicochemical and rheological characteristics and provide anti-aging effects (new potentialities). Finally, the recycled asphalt mixtures were designed, assessed, and functionalized with TiO_2 and PTFE particles in order to improve the photocatalytic and the superhydrophobic capabilities aiming the improvement of the particle's fixation over their surface.

1.1. Objectives

The main objective of this thesis is the development of ecological asphalt mixtures, functionalized and optimized in terms of their functional characteristics. This design can be achieved through an appropriate articulation between recycling techniques (enabling the reduction of raw material) and the incorporation of nano/micromaterials to provide them with new properties and the appropriate selection of grading. These asphalt mixtures should not only be technically viable, that is, they should be able to

withstand traffic and weather conditions, but they should also be improved in terms of surface characteristics when used as top layer to increase the ecological character of the pavements and also improve road safety. Among these new capabilities, it is intended to develop asphalt mixtures with the following functionalities: (i) photocatalytic, to be capable of photodegrading organic pollutants to clean the environment. The application of this technique will contribute very positively so that pavements can become ideal locations (given its large surface area) for the photodegradation of pollutant gases that are systematically emitted by vehicles exhausts; (ii) superhydrophobic to guarantee higher levels of safety during periods of rain and low temperatures; and (iii) self-cleaning to avoid skidding problems and facilitate water drainability. Also, it is intended to provide anti-aging effects to the asphalt binders with the incorporation of semiconductor nanoparticles. Thus, for this thesis, the following specific objectives are drawn:

- To carry out an extensive literature review about photocatalytic asphalt mixtures considering the main material application methods (materials, scale, technique of application, among others), test methods and analysis, gaps in literature, real scale section experiences, modelling, cost analysis, among others;
- To perform a literature review about superhydrophobic asphalt mixtures regarding the materials used, application methods, analysis and literature gaps and results;
- To review the literature considering other smartness applied on asphalt mixtures and to compare, summarize and analyze them;
- To apply semiconductor materials (TiO_2 nanoparticles and/or ZnO microparticles) by spraying on different asphalt mixtures (different substrates) and analyze them under chemical and morphological, mechanical and functionalization points of view and evaluate the influencing parameters;
- To analyze the mechanical impacts (fatigue, rutting and water sensitivity) of the functionalization process and evaluate the impacts of weathering and traffic on photocatalytic efficiency;
- To evaluate the functional impacts (macro and microtexture and friction) of the functionalized asphalt mixtures;
- To modify the asphalt binders with TiO_2 nanoparticles in order to assess the physicochemical and rheological characteristics and anti-aging effects of this application;
- To design and evaluate the recycled asphalt mixtures using Reclaimed Asphalt Pavement (RAP) and Steel Slags (SS) in order to present ecological asphalt pavement layer from the begging of the lifetime;

- To functionalize the recycled asphalt mixtures (with RAP and SS) in order to obtain an ecological and multifunctional material and evaluate them under photocatalytic and superhydrophobic capabilities;
- To analyze the effectiveness of application of different materials (TiO₂ and PTFE particles with different contents and solvents) on the functionalization process of recycled asphalt mixtures using a diluted resin;
- To evaluate different application methods of nano/microparticles on asphalt mixtures (volume incorporation, asphalt binder modification and spraying coating).

1.2. Thesis Organization

During the Ph.D. period, different research works were published, allowing and encouraging the thesis organization to be written by scientific articles. It is supported by 9 scientific articles published in 6 international journals (presently, one of them is still under review), 2 indexed conferences and 1 national conference. Other publications using results that are not presented in this Ph.D. thesis are described in the Parallel Work reported in the last chapter. Thus, this thesis is organized as follows:

i) Chapter 1 – Introduction

In the first chapter, the subject under study is introduced, and the thesis objectives and organization are presented.

ii) Chapter 2 – Literature review: photocatalytic asphalt mixtures.

In the second chapter, a literature review about photocatalytic asphalt mixtures is presented and the main findings discussed. This chapter is related to the journal article (Smart, Photocatalytic and Self-Cleaning Asphalt Mixtures: A Literature Review) published in Coatings (MDPI). In this chapter, it is expected to compile and discuss the most important information in literature regarding the photocatalytic asphalt mixtures.

iii) Chapter 3 – Literature review: superhydrophobic asphalt mixtures

In the third chapter, a literature review about superhydrophobic asphalt mixtures is carried out and the main issues are reported. This chapter is related to the document Superhydrophobic Asphalt Pavements: Surface Improvement published in EOSAM 2020 (EPJ WEB OF CONFERENCES).

The objective is to show the most important information in the literature about the superhydrophobic asphalt mixtures.

iv) Chapter 4 – Literature review: smart asphalt mixtures

In the fourth chapter, the literature review about other new capabilities applied to asphalt mixture is presented and discussed. Currently, with the results of this chapter, a manuscript (Review and analysis of advances in functionalized, smart, and multifunctional asphalt mixtures) was submitted to a prestigious scientific journal. In this chapter, deicing-anti-icing, self-healing, thermochromic, and latent heat thermal energy storage capabilities applied on asphalt mixtures are compared and analyzed concerning future perspectives.

v) Chapter 5 – Development of Photocatalytic and Superhydrophobic Asphalt Mixtures

In the fifth chapter, the first laboratory research work was carried out considering the application of TiO₂ and ZnO semiconductor nano/microparticles aqueous solution to the asphalt mixtures to provide them with new capabilities. This chapter is related to the journal article (Assessment of photocatalytic, superhydrophobic, and self-cleaning properties on hot mix asphalts coated with TiO₂ and/or ZnO aqueous solutions) published in Construction and Building Materials (Elsevier). The main objective is to set up a procedure to develop the photocatalytic, superhydrophobic and self-cleaning capabilities on asphalt mixtures. In this procedure, the effect of factors as different materials, mixtures, wearing testing are analyzed.

vi) Chapter 6 – Mechanical impacts and photocatalytic efficiency of asphalt mixtures

In the sixth chapter, mechanical impacts and photocatalytic efficiency were evaluated when semiconductor nanoparticles are applied by two methods: bulk incorporation and spraying coating. This chapter is related to the journal article (Photocatalytic asphalt mixtures: Mechanical performance and impacts of traffic and weathering abrasion on photocatalytic efficiency) published in Catalysis Today (Elsevier).

vii) Chapter 7 – Functional impacts of functionalized asphalt mixtures

In the seventh chapter, the functional impacts were assessed when the semiconductors are applied by bulk incorporation and spraying coating. This chapter is related to the journal article (Photocatalytic asphalt mixtures: semiconductors' impact in skid resistance and texture) published in Road Materials and Pavement Design (Taylor and Francis). The functional characteristics texture and skid

resistance are assessed after the functionalization process to check if changes negatively affect road safety.

viii) Chapter 8 – Effects and potentialities of modification of asphalt binders with TiO₂

In the eighth chapter, TiO₂ nanoparticles were used to modify two asphalt binders, one used currently and another transparent. The work carried out took place during two academic exchange mobilities, the first one at the Federal University of Ceará (Brazil) and the second one at the University of Antwerp (Belgium). The main objective is to analyze an asphalt binder modified with nano-TiO₂ and evaluate new potentialities, for example, the use of these nanoparticles in a transparent asphalt binder. Thus, the purpose of these research work was to evaluate the effects of the modification of the asphalt binders with nano-TiO₂ under physicochemical and rheological viewpoints. With the results, two documents were published: i) Evaluation of physical and rheological properties of asphalt binder modified by nano-TiO₂ after aging in Portuguese Road Congress and ii) Physicochemical and Rheological Properties of a Transparent Asphalt Binder Modified with Nano-TiO₂ in Nanomaterials (MDPI).

ix) Chapter 9 – Recycled asphalt mixture using steel slags and reclaimed asphalt

In the ninth chapter, recycled asphalt mixtures were designed and assessed from the mechanical and functional points of view. This chapter is related to the document Incorporation of steel slag and reclaimed asphalt into pavement surface layers published in Wastes: Solutions, Treatments and Opportunities III (Taylor and Francis). This chapter aims to design and characterize recycled asphalt mixtures in order to provide them with new capabilities (next chapter).

x) Chapter 10 – Ecological, photocatalytic, superhydrophobic and self-cleaning asphalt mixtures

In the tenth chapter, recycled asphalt mixtures were functionalized and assessed using all the experience from the previous research works using TiO₂ and PTFE particles to improve the photocatalytic, self-cleaning and superhydrophobic capabilities and the immobilization of the micro/nanoparticles. These results were the last research work carried out; thus, currently, the submission to a scientific international journal is being prepared. This chapter reports how the new capabilities were provided to the recycled asphalt mixtures aiming the improvement of the smartness and the particle's immobilization.

xi) Chapter 11 – Conclusions and parallel and future works

In the last chapter, the general conclusions are presented, the parallel work is reported, and also future work is suggested considering the gaps and the sequence of this research.

It is important to mention that the scientific articles were not produced with the same sequence presented in the thesis. The literature reviews were submitted or published after most of the other research articles. Thus, the literature review includes the main results of these research articles. In order to understand better all the organization, the objectives and relationship between the chapters, Figure 1 and Figure 2 present the schematic representation of this thesis.

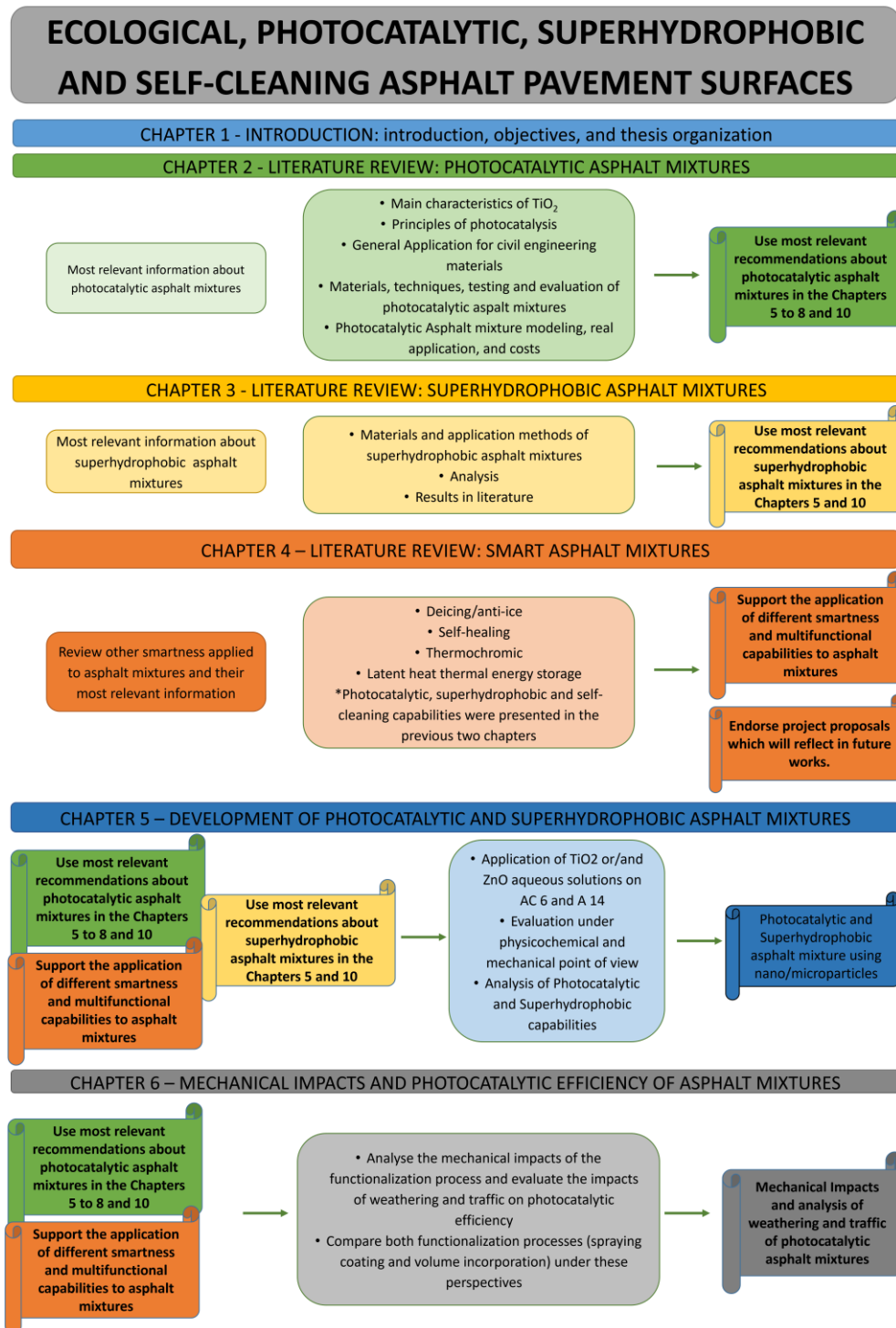


Figure 1: Schematic representation of this thesis: part 1

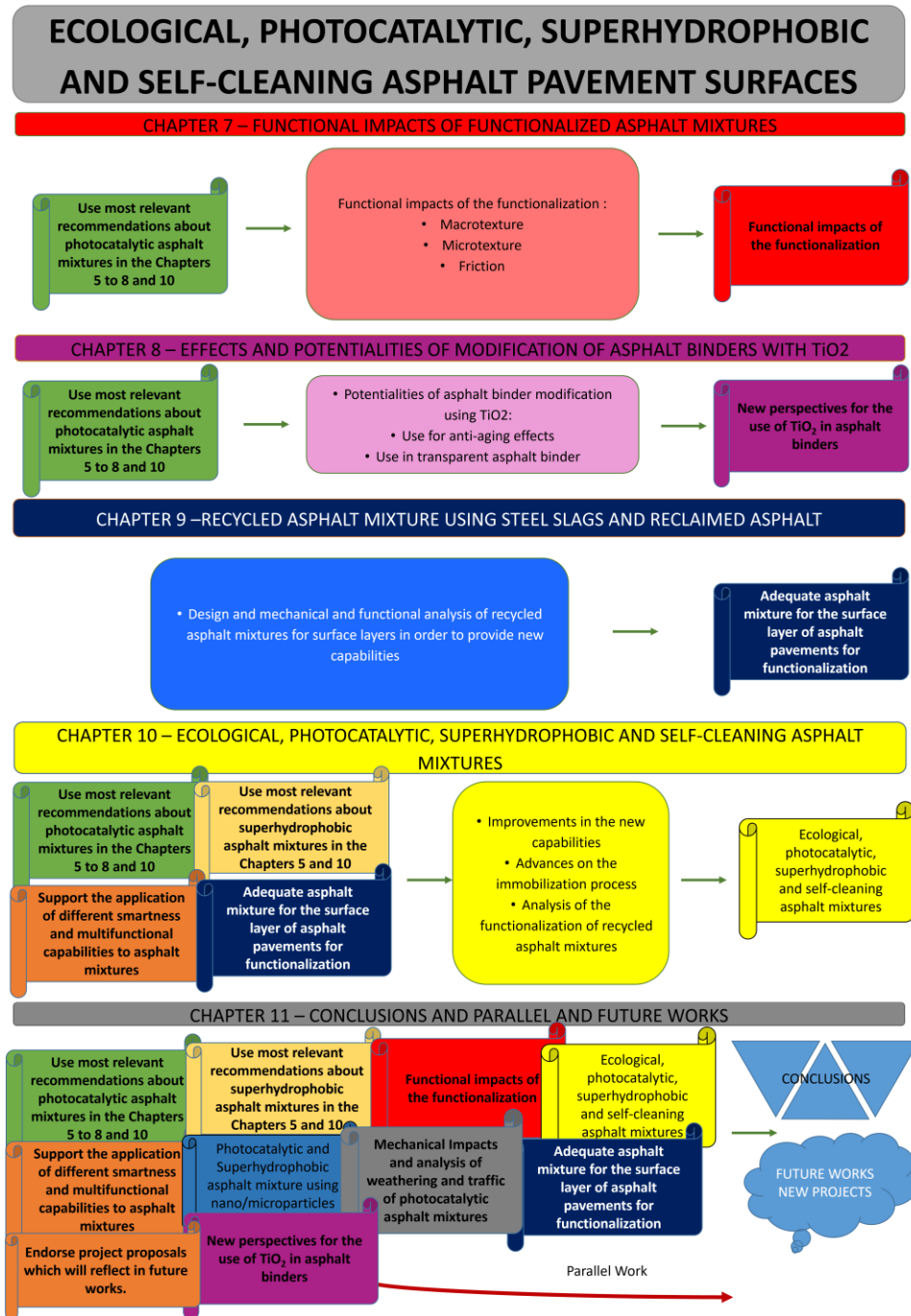


Figure 2: Schematic representation of this thesis: part 2

CHAPTER 2 – LITERATURE REVIEW: PHOTOCATALYTIC ASPHALT MIXTURES

This chapter refers to the literature review about photocatalytic asphalt mixtures “Smart, Photocatalytic and Self-Cleaning Asphalt Mixtures: A Literature Review” published in Journal Coatings (impact factor – if - 2.881). Figure 3 shows its first page. The content of this chapter is included in the article, which digital object identifier (DOI) is doi.org/10.3390/coatings9110696. The main objective of this chapter is to present the most relevant information on literature considering the application of the photocatalytic capability to the asphalt mixtures. The main findings of this chapter support the laboratory work carried out in the chapters 5 to 8 and 10 regarding the photocatalytic capability applied to asphalt mixtures.



Figure 3: First page of the research work published in Coatings [1]

2.1. Introduction

Since the findings of the photocatalytic capability of semiconductor materials, smart products have been gradually inserted in the market during the last three decades [2]. The global market of photocatalytic products is growing from \$848 million in 2009 to the expected value of \$2.9 billion by 2020 [3]. Nowadays, self-cleaning surfaces based on photocatalytic processes are applied in dissimilar areas such as buildings, road paving, vehicle side-view mirrors, lamps, and even in textiles. Among the semiconductor materials based on oxides, such as titanium dioxide (TiO_2), zinc oxide (ZnO) and tungsten oxide (WO_3), TiO_2 have received the highest attention.

Fujishima researched the photoelectrolysis of water using a TiO_2 electrode during the 1960s [4]. Following this revolutionary change in photo-electrochemistry and as a response reaction to the oil crisis of the 1970s, his research pointed to innovative methods for hydrogen production using TiO_2 semiconductor material. Nevertheless, due to the need to use ultraviolet (UV) light irradiation (accounting for only about 3% of the solar spectrum) for starting the photocatalysis, the H_2 production promoted by using TiO_2 appeared to be unattractive. Then, research has pointed out the investigations of TiO_2 to air and water-pollutant photodegradation [4].

Road pavements must be able to withstand the effects promoted by vehicle traffic and also by the climate actions (weathering), ensuring driving conditions meet requirements related to safety, comfort, economy, and with low environmental impact on the surrounding ecosystems. Most recent research on road pavements is intended to improve the mechanical behavior of asphalt mixtures, but recently the functionalization and multifunctional capabilities have become an important topic.

As described by Han et al. [5], a smart and multifunctional cement/asphalt/polymer concrete is a material with properties that differ from conventional concretes, which can react to external stimulus complying with those requirements, such as stress and temperature. These properties can be self-healing, self-sensing, electrically conductive, electromagnetic, and thermal. A smart and multifunctional material is accomplished by proper composition design, special processing, introduction of new functional components, or via the modification of the microstructure from the conventional one [5]. In this sense, a smart asphalt mixture is a material that holds another property besides ensuring good mechanical and superficial performance.

The smart and multifunctional concretes (by their smartness or function) are classified by its smartness, mechanical, electrical, optical, electromagnetic wave/radiation shielding/absorbing, water-

related, and energy-harvesting functions. The optical functions are light-transmitting, light-emitting, and photocatalytic ability [5,6].

Heterogeneous photocatalysis mediated by semiconductors has recently attracted significant interest due to its efficient capacity to convert solar energy into chemical energy, mainly in applications devoted to the field of environmental remediation. Several research studies achieved good and promising results related to the degradation of different pollutants emitted by fossil fuels used by road vehicles. Due to the huge surface area of photocatalytic road pavements and its vicinity to the exhaust gases from automobiles, they are quoted as promising surfaces for the reduction (in the presence of sunlight and moisture/O₂) of SO₂, NO_x, CO_x, HC, soot fouling and other volatile organic compounds (VOCs) present in the atmosphere [7–14]. Since in the presence of light irradiation, photocatalytic materials can degrade organic pollutants (such as oils and greases) adsorbed to their surface, these materials can also be classified as self-cleaning materials, a very important property in road engineering applications, because the self-cleaning function can contribute to a significant reduction of car accidents on oil-spilled areas.

The most important new functions imparted to asphalt mixtures are the photocatalytic and self-cleaning properties. Therefore, the main goal of this article is to present a review of the functionalization processes performed over asphalt mixtures and also the discussion of their most relevant features. Firstly, the general characteristics of titanium dioxide semiconductor material and its essential principles of photocatalysis will be discussed in Sections 2.2 and 2.3, respectively. Afterward, some applications related to civil engineering materials will be presented in Section 2.4. Concerning the particular applications for asphalt mixtures, Section 2.5 presents the main materials used and the corresponding published topics, application methods and its benefits and limitations, some surface modifications as a strategy to improve photocatalytic efficiency such as TiO₂ metal doping or coupled semiconductor photocatalysts (e.g., g-C₃N₄-TiO₂ or CdS-TiO₂ systems), analysis of results from literature, modeling of photocatalytic pavements, impact on the essential characteristics of asphalt mixtures and application to experimental and real road sections and also their related costs.

2.2. General Aspects and Characteristics of Titanium Dioxide

TiO₂ is the most widely used semiconductor material in the field of photocatalysis because of its great ability to promote the degradation of organic pollutants, superhydrophilicity, chemical stability, long-term durability, non-toxicity, visible light transparency [15], low cost and availability (0.44% of the elemental chemical composition of the Earth's crust is Ti) whose worldwide reserves are higher than 600 million tons [16,17].

As with different materials, TiO₂ is produced in four different geometric/dimensional shapes (0 to 3). The zero dimensions refer to spherical particles, one dimension is devoted to nanowires, nanorods, nanobelts, and nanotubes, the two-dimensional shapes are for nanosheets, and lastly, the 3D shapes usually refer to porous nanostructures. Obviously, the selection of the geometric/dimensional shapes depends on the ultimate application purposes [18]. TiO₂ nano or microspherical particles are mostly applied in smart materials. They have a high specific surface area as well as high pore volume and pore size, thus increasing organic pollutant adsorption and, consequently, improving the photocatalytic efficiency [15,19].

TiO₂ presents three crystalline phases: anatase, rutile, and brookite. Anatase is the most stable crystalline phase, while brookite is uncommon and unstable. Anatase phase can be converted to the rutile phase by heating higher than 700 °C. Anatase and rutile crystallize in the tetragonal system while brookite presents an orthorhombic form. The structure of the anatase phase shows bipyramid tetragonal symmetry with four units per elementary cell, and, for rutile, it is tetragonal, with two formula units per elementary cell [20]. Concerning the photocatalytic ability, the literature reports that TiO₂ anatase structure is more efficient than rutile due to its more exposed structure. Degussa P-25 is the trade name of TiO₂ particles that are most commonly used in different applications. These particles are composed of about 25% rutile and 75% anatase. This phase composition enables the formation of clusters or thin rutile layers onto the surface of anatase particles, or the presence of individual rutile and anatase nanoparticles, or even heterojunction of the two crystalline phases [21]. The literature refers to the fact that a combination of these two phases can improve photocatalytic efficiency when compared to the use of just one phase [22]. Regarding TiO₂ nanoparticles, there are some features that can influence photocatalytic efficiency, namely, their size, specific surface area, exposed surface facets, pore volume and structure as well as crystalline phase content [15].

Besides the photocatalytic properties, TiO₂ presents a superhydrophilic surface under photoinduction. A TiO₂ surface can change between a less photocatalytic and more superhydrophilic state depending on the chemical composition and processing techniques. When this semiconductor material is irradiated by UV light, the water adsorbed on the surface of TiO₂ spreads, forming a thin film, which is related to the reconstruction of hydroxyl groups under UV-light irradiation. Molecular oxygen captures the photo-excited electrons and holes diffuse to the TiO₂ surface where they can be trapped by surface lattice oxygen, as suggested by Nakamura et al. [23].

Hole trapping weakens the energy between the Ti atoms and lattice oxygen. Another adsorbed water molecule breaks this bond, forming a new hydroxyl group. The successive dissociative adsorption of water induces the trapping of these hydroxyl species leading to the photogeneration of a hydrophilic domain (size of about 10 nm). Given the unstable state of this surface, the bound photogenerated hydroxyl groups desorb gradually, and the surface returns to its initial state, presenting less hydrophilic behavior [11,24]. TiO₂ material's surface with flat or rough texture can exhibit hydrophobic or superhydrophobic behavior when coated with hydrophobic materials, for example, some silane compounds. Moreover, TiO₂ surfaces can also present a superhydrophilic state, which, in general, is characterized by a water contact angle less than 5° when irradiated with UV-light [15].

2.3. Basic Principles of Photocatalysis

Photocatalysis is commonly defined as the catalysis of photochemical reactions of adsorbed species on the semiconductor's surface [25].

Unlike metals that have a continuum of electronic states, semiconductor materials possess an electronic structure that is characterized by an empty energy space region where there are no energy levels available to promote the recombination of electron-hole (e⁻/h⁺) pairs generated by photoactivation in the solid semiconductor. The empty energy region is the so-called band gap energy (E_g), which extends from the top of the filled valence band (VB) to the bottom of the empty conduction band (CB) of the semiconductor material.

The TiO₂ VB mainly consists of oxygen 2*p* orbitals, whereas the CB is essentially formed by the 3*d* orbitals of the Ti⁺ cations [26]. Since photoexcitation (upon light irradiation) occurs via the band gap, the generated e⁻/h⁺ pairs have enough lifetime, to promote charge transfer to adsorbed species on the semiconductor surface (from the solution or from the gas phase in contact) and participate in redox processes [26]. The interaction of the photogenerated e⁻/h⁺ pairs with chemical species adsorbed to the semiconductor surface generally occurs via two main pathways. At the semiconductor surface, the electrons can be transferred to acceptor species, thus being reduced (usually the electron acceptor is oxygen in an aerated solution); in turn, the holes migrate to the semiconductor surface where they can be combined with donor species (e.g., OH⁻), which become oxidized. Competing with charge transfer to the adsorbed species is the phenomenon of electron-hole recombination. The recombination of the separated e⁻/h⁺ pairs can occur in the bulk of the semiconductor particle or on its surface, releasing energy as light or, more frequently, as heat. Obviously, the recombination of the photoexcited e⁻/h⁺ pairs

are detrimental for the photocatalytic performance and, therefore, this phenomenon should be retarded to enable the occurrence of an efficient charge transfer process on the photocatalyst surface. Charge carrier trapping can be used as an important mechanism that can be employed to suppress the recombination process and increase the lifetime of the separated e^-/h^+ pairs to participate efficiently in redox reactions. The most effective separation of the e^-/h^+ pair is achieved from the Ti defect states and surface Ti–O–Ti sites (or terminal Ti–OH), which can trap the electrons and holes, respectively. In general, oxygen vacancies [27], surface Ti^{3+} [28], Ti interstitial or even ions in the lattice or in the near-surface of TiO_2 [29] are responsible by the generation of intra-bandgap energy levels, which are of great importance in retarding the rate of e^-/h^+ recombination and simultaneously can enable the absorption of light by TiO_2 catalyst, not only in the ultraviolet, but also in the visible region of the electromagnetic spectrum [30–32].

Besides, the e^-/h^+ pairs can also be trapped by using other strategies comprising the semiconductor surface modification. For example, in TiO_2 photocatalysis, the addition of transition metals (so-called metal doping, for example, iron doping to the semiconductor can change its photocatalytic process by altering the semiconductor surface properties [33]. Upon photoexcitation, the electron migrates to the metal (covering a small area of the semiconductor surface), getting trapped there, and thus, the e^-/h^+ recombination is blocked. This occurs due to the creation of the so-called Schottky barrier that is produced at the metal–semiconductor interface, which acts as an effective electron trap avoiding electron-hole recombination and, therefore, increasing the photocatalytic efficiency [34].

Despite this, in several cases related to the preparation of some colloidal and polycrystalline photocatalysts, ideal semiconductors crystal lattices are not formed. Instead, surface and bulk defects occur quite regularly during the photocatalysts preparation process. The nature of surface defect sites depends on the semiconductor's preparation method. A particular example about the role of surface traps is the preparation of CdS colloids obtained by the addition of H_2S to a cadmium salt solution, which generates surface defect sites promoting radiation-less recombination of charge carriers in this semiconductor system. Furthermore, if a surface modification is performed by the addition of excess Cd^{2+} ions and with a proper pH adjustment toward a basic solution, then it induces the blocking of charge carriers trap sites, which also promotes radiation-less recombination of electron-hole pairs across the semiconductor bulk band gap, therefore being detrimental to the photocatalytic performance [34,35].

Figure 4 is a schematic representation of photoexcitation in a semiconductor material in which an electron is moved from its valence band to the conduction band, provided that light is absorbed with energy equal to or higher than the semiconductor's energy band gap.

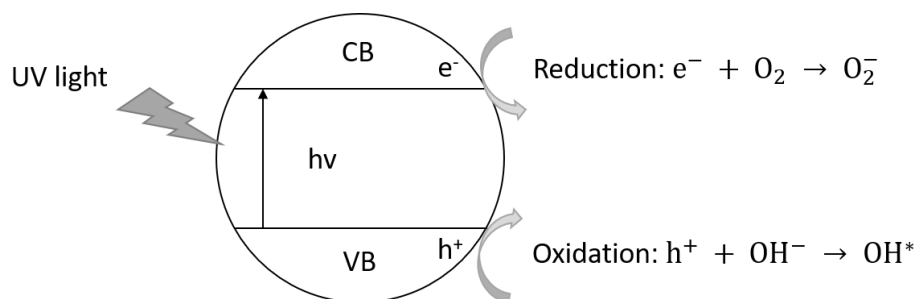


Figure 4: Schematic representation of the photo-excitation in a semiconductor material. Adapted from [36]

The general mechanism of photocatalysis using TiO_2 under UV light irradiation (wavelength less than 385 nm) follows several stages, which can be generically presented as photochemical reactions shown by Equations (1) to (4) [36–39]. Initially, an e^-/h^+ pair is photogenerated by the UV light irradiation on the semiconductor material (Equation (1)). Then, the electrons and holes react with oxygen and moisture, forming super-oxide ions (O_2^-) and hydroxyl (OH^*) radicals, respectively, which are highly reactive species (Equations (2) and (3), respectively). The O_2^- specie reacts with H^+ , dissociated from water, and forms HO_2^* . From these radicals, pollutant gases such as, for example, NO_x , can be degraded, according to Equations (5) and (6) [36–39]. For NO_x -type gases, the photocatalysis end products are essentially water-soluble nitrates, which can react by forming mineral salts that are harmless and very soluble in water [40,41]. In this sense, the end products can be easily removed from surfaces by rain or by simple washing. The soluble nitrates end products should be analyzed to assess their environmental damage. In fact, it is ideally desirable that, after photocatalysis of NO_x -type gases, nitrates would be produced with a very low concentration, therefore, without harming the environment.



Additionally, the TiO₂ semiconductor material can also degrade organic compounds through dissimilar oxidation reactions that, ideally at the last stage, lead to the formation of carbon dioxide and water (Equation (7)). The chemical reaction shown below can be extended to other organic materials such as oil and greases [12], for example, and/or bio microorganisms [42].



The understanding of the charge carriers' kinetics and the associated energies of the VB and CB can be accessed from different characterization techniques. For example, diffuse reflectance spectroscopy studies analyzed in light of the Kubelka–Munk theory are commonly utilized to determine the semiconductor's energy band gap [43,44]. Time-resolved spectroscopy and electron spin resonance are applied to monitor the e⁻/h⁺ pairs dynamics and to identify the radicals formed upon the transfer of the charge carriers [45]. Therefore, these results are essential for understanding the mechanisms underlying photocatalysis.

Figure 5a shows the measured values for diffuse reflectance spectroscopy of TiO₂ nanoparticles, TiO₂ nanoparticles milled at 350 rpm, and TiO₂ nanoparticles milled with Fe (at 350 rpm) by using the ball-milling technique. Figure 5b presents the Kubelka–Munk transform, which enables the energy band gap calculation of TiO₂ particles.

After acquisition of the TiO₂ reflectance curve (reflectance (R) versus wavelength), the Kubelka–Munk function can be expressed as $F(R) = (1 - R)^2/2R$ and the Kubelka–Munk transform is given by $[F(R) \times E]^{\frac{1}{2}}$ in which E corresponds to the incident photon energy (see Figure 5b). Taking the curve shown in Figure 5b, the value of the energy band gap was calculated by drawing a line tangent to the curve (drawn from the curve's inflection point) to its intersection point with the energy horizontal axis. Such an intersection point corresponds to the E_g value. For this specific case, the E_g value for TiO₂ without milling, milled with and without Fe powder was 3.0, 2.68, and 2.45 eV, respectively. These results, that is, the changes on the TiO₂ energy band-gap, showed that the milling process, as well as doping of the semiconductor by a transition element (iron), influenced the semiconductor's optoelectronic properties [43].

As mentioned before, the TiO₂ semiconductor activates the photocatalysis when it is irradiated by UV light. However, the sunlight is mostly composed of visible and infrared photons, having a very low UV light irradiance, since only about 3%–5% of the solar spectrum comprises the UV range [43]. In this sense,

one of the most important concerns reported in literature review to obtain improved photocatalytic materials is the doping of TiO_2 particles with different materials in order to decrease its E_g to the wavelength range of visible light (indicated in Figure 5) or forming localized mid-gap states above the valence band [27], thus promoting the degradation of pollutants when subjected to the incidence of photons in the visible range [43,46]. As already pointed out, some TiO_2 doping approaches have been studied, such as, for example, via the utilization of transition metals: Cu, Co, Ni, Cr, Mn, Mo, Nb, V, Fe, Ru, Au, Ag, Pt; and non-metals: N, S, C, B, P, I, F [47] or by chemical doping or physical ion-implantation methods [27]. These strategies not only ensure the absorption in the UV range, but also promote the visible-light absorption, thus improving the photocatalytic efficiency under natural solar irradiation [48].

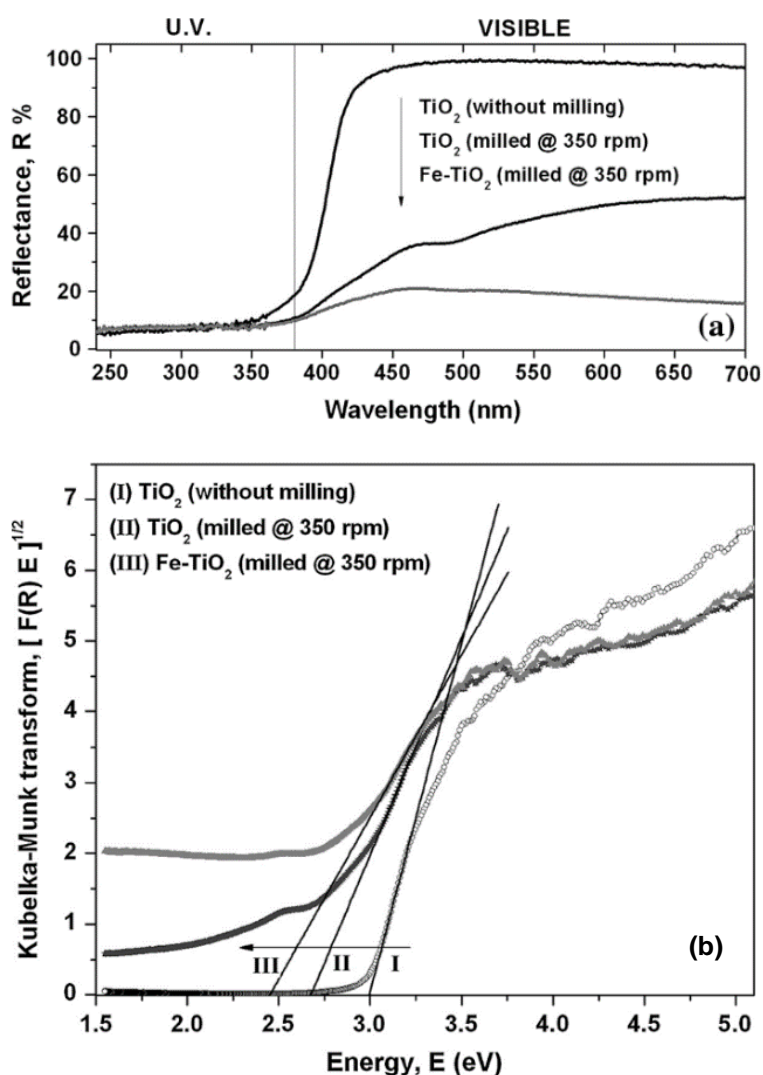


Figure 5: Diffuse reflectance spectroscopy of TiO_2 nanoparticles (a) and calculation of the TiO_2 energy band gap by the Kubelka-Munk theory (b) [43]

2.4. General Application for Civil Engineering Materials

Semiconductor materials have been extensively used in many applications from common products, such as sunscreens, to advanced and smart materials in the materials science context. The literature refers to the use of semiconductors for chemical (paints), automotive (glasses), aerospace (sensors), photovoltaic (self-cleaning glasses for the optimization of optical transmission), biomedical (functionalization of biomedical prostheses), textile (textiles for treatment of effluents from processing tasks), and civil engineering materials (facade tile materials, glass and pavements) mainly devoted to environmental and energy-related fields [15,49]. The use of the semiconductor materials can consist of the promotion or improvement of some properties, such as self-cleaning, photodegradation of air and water-pollutants, anti-fogging, anti-microbial, anti-aging, cooling surfaces, among others.

In the last few decades, research activity in civil engineering has mainly focused on studying the composition and design of more eco-friendly materials due to the natural resources depletion and environmental damages caused by this activity sector. For the construction of buildings and road pavements, non-renewable sources, i.e., aggregates, cement, and oil products, are required. On the other hand, there has been growing motivation for recycling wastes, the life-cycle study of different materials, and also their emissions [50,51]. More recently, TiO₂ nanoparticles have been incorporated in this sector, for example, in the production of more eco-friendly cementitious and asphalt materials, paints, and finally glasses, which can be devoted to many purposes, mainly for air-cleaning applications.

Ohama and Gemert have divided the use of TiO₂ semiconductor in construction materials into 3 different applications: (i) horizontal: concrete pavements, paving block and paving plates, coating systems for pavements and roads, roofing tiles, roofing panels, and cement-based tiles; (ii) vertical: indoor and outdoor paints, cement-based materials, permanent formworks, masonry blocks, sound-absorbing elements for buildings and roof applications, traffic divider elements, street furniture, retaining fair-faced elements; and (iii) tunnels: paints and coatings, concrete panels, concrete pavements, ultrathin white toppings [52].

Industrial activities and road traffic are the main causes of pollutant gas emissions such as SO₂, NO_x, and VOCs. For example, in France, the health costs only related to road traffic air pollution represent about 0.9%–2.7% of its gross domestic product (GDP) [53]. This type of pollution also reduces the appearance and durability of building materials. The use of inorganic photocatalysts, such as TiO₂, has proven to be relatively cheap and an effective strategy to remove toxic organic compounds and pollutant

gases from air and aqueous environments. An important and smart application of the TiO_2 photocatalyst is concerned with its use in construction and building materials. Moreover, given the building's large surface areas, they can also be used to promote the removal of pollutant gases from the surrounding air [54].

Cementitious materials, especially those used for outdoor applications, are permanently exposed to the action of atmospheric pollutants, microorganisms, and different weather conditions, in which all of them can be related to the deterioration and modification of the material properties. In this context, the use of TiO_2 can contribute to increasing the material life cycle while simultaneously promoting air-depollution of polluted areas or the depollution of some specific industries [52,55]. Also, the photocatalytic mortars can remove soot fouling, which deteriorates the architectural appearance of buildings [13].

Besides the self-cleaning effect and photodegradation of air pollutants, TiO_2 can be applied to provide passive cooling on the surface of building facades. Under solar light irradiation, TiO_2 -coated building surfaces become superhydrophilic if subjected to some cooling process, such as spraying water droplets on its surface facades, which spread to form a thin film of water covering large areas of the building's facade. It is important to emphasize that the cooling of a warm building surface (typical case of summer season) is due to a thermodynamic process, which results from the release of heat due to water evaporation when it comes into contact with the building's warm surface. This smart process for cooling down the buildings would decrease the electric energy that is consumed by using conventional air conditioning. Regarding the self-cleaning effect, the use of TiO_2 can maintain heritage buildings and also cleaner facades over time [4,19,49]. For this purpose, the pioneering use of TiO_2 in Europe took place in the Church Dives in Misericordia, Italy, and in the Music and Arts City Hall in France, which ensured that the original color of their facades was preserved [52].

Another pioneer application of photocatalysis in the civil engineering area refers to the coating of self-cleaning glasses for tunnel lighting in Japan. Uncoated lamps tend to lose brightness due to contaminants from vehicle exhaust gases that are adsorbed onto the lamp exterior. Sodium lamp glasses coated with TiO_2 semiconductor emit enough UV light ($\sim 3 \text{ mW/cm}^2$) to enable catalytic reactions and photodecompose adsorbed contaminants [11].

For indoor applications, TiO_2 coated ceramic tiles, and mortars are considered to be very effective against bacteria [56] and also fungi [57]. The bacteria are killed faster than they can grow on

photocatalytic ceramic tiles. This application in hospitals and health centers can be used to reduce the spread of infections. Moreover, it can be used for public, commercial, and residential buildings to improve the hygienic conditions [56].

Considering the antifungal application on mortars, Jerónimo et al. evaluated the growth evolution of the *Cladosporium* fungus. They found that after 49 days, in the case of the mortar without TiO₂, the fungus began to develop while the one with 4% of TiO₂, the fungus was still practically germinating [57].

The TiO₂ semiconductor material has also been applied on (window) glasses for anti-fogging and self-cleaning purposes [58,59]. The use of self-cleaning properties on glass windows can save money on building maintenance budgets, like cleaning by using conventional methods which is expensive and laborious, especially when dealing with high-rise buildings. Its main benefit is the combination of hydrophilicity and pollutant photodegradation, which significantly helps the cleaning process [59]. The next section presents additional aspects related to the application of TiO₂ on asphalt pavements, especially those related to de-pollution purposes.

2.5. Photocatalytic Asphalt Pavements

Road pavements are ideal places for reducing air pollution due to their large paved surface areas, which are in close vicinity with the toxic gases emitted by the vehicles circulating there [60]. Figure 6 schematizes the operational mechanism of the asphalt mixtures with photocatalytic ability, one of the most evaluated characteristics in multifunctional road pavements.

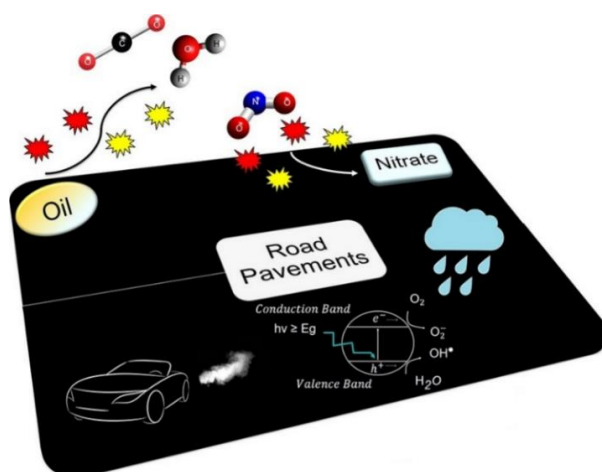


Figure 6: Photocatalytic asphalt mixture from [9]

Photocatalytic surfaces are also considered self-cleaning due to their ability to degrade organic pollutants, such as adsorbed oils and greases. In a road safety context, the ability to degrade organic

compounds adsorbed on paved surfaces can prevent problems related to vehicle skidding, thus contributing positively to the reduction of road accidents [7].

The number of articles published on topics related to photocatalytic asphalt mixtures has been steadily increasing. When looking for the keywords “photocatalytic” and “asphalt mixtures” (using Google Scholar), it is possible to observe that the research about this topic rose from 2 to 40 occurrences between 2006 and 2018, respectively, excluding citations. When carrying out the same analysis but only searching the keyword “asphalt mixtures”, it is possible to count the total occurrences of 904 and 3220 for the same period, respectively. This number means that in 2018, only 1% of occurrences refer to research about the topic of photocatalytic asphalt mixing. On the other hand, for this research topic, the number is increased by about 65% when the word “mechanical” is included in “asphalt mixtures”, thus showing that the mechanical behavior of asphalt mixtures is the most important issue related to asphalt pavements. Moreover, it can be concluded that the research in photocatalysis applied to asphalt mixtures is quite innovative and is of great interest to researchers.

2.5.1. Materials and Techniques for Application of Photocatalytic Effect on Asphalt Mixtures

Like many other applications in the field of material science, the most important semiconductor material in photocatalytic asphalt mixtures also refers to TiO_2 [7,61,62]. Meanwhile, the literature also presents information regarding the use of other materials, such as ZnO [8] and graphitic carbon nitride (g-C₃N₄) [63,64]. ZnO is also a semiconductor material with a band gap of about 3.3 eV [65,66], while g-C₃N₄ is a new type of non-metal photocatalyst that has a band gap of ~ 2.7 eV [63,64,67]. TiO_2 is commonly used on a nanometer scale (between 6 and 40 nm) [39,68–70]. In photocatalytic asphalt mixtures using TiO_2 , the crystalline phase of anatase [10,68,69,71,72] and the TiO_2 nanoparticles P-25 [7,8,62] are commonly used. Analyzing the photocatalytic capacity applied to asphalt materials, quite a few works can be found on conventional asphalt mixtures [7,60], asphalt mixtures with lower production temperature (warm mix asphalt) [71], slurry seals [63], fog seals [73], asphalt emulsions [64,74], among others. Also, other issues have been studied, such as their application in real context or just small test sections [62,69,70,72,74,75], and the computational modeling of the photocatalytic capability of road pavements [75,76].

In order to obtain photocatalytic asphalt mixtures, it is possible to highlight four main techniques that can be utilized to apply the semiconductor materials in the asphalt mixtures: (i) spraying coating [7,10,40,46,68,71,73], (ii) volume incorporation [7,68,73,77], (iii) bitumen modification [71],

and (iv) spreading [68,73,78,79]. Bitumen modification is developed before the manufacture of the asphalt mixture. The semiconductor particles are mixed just with the binder. The technique by volume incorporation is carried out during the asphalt mixture production where the particles are inserted and combined with the aggregates and/or the filler. The spraying coating and the spreading processes are applied over the asphalt mixture after its compaction. The first one, that is, the spraying coating, is carried out using a spray-painting gun and the second one (spreading process) is carried out by using a specific solution that is deposited over the surface like a chip sealing or even using paintbrushes. There are other techniques that can be used to functionalize asphalt mixtures, but probably implying a higher degree of application difficulty and also leading to a higher cost of implementation in a real context, such as the use of the atmospheric plasma-spraying technique [70].

Spraying coating is probably the most efficient functionalization technique, and it also uses smaller amounts of semiconductor material. However, the immobilization of the semiconductor particles over the asphalt mixtures surface is still a major challenge. The second and third functionalization processes, i.e., the volume incorporation and bitumen modification, respectively, probably guarantee the best immobilization characteristics, but more material needs to be used compared to the other ones. Nevertheless, traffic abrasion is required to expose the semiconductor material that is covered by bitumen.

The modification technique improves the aging resistance of asphalt binders mainly due to the capability of the semiconductors to reflect and absorb the UV light, which is the most important issue for the long-term aging process [71,80–82]. Additionally, TiO₂ nanoparticles as bitumen modifier decrease the acid component and increase the alkaline component and also the surface-free energy of the asphalt binder, leading to improvements in the adhesion between the asphalt binder and the aggregate [83].

Regarding the spraying coating technique, the literature reports the application of aqueous solutions [7,10,40,71,73] and other ones with emulsions [74], cement and resins [39,78], polymers [84] and rubber [69] in order to achieve a better immobilization process. A significant concern that should be taken into account when it is desired to obtain photocatalytic aqueous solutions is the dispersion of the TiO₂ nanoparticles; otherwise, they may agglomerate and, consequently, decrease the photocatalytic efficiency. Some authors submitted TiO₂ solutions to ultrasonic treatment [46,68] or prepared aqueous solutions with a value of zeta potential different from the isoelectric point [7].

The previous preparation reduces particle agglomeration because of the van der Waals attraction forces that should be competing with the Coulomb's repulsive electrostatic forces [7]. For the preparation of the TiO₂ aqueous solution, the suggestion is to use a pH equal to 8 [7].

To improve the photocatalytic efficiency and the immobilization of the nanoparticles, Leng and Yu proposed an interesting spraying technique called Breath Figure (BF). The process consisted in a solution with TiO₂ nanoparticles mixed with asphalt binder, polymer (polystyrene) and solvent (tetrahydrofuran). This process can create porous microstructures in bitumen, thus creating suitable conditions for TiO₂ particles to enter and be deposited inside the pores. The photocatalytic efficiency of the BF asphalt mixture was higher than that obtained with the asphalt mixture sprayed with TiO₂ aqueous solution before and after abrasion condition. The best proportion was 2:1:1 of TiO₂, binder, and polymer, respectively, and the concentration of all solutes was 120 mg/mL [84].

For the case of asphalt mixtures, the application of TiO₂ doping by using dissimilar materials, the literature reports the its functionalization by La [46], Ce [68,85], Cu and Fe by ultrasonic-assisted sol-gel [85], N by simple mixing [86], and C [62] and Ag [69]. The authors concluded that TiO₂ doped with 0.5% of La (mol%) [46] and 0.2% of Ce (mass ratio) [68] presented the optimal photocatalytic efficiency. Chen et al. mixed TiO₂ and urea at a 2:1 ratio in molar proportions [86]. Unfortunately, neither C nor Ag content was reported by Fan et al. [62] and Liu et al. [69], respectively. Under visible light, all of these treatments were able to degrade pollutants (such as NO_x) and improved photocatalytic efficiency because, considering the solar spectrum on Earth, visible light irradiance is much higher than UV. Other materials have been added to TiO₂ in order to improve its photocatalytic efficiency or even to improve another capability, such as the superhydrophobic ability. The non-metal g-C₃N₄ improved the NO degradation [64] and ZnO increased the water contact angle of the asphalt mixtures [8] when they are combined with the TiO₂ semiconductor material.

Considering the UV light resistance of asphalt binders modified with TiO₂ doped with Cu, Fe, and Ce (molar mass ratio of [Ti⁴⁺/Metal ion] equals to 3/1), Jin et al. [85] concluded that the optimal content of these materials is 5% (in the binder mass). Comparing the results obtained, the best performance was achieved by using Ce. The photocatalytic efficiency increased by at least 27% for NO and 40% for HC, after 90 min of testing, when the TiO₂ was doped when compared to the samples with only TiO₂. Regarding the HC and NO degradation, the best doping materials, presented in ascending order, are Cu, Ce, and Fe [85].

2.5.2. Testing, Results Analysis of Photocatalytic Asphalt Mixtures

In order to evaluate the photocatalytic ability, the literature presents gas degradation tests, such as NO_x and VOCs, most of them according to the standards ISO 22197-1 and JIS TR Z 0018 [61,68,71], and tests of photocatalytic efficiency via the degradation of different organic dyes, such as methylene orange (MO) [62], methylene blue (MB) [7,68] and rhodamine B (RhB) [8,9], which use spectrophotometric techniques (Figure 7b). Both tests can be used to evaluate the photocatalytic gas degradation, considering both air depollution and dye degradation for self-cleaning applications. Nevertheless, both tests are clearly related as they are used for measuring the ability of pollutant photodegradation.

Regarding the first test, some gases have been used: some VOCs: HC [85], benzene, toluene, xylene and trimethylbenzene [60], SO_2 [10] and mainly NO , NO_2 or NO_x [69,72,84]. Briefly, the gas flow with a controlled concentration passes into a chamber where the sample containing the semiconductor material resides inside and is subjected to light irradiation (Figure 7a). The gas concentration is monitored at the outlet of the system and the photocatalytic efficiency can be further evaluated. It is possible to control humidity, temperature, light irradiation (wavelength and power), gas flow rate and concentration, and other physical parameters.

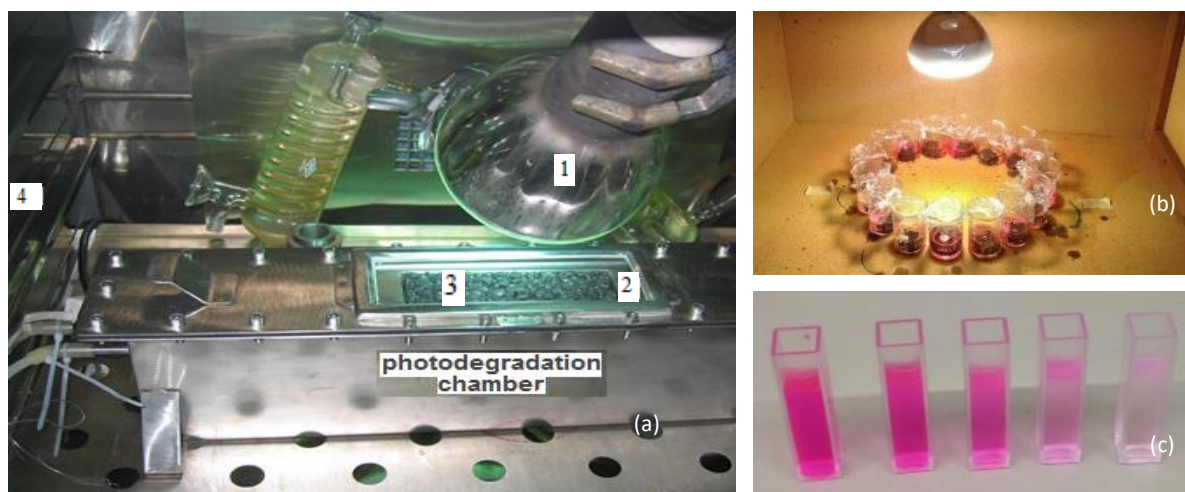
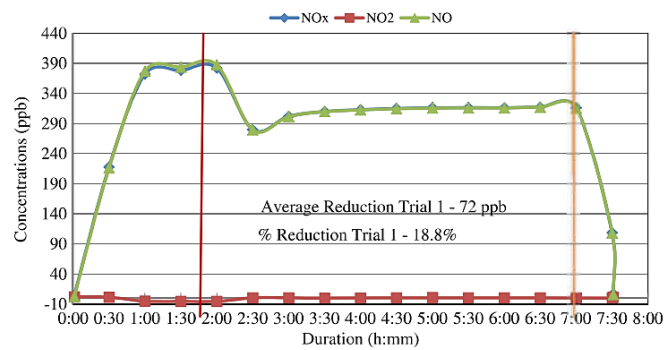


Figure 7: Experimental tests to measure the photocatalytic activity: (a) NO_x degradation efficiency (1: lamp for light irradiation, 2: quartz window, 3: test specimen, and 4: temperature stabilizer); (b) degradation of an organic dye; (c) aqueous solution of an organic dye of different color intensity over time, thus indicating its degradation

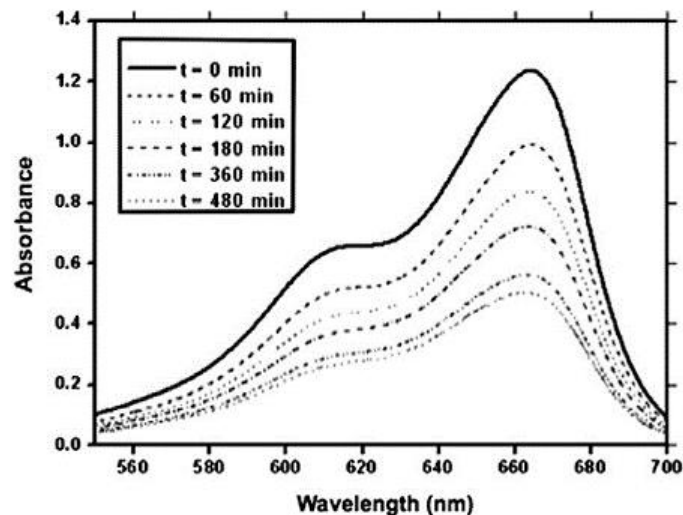
Regarding the second test, that is, the organic dye degradation, the asphalt mixture samples under study are dipped into a dye's aqueous solution of known initial concentration. Subsequently, the sample already immersed in the dye's aqueous solution is exposed to light irradiation and, over time, the variation in solution concentration is monitored by spectrophotometry (Figure 7b,c). The photocatalytic efficiency

can be calculated from detected variations (decrease) in the maximum absorbance values recorded on the absorption spectrum by using visible spectroscopy. As before, it is also possible to control light irradiation (wavelength and power), the dye's solution concentration, volume, and pH.

Figure 8 shows the results related to the two types of tests mentioned previously. For the gas degradation (Figure 8a), a plot of gas concentration, in this case, NO_x , versus duration (degradation time) is presented [61,87]. During the test beginning, the UV light is turned off. After reaching the equilibrium condition (after about 1 h 45 min), the UV-light source is turned on. Next, the gas is released, flowing into the chamber, and it is observed that the NO gas concentration decreases over time, thus showing a photodegradation capability. Actually, after 5 h of testing, the NO gas concentration becomes essentially constant, showing a reduction in its concentration of 72 ppb, which is a value that corresponds to about 18.8% when compared to the initial gas concentration (it was about 390 ppb). After 7 h of testing, the gas flow and the UV light source were turned off.



(a)



(b)

Figure 8: Results of photocatalytic tests: (a) variation (over time) of gas concentration, indicating its photodegradation from [61] (b) absorbance variation (over time) of the dye's aqueous solution, indicating its photodegradation from [7]

Figure 8b shows the absorbance spectra of the methylene blue aqueous solution acquired for different UV light irradiation times [7]. For the calculation of photocatalytic efficiency, the decrease of the maximum absorbance (wavelength equals to 662 nm) is observed. Using the Beer–Lambert law and considering that the molecular extinction coefficient and the light path length are constant, the concentration and the absorbance are directly proportional (Equation (8)), and the photocatalytic efficiency can be calculated from Equation (9). It is observed that the sample’s photocatalytic efficiency increases over time of photo-irradiation, because the absorbance of the dye’s aqueous solution decreases (or similarly, its concentration decreases over time), thus indicating the occurrence of the photodegradation process. In this specific case, the tests were conducted for 480 min. Thus, it is possible to present a plot of photocatalytic efficiency versus photo-irradiation time.

It is also important to emphasize that some details can be carried out to evaluate the photocatalytic ability better, thus avoiding some errors or misunderstandings. When the samples are immersed in the aqueous dye solution, still without UV light irradiation, a first phenomenon occurs, which is the adsorption of the dye onto the sample’s surface. Therefore, it is recommended that samples should be kept in the dark until the adsorption–desorption equilibrium is reached [88]. Additionally, due to the granitic nature of the aggregates, some photocatalytic efficiency also occurs for blank samples, that is, those that have not been modified by the addition of semiconductor material. In order to avoid or even eliminate the side effect of exposed aggregates, the side and bottom faces of the samples should be coated with bitumen, thus only showing their upper face that is the traditional condition. If this procedure is not performed, this must be considered for the results, that is, photocatalytic efficiency for the blank samples [9].

$$\frac{A}{A_0} = \frac{C}{C_0} \quad (8)$$

$$\Phi (\%) = \left(\frac{A_0 - A}{A_0} \right) \times 100 \quad (9)$$

where A and A_0 are the maximum absorbance of the dye’s aqueous solution for a determined instant of time, t and for initial time $t=0$ h, respectively; meanwhile, C and C_0 represent the concentrations of the dye’s aqueous solution for the same instants of time mentioned previously and Φ is the photocatalytic efficiency.

In these tests, the source light used to promote the samples irradiation may be only the UV light (shorter wavelengths of about 300 nm) [7] or simulation of sunlight spectra [8,9] and also visible light

(for example, by using a halogen lamp with a wavelength of 400–800 nm or light-emitting diodes (LEDs) in different wavelengths) [46,68,86]. The first option, that is, the use of UV light irradiation takes into account only the photocatalytic process activated in this region of the electromagnetic spectrum. The irradiation that simulates the sunlight considers real situations of outdoor applications. The last one, i.e., the samples irradiation over the visible range of the electromagnetic spectrum, is carried out in order to study the effect of semiconductor doping on the photocatalytic efficiency. For example, in order to evaluate the photocatalytic efficiency of doped-TiO₂ coated asphalt mixtures, Chen et al. used lamps operating in different wavelengths, namely 330–420 nm, 430–530 nm (blue LED), 470–570 nm (green LED), and 590–680 nm (red LED). They have concluded that the N-doped TiO₂ asphalt mixture presented a better photocatalytic efficiency than the conventional TiO₂-coated asphalt mixture. Besides, the photocatalytic efficiency decreases with the increase of the wavelength [86].

Another technique, proposed by Osborn et al., consists of adding water over the photocatalytic surface and, after 5 min, collecting this aqueous solution with a syringe to analyze the number of existing nitrates [10,61]. This technique resulted in 48% of the nitrate removal when compared to the standard method, that is, the ISO 22197-1 standard. It is a simple procedure that does not require the acquisition of asphalt samples from the field.

The oil/grease degradation could also be analyzed. For example, instead of evaluating the photocatalytic efficiency through the degradation of some organic compounds (dyes or soot) [4,14], there is the opportunity to evaluate this ability via the degradation of some simple oil/grease compounds that can be analyzed by spectrophotometry, for instance.

The photocatalytic efficiency can be influenced by several factors, such as pollutant flow rate and concentration, solar irradiation, humidity, environmental temperature, among others. Due to the action of traffic and wind speed on the photocatalytic asphalt mixture, a decrease in its photocatalytic efficiency in NO_x degradation usually occurs by about 60% and 42%, respectively [72]. An increase of the solar irradiation also leads to the concomitant increase in photocatalytic efficiency. The presence of excessive water inhibits the photocatalytic reaction as humidity competes with pollutants for adsorption over the surface, thus decreasing the photocatalytic efficiency [10,70,72]. On the other hand, the increase of gas flow rate decreases the photocatalytic efficiency due to an insufficient photocatalytic reaction under high-speed gas flow, because it reduces the contact time between the reactants and the catalyst [10,46].

Moreover, the gas concentration also influences the photocatalytic efficiency. The higher the concentration, the lower the photocatalytic efficiency [46,69]. Light irradiation with shorter wavelengths is more effective than for longer wavelengths [69,70]. A decrease in photocatalytic efficiency when the samples are submitted to higher temperatures has also been observed, which can be explained by the higher kinetic energy of the molecules, thus accelerating their gasification and reducing the contact of the gas with the semiconductor material [69]. Additionally, the dust particles over the asphalt mixtures also contribute to reducing the photocatalytic efficiency [77]. Besides the photocatalytic effect, this technology promotes a temperature decrease in the urban environment. Due to the color and light reflection, the TiO₂ treatment over the asphalt mixtures surface can reduce their surface temperature. This application can mitigate urban heating island (UHI) and building cooling demand [89]. The registered maximum temperature decrease, in a summer day, was 5.5 °C for a cool off-white asphalt when compared to the conventional asphalt mixture.

2.5.3. Photocatalytic Asphalt Mixtures Modeling

Some authors developed models related to the NO degradation promoted by photocatalytic asphalt pavements. Equations (10) to (12) describe NO concentration by factors related to the number of vehicles per hour (T), relative humidity (H), wind speed (V) in m/s, ambient temperature (T_{Ambient}) in °C and solar radiation rate (S) in W/m² [75].

$$\text{NO}_{\text{before}} = 0.96 \times T + 0.22 \times H - 1.33 \times V_{\text{Ambient}} - 10.5 \times V + 0.02 \times S \quad (10)$$

$$\text{NO}_{\text{after}} = 0.31 \times T + 0.06 \times H - 0.1 \times T_{\text{Ambient}} - 0.75 \times V + 0.0003 \times S \quad (11)$$

$$\text{NO}_{\text{reduction}} = \text{NO}_{\text{before}} - \text{NO}_{\text{after}} \quad (12)$$

where $\text{NO}_{\text{before}}$ and NO_{after} correspond to the hourly average of NO (ppb) concentration before and after the application of TiO₂, respectively and the $\text{NO}_{\text{reduction}}$ corresponds to the difference between these values. The modeling presented a R^2 of 0.79 for the untreated samples and 0.67 for the treated ones. As there are just a few studies about the photocatalytic efficiency of asphalt mixtures, therefore this must be better evaluated.

Kruschwitz et al. [76] report a 3D simulation of the whole length of photocatalytic asphalt pavement, showing similar results between the finite-element simulation technique and the experimental measurements of NO vs. time. They present some variables, such as the initial concentration of NO, vehicle distribution, NO emission by vehicle, road geometry, solar effects on NO (natural conversion from

NO to NO₂), and pollution-reducing effects. They also showed uncertainties in the weather condition (for example, UV irradiation, wind, and rain) [76].

2.5.4. Mechanical and Surface Impacts and Design of Photocatalytic Asphalt Mixtures

The mechanical characterization of photocatalytic asphalt mixtures has already been carried out. By volume incorporation, TiO₂ leads to a decrease in moisture resistance, while fatigue and rutting may also be affected. A high content of TiO₂ (6%) improved the rutting resistance but decreased the fatigue resistance, whereas a low content of TiO₂ (3%) slightly increased the rutting but maintained the fatigue resistance [9]. Furthermore, the functional impact was also evaluated. The functionalization techniques by spraying coating using aqueous solution and volume incorporation led to a difference in friction between -7% and 3%. The microtexture amplitude parameters were not affected by any functionalization technique except the skewness of AC 14 with 6% TiO₂ by volume incorporation [90].

Wang et al. [79] concluded that the friction and texture depth of the asphalt mixtures decreased when the spreading TiO₂ coverage rate (by emulsion spreading) is increased. Considering the local technical requirements, 550 g/m² is the maximum coverage rate that respects these parameters. The same authors studied the water permeability of the photocatalytic asphalt mixtures. They concluded that the covering rate did not affect the water permeability. They recommended 8% TiO₂ with a covering rate of 400 g/m².

A very interesting article was published taking into account the smart asphalt mixture design. Analyzing a mortar composed of asphalt binder, filler, and TiO₂, Zhang et al. [77] showed that the stiffness modulus was not influenced by the TiO₂ content. The increase of TiO₂ content raises the cone penetration values at 60 °C, which can indicate lesser performance of permanent deformation resistance. Analyzing the mechanical behavior of the asphalt mixture functionalized by volume incorporation, they concluded that the TiO₂ content did not affect the water sensitivity and the low-temperature anti-cracking performance, but it affects the permanent deformation.

Considering the maximum value for the deformation, the same authors reported that the maximum content of TiO₂ that respects the mechanical behavior of the asphalt mixture is 4%. Regarding the accumulative decomposition ratio of automobile exhaust degradation, they reported that the best content of TiO₂ is 3.1% in mass of the aggregates by volume incorporation. Considering the voids content of the asphalt mixture, the efficiency increases with the increase of voids content because of the higher contact area between automobile exhaust and asphalt mixtures.

Considering the compaction, they observed that increasing in the number of gyrations by the Superpave Compactor leads to the decrease of the photocatalytic efficiency. They suggest the application of an asphalt mixture with high air voids content, for example porous asphalt concrete. Thus, obviously, during the service period of the photocatalytic asphalt pavement, the photocatalytic efficiency decreases due to the compaction.

These concerns consist of the design of smart asphalt mixtures taking into account the essential parameters (mechanical and superficial performance) and the new capabilities. For coatings by spreading or spraying over asphalt mixtures, the functional (superficial) characteristics should be respected. For the volume incorporation, besides the functional characteristics, the mechanical performance should be assessed. Last but not least, those functionalized by bitumen modification must be evaluated under aging resistance, mainly by UV light. Under these circumstances, it is possible to obtain the optimization of the new capabilities (in terms of content, covering rate, etc.), respecting the standard requirements for real applications.

2.5.5. Photocatalytic Applications in Real Context or Small Road Sections

Regarding the application in real scenario context or small test sections, some first approaches were performed (Figure 9). Bocci et al. applied a bituminous emulsion containing TiO_2 and cement mortar made of sand, cement, additives, and TiO_2 sprayed over asphalt mixtures onto Highway A14 in Italy. The coatings were applied to the right and emergency lanes of the road and their performance was monitored for 527 days. The most important variables that contributed to the decrease in emulsion efficiency were the low temperatures and rainfall. Its efficiency has been reduced by about 80% in just 100 days.

The authors concluded that, for tunnel applications, where weathering would be avoided, the best alternative should consist of the application of a bituminous emulsion, while, for the case of emergency lanes, the best option could fall on the use of cement mortar [74].

Meanwhile, Lui et al. applied a composite material (composed by Ag-doped TiO_2 nanoparticles dispersed in silane-bound rubber powders and dissolved in ethanol) to coat the asphalt mixture surface layer of the Wenxing Tunnel in Xiamen, China. According to their study, the results obtained showed that when the technology was applied to zones in the middle of the tunnel, a NO_x gas uptake of at least 62.4% was registered. When this result was compared to that obtained for tunnel exit sites, they found a decrease in gas uptake by about 26.3% because of the easier gas exit from the tunnel (i.e., at the tunnel end sites, the gas is closer to the outside) [69].

Moreover, Chen and Liu also applied a photocatalytic coating composed of TiO_2 nanoparticles dispersed in silane on the asphalt mixture of Highway G11 from Tsitsihar to the Nehe River, China. They showed a photocatalytic efficiency from 6% to 12% under real scenery of outdoor road traffic [70].

Wang et al. [78] spread cement mortars containing TiO_2 particles bound by epoxy resin in asphalt pavements of a test section at the Institute of Highway Engineering at Aachen, Germany. The authors observed that, without using the polishing process, the technology presented a photodegradation capacity of about 25.2%, while after 300 min of the polishing task (equivalent to a period of 8–15 years of traffic), the samples showed a photocatalytic efficiency of about 10.7%.

Fan et al. [62] sprayed a C- TiO_2 aqueous solution over a 90 m² section of asphalt road in Sheung Shui District, New Territories, Hong Kong. After applying the treatment, they heated the asphalt road surface by using an infrared heating lamp in order to immobilize the C- TiO_2 nanoparticles and concluded that heating treatment was successful. Besides out-of-the-wheel tracks, the nanomaterials remained since there is no traffic wearing [62].

Another study suggests that the durability (permanence) of TiO_2 nanoparticles sprayed over asphalt pavement surfaces ranges from 10 to 16 months [61]. Recently, Chen et al. applied a spraying coating of N-doped TiO_2 (by using a silane coupling reagent) over an asphalt road and showed that the coating's durability kept working during about 13 months [86].

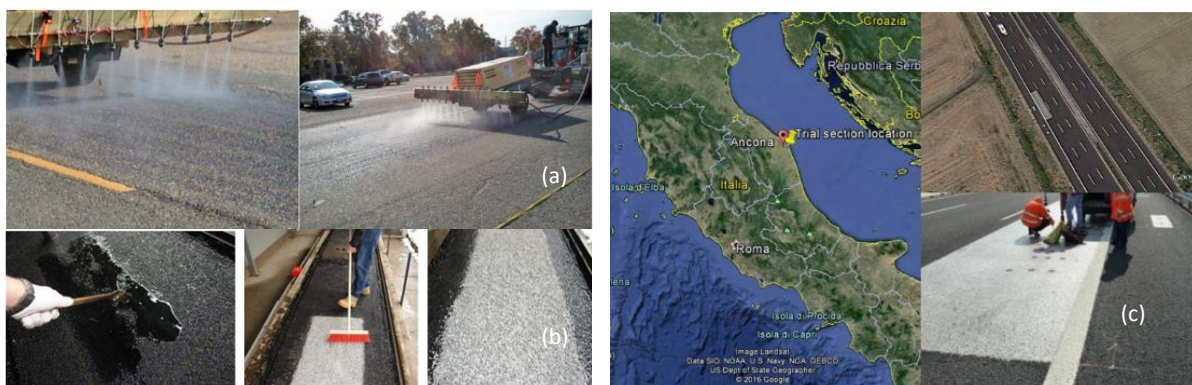


Figure 9: Photocatalytic test sections: (a) by Hassan et al. [10]; (b) by Wang et al. [78] , and (c) by Bocci et al. [74]

The literature points out that the application of photocatalytic treatments on asphalt mixtures is still being studied. There are just a few articles published about the analysis in a real context. In fact, ensuring the nanoparticles immobilization over surfaces still remains the major problem and challenge for researchers. The main and most commonly used application techniques are those that interact with the surface: spreading and mainly spraying coating. The others, that is, the bitumen modification and

volume incorporation techniques, should be tested since there is a lack of information on these approaches under test section or real context applications.

2.5.6. Cost Analysis

Regarding the costs, probably between the known four application methods, those that use the least amount of semiconductor material and also is more efficient, refers to the spraying coating technique. Hassan et al. carried out an economic analysis of a photocatalytic coating of TiO₂ aqueous solution sprayed over the asphalt pavement surface layer. This solution was composed of anatase phase of TiO₂ nanoparticles (2% by volume), and it was applied covering 0.05 L/m². They concluded that the photocatalytic coating costs were about USD 2.25 per m² (in 2012). When compared to the application cost around 9 cm asphalt mixture layer, the coating application increased by 11% the initial budget [10]. Fan et al. reported that the fabrication cost of the C-TiO₂ aqueous solution coating applied by spraying is estimated in USD 1–3 per m² covering about 7 g/m² (in 2018), but the other costs need to be evaluated in further studies. Bocci et al. studied bituminous emulsion containing TiO₂ and cement mortar made of sand, cement, additives, and TiO₂ sprayed over asphalt mixtures. They reported a cost of €6.50 per m² (0.067 kg/m²) for the first one and €20 per m² (1 kg/m² except for water) for the second one, in 2015.

As a typical example related to the costs of raw TiO₂ nanoparticles, one can highlight the case of Evonik Aeroxide P-25, which presents a cost of about USD 45 per kg [91]. Nevertheless, it is well known that TiO₂ nanoparticles are still quite expensive due to very low industrial production. It is predictable that, in the next years, this cost would decrease significantly due to the very high application versatility of TiO₂ nanoparticles. Besides, since these researchers report very small test sections, the application over asphalt roads in a real context that covers much larger areas necessarily requires the acquisition of a large amount of nanomaterials, thus leading to a decrease in the nanoparticles' price. Because there is a lack of information about the cost analysis, this approach could be evaluated by researchers in further studies.

It can be concluded that photocatalytic road pavements are very important since if they are close to the largest emissions, they have a large area, and the pavements are mostly bituminous. As mentioned, there are important references related to the functionalization of asphalt mixtures to impart photocatalytic function. However, there is still limited experience on this topic, thus the surface immobilization techniques of semiconductor materials need further studies. Other aspects also require further investigation, such as the application of semiconductor materials in different substrates (asphalt

mixtures), the impact of functionalization on the functional and mechanical characteristics, application costs, and real application analysis.

2.6. Conclusions

Photocatalytic asphalt mixtures behave like smart materials since they present new capabilities when subjected to the action of light (optical interaction). Photocatalysis applied in this field is very innovative and is of great interest to researchers. This new capability is mainly provided by the presence of semiconductor materials, mostly TiO_2 , usually at the nanometer scale (anatase phase or P-25) and applied by using four major methods: spraying coating, bitumen modification, volume incorporation and spreading.

When irradiated by UV light from sunlight, the TiO_2 semiconductor material activates the photocatalysis process. Nevertheless, the sunlight is composed of only 3%–5% of the UV range light. Therefore, many research efforts have been carried out in order to shift the TiO_2 absorption energy to the visible range of the electromagnetic spectrum; a common strategy consists of using a TiO_2 -doping process with different chemical elements in order to obtain an improvement in the photocatalytic efficiency. Under the scope of road pavements, the photocatalytic efficiency can be evaluated by degradation of a harmful gas (mainly NO_x) and monitoring over time the variation of the concentration of a particular organic dye's aqueous solution (MB, MO or RhB).

There exist some variables that can influence the photocatalytic efficiency, such as pollutant flow rate and concentration, solar irradiation, humidity, and environmental temperature. In general, a high concentration of pollutants, high environmental temperature, high relative humidity, high gas flow rate, high traffic, and wind speed contribute to decreasing the photocatalytic efficiency. On the other hand, a high level of solar irradiation increases photocatalytic efficiency. In addition, the incidence of higher energy photons on a semiconductor material becomes more effective than when the incidence occurs with less energetic photons (longer wavelengths). Additionally, higher asphalt mixture air voids and cleaner surfaces improve the photocatalytic efficiency.

In order to design a smart asphalt mixture, the researchers must consider the essential characteristics (mechanical and superficial) and the new capabilities. They should optimize the new capabilities (in terms of content, covering rate, etc.), respecting the standard requirements for real applications. Regarding the costs of the application, TiO_2 nanoparticles are still quite expensive because their industrial production is still quite low. However, it is predicted that the cost will decrease significantly

in the next years. Since there is a lack of information about the cost analysis, this approach could be evaluated by the researchers in further studies.

It can be concluded that photocatalytic road pavements are very important since they can be used in places where there are high emissions of pollutants (typically in areas with a high density of urban mesh), since these modified road structures are characterized by having a high surface area and, therefore, present a great potential to effectively promote photocatalytic reactions with the surrounding pollutants, thus contributing to the improvement of health conditions of populations that live in those urban centers. However, in real contexts (functionalized pavements with great extension, tens or hundreds of kilometers) the existing experience on application techniques is unsatisfactory, and some problems mostly associated with the surface immobilization of the semiconductor materials need further study.

CHAPTER 3 – LITERATURE REVIEW: SUPERHYDROPHOBIC ASPHALT MIXTURES

This chapter presents the most relevant information on literature considering the application of the superhydrophobic capability to asphalt mixtures. It was published in EPJ Web of Conferences 238, 12012 (2020) “Superhydrophobic Asphalt Pavements: Surface Improvement”. Figure 10 shows its first page. The content of this chapter is included in the article, which DOI is the following one: 10.1051/epjconf/202023812012. The findings of this chapter were mainly used in chapters 5 and 10 considering the application of nano/microparticles on asphalt mixtures in order to provide superhydrophobic capability.

EPJ Web of Conferences **238**, 12012 (2020)
EOSAM 2020

<https://doi.org/10.1051/epjconf/202023812012>

Superhydrophobic Asphalt Pavements: Surface Improvement

Ivan Rocha Segundo^{1}, Salmon Landi Jr.^{2,3}, Elizabete Freitas¹, Verônica Castelo Branco⁴, Manuel F. M. Costa², Joaquim Carneiro²*

¹Civil Engineering Department, University of Minho, Azuém Campus, Guimarães, Portugal

²Physics Department, University of Minho, Braga & Guimarães, Portugal

³Federal Institute Goiano, Rio Verde – GO, Brazil

⁴Transportation Engineering Department, Federal University of Ceará, Fortaleza, Brazil

Abstract. The most adverse weather condition for road safety happens when there is water, snow, or ice on the road surface because their presence highly decreases friction. Therefore, it is essential to drain or repel them quickly. If the water drops are repelled from the surface or the ice/snow formation is avoided with the application of superhydrophobic coatings, roads become safer. In order to functionalize the asphalt mixtures used in road pavements, nano/micromaterials, such as Polytetrafluoroethylene (PTFE), TiO₂, and SiO₂, among others have been applied by spraying coating. The mixes are usually characterized by the water contact angle, and the surface roughness is typically assessed by optical and electron analysis. This research work aims to present a brief overview of superhydrophobic asphalt mixtures.

1 Introduction

The water, snow, and ice over the surface of the road pavements cause time waste, economic loss, polluting the environment and endangering passenger safety, and traffic congestion. Also, due to the presence of ice/snow over airport roads, flights are cancelled, causing personal problems for travellers and millions of losses for the airline companies and airports [1]. The conventional method to melt the ice/snow over the pavement's surface is spreading salt (mainly chloride salts, for example, NaCl and CaCl₂) and chemical compounds, which affect the asphalt pavement performance and oxidize vehicles and special structures (i.e., bridges), and, at long-term period, it causes environmental problems [2].

One of the main functional characteristics of road pavements is friction. It expressively reduces when there is water or ice on the road surface. Thus, it is essential to drain or repel the surface water quickly. Superhydrophobic materials can do it fast, and, by their self-cleaning effect, the dirt particles are removed [1,3]. This research work aims to present an overview of superhydrophobic capability applied to asphalt mixtures.

2 Superhydrophobic Asphalt Mixtures Using Nano/microparticles

Wetting is the ability of a liquid (mainly water) to maintain contact with a solid surface, resulting from intermolecular interactions. As reported by Wenzel (1936), wettability is described by a thermodynamic process. Regarding the hydrophilic surfaces, the process is spontaneous since the wet interface free energy is inferior to that of the dry interface. Whereas for

hydrophobic surfaces, the process is non-spontaneous because the dry interface free energy is lower than that of the wet interface [1,3,4]. Furthermore, the wettability is also directly related to the surface roughness. Increases on roughness raise the contact angle (CA) between the (water) drop and the material surface; that is, it can improve the hydrophobicity [4].

The superhydrophobic capability is achieved when the CA is higher than 150° [5]. While, according to some authors, CA should be lower than 5 or 10° to have a superhydrophilic, or super-wettable surface [5].

Superhydrophobic surfaces are not wetted by water, presenting low surface energy. They are usually designed by two methods: i) applying surface treatments with low-surface-energy, and ii) creating a rough surface [6]. The benefits of the promotion of this capability for the materials are diverse, providing functions such as water-resistant, anti-icing, antibacterial, contaminant-free, self-cleaning, and anticorrosive [5].

3 Application Method

Some nano/micromaterials (with a grain size between 6 nm and 45 µm) have been applied on asphalt mixtures: TiO₂, ZnO [3], modified-SiO₂ [7], modified fluorine-containing polymer with nano-CaO [4], Magnesium-Aluminum layered double hydroxides (Mg-Al LDHs) [2], and PTFE [1]. Usually, solutions (or dispersions) are prepared containing the nano/microparticles. They are applied by spraying over the asphalt mixture surfaces. In some cases, there is just one spraying process or even two. For the case of two spraying processes, the binder layer is applied, then the dispersed particles are sprayed over the binder layer [1,3].

*Corresponding author: ivan_romez@hotmail.com

Figure 10: First page of the research work published in EPJ Web of Conferences [92]

3.1. Introduction

The water, snow, and ice over the surface of the road pavements cause time waste, economic loss, polluting the environment and endangering passenger safety, and traffic congestion. Also, due to the presence of ice/snow over airport roads, flights are canceled, causing personal problems for travelers and millions of losses for the airline companies and airports [93]. The conventional method to melt the ice/snow over the pavement's surface is spreading salt (mainly chloride salts, for example, NaCl and CaCl₂) and chemical compounds, which affect the asphalt pavement performance and oxidize vehicles and special structures (i.e., bridges), and, at long-term period, it causes environmental problems [94].

One of the main functional characteristics of road pavements is friction. It expressively reduces when there is water or ice on the road surface. Thus, it is essential to drain or repel the surface water quickly. Superhydrophobic materials can do it fast, and, by their self-cleaning effect, the dirt particles are removed [8,93]. This research work aims to present an overview of superhydrophobic capability applied to asphalt mixtures.

3.2. Superhydrophobic Asphalt Mixtures Using Nano/microparticles

Wetting is the ability of a liquid (mainly water) to maintain contact with a solid surface, resulting from intermolecular interactions. As reported by Wenzel (1936), wettability is described by a thermodynamic process. Regarding the hydrophilic surfaces, the process is spontaneous since the wet interface free energy is inferior to that of the dry interface. Whereas for hydrophobic surfaces, the process is non-spontaneous because the dry interface free energy is lower than that of the wet interface [8,93,95]. Furthermore, the wettability is also directly related to the surface roughness. Increases on roughness raise the contact angle (CA) between the (water) drop and the material surface; that is, it can improve the hydrophobicity [95].

The superhydrophobic capability is achieved when the CA is higher than 150° [96]. While, according to some authors, CA should be lower than 5 or 10° to have a superhydrophilic, or super-wettable surface [96].

Superhydrophobic surfaces are not wetted by water, presenting low surface energy. They are usually designed by two methods: i) applying surface treatments with low-surface-energy, and ii) creating a rough surface [97].

The benefits of the promotion of this capability for the materials are diverse, providing functions such as water-resistant, anti-icing, antibacterial, contaminant-free, self-cleaning, and anticorrosive [96].

3.3. Application Method

Some nano/micromaterials (with a grain size between 6 nm and 45 μm) have been applied on asphalt mixtures: TiO_2 , ZnO [8], modified- SiO_2 [98], modified fluorine-containing polymer with nano- CaO [95], Magnesium–Aluminum layered double hydroxides (Mg–Al LDHs) [94], and PTFE [93]. Usually, solutions (or dispersions) are prepared containing the nano/microparticles. They are applied by spraying over the asphalt mixture surfaces. In some cases, there is just one spraying process or even two. For the case of two spraying processes, the binder layer is applied, then the dispersed particles are sprayed over the binder layer [8,93].

3.4. Analysis

The superhydrophobic capability is mostly evaluated by optical and electron analysis. The main method is by measuring the CA of the water and the surface. As mentioned before, CA must be higher than 150° to guarantee the superhydrophobic surface.

As previously described, the surface should be rough, being essential to the analysis of the microtopography of the surface. The surface roughness is usually analysed by optical methods, for example, by optical triangulation based-microtopography (Figure 11). In this case, surface parameters can be assessed in order to characterize it and compare materials and treatments.

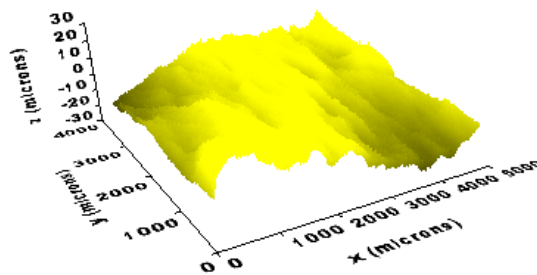


Figure 11: Microtopography of an asphalt mixture

Also, the images by Scanning Electron Microscope (SEM) are essential to understand the microtopographic structure of the surface. In Figure 12, the self-cleaning effect is showed by water drops carrying the dirt particles that were previously deposited, as the effect of the Lotus Flower [99].

A biomimetic approach is developed to provide a self-cleaning effect. Tests to check the feasibility are also conducted: friction [93,100], water drop freezing [94], and durability [94,95].

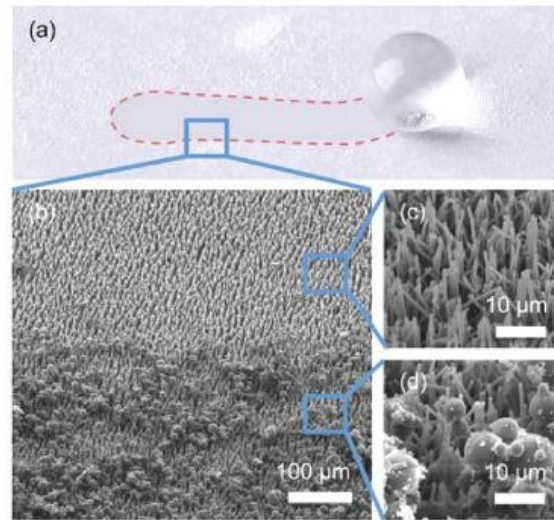


Figure 12: a) Water drop carrying dirt. Adapted from [99]

3.5. Results on Literature

Table 1 summarizes the main results in the literature. Most of the research work has used nanoparticles. The CA ranges from 150 to 166°, depending on the material and application method.

Table 1: Superhydrophobic Asphalt Mixtures.

Material	Grain size (nm)	Dispersion Medium	CA (°)	Reference
TiO ₂	23 – 28	Water	150	[8]
Modified- SiO ₂	20	Silanes, Water, Ethanol, and Ammonia	151	[98]
TiO ₂ ZnO	23 – 28, 45000	Water	155	[8]
Mg-Al LDHs	100	Naphtha	152	[94]
*	*	*	157	[100]
Fluorine polymer with nano-CaO	6 – 20	Water	163	[95]
PTFE	12000	Acetone**	166	[93]

*Not described by the authors, **One binder layer composed of epoxy resin dissolved in xylene was sprayed before the application of the particles.

The highest CA was achieved by using microparticles of PTFE [93]. The superhydrophobic asphalt mixtures can present rough surface [94,95], delay water freezing [94,98], decreasing the ice adhesion force [94]. Besides, friction was slightly influenced by water and ice [100]. Durability should be further explored.

3.6. Conclusions

Superhydrophobic coatings containing PTFE, TiO_2 , TiO_2 and ZnO, SiO_2 , Mg-Al LDHs, and fluorine polymer with nano-CaO nano/microparticles have been applied over asphalt mixtures to improve safety. They are tested under optical and electron analysis (CA, surface roughness, and SEM images), friction, water drop freezing, and durability. Relevant literature results indicate that road can be safer with superhydrophobic asphalt mixtures.

CHAPTER 4 – LITERATURE REVIEW: SMART ASPHALT MIXTURES

This chapter presents the literature review about smart asphalt mixtures “Review and analysis of advances in functionalized, smart, and multifunctional asphalt mixtures” submitted to a prestigious scientific journal. Figure 13 shows its first page. The sections about photocatalysis, superhydrophobicity, and self-cleaning were removed as they were already addressed in chapters 2 and 3. In this chapter, only the other capabilities were considered. Thus, the main objective of this chapter is to present the most relevant information on literature considering the application of several types of capabilities to the asphalt mixtures as: deicing/anti-ice, self-healing, thermochromic, and latent heat thermal energy storage. The findings of this chapter supported the application of different smartness to asphalt mixtures (techniques, materials, and combination of them) and suggest the need of provide multifunctional capabilities to asphalt mixtures. They endorsed the project proposal included in 11.2 Parallel Works which will reflect in 11.3. Future Works.

1 **Review and analysis of advances in functionalized, smart, and**
2 **multifunctional asphalt mixtures**
3 **I. Rocha Segundo^{1*}, E. Freitas², V. T. F. Castelo Branco³, S. Landi Jr.⁴, M. F.**
4 **Costa⁵, J. O. Carneiro⁶**
5 ¹Civil Engineering Department, University of Minho, **Azúem** Campus,
6 **Guimarães**, Portugal, *iran_gomes@hotmail.com; ²Civil Engineering
7 Department, University of Minho, **Azúem** Campus, **Guimarães**;
8 ³Transportation Engineering Department, Federal University of Ceará,
9 Fortaleza, Brazil; ⁴Physics Department, University of Minho, **Azúem**
10 Campus, **Guimarães**, Portugal and Instituto Federal **Goiano**, Rio Verde – GO,
11 Brazil; ⁵Physics Department, University of Minho, **Gualtar** Campus, Braga,
12 Portugal; ⁶Physics Department, University of Minho, **Azúem** Campus,
13 **Guimarães**, Portugal.

14 **Abstract**
15 The asphalt pavements must resist the efforts of road traffic and weathering and assure
16 riding conditions with comfort, economy, and safety with low damage to the
17 environment. A smart and multifunctional asphalt mixture presents additional abilities,
18 different from the original ones, or reacts upon the external stimulus. Currently, new
19 capabilities such as: photocatalytic, superhydrophobic, self-cleaning, deicing/anti-ice,
20 self-healing, thermochromic, latent heat thermal energy storage, among others, have been
21 investigated in asphalt mixtures. They are mostly applied by spraying coating, volume
22 incorporation, or asphalt binder modification. The spray method is used for
23 superhydrophobic, self-cleaning, and photocatalytic capabilities because it is easy to
24 apply in a real context, that is, during the asphalt paving process of road pavement and with
25 the added advantage of using a smaller amount of material than the other techniques. This
26 research work addresses the review of the new capabilities applied to asphalt materials
27 and provides recommendations.
28
29 **Keywords:** asphalt mixtures; smartness; multifunctionality; spraying coating;
30 photocatalytic materials; superhydrophobic; deicing/anti-ice; thermochromic; latent heat
31 thermal energy.
32

Figure 13: Manuscript first page submitted to a prestigious scientific journal

4.1. Introduction

The genuine idea of the design of smart and multifunctional cement concrete was first proposed in late 1980 by Japanese investigations [5]. After extensive researches about the design, manufacturing, characterization, performance, and mechanisms, some sorts of smart and multifunctional cement concretes have successfully been employed in a real-scale scenario [5]. For asphalt mixtures, the concept is recent, and, in terms of practical experiences (test sections), there are very few applications [62,69,70,72,74,75,101–103].

According to Han's definition [5], a smart and multifunctional concrete is either an intelligent material with different abilities/characteristics from the original ones or is able to react upon external stimuli, for example, temperature and stress. This concrete can be composed of cement, asphalt, or polymer. These abilities can be classified by the smartness or function: smartness, optical, electrical, mechanical, and electromagnetic wave/radiation shielding/absorbing, energy-harvesting, and related to water. They are designed through special processing, composition design, introduction of new functional materials, or microstructure modification of the original ones [5,6].

The design and implementation of asphalt pavements should meet relevant requirements to withstanding the actions of road traffic (different mechanical efforts) and weathering, apart from ensuring comfortable driving conditions, economy, and safety, as well as causing low environmental damage (e.g., low noise levels). The smart and multifunctional capabilities have been applied to asphalt mixtures, becoming a significant subject to the road engineering field once the road pavements present a vast surface area and can show other benefits that will be addressed in this research work. The literature has already shown important results on the functionalization of the asphalt pavements and also the development of smart and multifunctional asphalt mixtures, mostly for the top layer [104].

Previous literature review works generally covered issues related to road infrastructures features, as paintings, and flexible and rigid pavements, from the concept of nanotechnology to the results of mechanical and multifunctional performance [105–108]. These works concluded that nanomaterials can be used to provide new capabilities by improving mechanical properties, and the use of nanoscale tests are essential to design these materials.

This article addresses the main results and discussion of the functionalized, smart, and multifunctional asphalt mixtures imparted by different materials. The latest literature reviews have approached nanotechnology in Transportation Engineering (namely pavements, bridges, vehicles),

differently from this work that discusses the multifunctionality of smart asphalt mixtures. Also, literature reviews only refer specifically to photocatalytic asphalt mixtures [1] but not to other new capabilities.

The purpose of this literature review is to discuss the main capabilities imparted to asphalt mixtures, namely deicing/anti-ice, self-healing, thermochromic, and latent heat thermal energy storage. Their contextualization, application methods, results, conclusions, and limitations are presented and critically discussed.

4.2. Deicing and Self Ice-Melting Capabilities

In very cold countries and during the winter, it is usual to observe a rapid formation of ice on the pavements' surface, contributing to the reduction of friction and, therefore, resulting in road accidents, traffic congestions, and economic losses. To prevent this problem, the road administrations usually use deicing solutions or chlorine salt to melt the snow/ice over the pavement surface, requiring high financial resources [109,110]. The application of anti-ice or self-ice-melting additives into asphalt mixtures can present advantages such as the prevention of traffic jams when compared to conventional methods, which are time-consuming processes and require intensive work. Usually, there are two ways to obtain an asphalt pavement holding this capability: i) using anti-icing additives as an asphalt binder modifier or filler, and ii) using a conductive material as aggregates or fibers.

4.2.1. Self-Ice-Melting Pavements Using Anti-Icing Additives

The incorporation of anti-icing additives into asphalt pavements creates an anti-icing liquid layer between the ice/snow and the surface, which contributes to slow or avoid the ice formation, facilitating the melting process of snow and ice and, consequently, keeping the original friction of asphalt mixtures. For this purpose, some additives were applied into asphalt mixtures as asphalt binder modifier or filler, such as Potassium Formate (HCOOK) with Styrene-Butadiene-Styrene (SBS) matrix [111]; MgAl Cl-Layered Double Hydroxide (LDH) [109]; Commercial fillers, such as IceBane (composed by chloride salt - CaCl₂ and NaCl) [110] and Mafilon (composed by NaCl, SiO₂, MgO and CaO) [112]. The most used materials were those based on the chloride-based anti-freeze [110,113]. Other options were also investigated i) liquids: glycol base fluids and potassium acetate base fluids and ii) solids: urea, Calcium Magnesium Acetate (CMA), Sodium Formate (NaF), and Sodium Acetate (NaAc) [114].

The tests most used to evaluate this capability are the conductivity tests, ice layer rupture tests (shear strength and pullout), and the one that consists in the observation of the melting process after the

accumulation of snow, taking into account the thickness of the ice/snow, temperature and melting time [110,112,113]. The anti-icing additives as a filler do not require changes in the asphalt mixtures design but can negatively affect mechanical properties, as permanent deformation, thermal cracking, and water sensitivity resistances. To prevent the damages caused by the introduction of anti-icing additives and maintain the mechanical characteristics, 0.3% polyester fibers by the aggregates' weight can be used. Using the content of 6% of anti-icing additives (as filler by the mass of the aggregate), the melting of snow over the asphalt pavements was facilitated, and the ice layer's strength was reduced by half [113]. This material was already tested on the road, which one year after the application still holds this capability [101].

Regarding the commercial anti-freeze filler IceBane, Liu et al. reported that it is desirable to use coarser size of anti-freeze filler (the 0.075 mm sieve size passing rate of 21% was the most efficient). They concluded that the anti-freeze filler with large particles dissolved into the water more quickly than smaller salt particles [110].

Ionic salts as anti-icing additives are being used to reduce the ice formation on asphalt surfaces. The problem of using these salts is related to their high corrosive power in bridges, buildings, and airports. There are regulations about this type of material for airfield asphalt pavements, which can limit its use [114]. Also, these salts negatively influence the mechanical characteristics of asphalt mixture and harmful to the environment when used in high contents. Therefore, it is essential to evaluate the environmental impact of these materials and include the anti-icing additives in designing the asphalt mixtures to guarantee adequate mechanical performance.

4.2.2. Deicing Pavements Using Conductive Materials

The Joule effect is the physical phenomenon that justifies the incorporation of conductive materials into asphalt mixtures to remove the snow and/or prevent ice formation over the pavement surface. This effect can be described by the occurrence of an electric current passing through the composite material that can generate heat, thus reducing the snow and ice accumulation over the asphalt mixture surface. Three conductive materials are being used in asphalt mixtures: i) powders like graphite, aluminum chips, and carbon black; ii) fibers, including Carbon Fiber (CF), Steel Fiber (SF), Steel Wool (SW), and Carbon Nanofiber (CNF); iii) conductive coarse and fine aggregates such as Steel Slags (SS) [115]. When irradiated by microwave radiations, road pavements composed of these materials can melt the ice on their surface during the winter more quickly than traditional road pavements (i.e., pavements without

conductive materials) [116]. To assess the deicing capability, some properties, such as electrical resistivity and thermal conductivity, and the asphalt mixture's behavior when submitted to Microwave Heating (MH) were evaluated.

While the asphalt binder resistivity is around 10^{11} and 10^{13} Ωm , the asphalt mixtures resistivity is between 10^7 and 10^9 Ωm due to the presence of aggregates and air, being classified as insulating materials. Adding some materials such as graphite, steel fiber, and CF, the resistivity of the asphalt mixture can be reduced to values between 10 and 10^3 Ωm , thus greatly improving the electrical conductivity, as graphite and CF have an electrical resistivity of about 10^{-5} and 10^5 Ωm , respectively [117]. In general, the asphalt mixture's conductivity for the electrical heater would not exceed 100 Ωm [115].

The volume incorporation of SS into asphalt mixtures for the MH pavement offers a new potential for recycling of SS, which mitigate the use of natural raw material and its depletion and increase road safety during winter. The SS as an aggregate for deicing asphalt mixture presents other advantages when compared to CF, graphite, and steel fibers of wide sources because, for instance, this material is eco-friendly and low-cost. Nevertheless, it also has limitations; for example, it should be pretreated to avoid use during its expansion phase. Moreover, as this material has a high density, it could bring extra costs for transport. Gao et al. suggest a SS content between 40 and 60% and the aggregate sizes of 9.5, 2.36, and 0.6 mm regarding the promotion of MH, the thermal conductivity, and the surface temperature [116].

It is crucial to consider in the design of the asphalt mixtures the effect of shape, size, composition, and conductivity of the raw materials besides the final conductive and the mechanical characteristics of asphalt mixtures. The average melting speed of snow for asphalt mixtures with SF and SS using MH achieves 53.9 and 48.5 g/min, respectively [118]. Although both techniques are feasible to provide this capability, the use of fibers is probably more efficient, but the use of SS contributes to recycling materials, and it is eco-friendly.

The use of salt has a negative effect on the performance of asphalt mixtures SF and graphite. After performing few freeze-thaw cycles, the saltwater led to an increase in air voids and reduced resistance of moisture, compared to distilled water, probably due to the loss of aggregates-binder adhesion [117]. It is essential to consider the oxidation of these materials during the design and performance of asphalt mixtures. The anti-icing additives can be used combined with CF to obtain good mechanical capacities and prevent and facilitate snow/ice formation. The use of the recycled material, such as SS, is strongly recommended due to the associated eco-friendly and low-cost benefits.

4.3. Self-healing Capability

For conventional asphalt mixtures, the typical mechanical distresses are fatigue (and temperature) cracking, water degradation (moisture damage), and rutting [115]. Self-healing capability aims to assist the materials to heal after damage. It is defined as “the ability to substantially return to an initial, proper operating state or condition prior exposure to a dynamic environment by making the necessary adjustments to restore to normality and/or the ability to resist the formation of irregularities and/or defects [119,120]. This capability is also based on biomimetics from the biological systems of wound healing in living organisms' skin [121–123].

Asphalt binder is a self-healing material. After rest periods, asphalt mixtures are able to recover their strength and stiffness by closing the microcracks that open after traffic loading [102]. The cracks heal instantly after the load is removed. Two phenomena occur during this process: firstly, viscoelastic recovery and then healing in the cracked area. Their difference is that the former is due to the molecules' rearrangement, and the consequence is the wetting and inter-diffusion between the crack faces. The following stages explain the self-healing mechanism: i) both faces of a nano-crack are wetted, ii) immediate strength gain by interfacial cohesion between the crack faces, and iii) long term strength gain due to the diffusion and randomization of molecules from one face to the other [124].

Improving the self-healing ability of the asphalt mixtures can provide a higher life cycle to the pavements. The surface free energy is the most important aspect causing the first cracks to shrink and then progressively disappear in asphalt binder with the increase of temperature [125]. Two techniques enhance the self-healing in asphalt mixtures: i) heating the asphalt material improved by good electrically conductive materials, and ii) adding nanomaterials or healing agents to their composition [102].

4.3.1. Self-healing Capability by Heating

With the incorporation of materials like graphite, carbon black filler, carbon and steel fibers, SW and slags, and some nanomaterials (carbon nanotubes and nanofibers), the asphalt mixtures improve their electrical conductivity. By Induction Heating (IH), the cracks will be repaired, and the raveling effect (loss of aggregates) is prevented, self-repairing, preserving, and renewing the asphalt pavements.

Also, for this purpose, microwaves have been used to heat the asphalt mixtures; although they are fast and easy to apply, the high cost and difficulty of controlling heat deepness penetration are the main drawbacks of this technique [124]. Besides that, MH increases the temperature of the asphalt

binder but not of the aggregates. Consequently, the asphalt mixtures' surface temperature is inferior to the asphalt binder temperature when both are submitted to this procedure. Therefore, metallic fibers or particles are used to improve the effectiveness of the microwave [126]. IH, based on the electromagnetic induction phenomenon, is another possibility to increase the temperature of pavements. It is fast, but it is high-cost and has a complex heating mechanism [124]. IH does not heat the asphalt binder or the aggregates. The metallic particles are needed to increase the temperature of the asphalt mixture after heating [126]. MH heals the cracks better than IH due to the increase in the asphalt binder's temperature [126].

There is an optimal time to heal an asphalt mixture. The heating should not be too late or too early [127]. On one hand, when the heating is early, it is useless because the asphalt mixture heals the crack by itself. On the other hand, when it is too late, the healing process is drastically decreased because the asphalt binder is aged, and it is not effective on large cracks. Besides that, mechanical damage such as rutting or raveling could happen before [126].

This property, self-healing, can be measured in binders, mastics, and asphalt mixtures by the electrical conductivity, temperature rate after IH, and rate between healed strength/modulus and initial strength/modulus and of asphalt mixtures. Factors like achieved temperature influence this property, number of cycles of heating, healing time, and the IH's confining pressure. The rest periods are essential as well for healing [124]. While the temperature has an exponential relationship with the self-healing mechanical property, the healing time has a linear relationship with the self-healing index. Confining pressure can accelerate crack healing. Fan et al. concluded that the confining pressure effect on self-healing capability is relevant for temperatures inferior to 60 °C, and a deeper crack has a greater self-healing potential than a surface crack [128].

The asphalt mastic (in this specific case, crushed sand less than 2 mm, asphalt binder, and SW) can be healed several times using IH. The stiffness of asphalt mixture with SW recovered faster with IH's application when compared only when it is submitted only to the rest period. The modified asphalt mixture's fatigue life was expressively prolonged due only to the heating (135,408 cycles more – H₃). Figure 14 shows the fatigue recovery of porous asphalt mixture containing SW before and after healing [127].

H_1 and H_3 were caused by the rest period and IH, respectively, while H_2 is the increase of fatigue life due to IH and rest periods. One limitation of the use of this type of material is oxidation (corrosion). Contrarily, CF can be used without this problem.

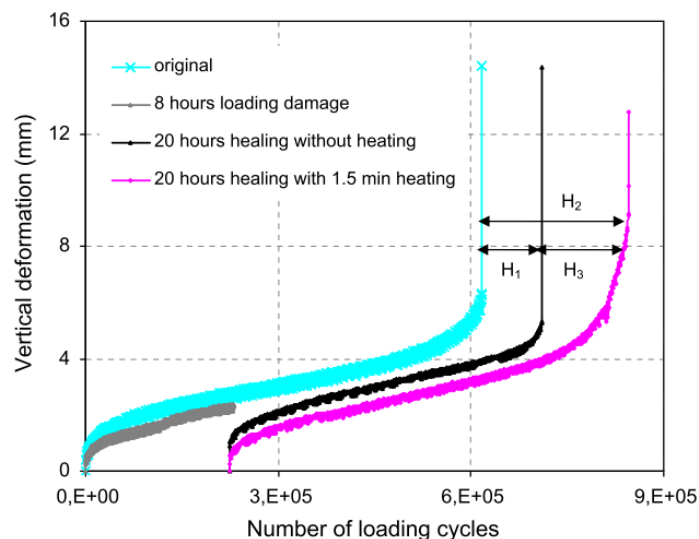


Figure 14: Fatigue life of porous asphalt mixture with 8% steel wool [127]

4.3.2. Self-healing Capability by Adding Nanomaterials or Healing Agents

Considering this approach, three techniques can be applied in asphalt mixtures to provide self-healing capability, namely incorporation of: i) microcapsules of high percent maltene oils with a shell; ii) ionomers, and ii) nanomaterials. The first one consists of the microencapsulation of high percent maltene oils by a shell (usually polymeric). In the asphalt binder (Figure 15a), when a crack achieves the microcapsules, the shells break, releasing the healing agent (Figure 15b), and restoring the ratio of asphaltene/maltenes (Figure 15c) [129]. This technique has a good recovery ratio and compatibility, nevertheless, it works only once and should be applied just for top layers.

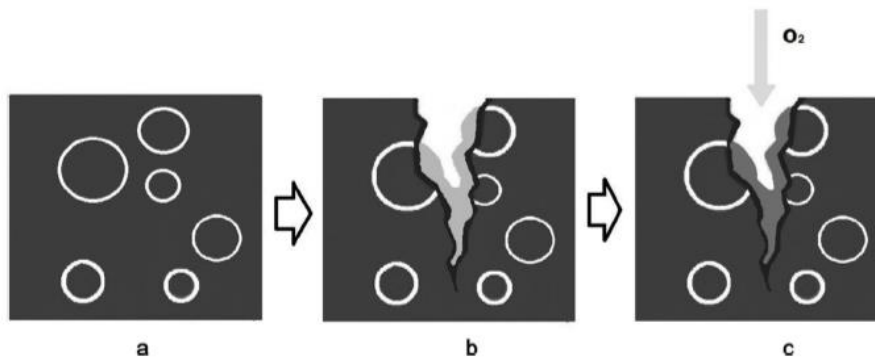


Figure 15: a) Asphalt with microencapsulation, b) microcapsules are broken by the crack, and c) release of the healing agents [130]

Chung et al. tested microcapsules of urea/formaldehyde resin (forming the shell) and solutions of Triethylenetetramine (TETA) with only Dimethylphenol (DMP) or with SBS (consisting of the core). The microencapsulated asphalt binders showed an increase in the parameter ratio strength upon rest periods and original strength. SBS/DMP microcapsules showed a faster self-healing effect than DMP alone [130]. Using sunflower oil (core) capsules with cement and epoxy (shell), Garcia et al. concluded that gradually during the load cycles, the capsules break, releasing the oil and rejuvenating the asphalt mixture (Figure 16). One limitation of this technique was the dispersion of the capsules, which was not uniform [131].



Figure 16: Detail of the sunflower oil coming out [131]

However, high percent maltene oils' microencapsulation requires that these agents have good compatibility with the asphalt binder, high stability, good thermal properties during the mix at high temperatures (150 to 180 °C). Besides, it needs to be activated at the service temperature of asphalt pavement (from -30 to 70 °C) [132].

On one hand, microencapsulation can repair the first cracks of the top layer only once. On the other hand, the use of ionomers or nanoparticles can be activated more times because the ductile polymer can elastically rebound to its original position and the nanoparticles' movement, respectively.

The second self-healing technique consists of the application of ionomers, a thermoplastic copolymer containing ionic groups (less than 30% mol) in their backbone. The ductile polymers can elastically rebind the crack to its original position. They can be recovered multi-times and provide high thermal stability and good compatibility, but they blend and are limited to first-stage cracks [124]. Their healing process is due to the attraction of the ionic bonds.

Regarding ionomers' use, the physical ionic clusters crosslinking can present the network structure of polymer-modified asphalt [133]. Shi [134] addressed the rheological properties, only, of an asphalt binder modified with an ionomer (ethylene and methacrylic acid systems), reporting a best ionomer content of 5% [134]. Chen et al. [135] incorporated Ethylene Methyl Acrylate (EMAA), zinc ion, sodium ion, and lithium-ion ionomer polymer as an asphalt binder modifier with a content of 3%. Analyzed by T-peel test, the EMAA asphalt binder presented higher self-healing ability with lower peel force when compared to the unmodified samples. This fact was shown by lower values of the destructive forces of EMAA asphalt samples since the rupture mainly occurred in the interface tape-asphalt (weak) instead of in the asphalt-asphalt (strong).

Finally, the last one is the incorporation of nanoparticles. The nanoparticles relocate towards the crack tip, stimulated by the high surface energy, stopping its propagation and, consequently, healing the composite material [132]. Researches assessed different nanomaterials, like rubber, clay, SiO₂ and TiO₂ as modified asphalt binder. In addition to the self-healing capability, these materials can improve the adhesion between asphalt binder and aggregate due to their high specific surface area [136] and improve water sensitivity and rutting resistances of asphalt mixtures [137].

Using nanomaterials for self-healing effects, Amin and Esmail [138] modified asphalt binders with different contents of nano-SiO₂ (from 0% to 5% increasing 0.5%). SEM showed the asphalt mortar flowing into micro cracks. By the analysis of the resilient modulus of the asphalt mixtures composed of nano-SiO₂, they concluded that the increase of the nanomaterial content from 0% to 3% enhances the healing index from 71% to 89%. Contents higher than 3% will absorb a large volume of binder due to this nanomaterial's high specific area, increasing the viscosity of the binder, restricting its mobility, and, consequently, interfering the self-healing process.

Considering the use of ionomers and nanomaterials to promote self-healing effects, there are few research works addressing self-healing effects. Figure 17 presents the self-healing mechanism for these materials. In the case of the ionomers, the self-healing effect is carried out by the ionic group rearrangement (due to the attractions of ionic bonds). For the nanomaterials, the crack is repaired because these materials tend to move to the crack tip led by the high surface energy.

Self-healing technology was already applied in a highway in the Netherlands, where 400 m of a self-healing porous asphalt concrete containing SW fibers to avoid the raveling effect were laid [102,103,139]. Research on this highway is still ongoing. Tabakovic and Schlangen [102] referred that if the asphalt binder with self-healing agents was two times the conventional asphalt binder's price, the Netherlands, for example, would save €90 million per year to extend the lifespan 50% by investing in this capability.

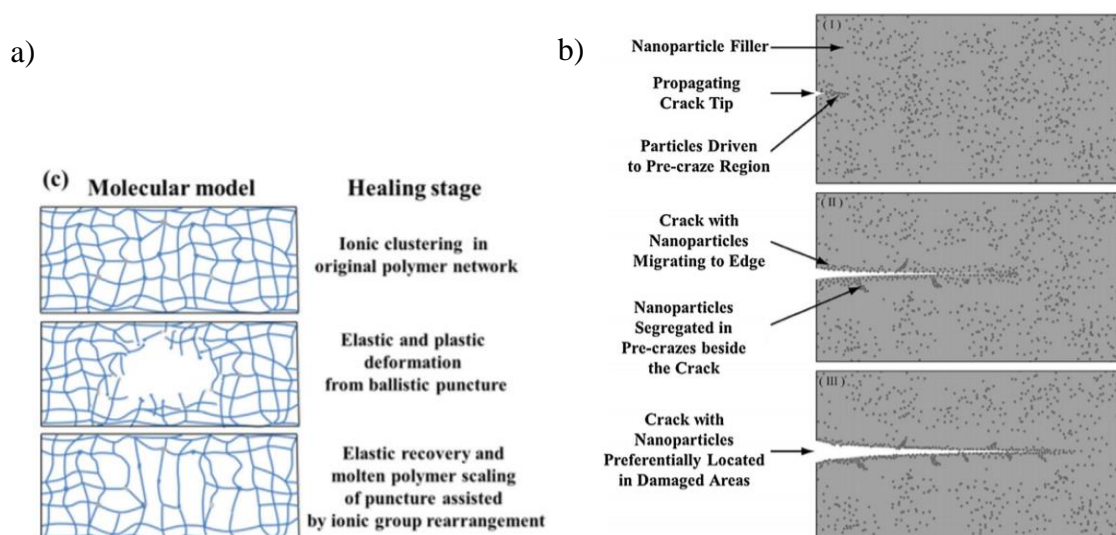


Figure 17: Mechanism of the healing effect due to: a) ionomers and b) nanomaterials [133]

Moreover, if pavements' lifetime is longer by applying the self-healing capability to asphalt mixtures, rehabilitation and paving of new roads will be less often carried out, requiring less raw material consumption, leading to less emission of CO₂ and traffic disruption.

4.4. Thermochromic Capability

Thermochromism is a phenomenon of reversible color change in response to a temperature change. The thermochromic materials are classified as conjugated oligomers, metallic oxides, leuco dyes, among others [140]. In inorganic compounds, the color changes can result from phase transitions and

variations in the coordination geometry [141], while inorganic compounds can result from reversible chemical reactions and molecular rearrangements [142].

The application of thermochromic materials in the Civil Engineering field must take into account the temperature transition. Vanadium Dioxide (VO_2) and vanadate compounds have been intensively studied, but their temperature transition is too high for this kind of application, 68 °C for VO_2 [141], and 255 °C for BiVO_4 , for example [140]. Due to their black color, asphalt binders strongly absorb the energy from sunlight. During the summer season, the asphalt pavements' surface temperature may increase up to almost 70 °C, impacting their durability due to the acceleration of some distress mechanisms. On the other hand, during the winter season, the low temperature of asphalt pavements worsens the low-temperature cracking phenomenon and also promotes ice formation [143]. Therefore, it is crucial to control the asphalt mixtures' temperature by cooling the surface during summer and warming it during winter. To achieve this goal, the new thermochromic capability has been applied to asphalt mixtures using materials as leuco dyes, like an asphalt binder modifier.

The reflectivity of asphalt mixtures changes with the introduction of thermochromic materials due to the color variation with temperature. This composite material can, at high temperatures, reflect more solar energy and, at low temperatures, reflect less solar energy [143]. Besides, during the winter night, treatment helps control the surface temperature of the functionalized asphalt mixtures compared to the conventional ones, thus mitigating the low-temperature cracking effects [143]. The main goal for introducing thermochromic materials is to promote control of the temperature variation and amplitude to improve the performance of the asphalt mass since the climate is one of the essential sources that help reduce its mechanical performance.

The properties that can be considered to evaluate this capability are the color change with different temperatures combined with color coordinates, physical (penetration, softening point, photoluminescence, and reflectance), and rheological properties, besides aging behavior when the asphalt binder is modified [142–146].

A few studies have been carried out on the application of thermochromic capability in asphalt mixtures. Hu and Yu evaluated the use of 10% of black, blue, and red thermochromic powders (leuco dyes with a transition temperature of about 31 °C) as an asphalt binder modifier to decrease the surface temperature of the asphalt binder by changing its color. On the other hand, for high temperatures, the maximum reduction in the asphalt binder's surface temperature was 6.6, 2.7, and 4.9 °C for the black,

blue, and red asphalt binders, respectively. Moreover, for low temperatures, the thermochromic powders increased the maximum surface temperature of about 1 °C [143].

The asphalt binder modification by thermochromic powders (Figure 18) improves its high-temperature stability, increases complex modulus, viscosity, and softening point, and decreases the phase angle and penetration when compared to conventional asphalt binders'. These materials can also extend the Performance Grade (PG) of asphalt binders. The modified asphalt binder with thermochromic powder showed better aging resistance after RTFOT, PAV, and UV aging. The best anti-aging properties were achieved using the value of 6% of red thermochromic powder [144].



Figure 18: Thermochromic powders (blue, black and red) disactivated under 31 °C (left) and activated above 31 °C (right) [144]

Besides the surface temperature, Hu et al. also studied the physical and rheological characteristics of the modified asphalt binders with thermochromic powders (black, blue, and red), composed of organic mixtures of leuco dye (electron donor), a developer (electron acceptor) and a solvent, all encapsulated by trioctanoin. The increase in the reflectance spectra is associated with a reduction of solar absorption on the surface. The highest reflectance in visible wavelengths of the electromagnetic spectrum was obtained for the blue powder, then for the red, and finally black powders. Also, the thermochromic asphalt binder was more reflective than the conventional asphalt binder. The highest reflectance was achieved for the black (when disactivated) thermochromic asphalt binder, followed by blue and red thermochromic asphalt binders. The authors recommended that the use of these thermochromic powders should be less than 5–6% (by the mass of asphalt binder) to assure the physical and rheological properties [142].

Thermochromic powder improves low-temperature cracking behavior and aging resistance. When only the anti-aging properties of asphalt binders were considered, the ideal content to achieve the best performance was 4%, as Zhang et al. [97] concluded. The results showed higher spectral reflectance for higher contents of powder [145].

Considering the results of the reflectance spectra of thermochromic asphalt binders at different temperatures, it was possible to develop some equations to simplify the design of these materials for road pavements. Maxwell (Eq. 3), Effective Medium Theory (EMT) (Eq. 4), and Mori-Tanaka (Eq. 5) models were the best ones evaluated. They are used to predict the effectiveness of reflectance spectra capacity of thermochromic asphalt binders [146].

$$R_{mix} = \left(1 + \frac{3(\alpha - 1)\emptyset}{(\alpha + 2) - (\alpha - 1)\emptyset} \right) R_m \alpha = \frac{R_p}{R_m} \quad (13)$$

$$(1 - \emptyset) \frac{R_m - R_{mix}}{R_m + 2R_{mix}} + \emptyset \frac{R_p - R_{mix}}{R_p + 2R_{mix}} = 0 \quad (14)$$

$$\frac{R_{mix} - R_m}{R_p - R_m} = \frac{\emptyset}{1 + (1 - \emptyset)(R_p - R_m)/3R_m} \quad (15)$$

In the equations above, α , R_m , R_{mix} , R_p , and \emptyset represent, respectively, powder dimension (μm), original asphalt binder reflectance (%), thermochromic asphalt binder reflectance (%), thermochromic powder reflectance, and volume fraction of the dispersed powder.

UHI could also be mitigated controlling the thermochromic asphalt pavement color at high-temperature conditions. It can be concluded that thermochromic materials can positively affect the mixtures' mechanical performance due to the control of their surface temperature and improving aging resistance. For this new capability, the literature review shows a very short experience. Thus, there are many opportunities to explore this capability, including mechanical performance, cost analysis, among others.

4.5. Latent Heat Thermal Energy Storage (LHTS) Capability

Phase Change Materials (PCM), under the principle of LHTS, absorb energy in large amounts when there is excess and release it when there is deficit. PCM provide a reduction in peak heating and cooling loads when applied to materials in different areas [147]. PCM are applied in Civil Engineering, mostly in floors, roofs, wallboards, and concrete, to improve building energy efficiency (reducing the energy per area needed for heating/cooling). For building applications, PCM increase the thermal comfort due to smooth temperature fluctuation at inner spaces, reducing the energy needed by heating/cooling equipment, i.e., heaters and air-conditioners. In this way, there are benefits for the environment since energy consumption from power station will decrease, resulting in less emissions.

When PCM are incorporated into asphalt mixtures, the primary purpose is to prevent rutting [148] and avoid thermal cracks or quick temperature change due to the reduction of the magnitude of temperature fluctuations [149]. Besides the mechanical component addressed in the researches, another goal is to avoid the UHI by controlling the interaction between the asphalt pavement surface and environment, being a socioenvironmental goal [150].

For the design of the LHTS materials, including LHTS asphalt mixtures, it is essential to have at least three components: i) appropriate PCM with the desired temperature range of melting point, ii) a suitable heat exchange surface, and iii) an appropriate container compatible with the PCM [151].

The Differential Scanning Calorimeter (DSC) is the technique most commonly adopted to obtain the melting temperature through the phase change enthalpy of the materials [152]. The observation of temperature during heating, to calculate the heat and cooling rates, is also relevant to assess this capability.

There are dissimilar types of PCM with different relations between the melting enthalpy and melting temperature, as shown in Figure 19a and b [152,153]. Its phase transition can classify this material: solid-liquid phase transition, solid-solid phase transition, solid-gas phase transition, liquid-gas phase transition [150]. The most used PCM are fatty acids and esters, such as paraffin, salt hydrates, and ionic liquids [154].

The recommendation for rutting mitigation is using PCM with maximum phase change temperature between 3 and 5 °C below the softening point of the asphalt binder. With this limit, there is an acceptable trade-off between the amount of PCM and the energy absorbed. The material must not store much energy since the reverse process will happen and affect the air temperature, enhancing the UHI [148].

Silica powder, floating bead, and activated carbon with PCM used as raw materials via the sol-gel process can improve the high-temperature stability of asphalt mixtures [155]. Activated carbon with PCM has a larger latent heat storage capacity (phase change enthalpy 19 J/g) and proper phase change temperature transition (-3 °C). By using 0.3% of unsaturated organic acid and polypropylene as PCM in the mass of the asphalt mixture, this material decreases the rising and cooling rate of temperature and delays the occurrence time of extreme temperatures [154]. He et al. compared the performance of Polyethylene glycol 2.000 as PCM and SiO₂ as a matrix in asphalt binders. They concluded that the

modified asphalt binder had large phase change enthalpy (38.2 to 117.5 J/g), good chemical compatibility, and thermal stability [149].

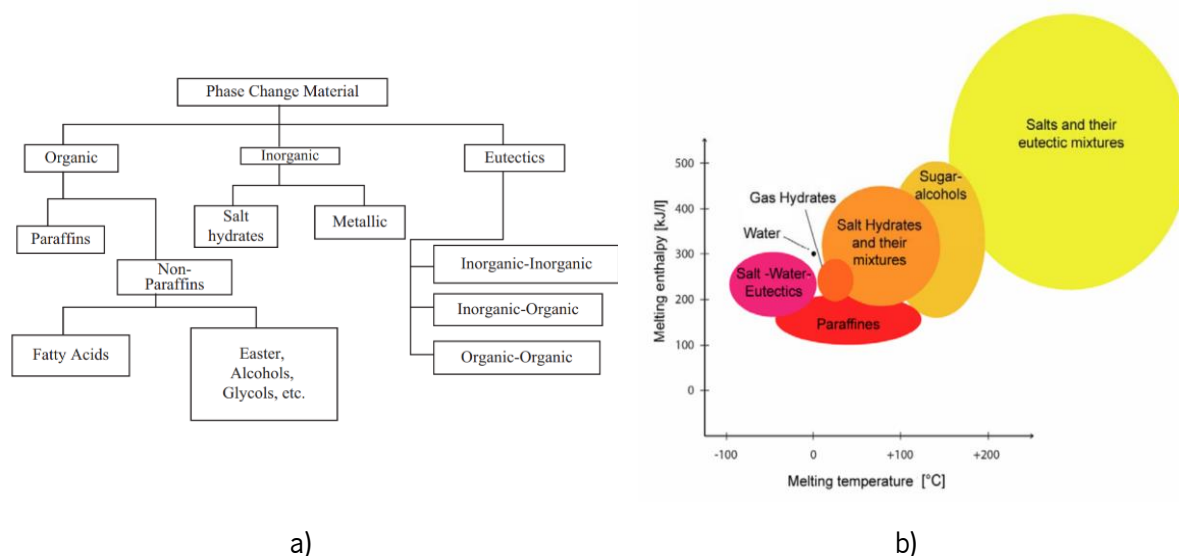


Figure 19: a) Different types of PCM [152] and b) Melting enthalpy versus melting temperature [153]

The PCM (phase change temperature among 40 and 50 °C and latent heat of 150 J/g) were used for lowering the temperature and preventing rutting by MeiZhu et al. [148]. These PCM were used since the dynamic stability of asphalt mixtures considerably decreases in the range of 48 to 52 °C. In this way, it was possible to reduce the temperature increase rate [148].

Granular-shaped solid-liquid PCM composed of unsaturated organic acid and polypropylene with a melting point of 22.1 °C and latent heat of 46.97 J/g were used as aggregate in a proportion of 0.3% of the asphalt mixture weight (added in bulk incorporation during the mix). The material decreased the temperature rising and cooling rate and delayed the occurrence in time of high temperature [154].

Manning et al. tested 1.25 and 2.5% paraffin waxes as PCM (by mass of the mixture) with phase changes at 6 °C to delay the freezing, decrease the cooling rate and reduce the frozen time [156]. Their results showed that this material has the potential to reduce cooling and heating rates. However, they did not conclude the effect on the extremely low temperature, and the phase changing the time above 5 h was a limitation. Besides that, there was no reduction of the extremely high temperature with the use of the PCM.

Ma et al. tested PCM composed of unsaturated acid, γ -linolenic acid, β -linolenic acid using SiO_2 as a matrix with phase changing temperature between 8 and 25 °C in a content of 20% (in the mass of

the asphalt binder) during the mixture. The results showed that incorporating the PCM in the mixture reduced the increasing and cooling rates, improving the low-temperature crack and rutting resistance [157].

After analyzing the mechanical behavior, Ma et al. recommend 0.3% of two types of PCM composed of hydrocarbon PCM with porous SiO₂ or unsaturated organic acid with polypropylene in the weight of asphalt mixture to adjust phase-change temperature meeting the technical requirements of roads [158].

To avoid the UHI, a solid-liquid phase transition PCM composed of unstable acids and SiO₂, resulting in latent heat of 95 kJ/kg and temperature of phase-changing of 17 °C, was tested with a content of 50% of asphalt binder by weight. The results show an increase in the asphalt mixture's specific heat, requiring more energy to change the temperature. With this, it is possible to have cooler roads, mitigating UHI [150].

For developing the LHTS capability, heating and cooling tests were carried out; however, conventional rutting, fatigue, and moisture resistance tests are also essential to design LHTS asphalt mixtures. PCM encapsulation could have advantages such as a larger heat transfer area, decrease of the PCM reactivity due to the external environment, and control of changes in the volume (expansion or retraction) of the storage materials when phase change happens [159].

The capsule shell prevents interactions between the PCM and the smart material [159], avoiding future mechanical problems. Researchers can also study the use of PCM to avoid UHI.

4.6. Summary

Table 2 summarizes all the capabilities detailed in the new capabilities, their influences, the most used materials, and the most important applications. The new capabilities are being investigated to enhance the performance of the surface and improve the pavement structural properties. Some of the capabilities are interrelated. The capabilities directly related to the socio and/or environmental impacts are the photocatalytic, thermochromic, and Latent Heat Thermal Energy Storage (LHTS), while those that directly impact mechanical behavior are superhydrophobic, LHTS, self-healing, and thermochromic capabilities. Lastly, the ones related to safety are superhydrophobic, self-cleaning, and deicing

capabilities.

Table 2: Influences, Benefits, Materials and Mains Applications of the Multifunctional Capabilities

Capability	Direct Influence	Indirect Influence	Benefits	Materials	Main application
Photocatalytic	Environmental	Social	Air and surface cleaning	Semiconductors, mostly TiO ₂	Spraying coating, bulk incorporation, asphalt binder modification, and spreading
Superhydrophobic	Safety and mechanical	Social and economic	Non-wetting pavements and better resistance	PTFE, nanoparticulate copolymer fluoroacrylate with CaO, TiO ₂ and TiO ₂ ZnO	Spraying Coating
Self-cleaning	Safety and Environmental	Social and economic	Surface cleaning and higher friction	Semiconductors/s uperhydrophobic treatments	Spraying coating, bulk incorporation, asphalt binder modification, and spreading
Deicing	Safety	Social and economic	Anti-snow/ice pavement	Salts and high electrical conductor materials	Asphalt binder modification bulk Incorporation
Selfhealing	Mechanical	Economic, environmental, and social	Crack healing: lifetime increase	High electrical conductor materials, microcapsules, nanomaterials, ionomers	Bulk incorporation asphalt binder modification
Thermochromic	Mechanical, safety, and social	Economic	Mitigate UHI or temperature control sensor	Leuco dyes	Asphalt binder modification
LHTS	Social, environmental or mechanical	Financial	Mitigate UHI or control of very high/low temperatures	Phase change materials	Bulk incorporation

From the review, it is clear that the optimization of some techniques could promote more than a single capability. The self-cleaning capability can be treated as the superhydrophobic or photocatalytic capabilities. On one hand, on a superhydrophobic surface, the rolling water drops remove the dirt particles. On the other hand, on a photocatalytic surface, oils and greases are removed by chemical reactions (heterogeneous photocatalysis).

A strategy to ensure the thermochromic capability for a longer time is the application of specific semiconductor materials in the thermochromic coating since, through their photocatalytic and self-cleaning capabilities, these materials have the ability to degrade oils and greases, thus eliminating these contaminants that block the path of light [160]. Moreover, with the application of high electrically conductive materials or nanomaterials, such as carbon nanotubes and nanofibers, it is possible to provide both capabilities: self-healing and deicing.

Thermochromic and LHTS capabilities can also be used to mitigate the UHI phenomenon. A photocatalytic coating applied over the surface can prevent this problem, as the treatment usually provides a white color (low absorptivity), thus covering the original surface black color (high absorptivity). The semiconductor nanomaterials could also provide the self-healing capability when applied by asphalt binder modification, as nanoparticles relocate towards the crack tip, stopping its propagation and, consequently, healing the composite material.

4.7. Critical Analysis and Conclusions

The main goal of this work is to perform a literature review on the smart and multifunctional capabilities applied to asphalt mixtures. The detailed and analyzed capabilities were the photocatalytic, superhydrophobic, self-cleaning, deicing/anti-ice, self-healing, thermochromic, and Latent Heat Thermal Energy Storage (LHTS) ones. In this section, the main conclusions are followed by a critical analysis, addressing the life cycle of smart asphalt pavement layers, from raw materials to the end of life, including costs:

- Considering the use of dissimilar materials, the nano/micromaterials incorporated to asphalt mixtures to provide new capabilities are semiconductor materials, fibers, microcapsules, and powders. Also, it is reported a new potential for the application of recycled materials, for example, SS (Steel Slags) from the steel industry.
- Essential characteristics of asphalt pavements must assured, namely resistance to traffic loading and climate actions, and rolling conditions as comfort and safety, with low impact for the environment and low cost. Therefore, besides the tests to evaluate the new capabilities, it is fundamental to carry out standard tests to guarantee adequate mechanical and functional performance, according to the technical requirements of asphalt mixtures.
- Regarding the design process of smart and multifunctional asphalt mixtures, different kinds of tests can be used to assess and characterize the new capabilities. The advanced material

characterization tests recommended are X-ray computed tomography, Scanning Electron Microscopy (SEM), Fourier Transform Infrared spectroscopy (FTIR), DSC, Atomic Force Microscopy (AFM). In this sense, and complementarily, the development of abrasion techniques, carried out on small samples, is an excellent opportunity to investigate the durability of new capabilities (mainly the capabilities applied by coating treatments) as well as to test the degree of immobilization of nanomaterials on functionalized surfaces.

- Regarding the methods of application of all the capabilities, they are simple and known by the paving industry, i.e., bulk incorporation, spraying coating, spreading, and asphalt binder modification.
- Considering the application of nano/micromaterials, their use on real scale is still a challenge for the Paving Industry. This chapter showed some use opportunities, which do not require expensive technological improvements. In fact, it is reasonable to state that, very soon, one of the potential destinations for the large-scale application of nanomaterials is the road sector, as it can act as a great lever to promote the dynamism and economic growth of industries related to the production of nanomaterials and nanotechnology use. With large-scale use, it is expected that their price will decrease since currently the production is limited, for that reason, the costs are still relatively high. There already exists the concern of the transfer technology from the laboratory to real scale roads for some capabilities. The application in real scale of the farther developed techniques as photocatalytic and self-healing did not imply relevant changes in the asphalt mixture manufacturing and paving processes. From these, it can be inferred that transfer technology of the capabilities not yet tested on the real scale will be easy and successful.
- Concerning the studies addressing the life cycle of smart and multifunctional asphalt mixtures, they are scarce but are important. Cost analysis is still a lack in the literature for all the capabilities. There is just a short economic analysis for a few techniques, for example, for the photocatalytic coatings. This evaluation is strongly recommended to guarantee economic feasibility. Furthermore, for those capabilities related to environmental benefits, some topics still need to be evaluated, such as environmental indicators, pollution reduction level, risk of cancer, biochemical analysis of the byproducts, and incorporated in costs analysis.
- Several researchers have carried out a significant number of works about different capabilities about the multifunctional effects of asphalt mixtures, but most of them focused on the application of just a single new function. For this reason, the combination of different techniques and/or

capabilities can result in the development of a better final product, a multifunctional asphalt mixture.

- Concerning the general design process, further studies should focus on a smart asphalt mixture, which must consider the requirements of traffic and weathering (mechanical and functional characteristics). It is recommended to design multifunctional asphalt mixtures made up of recycled materials and use techniques that cause less environmental damage and low noise. Combining these knowledges and techniques, the asphalt mixtures will be eco-friendly and provide several benefits of a social, environmental, and financial nature.

Actually, given the large surface area of paved roads (it may be talking about thousands of square kilometers), the functionalization process to provide them with multifunctional capability can deliver a very positive contribution to the citizens who utilize those roads, since, besides having a good mechanical structure and good surface properties that result from the application of new capabilities, they also bring benefits to the environment through, for example, the ability to photodegrade organic compounds adsorbed to the road surface or even toxic gases (NO_x and SO_x) that are exhausted by road vehicles.

CHAPTER 5 – DEVELOPMENT OF PHOTOCATALYTIC AND SUPERHYDROPHOBIC ASPHALT MIXTURES

This chapter refers to the research work about photocatalytic, superhydrophobic and self-cleaning asphalt mixtures “Assessment of photocatalytic, superhydrophobic and self-cleaning properties on hot mix asphalts coated with TiO₂ and/or ZnO aqueous solutions” published in Journal Construction and Building Materials (impact factor – if - 6.141). The content of this chapter is included in the article, which digital object identifier (DOI) is 10.1016/j.conbuildmat.2018.01.106 (Figure 20). The main objective of this chapter was to develop the photocatalytic, superhydrophobic and self-cleaning capabilities on asphalt mixtures by spraying TiO₂ or/and ZnO aqueous solutions.



Figure 20: First page of the research work published in Construction and Building Materials [8]

5.1. Introduction

Regarding the literature review chapters, it is shown that it is relevant to study the effect of the asphalt substrates (different asphalt mixtures) on the photocatalytic process. Therefore, the morphologic and chemical properties of asphalt bitumens were analyzed after spraying of different semiconductors on samples to verify if the use of this technique did not damage the bitumen, in a first stage. In a second stage, the photocatalytic efficiency and the wettability of asphalt mixtures were evaluated after spraying with aqueous solutions of: TiO_2 ; ZnO ; and, a combination of TiO_2 and ZnO . To guarantee that the effect still occurs after traffic, the asphalt mixture samples were submitted to an abrasion process. Finally, the effect of the best aqueous solution on mechanical properties of asphalt mixture samples was assessed.

5.2. Materials and Methods

5.2.1 Materials

In order to develop the research two bitumens were used: Cepsa® 35/50 and Elaster® 13/60, from Cepsa company, to compose two asphalt mixtures: AC 14 surf 35/50 and AC 6 surf Elaster 13/60 respectively. In order to functionalize these materials two semiconductors were used: nano- TiO_2 by Quimidroga (Aeroxide TiO_2 P25: 80% and 20% rutile); and micro- ZnO by Sigma Aldrich. The results of the bitumen characterization are presented in Table 3.

Table 3: Properties of the Bitumens

Properties	35/50	Elaster	Test specification
Softening point/ $^{\circ}\text{C}$	56	63	ASTM D 36
Penetration at 25 $^{\circ}\text{C}$ /0.1mm	30	46	ASTM D 5
Brookfield viscosity at 145 $^{\circ}\text{C}$ /Pa s	0.5607	1.2109	ASTM D 4402

The band gap of the semiconductors was measured by diffuse reflectance and calculated using the Kubelka-Munk equation [161,162]. This energy necessary to start the reaction is 3,20 eV for TiO_2 and 3,25 eV for ZnO , corresponding to UV-A light.

Three aqueous solutions were prepared with: TiO_2 nanoparticles (4 g/L); ZnO microparticles (1 g/L); and TiO_2 nanoparticles (4 g/L) + ZnO microparticles (1 g/L). The aim was to improve the photocatalytic efficiency by combining semiconductors to decrease the band gap (by doping) to trigger the photocatalytic property. All the solutions had pH 8 in order to prevent any negative impact into the bitumen and guarantee less aggregate agglomeration of the semiconductors [7].

The asphalt mixes were prepared following the standard EN 13108-1 and their temperatures of production and compaction following the bitumen curve viscosity *versus* temperature. The AC 6 mixture is characterized by an uniform granulometry, it is composed mostly by intermediate aggregates (4/6) and commercial asphalt bitumen which is modified by SBS. It also has a high volume of voids (10.9%). The AC 14 mixture is a conventional asphalt mixture that shows a dense granulometry, is composed by conventional asphalt bitumen 35/50 and has low volume of voids (4.7%). Both mixtures are used as structural and functional pavement layers but AC 6 has a very limited structural impact. Often it is used when improved superficial characteristics are required. The samples were compacted in two geometries: cylindrical following Marshall Design that is used to analyze the mechanical impact of the semiconductors; and, prismatic slabs by rolling compaction used to be cut and then to analyze the wettability and photocatalytic efficiency. The main characteristic of the AC 6 and AC 14 asphalt mixes of the slabs are given in the Table 4.

Table 4: Properties of Asphalt Mix Slabs

Asphalt Mix	Filler (%)	Fine Aggregates 0/4 (%)	Intermediate Aggregates 4/6 (%)	Intermediate Aggregates 4/8 (%)	Coarse Aggregates 6/14 (%)	Bitumen (%)	Maximum Bulk Density (g/cm ³)	Voids content (VC) (%)
AC 6	3	25	72	-	-	6	2.423	10.9
AC 14	3	41	-	12	44	5	2.474	4.7

For Marshall samples, used to analyze the mechanical impact of semiconductors, AC 6, compacted with 50 blows in each surface, presented a VC of 9.2%, and the AC 14, compacted with 75 blows in each surface, had a VC of 4.8%. The volume of voids of the mixtures was similar and independent of the geometry.

5.2.2. Sample Preparation

The method of application of the semiconductors was by spraying an aqueous solution onto the surface of the asphalt mixtures. This is the most efficient method when compared with others methods such as volume incorporation or bitumen modification [7,60,71]. This method consists of spraying the aqueous solution with an atmospheric air compressor at a distance of about 20 cm during 30 s, being the speed of the aqueous solution jet set at 100 mL/min, thus leading to coverage rates of around 5 mg/cm² to 12.5 mg/cm². The temperature of the asphalt mixes at spraying was 60°C, which is similar to the softening point temperature of both bitumens.

In this research, 2 approaches were carried out: analysis of the bitumens sprayed directly with the semiconductors; and, analysis of the asphalt mixtures sprayed with the semiconductors.

The bitumen damage/deterioration caused by the semiconductors was evaluated when applied directly onto bitumen samples. A hot drop of bitumen was carefully deposited on a glass microscope slide substrate, and spread out with a blade to form a film that covered the glass surface. Then the aqueous solutions were applied by spraying. Fourier Transform Infrared Spectroscopy (FTIR) and Atomic Force Microscope (AFM) results were compared including samples without treatment for control. The samples that were analyzed by FTIR were covered by a plastic film to protect the equipment.

In order to evaluate the photocatalytic property and efficiency, the solutions were applied in prismatic samples (25 x 25 x 15 mm³) cut from slabs. These samples were used to evaluate the water contact angle and the photocatalytic efficiency. To evaluate the semiconductors' fixation, the tests were carried out before and after abrasion using a metallic wire brush disc (at 200 RPM) conducting in 3 mass loss levels of the samples: 0.25%, 0.50% and 1%. The abrasion was carried out homogeneously over the asphalt mixtures' surface.

Finally, the best aqueous solution was applied to the asphalt mixes AC 6 surf Elaster 13/60 and AC 14 surf 35/50 Marshall samples to evaluate if there is a moisture impact into their mechanical properties. The Figure 21 shows the procedure used to prepare the samples for testing.

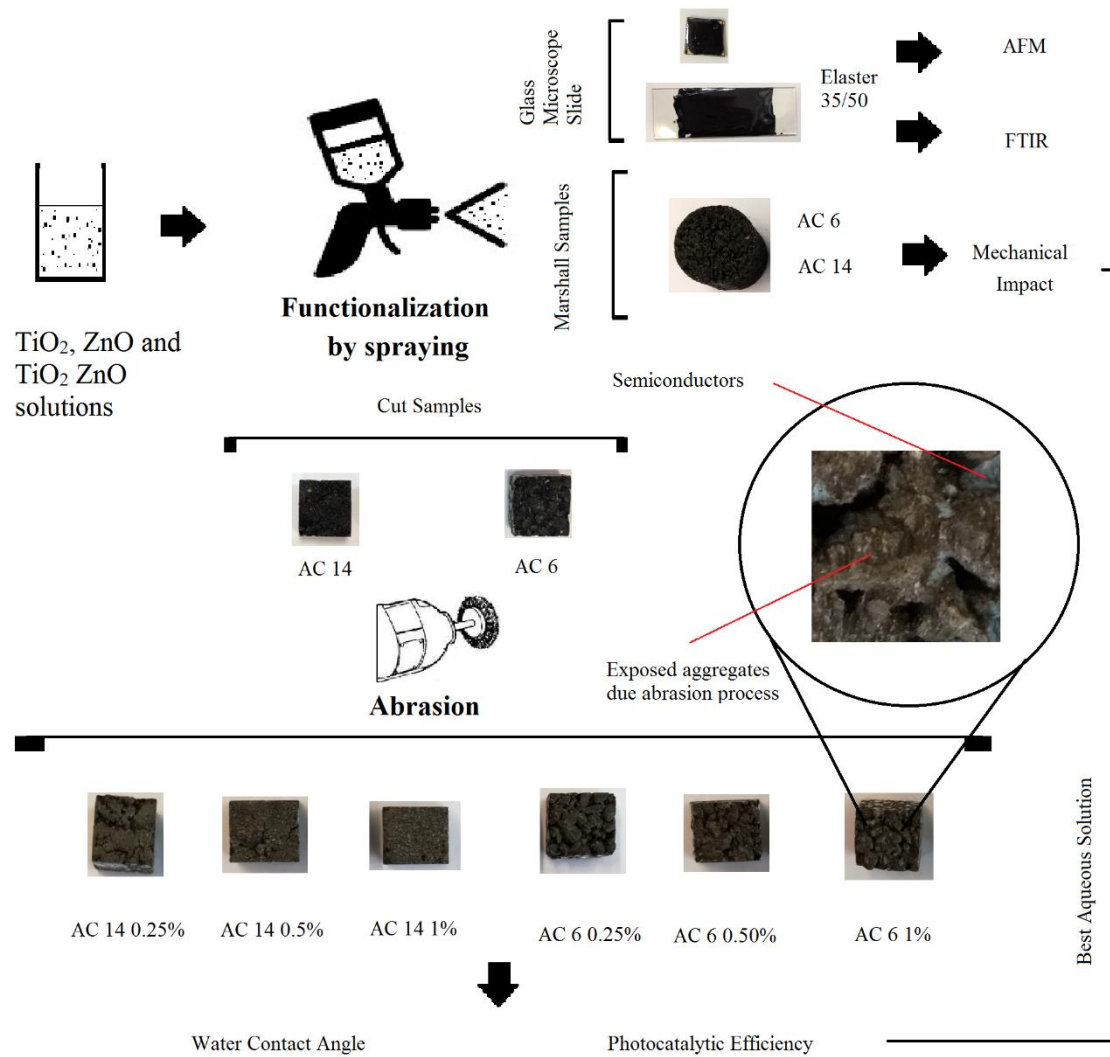


Figure 21: Sample preparation for AFM, FTIR, mechanical impact, water contact angle and photocatalytic efficiency measurements

5.2.3. Methods

5.2.3.1. Atomic Force Microscopy (AFM)

To study the bitumen surface morphology sprayed with semiconductors, the samples were evaluated by AFM. The structures of bitumen observed in this evaluation are: (i) *catana phase* or bee structures (pale lines as peaks and back lines as valleys). This phase could be related with the asphaltenes [163–165]; (ii) *periphase* pale region around the *catana* phase; (iii) *perpetual* phase: structural matrix. The samples were scanned over lengths of 5 μm to give a surface area of 25 μm^2 using the equipment Digital Instruments NanoScope III Atomic Force Microscope. The absence of the *catana* phase could indicate a superficial change in the bitumen, due to the degradation of the asphaltenes [7].

5.2.3.2. FTIR

Fourier Transform Infrared Spectroscopy (FTIR) was performed to analyze the bitumens sprayed with semiconductors and the control sample. The FTIR spectrum was recorded on an Avatar 360 FTIR system, Nicolet, 4000– 400 cm^{-1} spectral range, equipped with multi-bounce HATR and diffusion reflectance accessories. The semiconductors and bitumens' spectrums will be presented in Section 5.3.2.

5.2.3.3. Water Contact Angle (WCA)

The Water Contact Angle (WCA) test was carried out to evaluate the wettability of asphalt pavement and characterize its hydrophilicity/hydrophobicity. To measure this property Cassie-Baxter's model was considered because the water drop would be probably suspended on surface roughness, justified by the rough and hydrophobic surface [95]. Using the equipment OCA 15 plus Dataphysics, 3 readings of 5 μL water drops were carried out at 3 samples during 30 minutes, at room temperature and relative humidity, and the arithmetic mean was calculated. The analysis of variance (ANOVA) and PostHoc statistical test were done to evaluate the different parameters and their influence in the Water Contact Angle.

5.2.3.4. Photocatalytic Efficiency Evaluation

The new capabilities of materials on test, photocatalytic and self-cleaning, can be evaluated by the degradation of a dye [166,167]. It was carried out with the functional asphalt mixes by measuring the maximum absorption of Rhodamine B (RhB) (554 nm^{-1}) (using a Shimadzu 3101 PC spectrophotometer) with concentration of 5ppm (pH 5) as a function of a light that simulates the sun irradiation (with a power intensity of 11 W/m^2 , measured with a Quantum Photo Radiometer HD9021 Delta Padova) in different times. Each sample was immersed in 30mL of RhB aqueous solution distant 25 cm from the light. After 6h in dark condition (adsorption), the samples were irradiated with a 300 W - OSRAM UltraVitalux lamp. In order to avoid the evaporation of RhB solution that can increase the concentration, all the systems were closed with a transparent plastic film with at least 90% of transmittance in the wavelength range between 292 and 900nm. The photocatalytic efficiency (Equation (16)) was calculated using the Beer–Lambert law [7]. Also, ANOVA and Post Hoc test were done to evaluate better the photocatalysis results.

$$\Phi (\%) = \left(\frac{A_0 - A}{A_0} \right) \times 100 \quad (16)$$

where Φ is the photocatalytic efficiency; A and A_0 represent the maximum absorbance of RhB solution for time t and 0 hour, respectively.

5.2.3.5. Mechanic Impact of Semiconductors

To analyze the mechanical impact of the functionalized asphalt mixtures, tests of Indirect Tensile Strength (ITS) were carried out according to the standard EN 12697-23. Two groups of three samples were evaluated with and without TiO₂ + ZnO semiconductors after water immersion process. This water process was carried out due to different wettability of the materials which could cause different mechanical impacts. The parameter Resistance Index (RI), which is the ratio of the difference of the resistances of functionalized samples (ITS_f) and the not functionalized samples (ITS) to ITS (Equation (17)), was calculated.

$$RI = \frac{ITS_f - ITS}{ITS} \quad (17)$$

5.3. Results

5.3.1. Atomic Force Microscopy (AFM)

Figure 22 shows the AFM results. The absence of the catana phase could indicate a superficial alteration in the bitumen, that is, the degradation of the asphaltenes [7]. The bee structures were identified in the bitumen without the presence of semiconductors and after TiO₂ and TiO₂ + ZnO application. The ZnO solution presents an impact on the bitumen surface explained by the absence of the structure, indicating a superficial degradation of the bitumens.

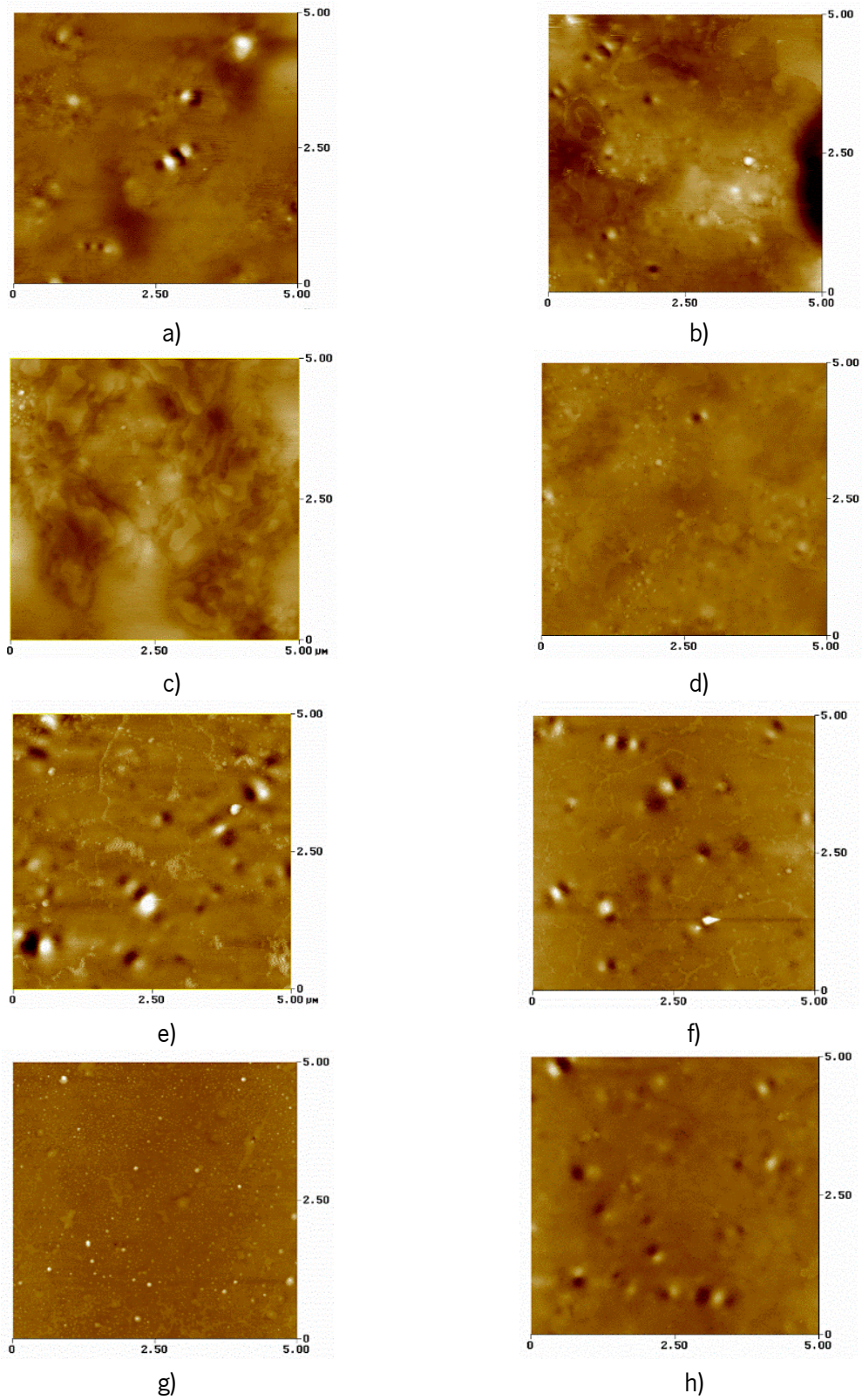


Figure 22: AFM Results: a) Cepsa 35/50; b) Cepsa 35/50 + TiO₂; c) Cepsa 35/50 + ZnO; d) Cepsa 35/50 + TiO₂ + ZnO; e) Elaster 13/60; f) Elaster 13/60 + TiO₂; g) Elaster 13/60 + ZnO; h) Elaster 13/60 + TiO₂ + ZnO

5.3.2. Fourier Transform Infrared Spectroscopy (FTIR)

Figure 23 shows the FTIR of bitumens with and without semiconductors. In the commercial Elaster bitumen when comparing with the bitumen 35/50 an accentuation is noticed in the peaks referring to the butadiene: 959.55 cm^{-1} , to the styrene: 684.76 cm^{-1} , both referring to SBS, and the aromatic C-H vibration [168]. For both bitumen, peaks 2923.11 and 2860.79 cm^{-1} are respectively related to the vibration of the asymmetric C-H (CH_3 and CH_2) shift and the symmetrical C-H (CH_3 and CH_2) stretching. Peak 1596.46 cm^{-1} is related to vibrations of aromatic C=C and C-H elongation and peak 1431.68 cm^{-1} , with C-H flexion.

It is possible to note that the ZnO solution sprayed onto the Elaster bitumen showed higher impact on this bitumen, having an impact on the transmittance of the functional groups. Differently from the Elaster, the bitumen 35/50 showed little change in its spectrum.

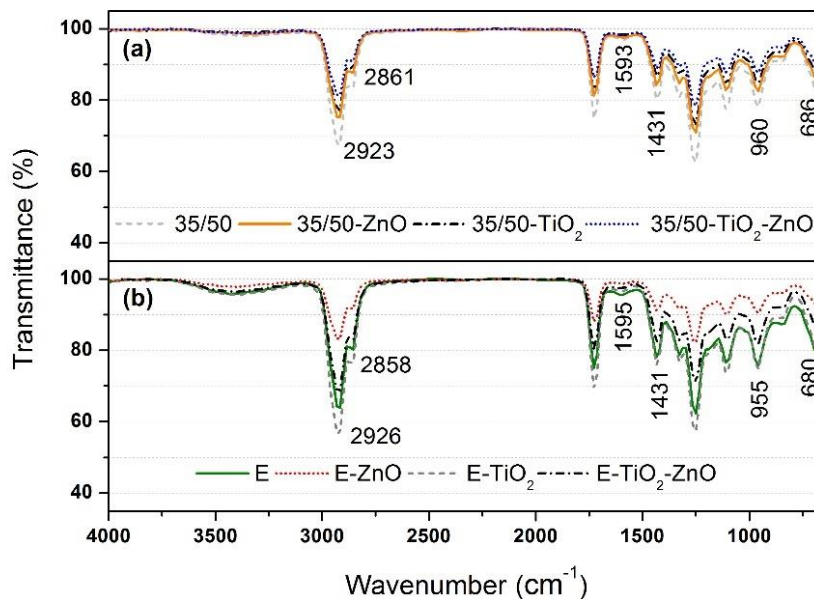


Figure 23: FTIR of 35/50 and Elaster (E) before and after the application of semiconductors

5.3.3. Water Contact Angle Analysis

Figure 24 shows the results of water contact angle (wettability) of the asphalt mixtures with the different treatments and wear levels. The initial contact angle for the mixtures before abrasion was higher than after abrasion. Initially, the asphalt mixtures had the aggregates' surface covered with bitumen, resulting in a smooth surface. After, with abrasion, the microtexture of the aggregate appeared. The

increase of the water contact after abrasion was probably due to the increase of the aggregates' roughness. But, in order to achieve higher hydrophobicity, the abrasion of the asphalt mixture is not recommended.

In general, after this first moment the result was the opposite. For both mixtures, the higher initial contact angle was found for the samples treated with TiO₂ and ZnO. The superhydrophobicity, WCA higher or equal to 150° was guaranteed for the mixtures AC 14 TiO₂, AC 14 TiO₂ ZnO and AC 6 TiO₂ ZnO. The initial WCA is the most important angle because the water drains in a very short time to the roadside. The lower WCA was obtained for AC 14 without treatment after 1% of abrasion (108°) and AC 6 without neither treatment nor abrasion (102°). After 30 min, it was possible to have WCA equal or higher than 40° for AC 14 ZnO 0.25% (63°), AC 14 TiO₂ ZnO (51°), AC 6 TiO₂ 0.25% (40°), AC 6 ZnO 0.25% (40°) and AC 6 TiO₂ ZnO 0.25% (40°). On the other hand, the sample AC 14 without treatment and abrasion had the lowest WCA, below 10°. Table 5 summarizes the maximum and minimum results for Water Contact Angle.

An analysis of variance, ANOVA (factors: abrasion, treatment, time, mixture), was carried out to determine if there is an interaction effect between the independent variables over the water contact angle for a significance level of $(1 - \alpha = 0.1)$. This parameter indicates the risk (%) of concluding that an effect exists when there is no actual effect. On the other hand, Mixture ($p < 0.001$), Time ($p < 0.001$), Treatment ($p < 0.001$) and Abrasion ($p < 0.1$) had a significant influence on contact angle measurements. Only the interactions of the following variables had a significant effect on the dependent variable results: i) Mixture and Treatment ($p < 0.001$); ii) Mixture and abrasion ($p < 0.01$); iii) Treatment and Abrasion ($p < 0.001$); iv) Mixture, Time and Treatment ($p < 0.01$).

Table 6 shows the ANOVA analysis: Degrees of Freedom (Df), Sums of Squares (SSq), Mean of Squares (MSq), Fisher (F value) and p.

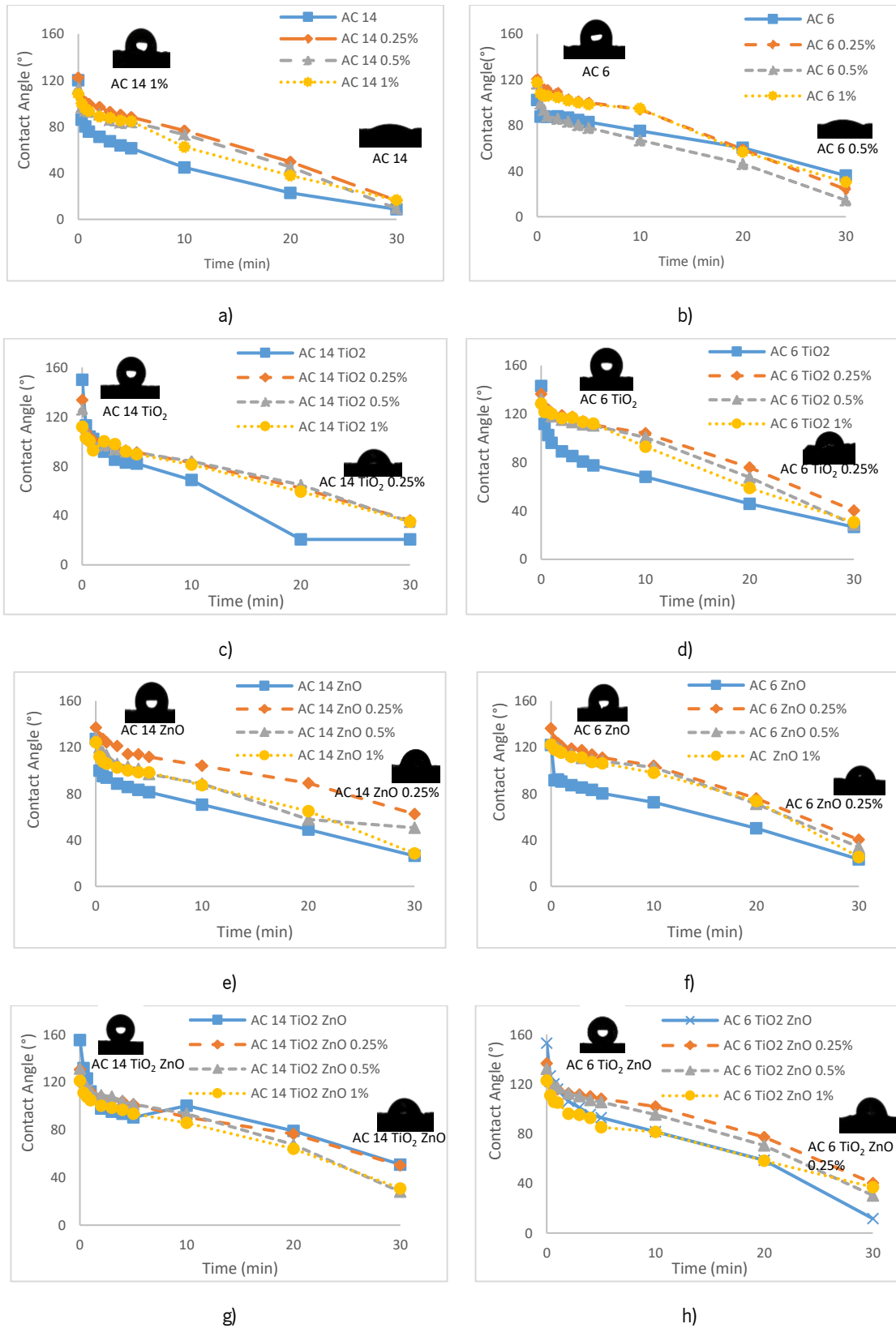


Figure 24: Water Contact Angle: a) AC 14; b) AC 6; c) AC 14 TiO₂; d) AC 6 TiO₂; e) AC 14 ZnO; f) AC 6 ZnO; g) AC 14 TiO₂ ZnO; h) AC 6 TiO₂ ZnO

Table 5: Maximum and Minimum Results for Water Contact Angle

Mixture	Treatment	Maximum WCA				Minimum WCA			
		Initial		Final		Initial		Final	
		Abrasion (%)	WCA (°)	Abrasion (%)	WCA (°)	Abrasion (%)	WCA (°)	Abrasion (%)	WCA (°)
AC 14	-	0.25	122	1.00	17	1.00	108	-	9
	TiO ₂	-	150	0.25	36	1.00	112	-	21
	ZnO	0.25	137	0.25	63	1.00	124	-	26
	TiO ₂ ZnO	-	155	-	51	1.00	121	0.50	28
	-	0.25	120	-	36	-	102	0.50	14
AC 6	TiO ₂	-	143	0.25	40	1.00	129	-	27
	ZnO	0.25	136	0.25	40	-	122	-	23
	TiO ₂ ZnO	-	153	0.25	40	1.00	123	-	12

Table 6: Results of ANOVA for Contact Angle

Variables	F value	p
Mixture	107.8	< 2×10 ⁻¹⁶ ***
Time	2248.411	< 2×10 ⁻¹⁶ ***
Treatment	90.119	< 2×10 ⁻¹⁶ ***
Abrasion	3.245	0.07192 .
Mixture and Time	0.048	0.82654
Mixture and Treatment	12.822	3.06E-08 ***
Time and Treatment	0.726	0.53651
Mixture and Abrasion	10.022	0.00159 **
Time and Abrasion	0.978	0.32284
Treatment and Abrasion	10.003	1.65×10 ⁻⁶ ***
Mixture, Time and Treatment	4.821	0.00243 **
Mixture, Time and Abrasion	1.546	0.21398
Mixture, Treatment and Abrasion	0.341	0.71113
Time, Treatment and Abrasion	1.126	0.3374
Mixture, Time, Treatment and Abrasion	1.907	0.14902

. p < 0.1, * p < 0.05, ** p < 0.01, *** p < 0.001

The Bonferroni Post-Hoc test for a level of significance (1 - α = 0.1) has the following factors:

Factor 1 - Time:

The average of the contact angle for time equal to zero were higher when compared to that of times equal to 0.3333s (p < 0.001). The averages of the contact angle of the times 0.6666 and 0.3333, 1 and 0.3333, 1 and 0.6666, 2 and 0.6666, 2 and 1, 3 and 1, 3 and 2, 4 and 2, 4 and 3, 5 and 2, 5 and 3, 5 and 4 did not present significant differences in average of contact angle (p > 0.1).

For all other times, the difference of the averages of the contact angle were significant ($p < 0.1$). It can be concluded that the initial WCA is the most important.

Factor 2 - Treatment:

The average of the WCA measurements of the treated samples were significantly higher when compared to the untreated samples ($p < 0.001$), but the averages of the WCA of the treated samples did not differ significantly. Therefore, the hydrophobicity was higher for the treated samples compared to the non-treated ones.

Factor 3 - Abrasion:

The averages of the WCA measurements of the worn samples were significantly different from the average of the samples without abrasion: 0.25% ($p < 0.001$); 0.5% ($p < 0.001$) and 1% ($p < 0.05$). Only the WCA averages for the samples with 0.25% and 1% wear level differ significantly ($p < 0.05$). It can be concluded that WCA for consecutive wear levels were similar.

Factor 4 – Asphalt Mixture:

The average of WCA measurements of the AC 14 samples was significantly lower than the AC 6 samples ($p < 0.001$).

5.3.4. Photocatalytic Efficiency

Figure 25 shows the results of photocatalysis for the asphalt mixtures. During 6 hours, the samples were submerged inside the dye solution in dark condition in order to analyze the adsorption without photodegradation reactions. When the adsorption was constant, the light was turned on. After 8h of irradiation, the best results for photocatalytic efficiency were achieved for the samples treated with TiO_2 (57%) and TiO_2 ZnO (56%) for AC 14 and TiO_2 ZnO for AC 6 (49%). The results show that the combination of these materials was more efficient for AC 6 due to the increase of 18% on the photocatalytic efficiency comparing with the results only with TiO_2 . AC 14 did not have any impact when combining the semiconductors. After abrasion, the worst situation was found for AC 14 treated with ZnO, which show a decrease, on average, of 59%. For AC 6, it was a decrease of 48%. The best fixation of semiconductors was for AC 6 TiO_2 , with a decrease of 8% in photocatalytic efficiency comparing with the average of the worn samples.

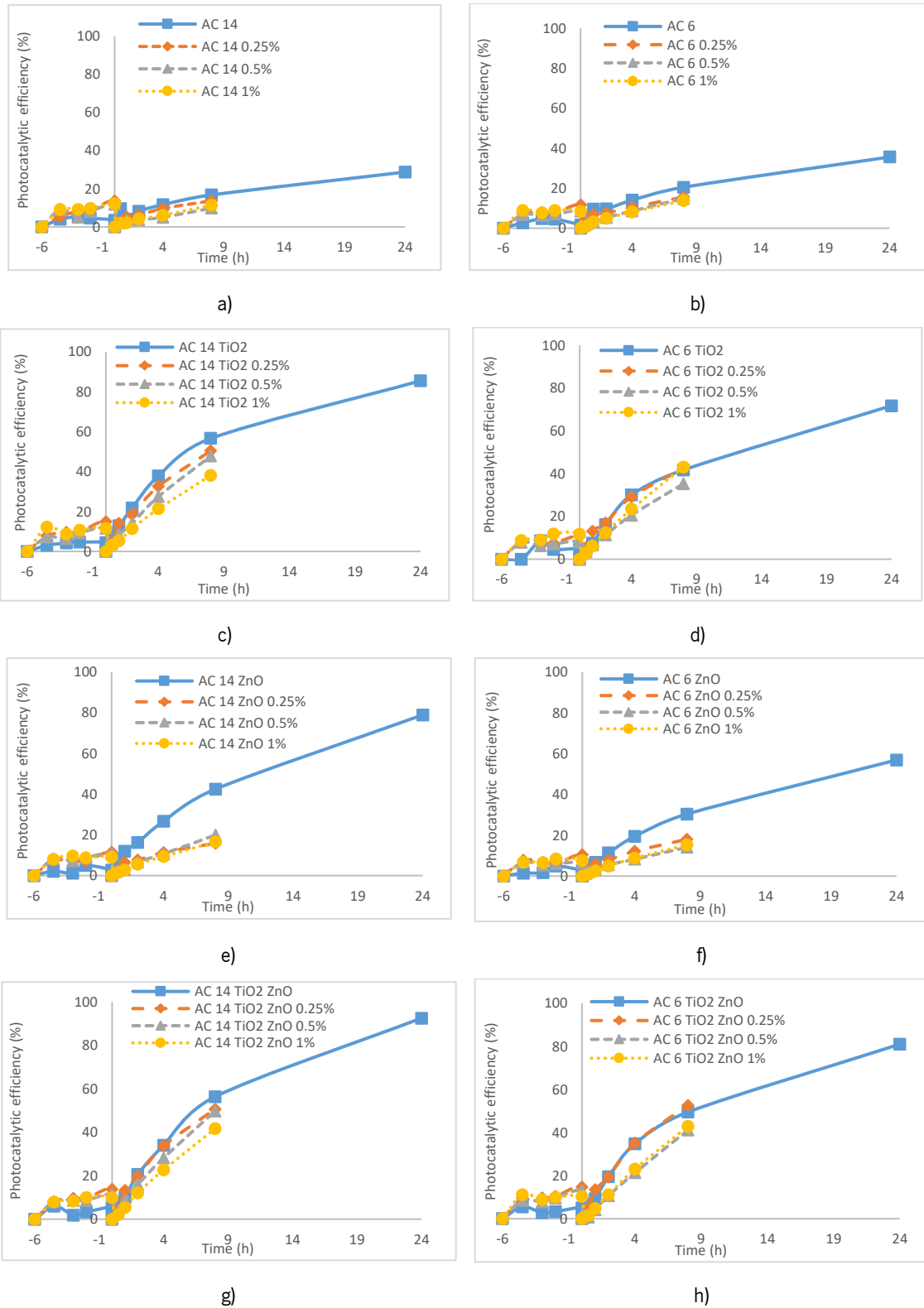


Figure 25: Photocatalytic Efficiency: a) AC 14; b) AC 6; c) AC 14 TiO₂; d) AC 6 TiO₂; e) AC 14 ZnO; f) AC 6 ZnO; g) AC 14 TiO₂ ZnO; h) AC 6 TiO₂ ZnO

The results after 24 hours of irradiation, done only for the samples before abrasion, show that the mixture before treatment has 29% and 36% of photocatalytic efficiency for, respectively, AC 14 and AC 6 samples. Probably this was caused by a presence of semiconductors in the aggregates exposed due to sample cutting.

It was possible to achieve photocatalytic efficiencies of 79% for AC 14 ZnO, up to 92% for AC 14 TiO₂ ZnO and 57% for AC 6 ZnO, and up to 81% for AC 6 TiO₂ ZnO samples. After doping, when the semiconductors were combined, the results showed an increase of 8% for AC 14 and 13% for AC 6 comparing with the samples treated only with TiO₂.

Analyzed by a variance analysis (ANOVA) for a confidence level of $(1 - \alpha = 0.1)$, the results of the independent variables Mixture ($p < 0.01$), Time ($p < 0.001$), Treatment ($p < 0.001$) and Abrasion ($p < 0.001$) have a significant influence on the measurements of the photocatalytic efficiency. The interactions of the following variables had a significant impact on the results of the photocatalysis: i) Mixture and Treatment ($p < 0.01$); ii) Mixture and Abrasion ($p < 0.05$); iii) Treatment and Abrasion ($p < 0.1$); iv) Time and Abrasion ($p < 0.001$); v) Mixture and Time ($p < 0.1$) and vi) Time and Treatment ($p < 0.001$). The interaction between the combinations of three independent variables has a significant influence on the measurements of the photocatalytic efficiency ($p < 0.1$). Table 7 show the ANOVA analysis.

The Bonferroni Post-Hoc test for a level of significance $(1 - \alpha = 0.1)$ has the following factors:

Factor 1 - Time:

The average of the photocatalytic efficiency at 0.5h and 1h did not differ significantly. The average of the photocatalytic efficiency at 1h and 2h presented significant differences ($p < 0.05$). For all the other times, the average of photocatalytic efficiency differed significantly with $p < 0.01$. This means, as expected, that the photocatalytic efficiency increases during the time irradiation.

Factor 2 - Treatment:

The average of the photocatalytic efficiency between treated samples and non-treated samples presented significant differences ($p < 0.01$), except for the samples treated with ZnO. In addition, the average photocatalytic efficiency of samples treated with TiO₂ ($p < 0.01$) and TiO₂ ZnO ($p < 0.01$) differs significantly from samples treated with ZnO. It is important to emphasize that the average of the photocatalysis results of the samples treated with TiO₂ did not differ significantly from the samples treated with TiO₂ ZnO. The average of the samples treated with ZnO did not differ significantly from the samples

without treatment. Therefore, it can be concluded that the use of ZnO did not have any improvement separated or combined with TiO₂ regarding only the photocatalytic properties.

Factor 3 - Abrasion:

The average of the photocatalytic efficiency of the samples before abrasion were significantly higher than the one of the samples at 0.5% ($p < 0.05$) and at 1% ($p < 0.001$), but not at 0.25%. However, the average of photocatalytic efficiency between the worn samples does not differ significantly between them. Low levels of abrasion do not effect photocatalytic efficiency.

Factor 4 – Asphalt Mixture:

The average of the photocatalytic efficiency of the different bituminous mixtures samples does not differ significantly. Therefore, the functionalization, considering the photocatalytic property, does not have influence on the different substrates.

Table 7: Results of ANOVA for Photocatalytic Efficiency

Variables	F value	Pr (> F)	
Mixture	10.708	0.001182	**
Time	1519.445	$< 2 \times 10^{-16}$	***
Treatment	166.017	$< 2 \times 10^{-16}$	***
Abrasion	133.83	$< 2 \times 10^{-16}$.
Mixture and Time	3.302	0.070131	**
Mixture and Treatment	4.899	0.002413	***
Time and Treatment	114.958	$< 2 \times 10^{-16}$	*
Mixture and Abrasion	5.813	0.016464	***
Time and Abrasion	11.384	0.000831	.
Treatment and Abrasion	2.565	0.054601	.
Mixture, Time and Treatment	2.317	0.075575	.
Mixture, Time and Abrasion	3.105	0.078988	.
Mixture, Treatment and Abrasion	2.112	0.09858	.
Time, Treatment and Abrasion	2.207	0.087211	.
Mixture, Time, Treatment and Abrasion	0.584	0.625899	.

. $p < 0.1$, * $p < 0.05$, ** $p < 0.01$, *** $p < 0.001$

5.3.5. Mechanic Impact of Semiconductors

The mechanical impact of the semiconductors on the mixture was assessed trough Indirect Tensile Strength after immersing the samples in water. The Resistance Index (RI) was for AC 6, -2.9% and, for AC 14, 0.1%.

After the semiconductors application, the asphalt mixtures had almost the same performance. Therefore, it can be concluded that the best aqueous solution of semiconductors, TiO_2 ZnO, applied by spraying had no mechanical impact.

5.4. Conclusions

This study aimed at developing and assessing photocatalytic, superhydrophobic and self-cleaning asphalt mixtures sprayed with TiO_2 or/and ZnO aqueous solutions. In the first stage bitumen samples were chemically and morphologically assessed in order to analyze if there was any bitumen deterioration after the solution spraying. Next, two types of asphalt mixtures functionalized with TiO_2 ZnO were assessed mechanically through indirect tensile strength after water immersion in order to find out if there were mechanical impacts caused by the semiconductors. Finally, the samples were evaluated by Water Angle Contact and by photocatalytic efficiency to analyze these new capabilities. Eight conditions of mixtures and semiconductors were evaluated: a) AC 14; b) AC 6; c) AC 14 TiO_2 ; d) AC 6 TiO_2 ; e) AC 14 ZnO; f) AC 6 ZnO; g) AC 14 TiO_2 ZnO; h) AC 6 TiO_2 ZnO. The results of the experimental activity led the following conclusions:

- Based on AFM, ZnO affects the bitumen physical integrity. The bee structure, or catana phase, disappeared. This is indicative of bitumen deterioration. The other solutions, with TiO_2 and TiO_2 ZnO, maintained the integrity of the bitumen.
- The FTIR showed on the one hand a high impact of the ZnO solution sprayed on the Elaster bitumen, and, on the other hand, little impact on the conventional 35/50 bitumen.
- The wettability of asphalt pavement and its hydrophilicity/hydrophobicity were evaluated by Water Contact Angle (WCA). The initial WCA before abrasion was higher than after. In general, for later times the relation was the opposite. The superhydrophobic property was developed for these samples: AC 14 TiO_2 , AC 14 TiO_2 ZnO and AC 6 TiO_2 ZnO (WCA higher or equal to 150°). Therefore, the combination of TiO_2 and ZnO was important to achieve the superhydrophobic property.
- The use of TiO_2 aqueous solution sprayed onto the surface of the asphalt mixtures was able to promote the photodegradation of an organic pollutant (Rhodamine B dye – RhB). After 24 hours of light irradiation, the maximum photocatalytic efficiency (92%) was obtained for samples functionalized with TiO_2 and doped with ZnO. After 8 hours of irradiation, the worst situation was for AC 14 ZnO, which had after abrasion a decrease in average of 59% of the photocatalytic efficiency, and the best situation, AC 6 TiO_2 , which has a decrease in average of 8%. After analysis

of Bonferroni Post-Hoc test, the use of ZnO is not recommended to promote the photodegradation neither separated nor in combination with TiO₂.

- The semiconductors TiO₂ ZnO applied by aqueous solution have no mechanical impact, assessed by Indirect Tensile Strength after water immersion.

The combination of TiO₂ with ZnO promoted the photocatalytic superhydrophobic and self-cleaning properties, providing the asphalt mixtures with these new capabilities. These functionalized pavement surfaces could degrade gases like SO₂ and NO_x, avoid accidents by removing the small dirt particles which are drained with water (lotus effect), degrade oils on the pavement surface and, additionally, it could prevent the pore clogging which happens in permeable asphalt mixtures. Great benefits to road safety and environment are foreseen with the construction of these layers.

CHAPTER 6 – MECHANICAL IMPACTS AND PHOTOCATALYTIC EFFICIENCY OF ASPHALT MIXTURES

This chapter refers to the research work about photocatalytic, superhydrophobic and self-cleaning asphalt mixtures “Photocatalytic asphalt mixtures: Mechanical performance and impacts of traffic and weathering abrasion on photocatalytic efficiency” published in Journal Catalysis Today (impact factor – if – 6.766) (Figure 26). The main objective of this chapter was to analyze the mechanical impacts of the functionalization process and evaluate the impacts of weathering and traffic on photocatalytic efficiency. Also, both functionalization processes (spraying coating and volume incorporation) were carried out and compared. The content of this chapter is included in the article, which DOI is 10.1016/j.cattod.2018.07.012. Its graphical abstract is presented in Figure 27.

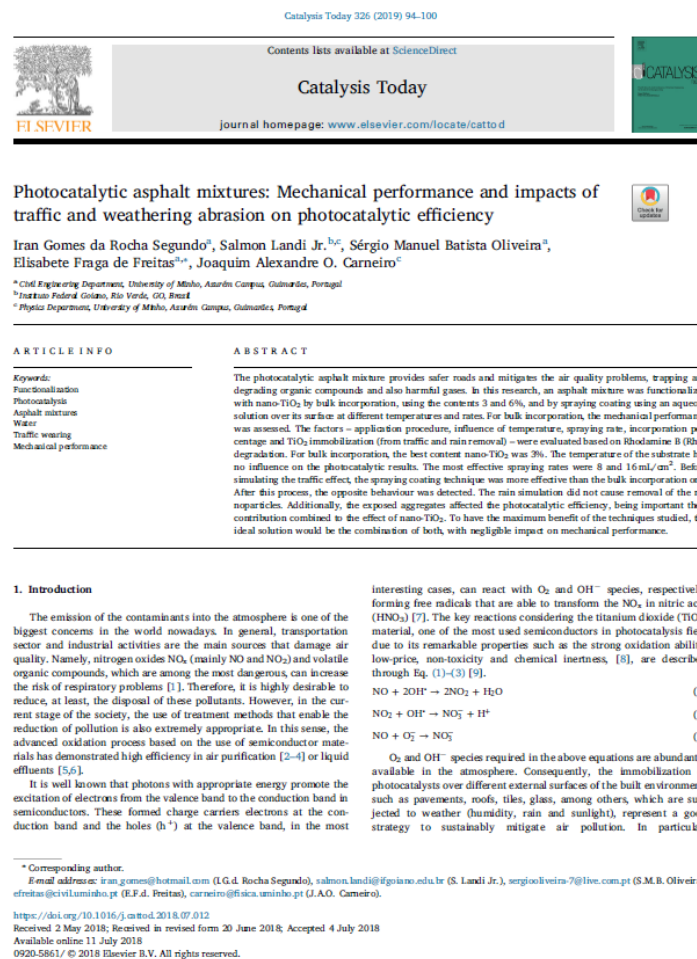


Figure 26: First page of the research work published in Catalysis Today [9]

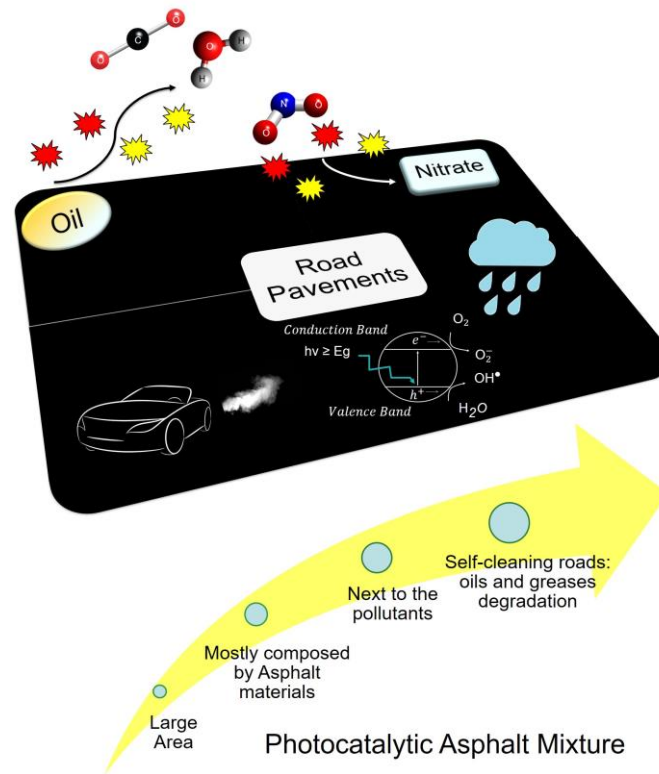


Figure 27: Graphical Abstract of the paper [9]

6.1. Introduction

The main goal of this chapter is to assess the immobilization degree of TiO_2 nanoparticles by using two experimental techniques (spraying coating and bulk incorporation) due to traffic and weathering and to analyse the mechanical behaviour of asphalt mixtures functionalized by bulk incorporation. In a first phase, the influence of TiO_2 nanoparticles on the mechanical properties for the bulk incorporation technique was studied due to the possibility of change the mechanical behaviour. Then, for the spraying coating, the effects of temperature and spraying rate in the immobilization of the nanomaterials were investigated. Lastly, the influence of traffic and water was analysed by applying abrasive wear through a rotary brush and simulating rain for both techniques.

6.2. Materials and Samples Preparation

In this research AC 14 surf 35/50 asphalt mixtures were formulated by the Marshall Method, using 92% of granite aggregates, 3% of limestone filler and 5% of asphalt binder in weight of the mixture, aiming 4% of voids content. The binder, Cepsa® 35/50, was characterized by: i) Penetration of 30×10^{-1} mm (EN 1426/2015); ii) Brookfield viscosity of 391 cP at 150 °C (EN 13302/2010) and iii) Softening

Point of 56 °C (EN 1427/2015). The aggregate composition of the mixtures was: i) limestone filler: 3%; ii) 0/4 mm: 41%; iii) 4/8 mm: 12% and iv) 6/14 mm: 44%.

In order to functionalize the asphalt mixtures, the semiconductor nano-TiO₂ by Quimidroga (TiO₂ P25: 80% anatase and 20% rutile) was used. Its purity is higher than 99.5% and the particle size is of about 23 to 28 nm [43]. The band gap of TiO₂ was 3.20 ± 0.03 eV, corresponding to the region of UV-A light. It was calculated using the Kubelka-Munk equation obtained from the diffuse reflectance spectrum [161,162].

The asphalt mixes were prepared following the standard EN 13108-1. The samples were compacted in two geometries: cylindrical to carry out the water sensitivity test (EN 12697-12) and prismatic slabs to assess the photocatalytic efficiency and to carry out mechanical characteristics tests, such as fatigue resistance (AASHTO TP 8-94), stiffness Modulus (EN 12697-26) and permanent deformation resistance (NP 12967-22).

Two techniques were adopted in order to obtain the photocatalytic asphalt mixtures: spraying coating (after compaction) and bulk incorporation (during mix). The first one consisted of spraying at the surface of the asphalt sample an aqueous solution of nano-TiO₂ (4 g/L) at pH 8 with an atmospheric air compressor at a distance of about 20 cm during 30 s, being the speed of the aqueous solution jet set at 100 mL/min [7,8]. The substrate temperatures during spraying were: room temperature (RT), 60°C (both considering an application during the use of the pavements), 100°C and 140°C (both considering the application during paving and compaction). Three spraying ratios were evaluated: 4, 8 and 16 mL/cm², according to the last studies [7,8,80]. The second technique, by bulk incorporation, consisted of partially replacing the filler with 3% and 6% of TiO₂ in mass of the bitumen [7], without granulometric changes.

In order to assess the photocatalytic efficiency, small cylindrical samples (3.6 cm diameter and 1.0 cm height) were drilled from the prismatic slabs and then sprayed with the nano-TiO₂ aqueous solution, the lateral of the samples was covered with bitumen to eliminate the effect of the granulates cut on the photocatalytic efficiency test results.

The samples were identified by characters representing the type of functionalization, the percentage of TiO₂, the spraying rate, the temperature, the percentage of abrasion and the water simulation. The code of the samples starts by C, BI or SC to indicate the control samples, the

functionalized samples by bulk incorporation or the functionalized samples by spraying coating, respectively. Initially, the lateral of some samples was not covered with the bitumen. This situation is represented by WC (without covering). The samples that were submitted to wearing and water simulation are indicated by the percentage of abrasion (e.g. 0.5% means 0.5% of a superficial abrasion) and by W (water simulation), respectively. By bulk incorporation, the samples were composed by 3 and 6% of TiO₂, indicated by 3%T and 6%T, respectively. By spraying coating, the samples were functionalized at 3 rates, 4, 8 and 16 mL/cm², indicated by 4R, 8R and 16R. The four temperatures of the asphaltic substrate during the spraying: room temperature, 60, 100 and 140 °C, were identified by RT, 60, 100 and 140. For example, the sample SC_8R_140_1%_W was functionalized by spraying coating using the rate 8 mL/cm² at 140 °C and submitted to 1% of abrasion and also rain simulation. The photocatalytic efficiency was evaluated in all samples, however only samples C, BI_3%T and BI_6%T were evaluated through mechanical performance. Last studies showed that the Indirect Tensile Strength after water conditioning (ITSw) of functionalized samples was not affected by spraying coating [8].

6.3. Methods

6.3.1. Water Sensitivity

In order to analyze the moisture resistance of asphalt mixtures with and without nanoparticles, the Indirect Tensile Strength Ratio (ITSR) test was carried out. Following the standard EN 12697-12, two groups of each mixture is produced considering their volumetric properties.

One group of samples was immersed in water at 40 °C during 72 hours, the other one was kept out of the conditioning. After this process, all samples were placed in a chamber at 15 °C during 2 hours to test them under indirect tensile Strength. The ratio between the wet samples (ITSw) and the dry samples (ITSd) was calculated and defined as ITSR.

6.3.2. Permanent Deformation

The permanent deformation of the asphalt mixtures was assessed by the Wheel Tracking Test (WTT) (EN 12697-22). Therefore, for each mixture, two prismatic slabs (30 × 30 × 4.0 cm³) were tested up to 10,000 cycles of a 700 N wheel at 0.44 Hz and 60°C. The curve deformation versus cycle and the maximum rutting of the asphalt mixtures with and without TiO₂ will be compared.

6.3.3. Stiffness Modulus

This property, used for pavement design, was assessed by the four-point bending test configuration (EN 12697-26) for the frequencies 0.1, 0.2, 0.5, 1, 2, 5, 8 and 10 Hz at 20 °C. The graph Stiffness versus Frequency (Hz) of the asphalt mixtures with and without TiO₂ will be compared.

6.3.4. Fatigue Test

This test aimed to measure the capacity of the mixtures to resist to cyclic loading through the four-point bending test procedure (EN 12697-24). In this test, samples at 20 °C are submitted to sinusoidal loading at 10 Hz, in strain control. When the stiffness modulus of the asphalt mixture samples reaches half of their initial value, theoretically, fracture occurs and the test stops. The fatigue resistance of the sample corresponds to the number of loading cycles at the end of the test. The graph strain level versus number of cycles will be presented.

6.3.5. Photocatalytic Efficiency

The photocatalytic efficiency tests are based on the measurement of the degradation of Rhodamine B (RhB) as a function of time irradiation with an artificial sunlight [7,8]. Therefore, each asphalt mixture sample was inserted into a beaker and completely immersed with 20 mL of RhB aqueous solution (5 ppm). After 3 h in dark condition (adsorption), the samples were irradiated during 8 h a light (300 W - OSRAM UltraVitalux lamp, 11 W/m² measured by Quantum Photo Radiometer HD9021 Delta Padova).

All the beakers were closed with a transparent plastic film with at least 90% of transmittance in the wavelength range between 292 and 900 nm in order to avoid the evaporation of RhB. The photocatalytic efficiency (Equation (18)) was calculated using the Beer–Lambert law [7]. For this test, 3 samples were used and the average of the result will be presented.

$$\Phi (\%) = \left(\frac{A_0 - A}{A_0} \right) \times 100 \quad (18)$$

where Φ is the photocatalytic efficiency, A and A₀ represent the maximum absorbance of RhB (553 nm) solution for time “t” and 0 hour after irradiation, respectively, which were measured using a Shimadzu 3101 PC spectrophotometer.

6.3.6. Traffic simulation

To assess the impact of the traffic wearing, i.e. the semiconductors' removal by traffic, the tests were carried out before and after mechanical abrasion carried out homogeneously over the asphalt mixtures' surface using a metallic wire brush disc (at 450 rpm), conducting in different mass loss 0.5%, 1%, 2% [8].

6.3.7. Rain simulation

In order to estimate a possible semiconductors' removal by rain, the samples were submitted a water simulation with a flow of 100 mL/min during 5 hours. It was calculated based on the precipitation of Portugal, estimating in average one year of rain.

6.4. Results and Discussions

6.4.1. Performance of the Asphalt Mixtures

6.4.1.1. Water sensitivity

The results of ITS and water sensitivity (ITSR) of the asphalt mixtures composed by TiO_2 incorporated in volume are presented in Figure 28a (3.7% average air voids). The ITS and the ITSR were affected by the content of TiO_2 . The lowest content of TiO_2 (BI_3%T) led to lower values of these parameters, while the highest content (BI_3%T) led to higher ITS and lower ITSR. It can be concluded that the use of TiO_2 by bulk incorporation reduces the water resistance. However, all results of ITSR are higher than 80%, the minimum value requested for this parameter of the water sensitivity of asphalt mixtures in Portugal.

6.4.1.2. Permanent Deformation

The permanent deformation test has a high importance in countries with hot climate where this phenomenon manifests itself with large significance. The permanent deformation was affected by the content of TiO_2 (Figure 28b). On the one hand, the lowest content of TiO_2 (3%) conducted to a slightly higher deformation (7.5 mm) than the conventional mixture (6.8 mm). On the other hand, the highest content of TiO_2 (6%) conducted to better results of this parameter (4.95 mm), reducing the permanent deformation.

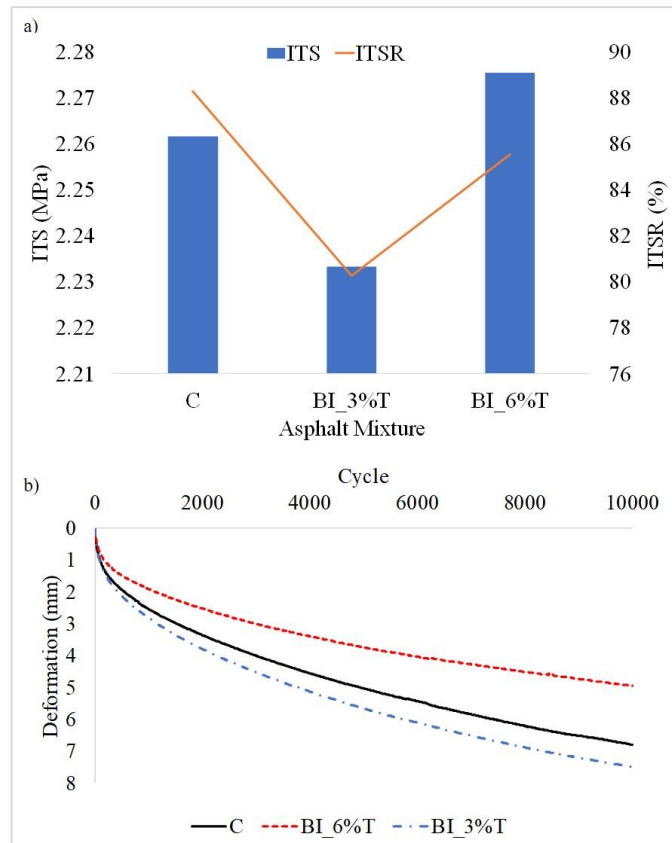


Figure 28: a) Water Sensitivity; b) Permanent Deformation Results [9]

6.4.1.3. Stiffness Modulus

The stiffness of the asphalt mixture was also influenced by the content of TiO_2 (Figure 29a). While the lowest content of TiO_2 (3%) conducted to a lower stiffness than the conventional mixture, the highest content (6%) conducted to similar stiffness moduli. This performance is in accordance with the results found the permanent deformation.

6.4.1.4. Fatigue Resistance

Figure 29b presents the fatigue curve (number of cycle versus applied strain) determined for the 3 asphalt mixtures. Good determination coefficients (R^2) were achieved, higher than 0.85. The asphalt mixture composed by 3% of nano- TiO_2 had the same behaviour as the conventional asphalt mixture, the fatigue curves are overlapped. The fatigue resistance of the asphalt mixture was affected only when 6% of nano- TiO_2 was used, reducing the fatigue resistance under very low strain, as can be seen the higher slope.

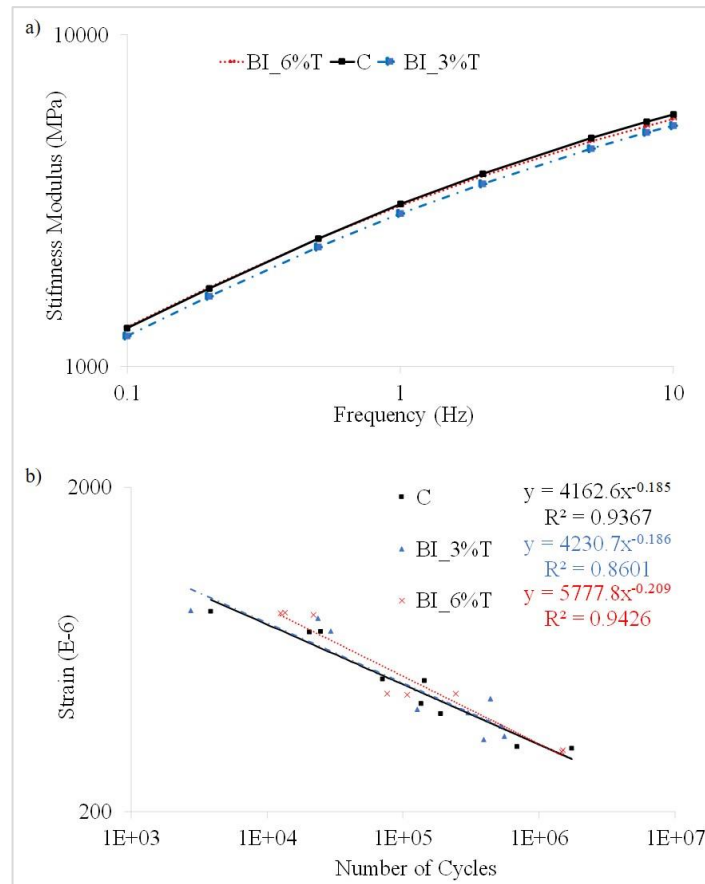


Figure 29: a) Stiffness Modulus; b) Fatigue Resistance [9]

6.4.2. Photocatalytic Efficiency

6.4.2.1. Evaluation of Substrate Temperature During Application

Figure 30 illustrates the dependence of the substrate temperatures (RT, 60°C, 100°C and 140°C) on the photocatalytic efficiency of the samples functionalized with TiO₂ by spraying. There was no substantial difference in the photocatalytic performance of the samples at different temperatures.

The results obtained for the samples with lateral surfaces not covered with bitumen (Figure 30a), suggest the increase of the photocatalytic efficiency due to the contact of the aggregates with RhB dye solution and exposed to light. The same situation, but with the sample's laterals covered with bitumen lead to a decrease of the photocatalytic efficiency (Figure 30b). After covering the laterals of the control samples, it decreased 29%. In average, a reduction of 17% was found for the functionalized samples. Thus, in order to eliminate the lateral effect of the exposed aggregates, all the experiments were carried

out with samples covered with bitumen, except in their superior faces (i.e. the functionalized faces). In this sense, the selection of aggregates seems important since their constitution can facilitate the photocatalytic process together with TiO_2 mainly for oil/grease degradation in order to reduce road accidents caused by contamination of these materials.

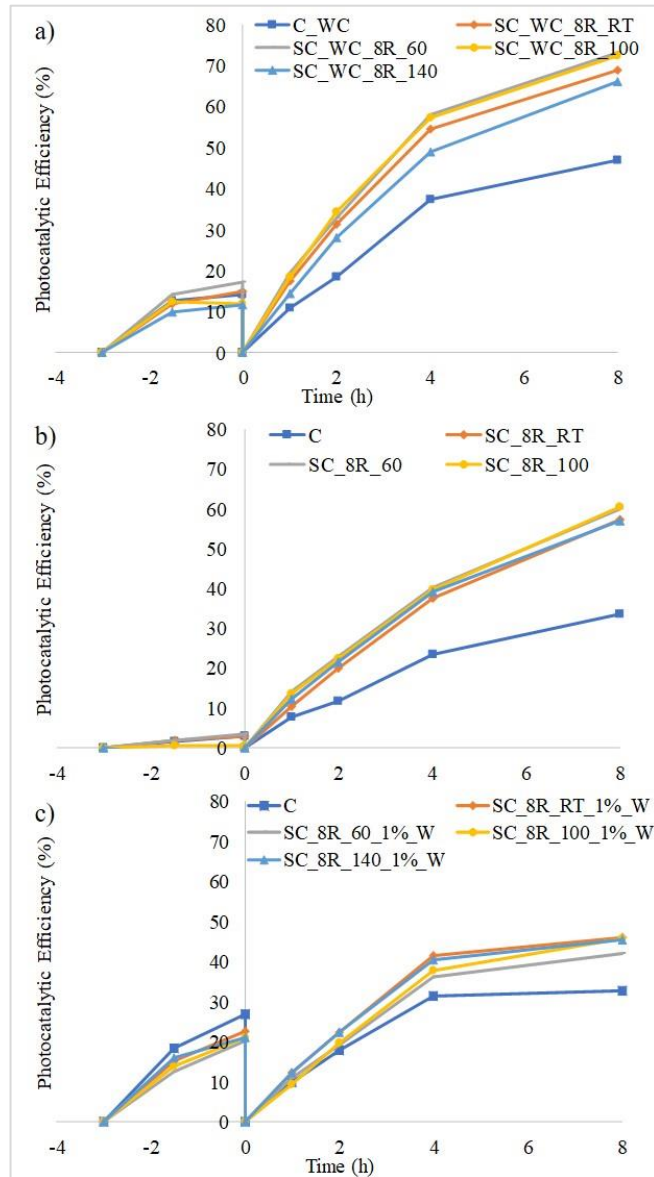


Figure 30: Photocatalytic Efficiency for Different Temperatures: a) before abrasion and without lateral covering; b) before abrasion and with lateral covering; c) after 1% superficial abrasion and rain simulation [9]

After the abrasion and weathering processes with 1% of superficial abrasion, this trend was the same (Figure 30c). However, in this case there was a decrease of about 10% on the photocatalytic efficiency compared to the samples that did not undergo the abrasion process, which probably is related to the removal of photocatalytic materials on the coated surfaces. From these results, it can be concluded that under the severe abrasion and the rain simulation processes, the functionalization of the pavements at room temperature is feasible. Therefore, the spraying technique may be applied at any time of the pavement life, including construction and use. Also, the reapplication of the technique is possible after the removal of the nanomaterials.

6.4.2.2. Evaluation of substrate spraying rate

To evaluate the spraying ratio effect, three rates were selected and applied at room temperature: 4, 8 and 16 mL/cm². Prior to abrasion process, the most effective rates were 8 and 16 mL/cm² which lead to a photocatalytic efficiency of about 60% (Figure 31a). Under abrasion of 0.125%, the best rates were in ascending order: 4; 8; 16 mL/cm² (Figure 31b). After rain simulation, also the most effective rates were 8 and 16 mL/cm² (Figure 31c). The other tests were carried out using the intermediate rate (8 mL/cm²) due to the similarity under rain simulation and before abrasion. Also, the rate uses half of the volume per cm², being more economic than the rate of 16 mL/cm².

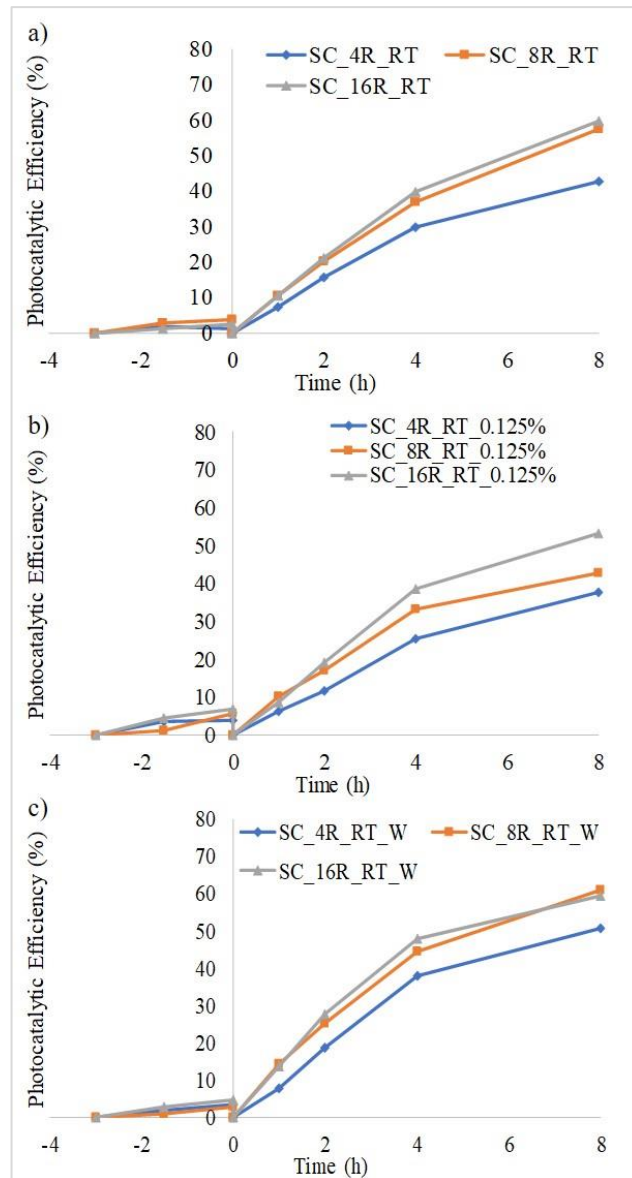


Figure 31: Photocatalytic Efficiency for Different Spraying Rates: a) before abrasion; b) after 0.125% of a superficial abrasion; c) after rain simulation [9]

6.4.2.3. Study of the fixation of the nanomaterials

The study of the fixation was carried out for 6 situations (Figure 32): a) before abrasion; b) after water simulation; c) with 0.5% of a superficial abrasion; d) with 0.5% of superficial abrasion and after rain simulation; e) with 2% of superficial abrasion; and f) with 2% of superficial abrasion and after rain simulation.

The photocatalytic efficiency was much higher for the spraying coating than the functionalization by bulk incorporation before abrasion (Figure 32a and b). Probably the low efficiency of these samples functionalized by bulk incorporation was due to the low content of TiO_2 over the surface (i.e. exposed to the light) and also because the superficial bitumen film covers the nanoparticles.

However, after the superficial abrasion, the photocatalytic efficiency of the sprayed samples decreases in opposition to the bulk incorporation process (Figure 32c-f). For example, the photocatalytic efficiency of BI_3%T increased from 32% (Figure 32a) to about 40% and 55% with 0.5% and 2% of abrasion, respectively (Figure 32c and e). For the BI_6%T, it was registered an increase of 4% and 41% under the same levels of abrasion. After the abrasion, the TiO_2 applied by the spraying technique was removed from the surface while by bulk incorporation it is more exposed. This effect is more important for higher levels of abrasion. In view of this, it is essential to evaluate the impact of the abrasion on photocatalytic materials which will be submitted to this process in their lifetime.

Contrarily to the expectations, which were the achievement of better results for higher percentages of nano- TiO_2 , for bulk incorporation, the highest photocatalytic efficiency was found for the samples with lower content of TiO_2 (BI_3%T). A possible explanation is that higher percentages can result in photocatalytic particle's agglomeration, thereby decreasing its surface area and consequently the photocatalytic efficiency. Additionally, the photocatalytic efficiency was not affected under rain simulation (Figure 32b, d and f). Also, the spraying coating technique leads to a very high photocatalytic efficiency, including under the rain simulation. However, when this process is preceded by abrasion, the TiO_2 nanoparticles are removed leading to lower efficiency. Therefore, the impact of rain simulation is very reduced since it did not remove the particles.

In practice, road pavements are submitted to traffic abrasion mostly the wheel tracks and also by weathering. The other areas of the traffic lanes and also the shoulders are mostly submitted to weathering. Taking into account the low impact on photocatalytic efficiency of the rain, it is expected a high performance of both techniques on field since the area submitted to the abrasion is significantly lower than the total area of the pavement.

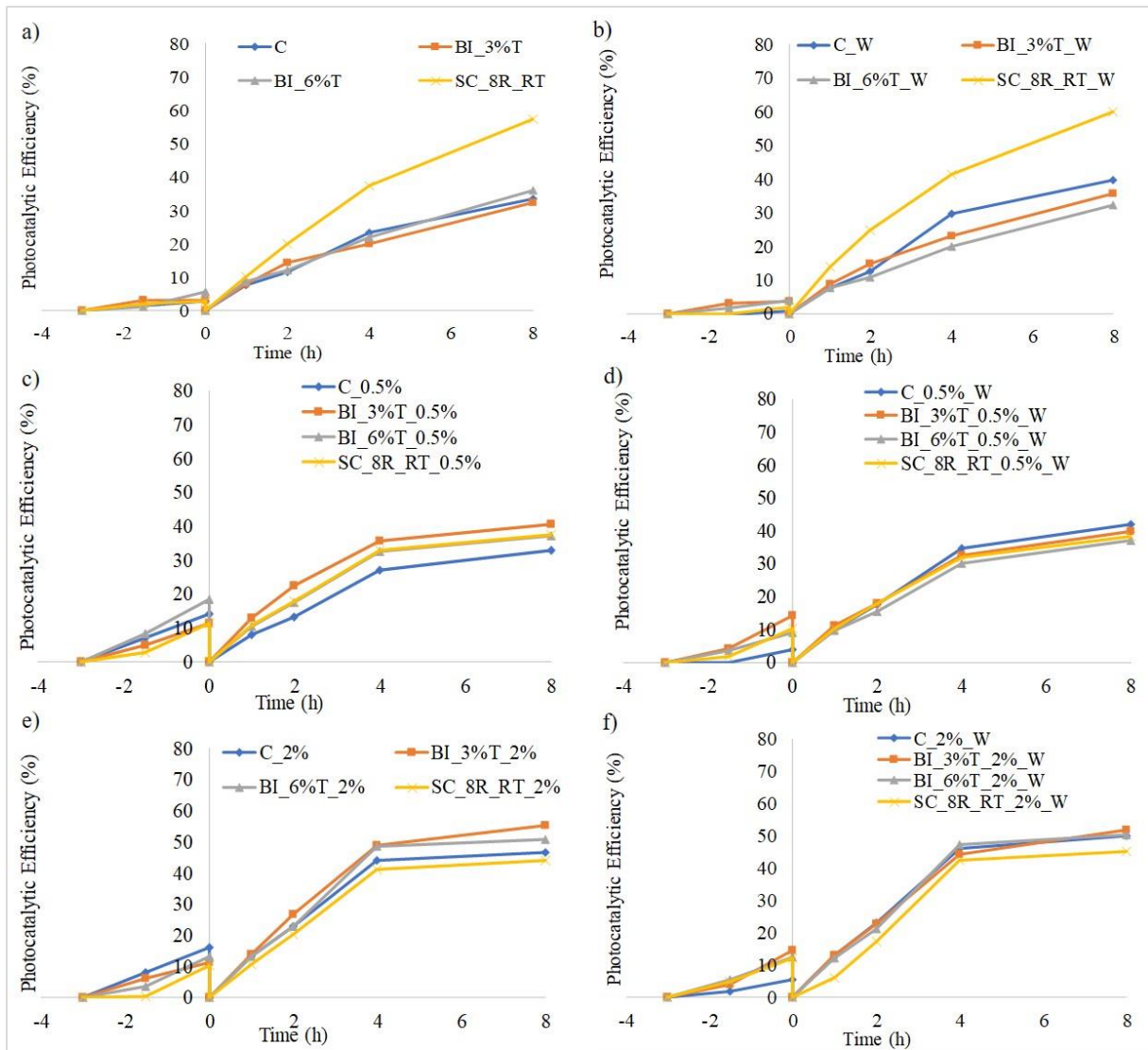


Figure 32: Photocatalytic Efficiency: a) before abrasion; b) after rain simulation; c) after 0.5% of a superficial abrasion; d) after 0.5% of a superficial abrasion and rain simulation; e) after 2% of superficial abrasion; f) after 2% of superficial abrasion and rain simulation [9]

6.5. Conclusions

The aim of this research was the analysis of the impact of photocatalytic asphalt mixtures functionalized by bulk incorporation on mechanical performance and by both bulk incorporation and spraying coating on photocatalytic efficiency considering the following factors: application temperature, traffic (wearing) and climate (weathering). Based on the results of this research, the following conclusions can be drawn:

- The mechanical impact of the bulk incorporation of nano-TiO₂ was mostly affected only in the moisture sensitivity. This property was reduced but respected the limit by the Portuguese specification for top layer asphalt mixtures. On one hand, the higher content of TiO₂ (6%) improved the permanent deformation, had similar results of stiffness modulus and reduced the fatigue resistance under very low strain, when compared with the conventional mixture. On the other hand, the lower content of nano-TiO₂ (3%) had a slightly higher permanent deformation, conducted to a lower stiffness, but remained the fatigue resistance, when compared with the conventional mixture.
- The granitic nature of the aggregates provided an increase of the photocatalytic efficiency. Thus, the selection of aggregates is important since it can improve the photocatalytic process together with TiO₂.
- The temperature of the substrate had no influence on the photocatalytic results before the abrasion process and after the high abrasive wearing conducted in this research. Therefore, the coating technique can be used at the construction or paving phase and also at any time of the pavement's use.
- The most effective spraying rates were 8 and 16 mL/cm² before the abrasion and after water simulation. Under abrasion of 0.125%, the best rates were in ascending order 4 mL/cm² < 8 mL/cm² < 16 mL/cm².
- The photocatalytic efficiency was much higher for the spraying coating than the functionalization by bulk incorporation before abrasion. The low efficiency by bulk incorporation was probably due to the low content of TiO₂ over the surface of samples.
- Only under water simulation, the photocatalytic efficiency was not affected. The spraying coating has a very high photocatalytic efficiency including after this process.
- After abrasion, the photocatalytic efficiency of sprayed samples was highly reduced, while for bulk incorporation samples it increased with the level of abrasion.
- The rain simulation in combination with abrasion washes the surface, removing the nanoparticles which were not immobilized.

In this work the main methodological issue was the simulation of the traffic wearing through an abrasion process. For big samples there are some recognized wearing techniques, however for small samples a traffic wearing procedure needs to be developed and validated. Nevertheless, the procedure adopted for this study seemed adequate and provided good results.

With these results seems acceptable to forecast a good performance of the photocatalytic road surfaces on field. The surface of road pavements is submitted to traffic wearing mostly in the wheel tracks. It represents a reduced percentage of the total area of the surface. In view of the low effect of rain on the photocatalytic efficiency, it is expected a good performance of the spraying coating technique, less expensive. The ideal solution would be the combination of both techniques, with negligible impact on mechanical performance, however it requires a cost-benefit analysis.

CHAPTER 7 – FUNCTIONAL IMPACTS OF FUNCTIONALIZED ASPHALT MIXTURES

This chapter refers to the research work about photocatalytic, superhydrophobic and self-cleaning asphalt mixtures “Photocatalytic asphalt mixtures: semiconductors’ impact in skid resistance and texture” published in *Journal Road Materials and Pavement Design* (impact factor – if – 3.792) (Figure 33). The main goal of the Chapter 7 was to analyze the functional impacts of the functionalization process. Also, both functionalization processes (spraying coating and volume incorporation) were carried out and compared here. The content of this chapter is included in the article, which DOI 10.1080/14680629.2019.1624398.

Road Materials and Pavement Design, 2019
<https://doi.org/10.1080/14680629.2019.1624398>



Photocatalytic asphalt mixtures: semiconductors’ impact in skid resistance and texture

I. Rocha Segundo ^{a,b,c}, S. Landi Jr. ^{b,c}, S. Oliveira^a, E. Freitas ^d, M.F. Costa ^b and J. Carneiro ^b

^aCivil Engineering Department, University of Minho, Azurém Campus, Guimarães, Portugal; ^bCentre of Physics, University of Minho Portugal, Azurém Campus, Guimarães, Portugal ^cFederal Institute Goiano, Rio Verde, Brazil

Photocatalytic asphalt mixtures have the capability of mitigating air quality problems and degrade oils/greases by using semiconductors. The techniques to do so can change their functional characteristics. This study aimed to analyse the functionalization effect on the essential surface characteristics, such as macrotexture, skid resistance, and microtexture. AC 14 and AC 6 mixtures were functionalised with nano-TiO₂ and micro-ZnO by spraying and bulk incorporation. Mean Profile Depth, British Pendulum and microtexture amplitude parameters were evaluated. TiO₂ application seemed to smooth the surface slightly. In dry condition, the skid resistance of functionalised asphalt and control mixtures was similar. In wet condition, the functionalization caused a maximum decrease of 7% in skid resistance. The amplitude parameters were not affected by any functionalization technique except the skewness of AC 14 with 6% TiO₂ by bulk incorporation. Furthermore, the application of the semiconductors can be used without high impacts in texture and skid resistance.

Keywords: photocatalytic asphalt mixtures; macrotexture; microtexture; skid resistance; optical non-contact rugometric characterisation

Introduction

Functionalization is the development of capabilities for materials, different from the essential ones, usually related to the surface. Implemented by semiconductors, such as TiO₂ and ZnO, photocatalytic and self-cleaning asphalt pavements can decrease the atmospheric concentration of gases NO_x and SO₂, mitigating air pollution (Dylla, Asadi, Hassan, & Mohammad, 2013; Tang, Liu, Huang, & Cao, 2017). Moreover, these materials can, by the self-cleaning property, degrade organic compounds, such as oils and greases, removing them from the surface to have safer roads (Rocha Segundo, Ferreira, et al., 2018). This is possible by the heterogeneous photocatalytic process, which results from the absorption of photons with energy equal to or greater than the band gap of the semiconductor, exciting the electrons, which go from the valence band to the conduction band. This migration generates an electron/hole pair (e⁻/h⁺). This pair, e⁻ and h⁺, provides oxidation–reduction reactions, forming respectively hydroxyl (HO*) and superoxides (O₂⁻) radicals in the presence of water and oxygen molecule. They react with the pollutants presented over the surface, degrading them (Dalton et al., 2002; Heller, 1995).

In general, three approaches have been carried out to develop photocatalytic asphalt pavements: (i) spraying deposition; (ii) bulk incorporation, (iii) bitumen modification (Cao, Yang, Li, Huang, & Liu, 2017; Carneiro et al., 2013; Hassan, Dylla, Asadi, Mohammad, & Cooper, 2012).

*Corresponding author. Email: iran_gomes@hotmail.com

© 2019 Informa UK Limited, trading as Taylor & Francis Group

Figure 33: First page of the research work published in *Catalysis Today*

7.1. Introduction

This chapter aimed to analyze the impact of the semiconductors on functional characteristics, such as skid resistance and texture. For this, two asphalt mixtures AC 6 and AC 14 were evaluated. Both were functionalized by spraying coating and one of them, AC 14, was also functionalized by bulk incorporation. Macrotexture, microtexture and skid resistance tests were carried out.

7.2. Materials and Methods

7.2.1. Materials

In this research, two asphalt mixtures were evaluated: AC 14 Surf 35/50 and AC 6 Surf Elaster 13/60, composed of 5% and 6% of binder, respectively. The aggregate composition of the mixtures was:

- AC 6 - limestone filler, 3%; 0/4 mm, 25% and 4/6 mm, 72%;
- AC 14 - limestone filler, 3%; 0/4 mm, 41%; 4/8 mm, 12% and 6/14mm, 44%.

The photocatalytic and self-cleaning properties were provided to the asphalt mixtures by spraying for AC 14 and AC 6; and bulk incorporation for AC 14. By spraying, an aqueous solution of nano-TiO₂ (4 g/L) and/or micro-ZnO (1 g/L) with pH 8 was sprayed over the AC 6 and AC 14 mixtures at 60 °C, covering the rate of 5 mg/cm² to 12.5 mg/cm². By bulk incorporation, the functionalization was achieved by partially replacing the filler with 3% and 6% of TiO₂ in mass of the bitumen, resulting in 2.84% and 2.68% of limestone filler respectively. This procedure was the same as those carried out on the last researches [8,9]. The designation of the conventional asphalt mixtures was AC 14 and AC 6. For those ones functionalized by bulk incorporation, it was AC 14 3% and AC 14 6% considering the content of TiO₂, 3 and 6%, respectively. Finally, those ones functionalized by spraying coating were named AC 14 TiO₂, AC 14 ZnO, AC 14 TiO₂ ZnO, AC 6 TiO₂, AC 6 ZnO, AC 6 TiO₂ ZnO, considering each treatment over the asphalt mixtures.

Table 8 identifies the mixtures selected for this research, how the semiconductors were applied, the Maximum Bulk Density (MBD) and the Void Content (VC) of the mixes.

Table 8: Properties of Asphalt Mixes

Asphalt mix	Semiconductors	Technique	MBD (g/cm ³)	VC (%)
AC 6	TiO ₂ and/or ZnO	Spraying	2.423	10.9
AC 14	TiO ₂ and/or ZnO	Spraying	2.426	4.4
AC 14 3%	3% TiO ₂	Bulk incorporation	2.377	3.8
AC 14 6%	6% TiO ₂	Bulk incorporation	2.356	4.4

7.2.2. Methods

The tests selected were skid resistance, microtexture, and macrotexture. Skid resistance and microtexture tests were carried out in all the mixtures. The macrotexture was assessed only in the mixtures without semiconductors and also in the mixtures functionalized by bulk incorporation since the application of the nano/micromaterials by spraying coating does not affect the macrotexture due to their very lower scale. All the tests were carried out before abrasion.

7.2.2.1. Macrotexture

To measure the macrotexture of the asphalt mixtures, profiles of their surfaces were acquired by a device equipped with a laser, and the Mean Profile Depth was calculated. This device allows determining with precision profiles of slabs with a surface of 25x25 cm², recording x, y, and z positions. It can acquire profiles every 0.2 mm with a vertical resolution up to 0.01 mm. The MPD was calculated in each profile for a 10 cm baseline. The baseline of the profiles is divided by half of the length, and the average of their two peak heights is used to calculate the MPD (Equation (19)).

$$MPD = \frac{1st\ Peak + 2nd\ peak}{2} - average\ level \quad (19)$$

7.2.2.2. Skid resistance

To access the skid resistance of the mixtures before and after the application of the semiconductors, Pendulum tests were carried out (EN 13036-4). This test is one of the most popular procedures to determine skid resistance and is widely used to analyse small samples of asphalt mixtures in the laboratory and also highway pavements in some situations. For highways, this test is still used due to the low cost and ease of operation [169].

7.2.2.3. Microtexture

To measure the microtexture, an optical microtopographer was used. With large measuring range, high versatility, robustness and reliability, good accuracy and resolution, the MICROTOP.06.MFC microtopographer (Figure 34) was used to inspect a wide range of surface types [170], including asphalt mixtures [171]. The system is based on discreet active triangulation. Basically, in this sensor, a beam of light shines on the surface at some angle, and the reflected light is collected at another angle.

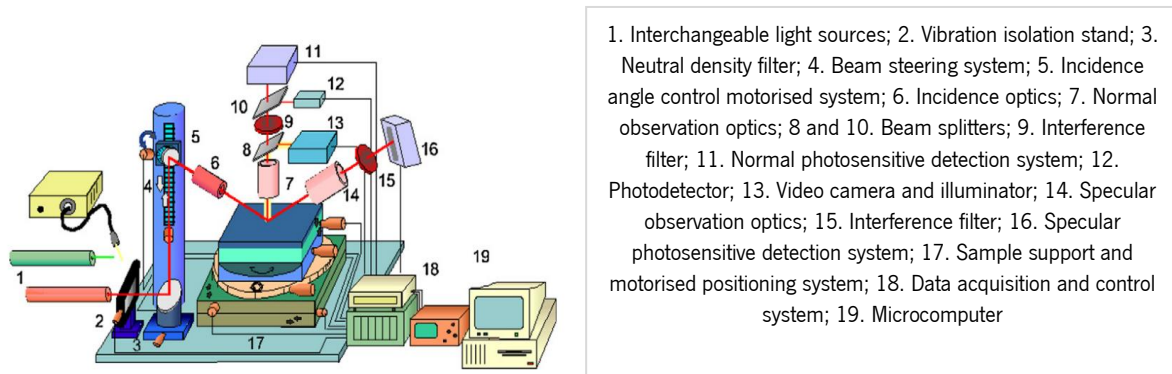


Figure 34: The MICROTOP.06.MFC [170]

The surface is scanned by an oblique light beam. The incident light is collimated and focused. A small, diffraction limited, bright spot is thus projected onto the surface. The bright spot is imaged both perpendicularly and specularly onto electronic photosensitive detection systems to assess its lateral position. The point-by-point scanning of the sample is carried out by the movement of a precision XYZ displacement on a rectangular array separated by distances down to 1.25 μm . By triangulation sensing of the reflected light at each scanning position, a full 3D inspection of the sample is achieved.

7.2.3. Testing set up and analysis

The macrotexture of each mixture was calculated by averaging the MPD of all profiles. The skid resistance test was carried out in wet and dry conditions at five different temperatures, resulting in 100 Pendulum tests. For the wet procedure, the water and the pavement were conditioned at the same temperature, which made possible the control of the system's temperature. This procedure was carried out to analyse whether the presence of the semiconductors could change skid resistance.

The microtexture of the surfaces of each asphalt mixture slab was acquired in 9 selected squares with 1 cm^2 . In each square, a silicone cast was applied to have a high-fidelity replica of the microtexture.

This material is composed of white liquid silica rubber and a catalyst that allows the hardening in some minutes. Its removal is easy and non-invasive. In total, 90 silicone casts were done to carry out the microtopography measurement within an area of 4 mm². This procedure was carried out due to the colour of the asphalt mixtures, naturally black, which affects the measurements due to light diffusion during the acquisition. With the use of the white silicone replicas, this measurement problem is prevented since the diffusion of the red light (632.8nm) into the silicone replica is low [172]. Also, it is clean and avoids the placement of large slabs of asphalt mixtures into the device.

The main roughness parameters calculated were: Arithmetic Mean Deviation of the Surface (Sa), Root-mean-square Deviation of the Surface (Sq), Total Height of the Surface (St), Maximum Peak Height of the Surface (Sp), Maximum Valley Depth of the Surface (Sv), Ten-point Height roughness of the Surface (Sz), Skewness (Ssk), Kurtosis (Sku). The parameters Sa and Sq were used to quantify significant deviations of textures. The symmetry of peaks and valleys of the surface about the average surface is established for $Ssk = 0$: normal distribution, that is, symmetry about the average line; $Ssk < 0$: predominance of valleys (negative texture); and $Ssk > 0$: indicates a higher number of peaks (positive texture). The Kurtosis (Sku) characterizes the presence of extremely deep valleys/high peaks for $Sku = 3$: normal distribution; $Sku > 3$: extremely deep valleys/high peaks; and $Sku < 3$: lack of them.

Analysis of variance (ANOVA), considering as factors mixture and treatment, was carried out to determine whether there was an interaction effect between the independent variables (Sa, Sq, St, Sp, Sv, Sz, Ssk and Sku) over the parameters for a significance level of $(1 - \alpha = 0.1)$. Bonferroni Post-Hoc analysis was also carried out to find patterns between subgroups by testing if there was a significant difference in the average of the parameters between samples. Figure 35 shows the flow chart of this study in order to facilitate understanding.

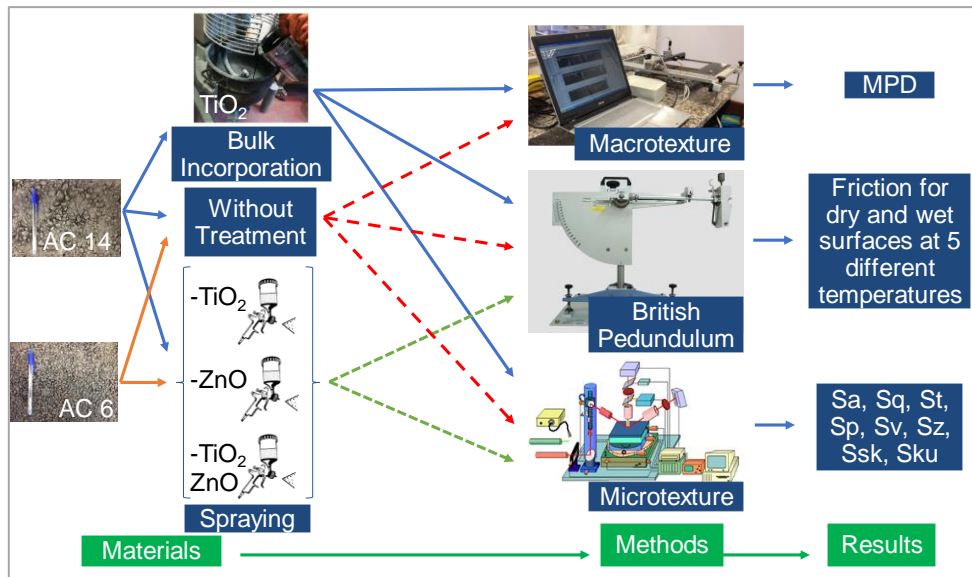


Figure 35: Flow Chart of this Study

7.3. Results

7.3.1. Macrotexture

Table 9 shows the macrotexture results. Explained by their formulation, the AC 6 was 21% rougher than the AC 14. The functionalization by bulk incorporation did not affect the macrotexture of the asphalt mixtures greatly. Both mixtures with TiO₂, independently to the content of nanomaterial, had similar MPD. However, when compared with the control mixture (AC14), the incorporation of TiO₂ seems to have affected the surface by smoothing it on average 7%.

Table 9: Macrotexture Results

Mixture	MPD (mm)
AC 6	0.85
AC 14	0.70
AC 14 3%	0.66
AC 14 6%	0.64

7.3.2. Skid resistance

Figure 36 shows the skid resistance versus temperature and Table 10 shows the linear regression fit parameters for each material (results in Pendulum Test Value – PTV).

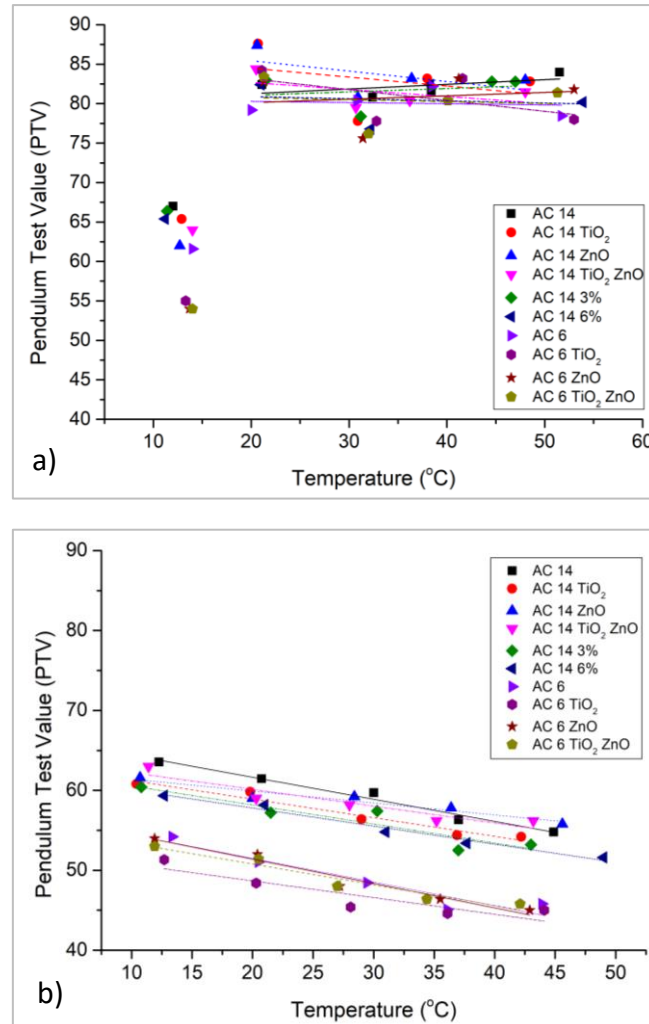


Figure 36: Results of Pendulum Test: a) Dry Condition and b) Wet Condition

In dry condition, the skid resistance of functionalized asphalt mixtures was similar to those without treatment. The AC 6 showed PTV values 2% lower than the AC 14, except for the lowest temperature. At the lowest temperature (10 °C), the surface got probably wet by water that condensed during the conditioning procedure, reducing the PTV value to those similar to the wet condition. Due to this, the results of the lowest temperature were removed from the linear trends for the dry condition. Moreover, R² values were lower than 0.35, indicating a low sensitivity of PTV to temperature variation.

In wet condition, the application of semiconductors on AC 14 did not have a pronounced impact on skid resistance. Furthermore, the trend lines of the AC 6 almost overlapped, except for AC 6 TiO₂. For both mixtures, after spraying, the minimum and maximum differences in PTV ranged between -6% (TiO₂ at 29 °C) and 3% (ZnO at 36 °C and TiO₂ ZnO at 43 °C). For bulk incorporation, the minimum and maximum differences in PTV were -7% (AC 14 3% at 22 °C) and 2% (AC 14 6% at 38 °C).

Table 10: Linear Trend Equations for Skid Resistance

Mixture	Dry Surface		Wet Surface	
	Linear Trend Equation	R ²	Linear Trend Equation	R ²
AC 6	PTV = -0.015T + 80.591	0.015	PTV = -0.296T + 57.405	0.907
AC 6 TiO ₂	PTV = -0.137T + 85.900	0.302	PTV = -0.208T + 52.838	0.813
AC 6 ZnO	PTV = 0.043T + 79.261	0.027	PTV = -0.305T + 57.490	0.958
AC 6 TiO ₂ ZnO	PTV = -0.025T + 81.246	0.011	PTV = -0.259T + 55.974	0.937
AC 14	PTV = 0.059T + 80.074	0.302	PTV = -0.277T + 67.182	0.978
AC 14 TiO ₂	PTV = -0.114T + 86.779	0.111	PTV = -0.233T + 63.555	0.958
AC 14 ZnO	PTV = -0.132T + 88.084	0.299	PTV = -0.149T + 62.891	0.921
AC 14 TiO ₂ ZnO	PTV = -0.089T + 84.458	0.228	PTV = -0.211T + 64.341	0.879
AC 14 3%	PTV = 0.043T + 80.189	0.053	PTV = -0.238T + 62.923	0.857
AC 14 6%	PTV = -0.027T + 81.439	0.020	PTV = -0.193T + 61.021	0.936

PTV = Pendulum Test Value for Skid Resistance and T = temperature (°C)

To summarize, for the spraying technique the maximum absolute difference was 6%, corresponding to a decrease from 48 to 45 PTV. For bulk incorporation, the maximum absolute difference was 7%, corresponding to a decrease from 61 to 57 PTV. The AC 6 mixture had on average a skid resistance 16% lower than the AC 14 mixture. This result indicates that skid resistance is higher for mixtures with higher nominal maximum aggregate size, according to results for asphalt concretes [173].

A linear trend of PTV and temperature was established with R² higher than 0.80, nevertheless lower for the AC 6 mixture. The skid resistance decreased with temperature which is according to literature results for conventional mixtures [174].

Considering all conditions, the linear trend of PTV and temperature (T) for the AC 14 and AC 6 resulted in Equations (20) and (21) with R² equals to 0,766 and 0.833, respectively. The lower slope of the AC 14 (-0.224) compared to the AC 6 (-0.268) shows that AC 6 was more sensitive to temperature.

The factor type of surface proved to be important when the pavement was wet. Also, the functionalized mixtures were less sensitive to the temperature than control mixtures, reporting a lower slope, except for AC 6 ZnO.

$$PTV_{AC14} = -0.224T + 63.195 \quad (20)$$

$$PTV_{AC6} = -0.268T + 55.937 \quad (21)$$

In conclusion, there is no change of skid resistance with temperature after the addition of the semiconductors when applied by spraying an aqueous solution or bulk incorporation. AC 6 was less influenced by the semiconductors when sprayed, which may have resulted from the higher porosity of the mixture. Also, either in dry or wet condition, the semiconductors did not cause a high impact in the skid resistance of the asphalt mixtures. This is important since the promotion of the new capacity did not cause a big impact on the most important functional characteristic of the pavement surfaces analysed.

7.3.3. Microtexture

Figure 37 shows the results of the microtexture assessment for the following parameters: Sa, Sq (both related to surface deviations), St (total height of the surface), Sp (maximum peak height of the surface), Sv (maximum valley depth of the surface) and Sz (ten-point height of the surface). In Figure 38 are shown the results of Ssk (symmetry) and Sku (presence of extremely deep valleys/high peaks).

The results of the roughness parameters are characterized by a large dispersion. In general, the results of AC 6 were more dispersed than the ones of AC 14. As the aggregates are smaller for AC 6, it may have influenced the sampling process.

For symmetry, the results show a normal distribution for most of the materials ($Sku = 3$, included between the first and third quartiles), except for AC 14 TiO_2 , AC 14 TiO_2 ZnO and AC 14 6%. These three mixture combinations have the first quartile higher than 3, identifying extremely deep valleys/high peaks. Regarding the skewness (Ssk), the mixtures had the first quartile higher than 0, excluding AC 14 6% and AC 6 TiO_2 , indicating only positive values, thus all of them conducting to a positive microtexture, and AC 14 6% and AC 6 TiO_2 , with a negative first quartile and positive third quartile (normal distribution).

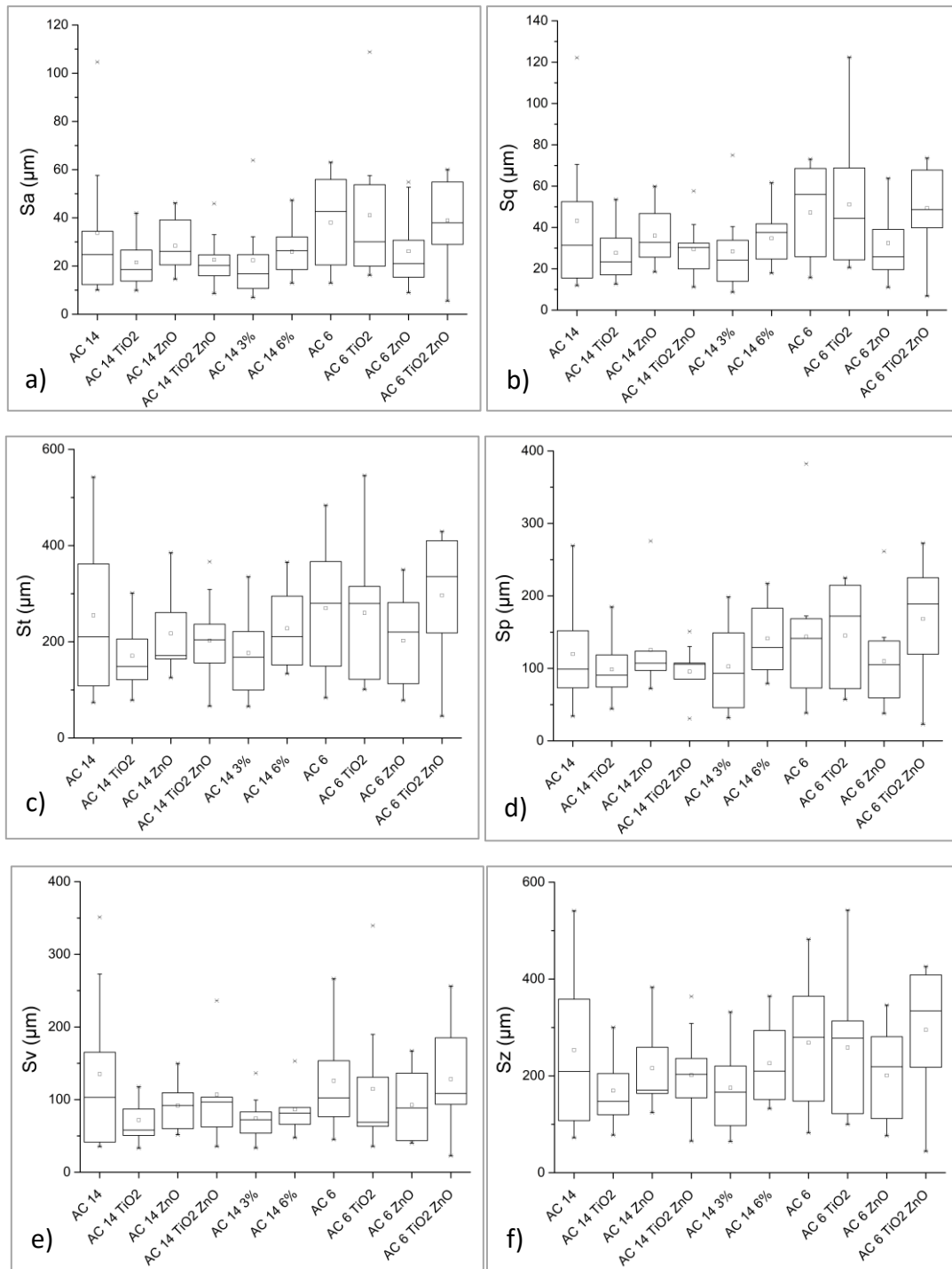


Figure 37: Microtexture Results: a) Sa, b) Sq, c) St, d) Sp, e) Sv and f) Sz

The analysis of the factors influencing the microtexture parameters by ANOVA shows, on the one hand, that the independent variable Mixture had a significant influence on Sa, Sq, Sp, St and Sz ($p < 0.1$). On the other hand, the variable Treatment had a significant effect only on skewness (Ssk). The interaction of Mixture and Treatment variables had no significant effect on the dependent variables results.

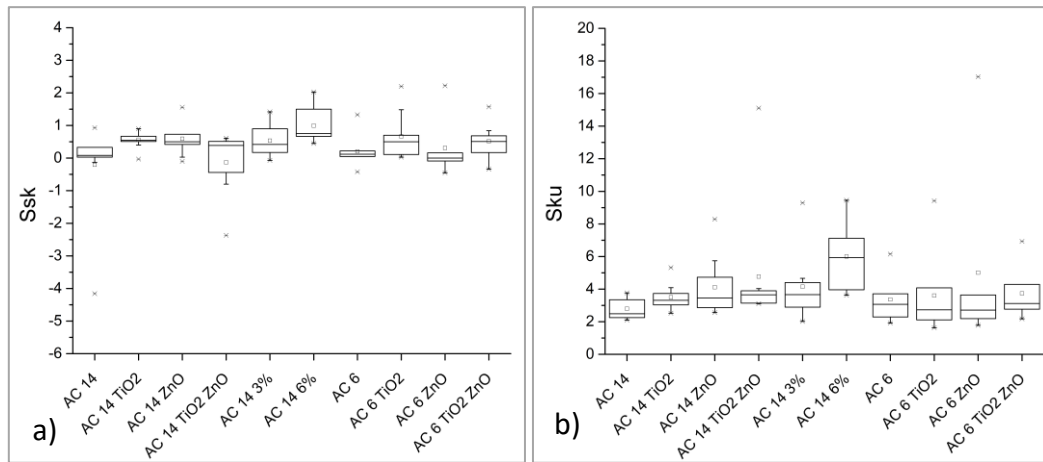


Figure 38: Microtexture Results: a) Ssk and b) Sku

The Bonferroni Post-Hoc test for a level of significance ($1 - \alpha = 0.1$) was carried out as well. The averages of Sa, Sq, St, Sp, Sz for the AC 6 samples were significantly higher than for the AC 14 samples ($p < 0.1$). Moreover, AC 6 microtexture deviation was higher ($> Sa$ and Sq) and was characterized by higher total height ($> St$), peaks ($> Sp$), valleys ($> Sv$) and ten-point heights ($> Sz$) than AC 14.

Therefore, the mixture with smaller aggregate size provided the roughest microtexture. However, it did not correspond to the mixture with the highest skid resistance. This relationship could be a consequence of the larger contact area offered by the AC14.

For the different treatments, the PostHoc test carried out showed just one difference on the average of the independent variables. The average of the skewness (Ssk) for the AC 14 6% was significantly lower than for the AC 14 ($p < 0.1$).

As final remarks, the asphalt mixture type was a significant factor for the microtexture characterization, and the functionalization had a low impact in this characteristic.

7.4. Conclusions

This research aimed to analyse the skid resistance and the texture of different asphalt mixtures after functionalization by spraying and bulk incorporation. This is one of the first researches contributing to the analysis of the functional characteristics, namely macro/microtexture and skid resistance, of functionalized asphalt mixtures.

When new capabilities are developed, it is important to assess these characteristics to guarantee road safety. The results of the experimental activity led to the following conclusions:

- For the macrotexture, the AC 6 was 21% rougher than the AC 14, that bulk incorporation of TiO_2 , may have slightly smoothed the surface.
- For skid resistance, in the dry condition, the asphalt mixtures had similar skid resistance independently of the temperature.
- For skid resistance, in wet condition, the surface type and temperature showed to be important factors. AC 6 had a PTV 16% lower than the AC 14 mixture and was also more sensitive to temperature changes, indicating that skid resistance is higher for mixtures with higher nominal maximum aggregate size and lower temperatures.
- Also in wet condition, the functionalization by spraying conducted to a difference in PTV between -6% (TiO_2 at 29 °C) and 3% (ZnO at 36 °C and TiO_2 ZnO at 43 °C). By bulk incorporation, this interval was between -7% (AC 14 3% at 22 °C) and 2% (AC 14 6% at 38 °C). Therefore, the maximum absolute difference was 7%, corresponding to a decrease of 4 PTV.
- For microtexture, only Sa, Sq, Sp, St, and Sz had a significant influence the asphalt from the mixture type with significantly higher averages for the AC 6. AC 6 also had more dispersed microtexture, higher peaks and ten-point heights than AC 14. It can be justified by the microtexture assessment for AC 14, which was carried out also over fine aggregates bonded with a binder, conducting to a smoother surface. Only the average of the parameter Ssk of the AC 14 6% was significantly lower than the AC 14 samples ($p < 0.1$).

In conclusion, in general, the treatments did not affect the amplitude parameters of microtexture. Thereby, the functionalization had a low impact on skid resistance and texture, allowing the application of the semiconductors by bulk incorporation and spraying. Road safety is in this way assured for the study conditions.

Although the goals of this research were achieved, it is important to carry out this kind of analysis in more and larger samples, since the microtexture is a very small surface area and skid resistance could be measured with other techniques. In addition, the next step of this research is the assessment of texture and skid resistance after abrasion.

CHAPTER 8 – EFFECTS AND POTENTIALITIES OF MODIFICATION OF ASPHALT BINDERS WITH TiO₂

8.1. Contextualization

This chapter aims to present the effects and potentialities of the modification of asphalt binders with nano-TiO₂. During the Ph.D. course, it was possible to study abroad for academic exchange mobility in two Universities: Federal University of Ceará, Brazil, and University of Antwerp, Belgium. The first period, in Brazil, was in June 2018, and the second one, in Belgium, was between October/2019 and January/2020.

In Brazil, the asphalt binder Elaster was modified with different contents of nano-TiO₂ and was physically and rheologically characterized. The second academic exchange mobility period was carried out to analyze photocatalytic asphalt mixtures using a transparent binder and modified with nano-TiO₂. In this chapter, the nanomodification was performed using a transparent binder for the characterization under physicochemical and rheological approaches.

Two scientific publications were produced: one in a Portuguese conference and another in a scientific journal. The results from work carried out in Brazil were published in the most important Portuguese conference about road pavements: Portuguese Road Congress (Congresso Rodoviário Português, in the Portuguese language) in 2019 (Figure 39a).

The results from the mobility in Belgium have been published in the scientific journal *Nanomaterials* from MDPI (if - 5.076). So, the second section of this chapter refers to the work about modification of transparent asphalt binder with TiO₂ “Physicochemical and Rheological Properties of a Transparent Asphalt Binder Modified with Nano-TiO₂”. Figure 39b shows its first page. The content of this chapter is included in the article, which DOI is doi.org/10.3390/nano10112152.

Thus, this chapter was divided into two sections: 8.2. Study of the anti-aging effect of TiO₂ on asphalt binder (work carried out in Brazil) and 8.3. Study of color-less asphalt binder modified with TiO₂ (work carried out in Belgium).

AVALIAÇÃO DAS PROPRIEDADES FÍSICAS E REOLÓGICAS DE LIGANTE ASFÁLTICO MODIFICADO POR NANO-TiO₂ APÓS ENVELHECIMENTO

Iran Rocha Segundo^{1,*}, Salmon Landi Jr.², Elisabete Freitas³, Verônica Castelo Branco⁴, Sandra Soares⁵, Jorge Soares⁶, Joaquim Carneiro⁷

¹Departamento de Engenharia Civil, Universidade do Minho, Campus de Azurém, Guimarães, Portugal;

²Departamento de Física, Universidade do Minho, Campus de Gualzaraz, Braga Portugal e Instituto Federal Goiano, Rio Verde – GO, Brasil;

³Departamento de Engenharia Civil, Universidade do Minho, Campus de Azurém, Guimarães, Portugal

email: efreitas@ceivil.uminho.pt;

⁴Departamento de Engenharia de Transportes, Universidade Federal do Ceará, Fortaleza – CE, Brasil;

⁵Departamento de Química, Universidade Federal do Ceará, Fortaleza – CE, Brasil;

⁶Departamento de Engenharia de Transportes, Universidade Federal do Ceará, Fortaleza – CE, Brasil;

⁷Departamento de Física, Universidade do Minho, Campus de Azurém, Guimarães, Portugal.

Sumário

A oxidação/envelhecimento do material betuminoso dos pavimentos rodoviários promove mudanças das suas propriedades físicas e reológicas, afetando o seu endurecimento e acelerando as degradações das misturas asfálticas. O dióxido de titânio (TiO₂) vem sendo aplicado em investigações da Engenharia para promover propriedades anti-envelhecimento e fotocatalítica. Neste estudo, um ligante comercial foi modificado com nano-TiO₂ e foi avaliado por ensaios físicos e por ensaio reológico antes e após envelhecimento pelo Rolling Thin Film Oven Test (RTFOT) e pelo Pressure Aging Vessel (PAV). Os resultados mostraram que a incorporação de nano-TiO₂ mitiga o envelhecimento do ligante, sendo o melhor potencial de modificação 0,25%.

Palavras-chave: ligante asfáltico; nano-TiO₂; envelhecimento; RTFOT; PAV.

1 INTRODUÇÃO

O envelhecimento por oxidação do material betuminoso dos pavimentos rodoviários tem efeitos irreversíveis, tais como a mudança das suas propriedades físicas e reológicas, como o seu endurecimento, o que acelera a sua degradação, que resulta no aparecimento de patologias, como por exemplo o fendilhamento. O envelhecimento envolve um processo físico-químico que se desenvolve geralmente em duas fases: a curto prazo e a longo prazo. O primeiro, ocorre durante o fabrico e a compactação das misturas betuminosas principalmente pela submissão a elevadas temperaturas. O último, ocorre durante a vida útil do pavimento em serviço sendo causado pelas intempéries [1,2].

O tráfego que solicita os pavimentos rodoviários é uma das principais fontes de poluição ambiental, principalmente em zonas industriais e urbanas. Algumas consequências no ambiente do tráfego é, por exemplo, a intensificação do efeito estufa, ocorrência de chuvas ácidas e problemas de saúde humana [3].

A aplicação de alguns semicondutores em materiais betuminosos das estradas pode contribuir para a redução desses dois efeitos que têm consequências económicas e sociais indesejáveis, da seguinte forma: i) promovendo a capacidade fotocatalítica para degradar compostos poluentes [3–6] e ii) desenvolvendo uma capacidade anti-envelhecimento para mitigar o aparecimento das patologias relacionadas com a oxidação dos materiais betuminosos [7–9].

Os semicondutores, como o óxido de zinco (ZnO), dióxido de titânio (TiO₂) e dióxido de cério (CeO₂) agem numa reação de redução e oxidação (redox) que promove a fotodegradação de poluentes. Esta reação inicia pela

a)



Article

Physicochemical and Rheological Properties of a Transparent Asphalt Binder Modified with Nano-TiO₂

Iran Rocha Segundo^{1,*}, Salmon Landi, Jr.², Alexandros Margaritis³, Georgios Pipintakos³, Elisabete Freitas⁴, Cedric Vuye⁵, Johan Blom⁶, Tom Tytgat⁴, Siegfried Denys⁴ and Joaquim Carneiro⁷

¹ Department of Civil Engineering, University of Minho, 4800-058 Guimarães, Portugal; efrilas@ceivil.uminho.pt

² Federal Institute Goiano, Rio Verde 75901-970, Brazil; salmon.landijr@fgoiano.edu.br

³ Energy and Materials in Infrastructure and Buildings (EMIB) Research Group, University of Antwerp, 2020 Antwerp, Belgium; alexandros.margaritis@uantwerpen.be (A.M.);

georgios.pipintakos@uantwerpen.be (G.P.); cedric.vuye@uantwerpen.be (C.V.);

johan.blom@uantwerpen.be (J.B.)

⁴ Research Group Sustainable Energy, Air and Water Technology, University of Antwerp, 2020 Antwerp, Belgium; tom.tytgat@uantwerpen.be (T.T.); siegfried.denys@uantwerpen.be (S.D.)

⁵ Centre of Physics, University of Minho, 4800-058 Guimarães, Portugal; carneiro@fisica.uminho.pt

* Correspondence: iran_gomes@hotmail.com

Received: 16 September 2020; Accepted: 23 October 2020; Published: 28 October 2020



Abstract: Transparent binder is used to substitute conventional black asphalt binder and to provide light-colored pavements, whereas nano-TiO₂ has the potential to promote photocatalytic and self-cleaning properties. Together, these materials provide multifunction effects and benefits when the pavement is submitted to high solar irradiation. This paper analyzes the physicochemical and rheological properties of a transparent binder modified with 0.5%, 3.0%, 6.0% and 10.0% nano-TiO₂ and compares it to the transparent base binder and conventional and polymer modified binders (PMB) without nano-TiO₂. Their penetration, softening point, dynamic viscosity, master curve, black diagram, Linear Amplitude Sweep (LAS), Multiple Stress Creep Recovery (MSCR), and Fourier Transform Infrared Spectroscopy (FTIR) were obtained. The transparent binders (base and modified) seem to be workable considering their viscosity, and exhibited values between the conventional binder and PMB with respect to rutting resistance, penetration, and softening point. They showed similar behavior to the PMB, demonstrating signs of polymer modification. The addition of TiO₂ seemed to reduce fatigue life, except for the 0.5% content. Nevertheless, its addition in high contents increased the rutting resistance. The TiO₂ modification seems to have little effect on the chemical functional indices. The best percentage of TiO₂ was 0.5%, with respect to fatigue, and 10.0% with respect to permanent deformation.

Keywords: asphalt binder; transparent binder; nanomaterials; TiO₂; viscoelastic properties; FTIR; photocatalytic asphalt; light-colored asphalt; self-cleaning

1. Introduction

For specific applications, it is important to control the light absorption and thermal energy storage in asphalt pavements, which can be carried out by the application of light-colored pavements [1]. Light and heat are essential influencing factors for asphalt pavements. Firstly, it is well known that they are essential keys for the asphalt binder aging, causing damage to asphalt roads [2,3]. The absence of light profoundly affects the visibility conditions, decreasing safety [1]. In contrast, a large amount of

b)

nanomaterials 2020, 10, 2152; doi:10.3390/nano10112152

www.mdpi.com/journal/nanomaterials

Figure 39: Publications in a) Portuguese Road Congress and b) Nanomaterials

8.2. Study of anti-aging effect of TiO₂ on asphalt binder

8.2.1. Introduction

This section aims to evaluate the anti-aging effects of an asphalt binder modified with the TiO₂ semiconductor on a nanometric scale. The binder was modified by the semiconductor in different percentages, and its physical and rheological characteristics were evaluated.

8.2.2. Materials and Methods

The materials used in this research were the commercial asphalt binder Elaster modified by SBS and the semiconductor TiO₂ in a nanometer scale. The asphalt binder was modified with three contents of nanoparticles of TiO₂ by mass, i.e., 0.25%, 0.5%, and 2%. Then, it was compared with the reference asphalt binder, named 0%. The modification was carried out with the asphalt binder at 150 °C for 30 minutes by a low-shear mixer at 1500 RPM.

For the characterization of the material after modification, tests of penetration (ASTM D5), viscosity (ASTM D4402), softening point (ASTM D36) and rheology (by the complex modulus through the DSR – Dynamic Shear Rheometer) (ASTM D7175) were carried out. Then, after short-term aging by RTFOT (ASTM D2872), the mass loss was registered. Also, after RTFOT, the asphalt binder was evaluated under penetration, viscosity, softening point, and rheology.

The residue aged by RTFOT was subjected to the PAV aging process (ASTM D6521), being characterized only by the complex modulus. Figure 40 presents the schematic representation of the methodology adopted to study the aging of the modified binder.

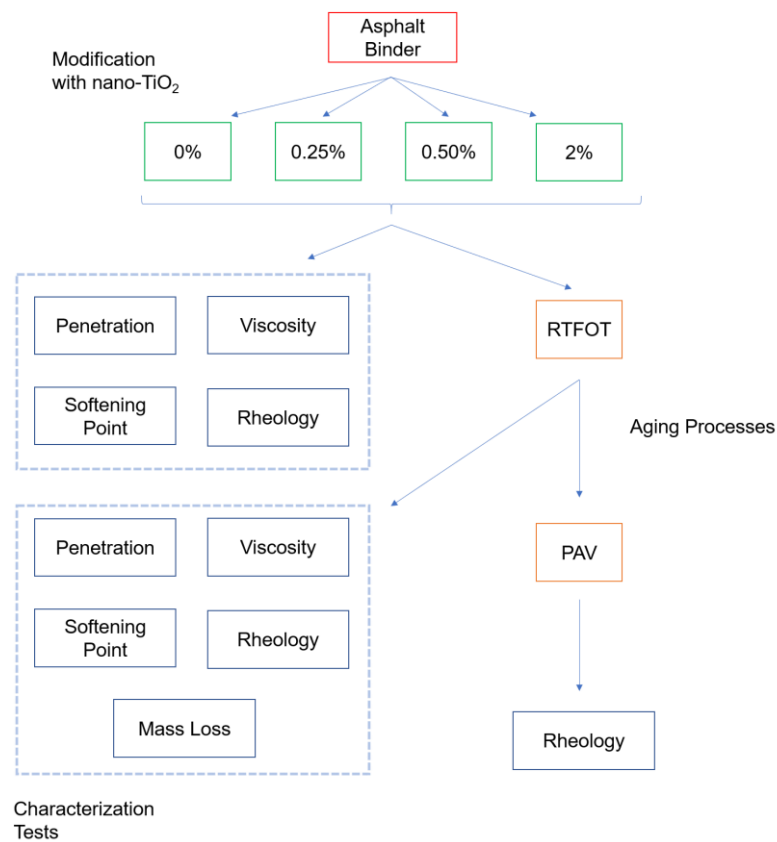


Figure 40: Schematic Representation of the Methodology of this section

RTFOT aging is intended to simulate short-term aging by applying compressed air (4 L/min) over an asphalt binder film subjected to a high temperature of 163 °C for 75 minutes. In turn, the PAV aims to simulate the long-term aging of the asphalt binder. The binder is subjected to 100 °C and a pressure of 2.1 MPa for 22 h.

8.2.3. Results and Discussion

Table 11 shows the results obtained and, in the following subsections, they are further explored.

Table 11: Results of penetration, softening point, and mass loss

Binder	Penetration (10 ⁻¹ mm)		Softening Point (°C)		Mass Loss (%)
	Before RTFOT	After RTFOT	Before RTFOT	After RTFOT	
0%	40	27	65	85	0.57
0.25%	39	29	71	78	0.53
0.50%	39	29	71	77	0.50
2%	39	27	72	78	0.48

8.2.3.1. Penetration

Figure 41 shows the results of the penetration tests before and after aging through the RTFOT. After the modification, the binders with nano-TiO₂ showed practically equal values, but 4.3% lower than the reference binder 0%. After aging, the binder samples 0% and 2% showed similar values, and the modified binder samples 0.25% and 0.5% too. However, the latter samples showed an increase in penetration of up to 10% compared to the reference binder.

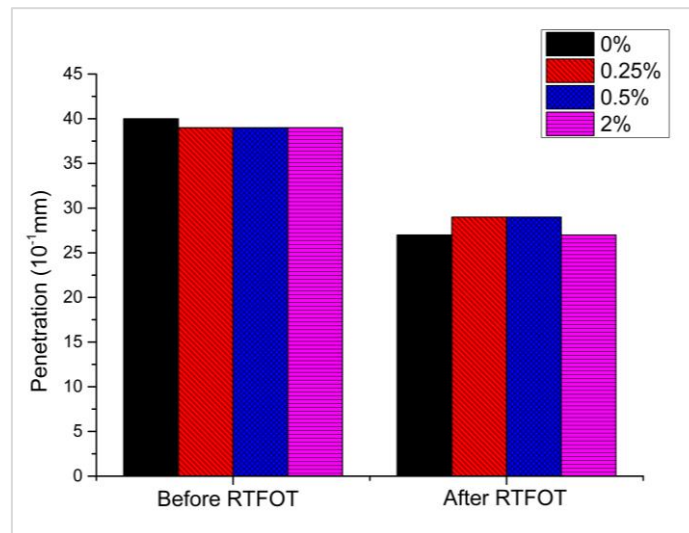


Figure 41: Penetration Results before and after aging by RTFOT

8.2.3.2. Softening Point

Figure 42 illustrates the softening point results before and after aging by RTFOT. The binder, when modified by nano-TiO₂ showed an increase in the softening point of up to 10% when compared to the reference binder. An inverse performance is observed after RTFOT; that is, the softening point of the modified binders showed a decrease of up to 9% concerning the reference binder.

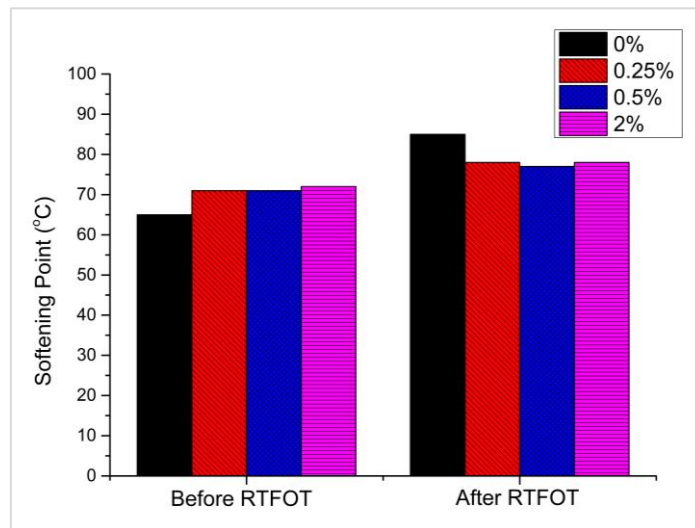


Figure 42: Softening point results before and after aging by RTFOT

Thus, based on the results of penetration and softening point, it can be concluded that the modified binders have better characteristics before the aging process, as the softening point increases. After short-term aging (RTFOT), the modification resulted in an anti-aging contribution, decreasing the softening point.

8.2.3.3. Mass Loss

Figure 43 shows the results of mass loss in the RTFOT test. It appears that there was a decrease in mass loss with the modification of the asphalt binder by nano-TiO₂. In general, with the percentage of TiO₂ increase, there was a gradual decrease in mass loss. It can also be concluded that the incorporation of the semiconductor has an anti-aging effect during the mixing and paving processes of asphalt mixtures (short term aging).

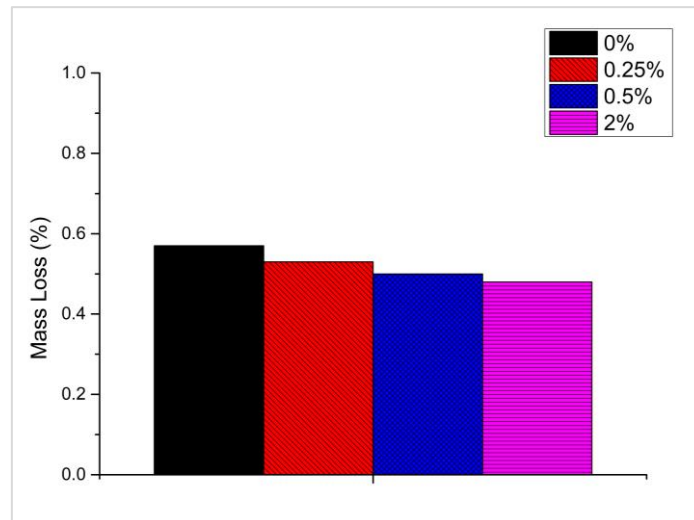


Figure 43: Results of mass loss after aging by RTFOT

8.2.3.4. Viscosity

Figure 44 illustrates the viscosity results before and after aging by RTFOT. Before the aging process, at temperatures between 135 °C and 150 °C, the 0.25% and 0.5% binders presented viscosities similar to that obtained for the reference 0% binder, while the 2% binder presented an increase in this parameter by up to 20%, depending on the temperature. At 177 °C, the binder 0.5% maintained the viscosity, and the binders 0.25% and 2% showed an increase of 14% and 16%, respectively, when compared to the reference binder. Finally, at 190 °C, the binders showed similar viscosity. In summary, with increasing the temperature, there is a convergence of the viscosity between the asphalt binders.

After RTFOT, up to the temperature of 177 °C, the binder modified with 0.25% TiO₂ showed a viscosity up to 10% lower than that of the reference binder. The 0.5% binder showed similar viscosity and the 2% up to 16% higher. At 190 °C, the 0.25% binder showed viscosity similar to the reference binder, while the others showed 14% higher viscosity. It can be concluded from the results of viscosity that, at high temperatures of manufacture and compaction, only the 0.25% binder had some anti-aging capacity.

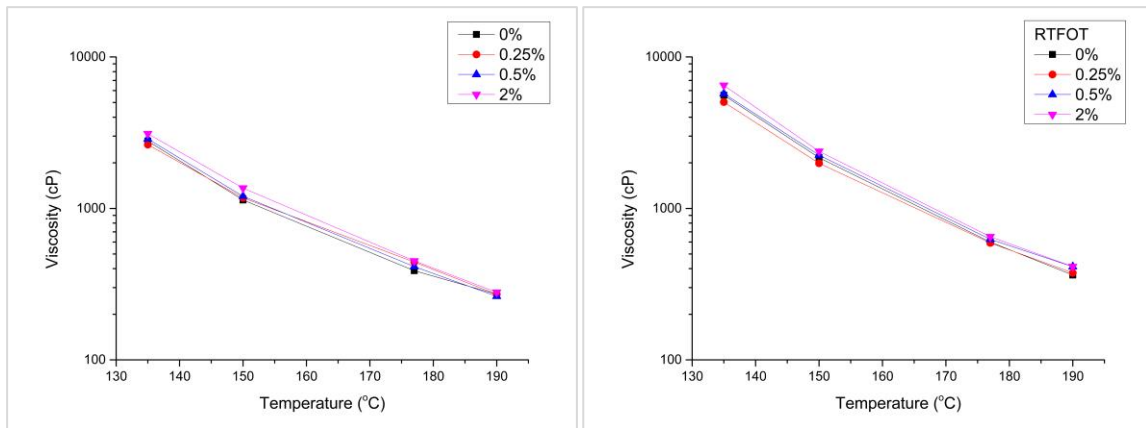


Figure 44: Viscosity results: before RTFOT (left) and after RTFOT (right)

8.2.3.5. Rheology

Figure 45 shows the results of the complex modulus before and after the RTFOT aging process and Figure 46 after the PAV and a detail of all evaluated situations. Before RTFOT, the binders showed similar complex modulus values. After RTFOT, the modified binders showed an increase in the complex modulus at low temperatures, but at high temperatures, the opposite occurred.

After aging by PAV, performed only at high temperatures, it can be seen that the modified binders have a lower value of complex modulus compared to the reference binder, showing the most significant difference in moduli between the three test conditions (Figure 46 right). This test method could not be performed at low temperatures due to the high stiffness of the binder, due to limitations of the plate geometries and the rheometer used (lower than 40 °C temperatures, the asphalt binder samples unstick from the plates of 8 mm). Thus, it is concluded again that the modification of the asphalt binder by nano-TiO₂ has an anti-aging effect when this rheological property is considered, with the best percentage of modification being 0.25%.

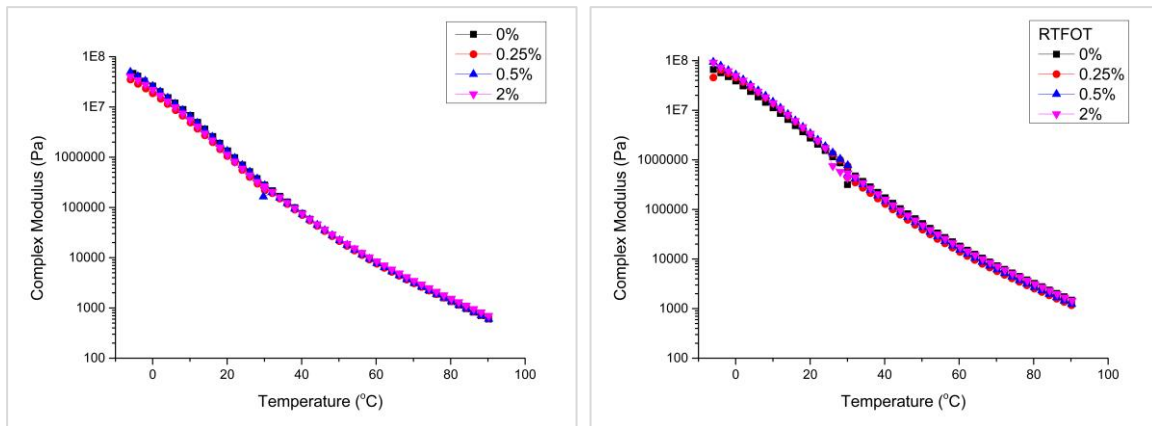


Figure 45: Complex modulus results before RTFOT (left) and after RTFOT (right)

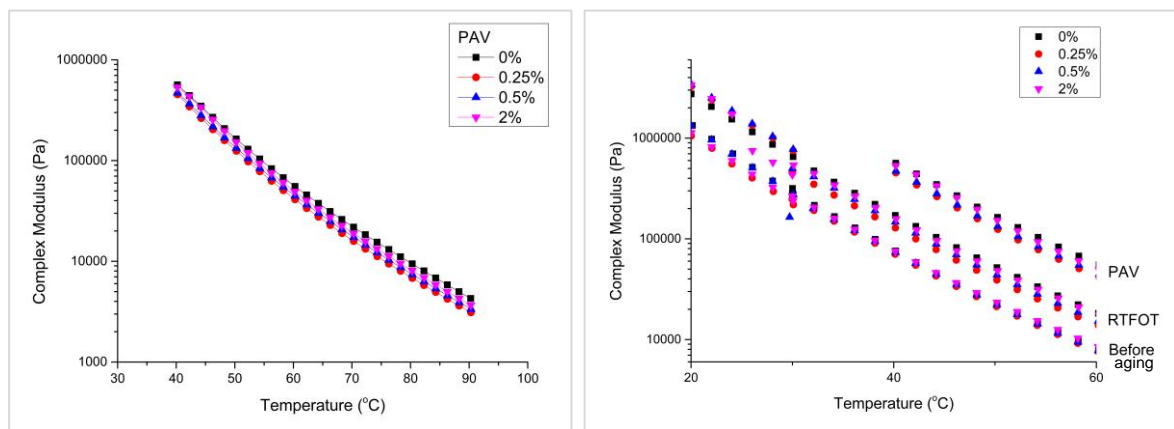


Figure 46: Results of complex modulus after PAV (left) and with the enlarged image of all situations evaluated (right)

8.2.4. Conclusions

This section aimed to evaluate the anti-aging effect of TiO₂ in an asphalt binder by conventional laboratory methods, namely, RTFOT in the short term and PAV in the long term. A commercial binder was modified by nano-TiO₂ with three different percentages and later subjected to physical and rheological tests. The following conclusions from this study are reported:

- After modification, the nano-TiO₂ provided maintenance of the penetration value when compared to the reference binder. After RTFOT, the 0.25% and 0.5% modified binders showed an increase in penetration, while the modified binder with 2% kept the penetration value. Thus, lower contents of TiO₂ can reduce this parameter.

- For the softening point, the addition of nano-TiO₂ led to an increase in this parameter of up to 10%. After submission to RTFOT, the softening point of the modified binders decreased by up to 9%; that is, they became less stiff.
- The increase of the percentage of TiO₂ led to a gradual decrease in mass loss.
- From the three previous tests, it can be concluded that the binders modified by nano-TiO₂ showed a positive effect on aging at short term.
- For the viscosity parameter, there was evidence an anti-aging effect only for the binder 0.25% at high temperatures.
- Before the RTFOT, the modified binders maintained the modulus value in relation to the reference binder from the rheological test. After RTFOT, at low temperatures, they showed an increase in the complex modulus. After the PAV, all modified binders showed a lower modulus than the reference binder.
- The best modification percentage among those evaluated was 0.25% of TiO₂, presenting the best results according to the penetration, viscosity, and rheology tests.

Briefly, nano-TiO₂ showed some anti-aging effect in the investigated asphalt binder, which can mitigate problems caused by increased stiffness. Thus, the incorporation of this material into asphalt mixtures would provide an environmental and sustainable gain extending the road lifetimes. Thus, the next phase of this investigation will address aging in the UV chamber to analyze this ability after radiation in order to consolidate the modification of asphalt binder using nano-TiO₂ for anti-aging effects.

8.3. Study of color-less asphalt binder modified with TiO₂

8.3.1. Introduction

Transparent binder is used to substitute conventional black asphalt binder and to provide light-colored pavements, whereas nano-TiO₂ has the potential to promote photocatalytic and self-cleaning properties. Together, these materials provide multifunction effects and benefits when the pavement is submitted to high solar irradiation.

For specific applications, it is important to control the light absorption and thermal energy storage in asphalt pavements, which can be carried out by the application of light-colored pavements [175]. Light and heat are essential influencing factors for asphalt pavements. Firstly, it is well known that they are essential keys for the asphalt binder aging, causing damage to asphalt roads [176,177]. The absence of light profoundly affects the visibility conditions, decreasing safety [175]. In contrast, a large amount of

heating can increase the Urban Heat Island (UHI) effect in urban areas [150]. The conventional black color of asphalt pavements absorbs light and stores a large amount of thermal energy.

The literature presents a small number of studies addressing the use of the transparent binder. For example, Bocci et al. (2012) produced a light-colored asphalt mixture with conventional aggregates, lime filler, light-colored binder, and TiO₂ powder (1% by aggregate weight). The coefficient of reflection related to night visibility and the luminance of this technology were much higher than those from the conventional asphalt mixture [175]. Bocci E. and Bocci M. (2014) continued their research on this subject, showing that light-colored dense-graded mixtures have similar mechanical properties when compared to the conventional asphalt mixture. They concluded that the light-colored asphalt pavement presented very high photometric properties even after five months from the traffic opening [178]. Sengoz et al. (2017) investigated the rheological properties of transparent binder in comparison to a traditional black bitumen. They concluded that the transparent and the traditional black bitumen had a similar performance [177].

The use of these two materials together would combine their benefits into one single product: an asphalt pavement capable to photodegrade pollutants and avoid the UHI. The main objective of this research is to analyze the physicochemical and rheological properties of a transparent binder modified with nano-TiO₂ (0.5%, 3.0%, 6.0%, and 10.0%) for the understanding of its limitations and definition of suitable destinations. For this, its physical (conventional), rheological, and chemical properties were assessed and compared to those of a conventional asphalt binder and a commercial PMB.

8.3.2. Materials

8.3.2.1. Binders

In this research, the transparent binder Kromatis 50/70 from Total (Rives-en-Seine, France) was used. According to the supplier, this light-colored synthetic binder presents properties similar to other bitumens. It is produced with hydrocarbon resins and low content of asphaltenes, which are removed and replaced with new elastomeric polymers [179]. A conventional 50/70 bitumen and a polymer-modified binder (PMB) (SBS-modified bitumen) were also used in this study. These reference binders were named as N50/70 and PMBTS, respectively.

8.3.2.2. TiO₂ Nanoparticles

The semiconductor selected to provide multifunctional properties was the nano-TiO₂ by Quimidroga (Aeroxide TiO₂ P25) (Barcelona, Spain). Its main properties are 80% anatase and 20% rutile crystalline phases, purity > 99.5%, and particle size about 23 to 28 nm.

8.3.2.3. Sample Preparation

The nanoparticles were incorporated into the binder (at 150 °C for 30 min in a low shear mixer with a rotational speed of 1500 RPM) with four different contents: 0.5, 3.0, 6.0 and 10.0% (in the mass of the binder) with a similar modification procedure adopted in the literature review [80,180–182]. The particles were placed when the low shear mixer was working, homogenizing the binder already heated to 150 °C. All safety precautions were taken, considering personal protective equipment, engineering control (ventilated enclosures), and hygiene, among other things.

The samples were named by the modification content: 0.5%, 3.0%, 6.0% and 10.0%. With the introduction of nano-TiO₂, the color of the binder changes from dark brown (0%) to light yellow (10.0%), see Figure 47. One blend was prepared for each content. Regarding the performed tests, the number of replicates respected the requirements mentioned in the relevant European standard.

8.3.3. Methods

Different tests were carried out, such as penetration, softening point, Dynamic Shear Rheometer (DSR) tests (complex modulus, Linear Amplitude Sweep—LAS, Multiple Stress Creep Recovery—MSCR), Dynamic viscosity and Fourier Transform Infrared (FTIR) spectroscopy, in order to determine conventional, rheological and chemical properties. Figure 47 presents the schematic summary of the preparation and characterization methodology adopted in this chapter.

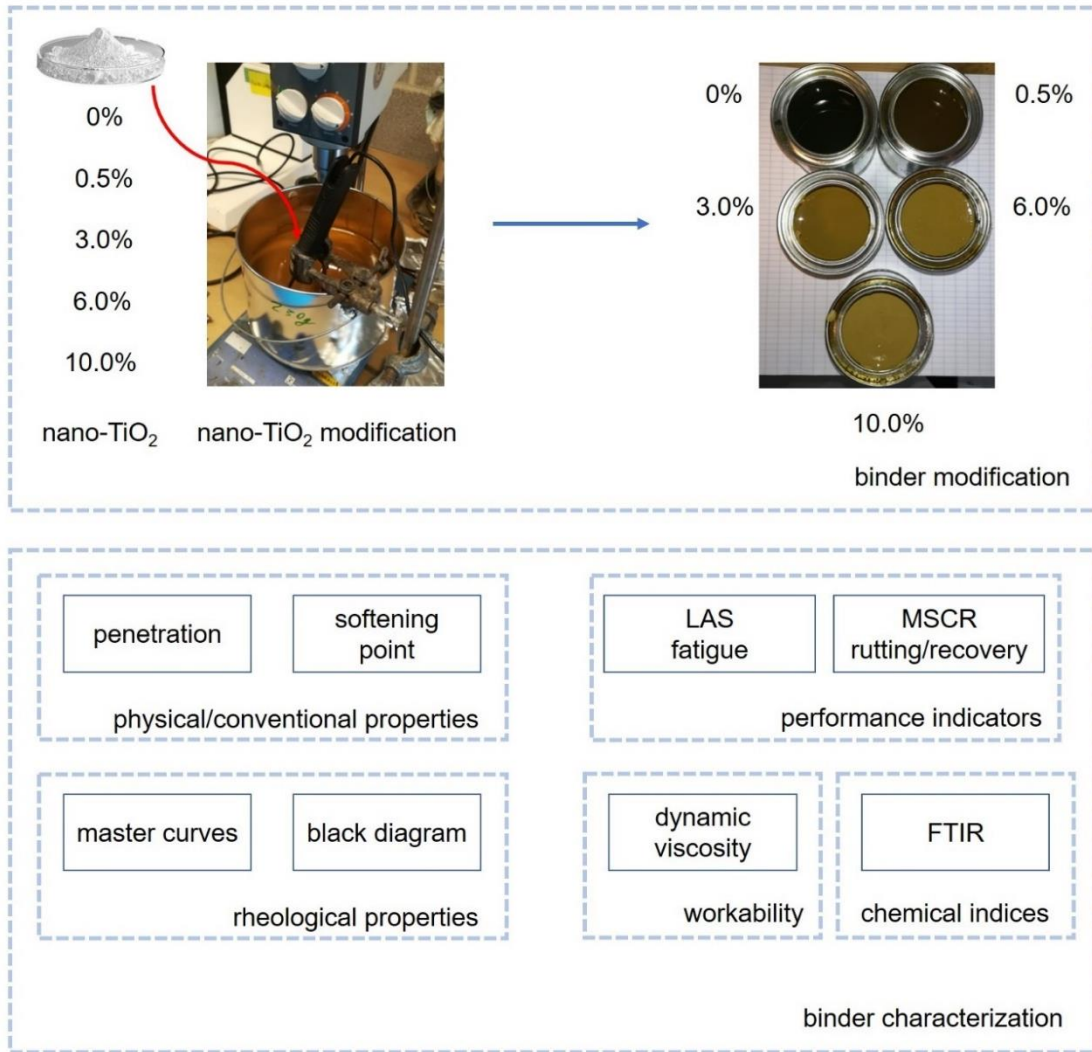


Figure 47: Schematic representation of this research

8.3.3.1. Penetration and Softening Point

Penetration and softening point were tested according to EN 1426/2015 and EN 1427/2015, respectively. They indicate the basic properties of asphalt binders.

8.3.3.2. Dynamic Viscosity

A dynamic viscosity test was carried out following the EN 13302/2010 standard, but only for the transparent binders (with and without nano-TiO₂). The objective was to evaluate the workability of the binders according to Superpave specifications. The highest allowed viscosity to respect the workability is 3×10^3 cP (or 3 Pa·s) at 135 °C [182,183].

8.3.3.3. Viscoelastic Behavior

The viscoelastic behavior of the binders was assessed using the Dynamic Shear Rheometer (DSR). The DSR used in this study is an Anton Paar MCR 500 (Graz, Austria). For temperature ranges from 0 °C to +40 °C and from +40 °C to +80 °C, the 8 mm and 25 mm plate geometries were used, accordingly, as described in EN 14770:2012. For each temperature step (increments of 10 °C), frequency sweep tests were performed (0.1–10 Hz) on two replicates per binder sample, within the linear viscoelastic region (LVER) of the binders. The data were further analyzed using the RHEA™ software (v2.0, Abatech, Blooming Glen, PA, USA) [184]. The shifting of the data was performed using the Gordon and Shaw procedure [185]. The phase angle and complex modulus master curves are presented in their original format, without fitting any mathematical or mechanical models.

Black diagrams (complex modulus versus phase angle) aim to identify discrepancies of the rheological data, breakdown of time-temperature equivalence, and thermo-rheological simplicity [186]. A smooth curve indicates time-temperature equivalence, a typical response of unmodified binders. On the other hand, discontinuities indicate the presence of high wax content bitumen, highly polymer modified bitumen, or a highly asphaltene structured binder [23]. Additionally, it is possible to notice whether there are different dominances when the binder is a composite [186]. This phenomenon happens, for example, when the complex modulus trend changes with the increase of the phase angle, a phenomenon known as curling.

8.3.3.4. Fatigue Resistance (LAS Test)

To evaluate the fatigue resistance of bituminous binders, the Linear Amplitude Sweep (LAS) test was performed. This test is an accelerated method that uses the DSR (8 mm parallel plate geometry at 15 °C), which consists of two steps: (i) firstly, a frequency sweep test, and (ii) secondly, an amplitude sweep test, as described in AASHTO TP 101-14. The frequency sweep test (0.2–30 Hz) is used to define the undamaged properties and fatigue law parameters, at a strain level of 0.1%. A linear amplitude sweep test is performed at 10 Hz, and the strain amplitude is linearly increased over 3000 cycles, from 1% to 30%.

The Viscoelastic Continuum Damage (VECD) theory is used to determine the parameters A and B of the fatigue law (Equation (22)) [187], in order to determine the fatigue life (N_f). The failure point is determined as the point when the product of the complex modulus (G^*) and phase angle (δ) sine is

reduced by 35% from its initial value. Both the fatigue curves and the N_f for strain levels (γ) equal to 2.5% and 5%, related to a strong and weak pavement [188], respectively, will be presented.

$$N_f = A \gamma^B \quad (22)$$

8.3.3.5. Rutting Resistance Indicator (MSCR Test)

The Multiple Stress Creep Recovery (MSCR) was performed using the DSR together with the 25 mm plate and 1 mm gap, as described in EN 16659:2015. The test was performed at 50 °C, at two different stress levels (0.1 and 3.2 kPa) over ten load cycles. Each cycle consists of 1 s loading followed by 9 s of a recovery period, from which two parameters are obtained: (i) the non-recoverable creep compliance J_{nr} (Pa⁻¹), which is the ratio between the residual strain and the stress applied; and (ii) the recovery R (%), showing proportionally how much strain the sample recovers at the end of the cycle. R (%) can be used to identify the presence of polymer modifications in the asphalt binders.

8.3.3.6. FTIR

Chemical characterization of binders has received attention in the literature as it can present functional groups related to the crude oil origin, the polymer modification, and the degree of oxidation [189–194]. Since this chapter aims to analyze the chemical characteristics of the transparent binder modified with nano-TiO₂, three approaches were carried out: (i) identification of FTIR peaks; (ii) establishment of a possible relationship between the TiO₂ modification level and related chemical groups; and (iii) comparison of standard indices with reference binders used in this study.

The Thermo Scientific Nicolet iS10 Fourier Transform Infrared (FTIR) spectrometer (Waltham, MA, USA) is equipped with an Attenuated Total Reflectance (ATR) fixture and a Smart Orbit Sampling Accessory. The average spectra were obtained after the acquisition of the spectra, 32 repetitive scans in the range 400 cm⁻¹ to 4000 cm⁻¹ with a resolution of 4 cm⁻¹ were performed to deliver an average spectrum. A hot droplet of each binder was placed on the crystal, and its respective spectrum was measured.

The chemical structure of the binders was analyzed using indices, I , from the obtained FTIR spectrum [195]. Each I (Equation (23)) is calculated by the ratio of the peak area of the identified band by the total area (Equation (24)) of the spectrum.

$$I_{Functional\ Group} = \frac{A_i}{\Sigma A} \quad (23)$$

$$\begin{aligned} \Sigma A = & A_{1700} + A_{1600} + A_{1460} + A_{1376} + A_{1030} + A_{864} + A_{818} + A_{743} \\ & + A_{724} + A_{(2953, 2923, 2862)} \end{aligned} \quad (24)$$

where A_i is the peak area of the specific functional group. The areas defined by the introduced baselines and the part of the spectrum were calculated using a specific software Origin. Each peak is attributed to a functional group remaining unaffected during service life, but also to groups responsible for aging or polymer presence [189,191]. When it comes to the groups responsible for TiO₂, echoing [196–198] in the region below 1000 cm⁻¹, several peaks are ascribed to TiO₂ presence. Previous researchers have demonstrated that the peak around 657 cm⁻¹ is attributed to Ti-O-Ti stretching vibration, whereas the peak around 590 cm⁻¹ is due to the vibration of Ti-O-O. A broader band of wavenumbers was calculated around these peaks in order to capture their increase by elevating the TiO₂ modification level. It should be noted that a horizontal baseline coinciding with the X-axis was used for the calculation of this area. R/I (Equation (25)) was calculated in order to check the relative increase of TiO₂ modification. $I_{Ti-O+Ti-O-O}$ is the index of each binder, and $I_{Ti-O+Ti-O-O0\%}$ is the index of the transparent base binder (0%).

$$R/I = \frac{I_{Ti-O+Ti-O-O} - I_{Ti-O+Ti-O-O0\%}}{I_{Ti-O+Ti-O-O0\%}} \% \quad (25)$$

More specifically, for asphalt binders, the sulfoxide, carbonyl, aromatic, aliphatic, branched aliphatic, long chains, polybutadiene, and polystyrene indices were calculated. Sulfoxide and carbonyl indices are both related to aging.

They were calculated considering the following method: (i) aromatic index: $A_{1600}/\Sigma A$; (ii) aliphatic index: $(A_{1460} + A_{1376})/\Sigma A$; (iii) branched index: $A_{1360}/(A_{1460} + A_{1376})$; (iv) long chain index: $A_{724}/(A_{1460} + A_{1376})$; (v) carbonyl index: $A_{1700}/\Sigma A$; (vi) sulphoxide index: $A_{1030}/\Sigma A$; (vii) polybutadiene index: $A_{966}/\Sigma A$; and (viii) polystyrene index: $A_{699}/\Sigma A$.

Aromatic, aliphatic, branched aliphatic, and long chains are the structural groups of asphalt binders. Polybutadiene and polystyrene are associated with SBS modified binders. For details concerning the determination of standard indices related to oxidative aging of the binder, the reader is referred to the

protocol described in [195]. Briefly, a common practice in this processing method is to introduce tangential baselines defined by limits around certain peaks [199].

8.3.4. Results and Discussions

8.3.4.1. Penetration and Softening Point

Figure 48 and Figure 49 show the resulting penetration and softening point of the studied binders. When compared to the transparent base binder, the inclusion of 0.5%, 3.0% and 6.0% TiO₂ nano-modification decreased the penetration from 49 to 47, 45, and 47 × 10⁻¹ mm, respectively. For 10.0% TiO₂, it increased to 53 × 10⁻¹ mm, which is similar to the N50/70 results. When compared to the PMBTS, all the penetration results were higher. Therefore, the penetration values of the Kromatis binder were between the conventional and the PMB binders. For the softening point, the results of the transparent binders were around 59 °C. The increase of the TiO₂ content gradually increased the softening point by about 4 °C. The transparent binders had a softening point again between those of the conventional and the PMB binders.

Comparing these results to those obtained by Sengoz et al. (2017) for the same binder from the same supplier, they showed that the penetration and softening points were 55 × 10⁻¹ mm and 56 °C [177]. Thus, in this research, the transparent base binder had a lower penetration but a higher softening point [177]. It can be concluded that the transparent binders had results between those of the conventional and the PMB binders, but closer to those of the conventional one. The incorporation of nano-TiO₂ gradually increased the softening point. For the penetration, the results were lower until 6.0%, but higher for 10.0%.

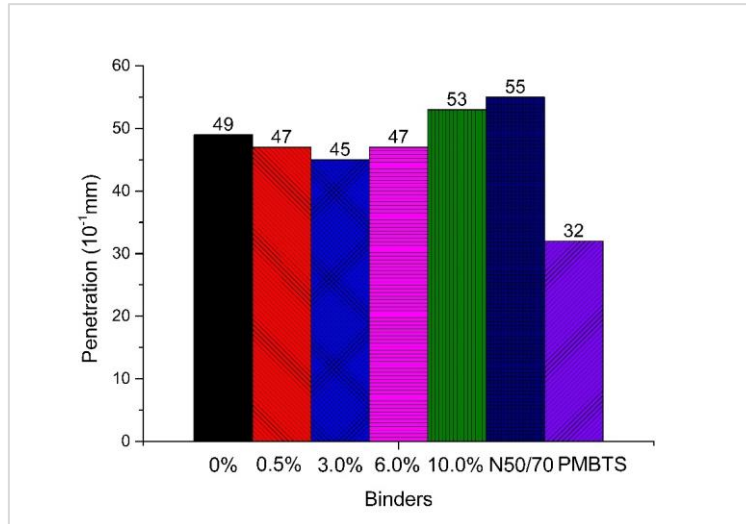


Figure 48: Penetration results of the binders of this study

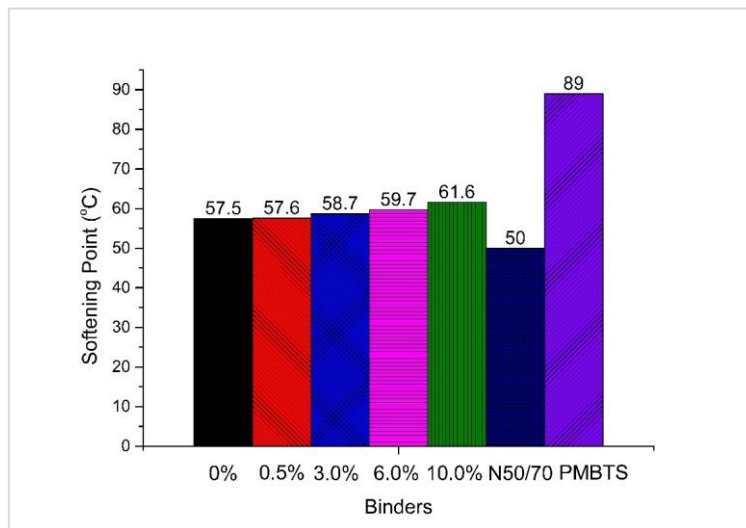


Figure 49: Softening point results of the binders of this study

8.3.4.2. Dynamic Viscosity

The dynamic viscosity, determined only for the transparent binders, is shown in Figure 50. The introduction of nano-TiO₂ increased dynamic viscosity. At 135 °C, the viscosity increased from 1×10^3 cP (for the base binder) to 2.3×10^3 cP (for the 10.0%). Additionally, all the binders had a viscosity lower than 3×10^3 cP, considered as the recommended maximum viscosity criterion under Superpave to guarantee proper binder pumping in the asphalt plant during production [200]. If this value is higher than 3×10^3 cP, excessive energy is needed for the mixing and compaction of asphalt mixtures [183].

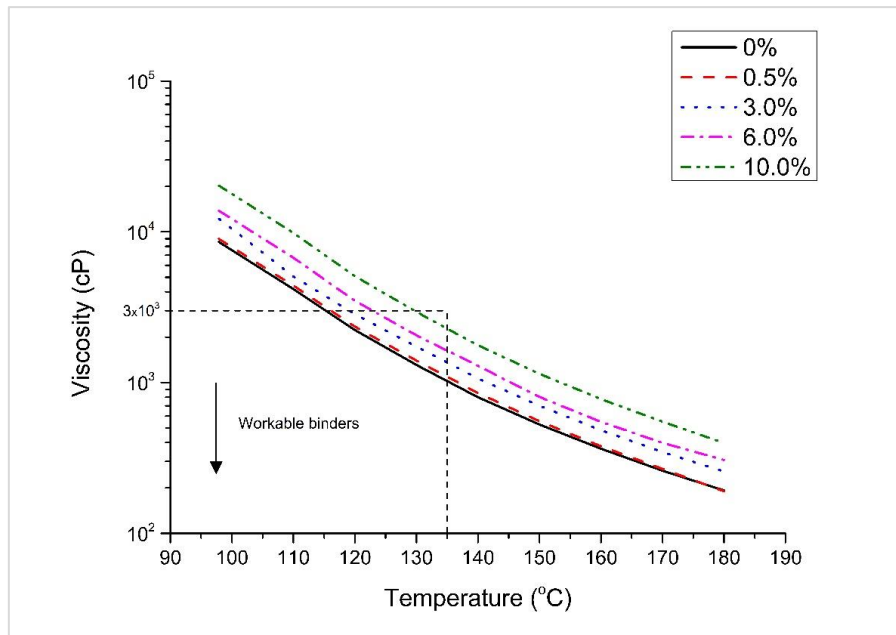


Figure 50: Dynamic viscosity results of the binders of this study

It can be concluded that all the modified transparent binders using the contents of nano-TiO₂ studied (from 0 to 10.0%) are feasible with respect to their workability. It is also interesting that the 10.0% TiO₂ appears to have the highest energy requirements as its viscosity is close to the Superpave threshold. Thus, from an economic point of view, it would be favorable to target lower TiO₂ levels.

In addition, the comparison of the results to those from the literature reveals that a higher viscosity was reached (1×10^3 cP). For example, Sengoz et al. (2017) presented 788 cP in dynamic viscosity for the same transparent binder [177].

8.3.4.3. Viscoelastic Behavior

The complex modulus and phase angle master curves are presented in Figure 51a and b. The addition of TiO₂ slightly alters the viscoelastic behavior of the transparent binder, leading to a simultaneous small increase of modulus and a decrease of the phase angle. The N50/70 shows a simple viscoelastic behavior with the phase angle gradually approaching the viscous asymptote of 90° at elevated temperatures, a typical response of an unmodified binder. Concerning the complex modulus, the N50/70 shows similar values to the PMBTS at frequencies above 10 Hz. At low frequencies (related to high temperature), N50/70 shows the lowest complex modulus compared to other binders, which was an expected observation, since the modulus of those binders is greatly influenced by the polymer modification.

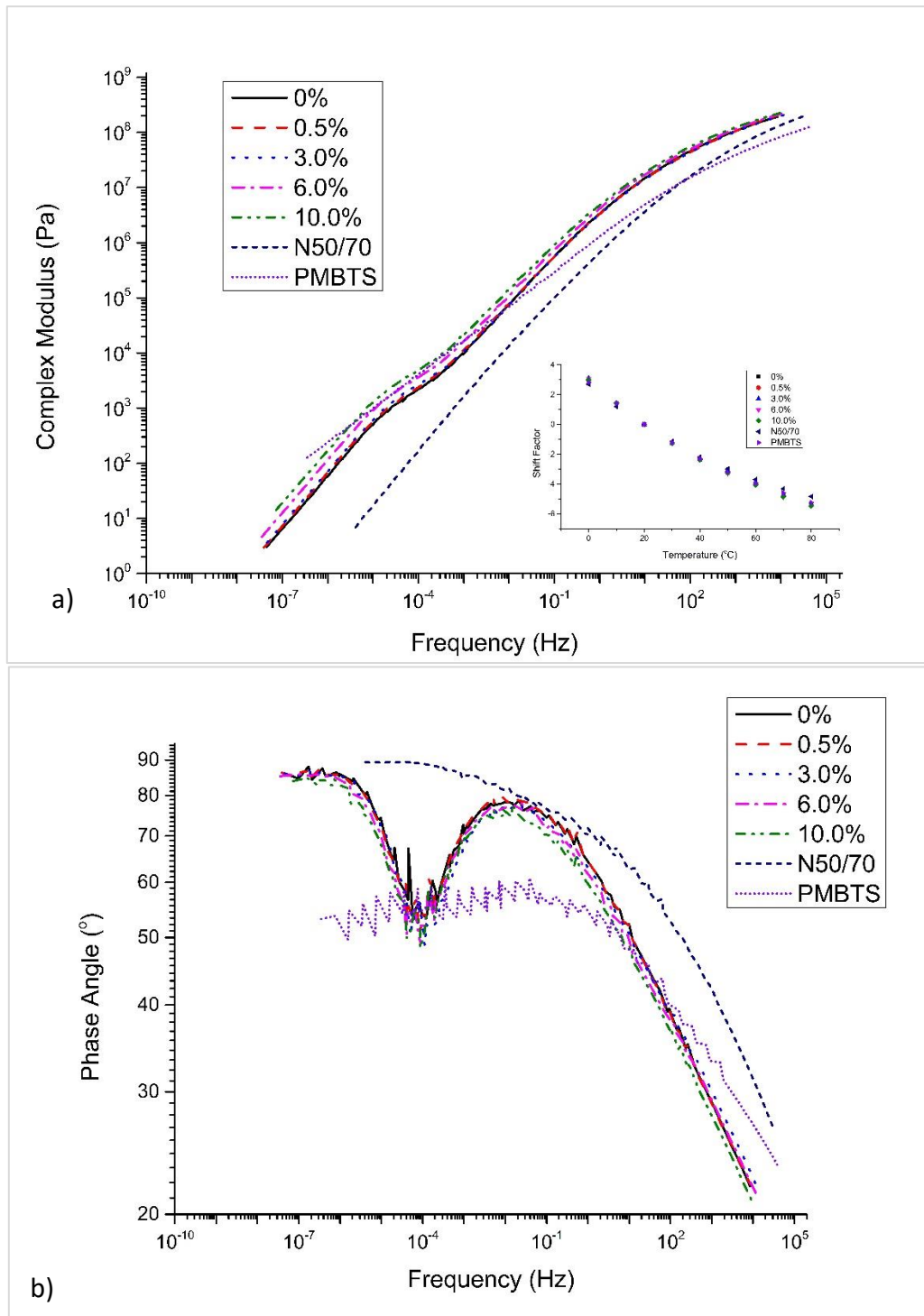


Figure 51: (a) Complex modulus and (b) phase angle master curves of the binders of this study

Comparing the transparent binder with the PMBTS, it can be seen that the complex modulus is similar at lower frequencies, while the PMBTS demonstrates a lower modulus at frequencies above 0.01 Hz. Looking at the phase angle, both reveal the presence of elastomeric modification, which is visible by the drop of the phase angle at a low reduced frequency. For the PMBTS, the dominance of the polymeric

phase starts below 1 Hz and shows at a steady plateau stage of 60°. On the other hand, the dominance of the polymeric phase for the transparent binders starts after 0.01 Hz (which can be translated that the polymer network is “active” at higher temperatures compared to the PMBTS), showing a significant drop of the phase angle and then gradually approaching the viscous asymptote of 90°.

The last part shows that the polymer network is no longer dominant. Those distinct differences can be attributed to the difference between the base binders as well as the compatibility between base and polymer [201]. Another possibility is the thermal history of the binders, which can significantly influence the rheological behavior of elastomeric binders, as demonstrated by Soenen et al. [202].

The black diagram (Figure 52) shows the combined effect of complex modulus and phase angle for the different binders. The N50/70 binder presents a conventional black diagram curve. Therefore, it is smooth, and the complex modulus decreases while the phase angle increases. The presence of a polymer can be seen by the shift of the curve towards a lower phase angle (higher elastic behavior) [186]. More specifically, for the PMBTS, the plateau near 60° (at a temperature of 58 °C) can indicate that the polymer forms a continuous elastic network when dissolved in bitumen, making it a polymer-dominant phase.

The shape of the curve of the transparent binders is different from the reference ones, showing three distinctive regions: (i) from 10⁸ to 5 × 10⁵ Pa, the complex modulus decreases with the increase of the phase angle; (ii) from 5 × 10⁵ to 5 × 10⁴ Pa, the complex modulus decreases when the phase angle increases; and (iii) from 5 × 10⁴ Pa, with the same pattern to that of the first region, including the shape. This viscoelastic response indicates an alternation of dominance between the materials that compose the transparent binders, as also observed in the phase angle master curve. Additionally, transparent binders seem to be more elastic than N50/70, with a partial shift towards the left. The addition of TiO₂ seems to have a small, rather insignificant, effect on the viscoelasticity of the transparent binder. Based on the observations of the master curves and black diagram, the addition of TiO₂ up to 10.0% seems not to introduce any noticeable effect on the structure of the transparent binders.

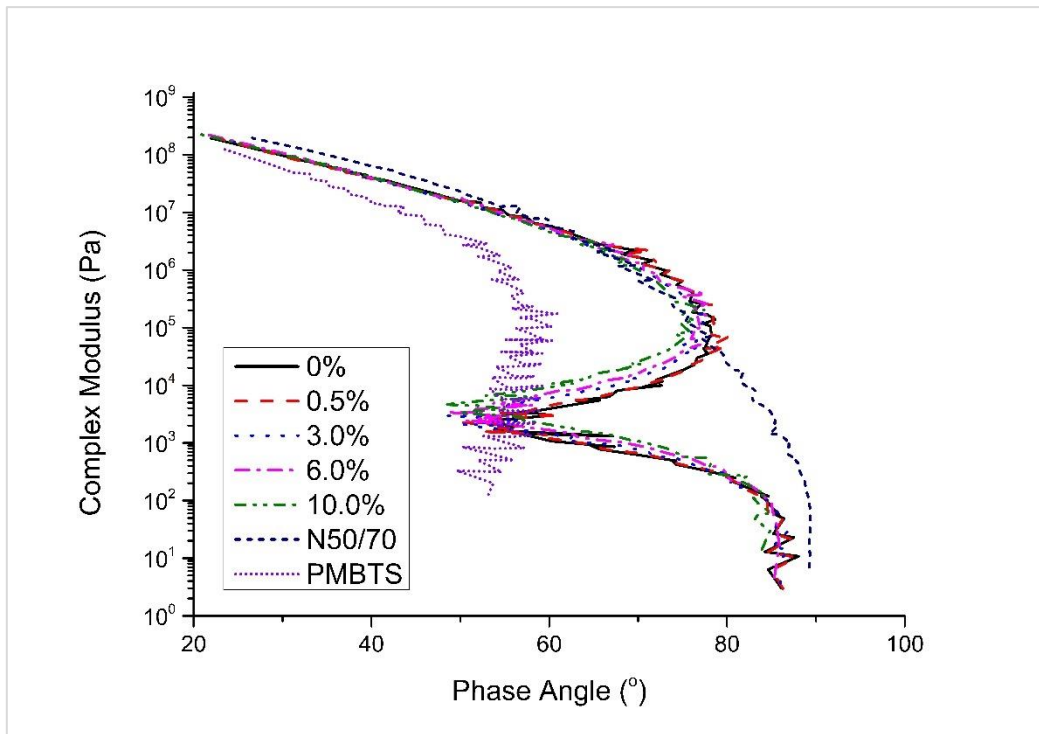


Figure 52: Black diagram of the evaluated reference and transparent binders

8.3.4.4. Fatigue Resistance (LAS Test)

The fatigue curves of each binder are presented in Figure 53 and the corresponding parameters are further elaborated in

Table 12. The PMBTS shows the highest fatigue resistance among the binder samples, while the transparent base binder and the N50/70 showed similar results. The addition of TiO₂ seems to harm the fatigue life of the transparent binder, except for the 0.5% dosage, where it shows a slightly improved fatigue life. In more detail, the addition of TiO₂ leads to a proportional decrease of the slope (parameter B), while no clear trend is evident on the effect of TiO₂ on the intercept (parameter A).

For all the binders, from the lowest to the highest fatigue performance considering the applied strain of 2.5% (representative strain level of a “weak” pavement structure), the progressive sequence is 10.0% < 6.0% < N50/70 < 3.0% < 0% < 0.5% < PMBTS. For the applied strain of 5% (representative strain level of a “strong” pavement structure), the progressive sequence is 10.0% < 6.0% < 3.0% < N50/70 < 0% < 0.5% < PMBTS. High contents of nano-TiO₂ slightly reduced the binder fatigue resistance. Additionally, higher differences are found for an applied strain level of 5%, related to the strong pavement structures.

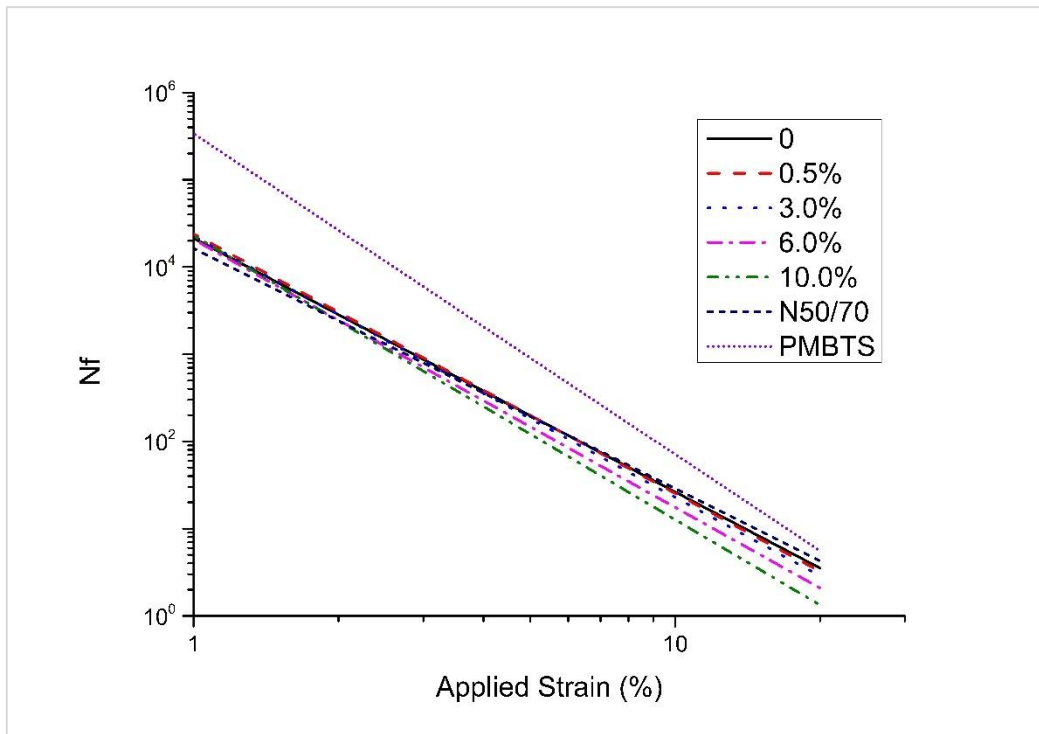


Figure 53: LAS Test: Nf versus applied strain

Table 12: LAS test results

Binder	Parameter			
	A	B	Nf 2.5%	Nf 5%
0%	21348	-2.9	1486	198
0.5%	23946	-3.0	1568	199
3.0%	22578	-3.0	1453	182
6.0%	20724	-3.1	1241	148
10.0%	22942	-3.3	1160	121
N50/70	16303	-2.8	1308	194
PMBTS	338013	-3.7	11631	909

8.3.4.5. Rutting Resistance Indicator (MSCR Test)

The MSCR test was introduced as a test to evaluate the resistance to permanent deformation (rutting) as well as a tool to evaluate the quality of polymer modified binders [203,204]. Generally, a combination of high recovery (R) and low non-recoverable compliance (J_{nr}) indicates a good quality PMB that can be used in high traffic pavements, as described in AASHTO M332. Such limits that distinguish between the acceptance levels for different traffic levels have not been established by the EN 16659. Therefore, a comparative evaluation of the rutting resistance of the binders in this study is presented.

The MSCR test results are presented in Table 13. Considering the %*R*, the transparent binders exhibit a recovery between the reference binders (higher than N50/70 but lower than PMBTS), but with values closer to PMBTS. At a stress level of 100 Pa, while the conventional binder N50/70 demonstrates recovery of only 9.0%, the transparent binders show at least 63.6% and the PMBTS 82.1%.

Table 13: MSCR test results

Binder	Parameter			
	Jnr,100 (kPa ⁻¹)	Jnr,3200 (kPa ⁻¹)	R100 (%)	R3200 (%)
0%	0.2	0.2	64.8	63.2
0.5%	0.2	0.2	63.6	62.3
3.0%	0.2	0.2	65.5	63.8
6.0%	0.1	0.1	69.9	64.4
10.0%	0.1	0.1	73.1	65.8
N50/70	0.6	0.6	9.0	6.0
PMBTS	0.0	0.0	82.1	85.7
Kromatis 50/70 from [177]	1.8	2.3	27.6	16.6

The incorporation of nano-TiO₂ increased the *R100* for the contents 6.0% and 10.0% when compared to 0%. The contents 0.5% and 3.0% had similar *R100* to 0%. For *R3200*, the transparent binders had similar results, from 63.2% to 65.8%, for 0% and 10.0% TiO₂ addition respectively.

Regarding the *Jnr* values, again, the transparent binders show an intermediate behavior between the reference binders N50/70 and PMBTS. The incorporation of nano-TiO₂ decreased the *Jnr* (100 and 3200 Pa⁻¹) for the contents 3.0%, 6.0% and 10.0% when compared to 0%. As can be expected, the content 0.5% had a similar *Jnr* to 0% (transparent base binder).

Sengoz et al. (2017) analyzed the same Kromatis 50/70 from the same supplier. They indicated values of *R*% between the N50/70 and PMBTS as well, 27.6% and 16.6% for 100 Pa and 3200 Pa, respectively [177]. Nevertheless, their results are closer to the N50/70 than the PMBTS. Considering *Jnr*, the results from Sengoz et al. (2017) are much higher than those obtained in this research for all the binders (base, modified, and reference ones).

It can be concluded that the transparent binders present better rutting resistance than the conventional N50/70 with higher recovery and lower non-recoverable creep compliance. This fact was expected, since the transparent binder contains elastomeric polymers. However, the transparent binders

presented lower rutting resistance than the PMBTS. The incorporation of nano-TiO₂ can increase the rutting resistance for high contents (mainly 6.0% and 10.0%).

8.3.4.6. FTIR Peak Identification

The FTIR spectra (absorbance versus wavelength) of the (TiO₂-modified) transparent binders, the reference binders, and the pure TiO₂ are shown in Figure 54. Peaks at 2953 cm⁻¹ and 2862 cm⁻¹ are associated with stretching vibrations of sp³ C-H in aliphatic chains, as asymmetric and symmetric stretches, respectively. Peaks at 1460 cm⁻¹ are characteristic of bending vibrations of methylene groups (-CH₂)_n. The peak at 1375 cm⁻¹ is attributed to the bending of methyl groups (-CH₃), which is related to aliphatic branched bands. The long-chain band can be seen at 724 cm⁻¹, associated with the rocking motion of -CH₂ groups in an aliphatic chain. The peak at 1700 cm⁻¹ is related to the stretching of carbonyl band C=O typical of carboxylic acids [205], being one of the most important peaks for the asphalt binder aging [206–208].

Stretching absorptions of C=C bond in aromatic rings occur at the peaks at 1600 cm⁻¹. The peaks that appear between 910 cm⁻¹ and 699 cm⁻¹ can be analyzed carefully to show ortho-, meta- and para-disubstituted rings presented in aromatic compounds and are associated with out-of-plane C-H bending vibrations in this structure. Due to the complex composition of the asphalt binders, all these compounds may be presented in the analyzed samples. For example, the pair 743 cm⁻¹ and 699 cm⁻¹ can match with monosubstituted rings; a single peak at 743 cm⁻¹ may be associated with 1,2-disubstituted rings; peaks at 864 cm⁻¹, 783 cm⁻¹ and 699 cm⁻¹ may be attributed to 1,3- disubstituted rings; and finally, the pair 864 cm⁻¹ and 814 cm⁻¹ can match to 1,4-disubstituted rings [206–208].

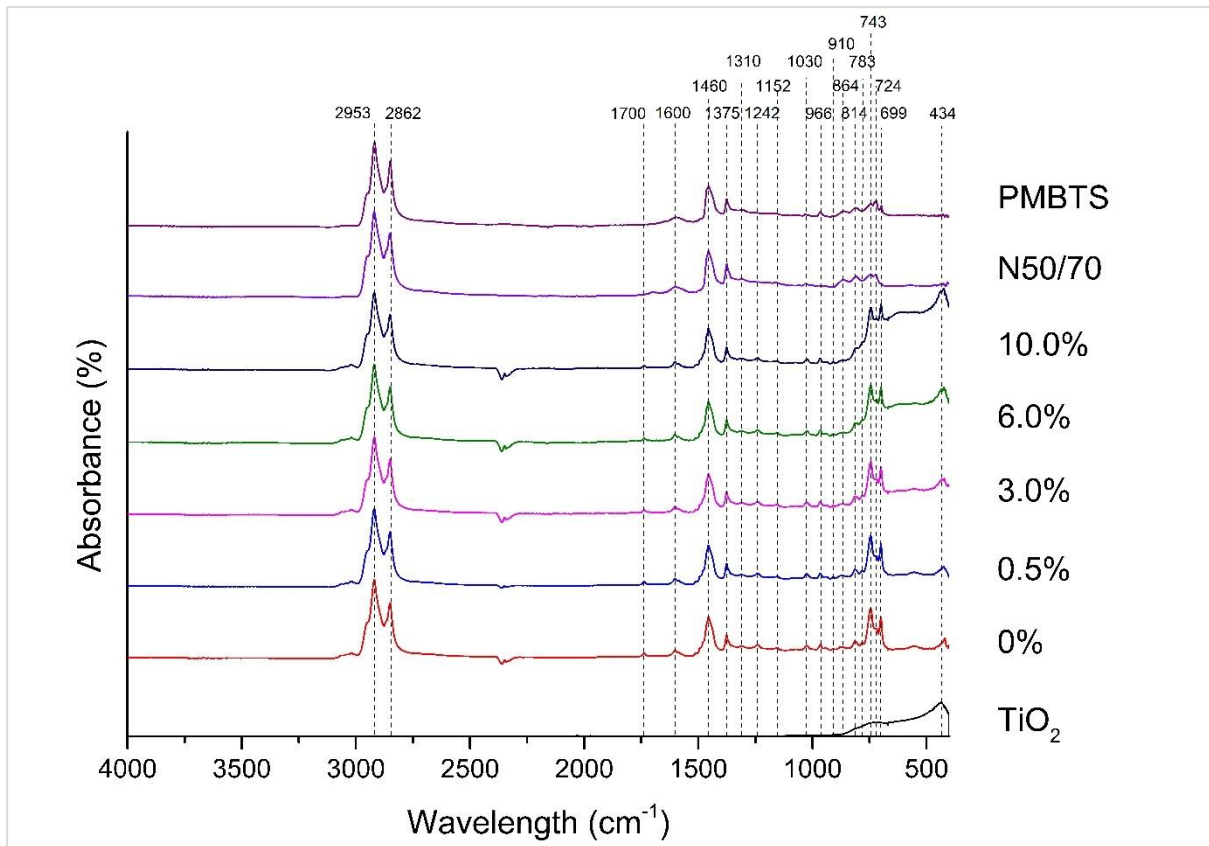


Figure 54: FTIR spectra of the binders of this study

The peaks at 966 cm⁻¹ and 699 cm⁻¹ may still correspond to the bending out-of-plane of C-H of trans-alkenes (from polybutadiene) and C-H out-of-plane bending in monoalkylated aromatics (from polystyrene) associated with SBS. The peak at 910 cm⁻¹ can also show terminal-alkenes [206]. The peak at 1375 cm⁻¹ may be associated with the asymmetric stretch of sulfonyl chlorides S=O bond. While the peaks at 1310 cm⁻¹ and 1152 cm⁻¹ are typical of respectively asymmetric and symmetric stretches of sulfones S=O bonds [209]. At 1030 cm⁻¹, there is the other peak directly related to asphalt binder aging, the stretch of sulfoxide S=O bond [206–208]. The peak 1242 cm⁻¹ can be linked to the asymmetric stretching vibration of sulfate esters [209].

For the transparent binders, the peak 434 cm⁻¹ represents a stretching vibration of metal oxides (M-O) bond (M can be Si, Mn, V, Ni, and others) [210–213]. This peak (434 cm⁻¹) is also attributed to stretch absorptions of Ti-O bond [214], and the increase in this peak area in the TiO₂-modified transparent binders may indicate the proper incorporation of the semiconductor in the asphalt binder.

8.3.4.7. Relationship between the TiO₂ Modification Level and the Chemical Responsible

Figure 55 shows the graph RI versus % TiO₂. It can also be seen that the addition of nano-TiO₂ increases the relative increase *R*/ (from TiO₂ related vibration area). A linear correlation of the nano-TiO₂ percentage and the *R*/ can be found. To some extent, this shift of the spectra with the addition of nano-TiO₂ is to be expected, as the vibrations become more evident when the binder is more diluted. The high correlation coefficient ($R^2 = 0.99$) of the increase of this index with the modification level (Figure 55) confirms the assumption that nano-TiO₂ can be used as a marker in bituminous blends [215,216]. This analysis can be used in order to assess the presence of TiO₂ and quantify its incorporation as a binder modifier.

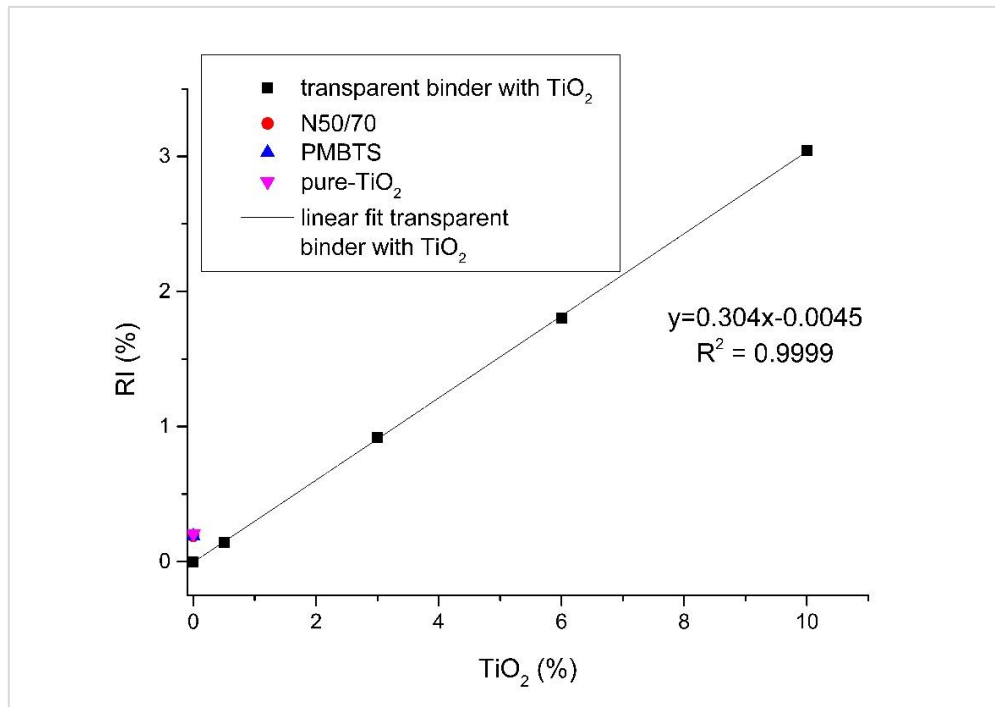


Figure 55: Correlation of the nano-TiO₂ modification level with the increase of the TiO₂-related index

8.3.4.8. Relationship between the TiO₂ Modification Level and the Chemical Responsible

The results of FTIR are presented in Figure 56 in terms of oxygen- and polymer-related indices. The chemical indices sulfoxide, carbonyl, polybutadiene, polystyrene, aromatic, aliphatic, branched aliphatic, and long chains are presented in terms of their normalized intensity. This study confirms that the initial sulfoxide and carbonyl levels of nano-TiO₂-modified are similar to the reference unmodified binder N50/70 and the SBS-modified PMBTS. This observation gives rise to the assumption that the presence of nano-TiO₂ does not introduce new functionalities in sulfoxide- or carbonyl-related groups such

as esters, carboxylic acids, and ketones. Furthermore, the modification of the binder with nano-TiO₂, according to other studies [82,217], can reduce the long-term oxidation performance due to its capability to reflect and absorb UltraViolet (UV) light during photocatalysis. It is also initially chemically neutral for the polar carbonyl groups.

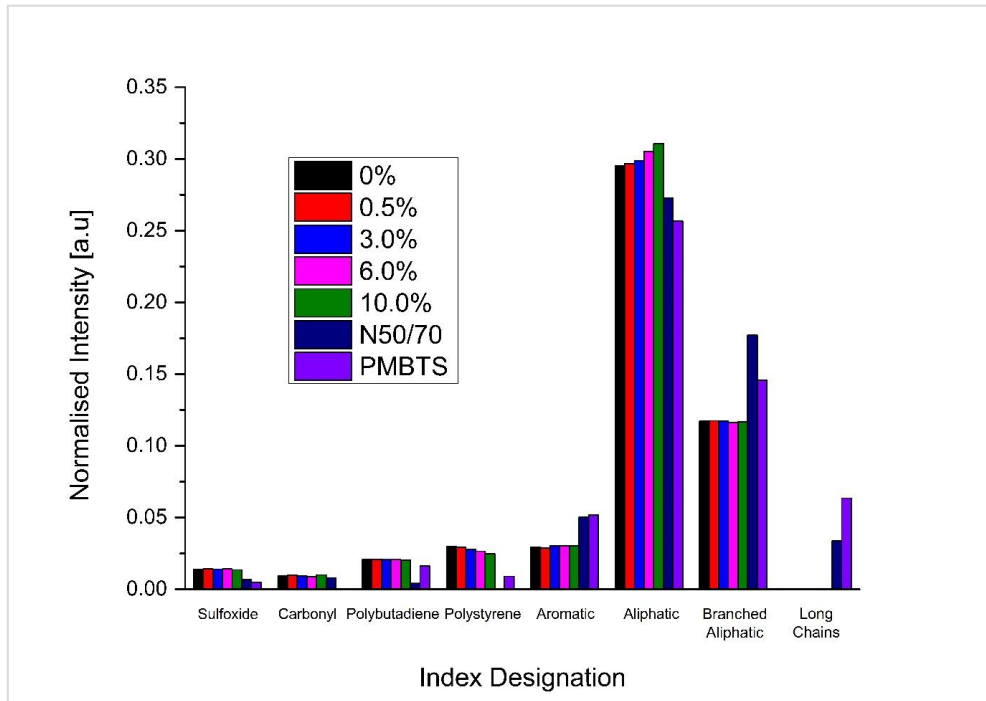


Figure 56: FTIR indices of the nano-TiO₂-modified, base and reference binders

A detailed observation of the two aging-related indices implies that, although of similar magnitude, slightly higher indices can be found compared to the two reference binders N50/70 and PMBTS. This fact can be explained to be the result of the different initial sulfur content for the sulfoxide index. In other words, the origin of the crude oils of the binders is different, and this has a clear implication for the S=O-containing groups. When examining the slightly higher carbonyl index of the nano-TiO₂-modified binders, one can highlight two important points. Firstly, the binder used for modification with nano-TiO₂ was different from the unmodified reference binder, and transparent binders show a carbonyl index of the same magnitude.

The level of modification seems to have a negligible effect on the initial carbonyl index. That is, the increased carbonyl level can be attributed to the binder used as the base for modification and not the nano-TiO₂ addition itself. Following the explanation provided for the higher carbonyl increase of nano-TiO₂-modified binders, the same line of thought can be followed for the slightly lower aromatic, branched aliphatic, and long chains indices and the higher aliphatic index compared to the reference binders.

In parallel, as the introduction of elastomeric polymers produces the binder selected as the base for TiO₂ modification, the polymer-related indices were evaluated. A comparison of the polybutadiene and polystyrene indices reveals that the binder used for modification (transparent base binder) is highly modified compared to the SBS modified reference binder PMBTS. For the binder N50/70, these indices are not applicable.

In contrast to the rheological parameters, the transparent binders did not show intermediate behavior between the reference binders N50/70 and PMBTS. They showed higher indices for sulfoxides, carbonyl, polybutadiene, polystyrene, and aliphatic but lower for aromatic, branched aliphatic and long chains. Their long chains were null. Moreover, the TiO₂ modification seems to have little effect on the indices, except for the polystyrene and aliphatic indices. The polystyrene index decreases, and the aliphatic index increases with the increase of nano-TiO₂.

8.2.5. Conclusions

A transparent binder modified with nano-TiO₂ was characterized with respect to its physicochemical and rheological properties in this chapter. This is useful for specific applications, such as tunnels, calming traffic areas, among others, as the nano-TiO₂ provides to the pavement a photocatalytic function and better visibility. Modified transparent binders, with 0.5%, 3.0%, 6.0%, and 10.0% of nano-TiO₂, were compared to the transparent base binder and two commercial asphalt binders (conventional and PMB).

Based on the results, the transparent binders (base and modified) performed similarly to the conventional binder and PMB, being workable in terms of their viscosity. The transparent binders clearly revealed the presence of an elastomeric modification, indicating polymer modification, and suggested an alternation of elastic/viscous behavior between the materials that compose the transparent binders.

The incorporation of nano-TiO₂ gradually increased the softening point and decreased the penetration by up to 6.0% of modification, causing no substantial changes in the Complex Modulus of the transparent binder. There is no evidence that the addition of TiO₂ up to 10.0% significantly affects the structure or visco-elastic behavior of the chemical indices, except for the polystyrene and aliphatic indices, of either of the transparent binders. Additionally, the addition of TiO₂ would reduce the fatigue life of asphalt pavements using the transparent binder. On the contrary, it would increase the rutting resistance for high contents.

Transparent binders with TiO₂ give promising results, based on their conventional, rheological, and chemical performance. On the one hand, the best percentage for the addition of TiO₂, based on the results, without compromising the performance of the transparent binder, was 0.5% with respect to fatigue resistance. On the other hand, 10.0% nano-TiO₂ was the best with respect to permanent deformation.

Although the objectives of this research were achieved, it is essential to carry out this analysis on more samples, as limited numbers were used. The next steps of this research are to evaluate the light-colored and photocatalytic pavements considering the properties of color and photocatalysis and analyze the aging performance of the transparent binders with nano-TiO₂. Another topic that must be assessed is the analysis of the total life cycle cost (including environmental impact/benefits).

CHAPTER 9 –RECYCLED ASPHALT MIXTURE USING STEEL SLAGS AND RECLAIMED ASPHALT

This chapter refers to the research work about photocatalytic, superhydrophobic and self-cleaning asphalt mixtures “Recycled Asphalt Mixtures Composed of Steel Slags (SS) and Reclaimed Asphalt Pavement (RAP) for Surface Layers” published in conference Wastes in 2019. The content of this chapter is included in this publication which the digital object identifier doi is 10.1201/9780429289798-72 (Figure 57). The main objective of this chapter was to design the recycled asphalt mixtures and evaluate them under mechanical and functional point of view to be latter functionalized and assessed regarding the photocatalytic and superhydrophobic capabilities in the chapter 10.

Incorporation of steel slag and reclaimed asphalt into pavement surface layers

I. Rocha Segundo & E. Freitas
Civil Engineering Department, University of Minho, Guimarães, Portugal

V. Castelo Branco
Transportation Engineering Department, Federal University of Ceará, Fortaleza, Brazil

S. Landi Jr.
Centre of Physics, University of Minho, Guimarães, Portugal, and Federal Institute Goiano, Rio Verde – GO, Brazil

M. F. Costa & J. Carneiro
Centre of Physics, University of Minho, Guimarães, Portugal

ABSTRACT. There is an increasing concern about the recycling and reuse of wastes in different areas. This research aims to analyze the technical viability of the use of Reclaimed Asphalt Pavement (RAP) and Steel Slags (SS) for the composition of asphalt mixtures for surface layers. Therefore, three asphalt mixtures AC 10 were designed: without recycled materials (R), with 30% of RAP (F) and with 30% of SS (A). They were mechanically and superficially assessed. Their water sensitivity and the permanent deformation were similar. The mixture A presented higher stiffness modulus and lower fatigue resistance when compared to the other ones. The best sound absorption and mechanical impedance found were for A and the worst ones were for F. Mixture A had smoother macrotexture if compared to the other mixtures. The asphalt mixtures had similar friction. It can be concluded that these wastes can be incorporated in asphalt mixtures for surface layers.

1 INTRODUCTION

Currently, it is undeniable to say that there is an increasing concern about natural resources depletion and environmental damages. In Paving Industry, most used raw materials, generally, come from non-renewable sources, i.e. aggregates and oil products, which are used as binders. On the other hand, there has been growing motivation for recycling wastes by incorporating them into asphalt mixtures. With this it is possible to obtain more ecological pavements, guaranteeing greater sustainability. In this context, the potential of some wastes has been studied: Steel Slags (SS), Construction and Demolition (C&D) waste, tire rubber and some types of recycled polymers.

The main recycled waste incorporated in asphalt mixtures refers to the milled material from deteriorated asphalt pavement, which is called Reclaimed Asphalt Pavement (RAP). This material has already been studied in several replacement ratios in asphalt mixtures, and under different techniques of production, such as hot, warm and cold asphalt mixtures with or without additives. Its incorporation presents results which are even better than the ones found for conventional asphalt mixtures, while offering some benefits, for example, economical due to the use of aggregates and binder from RAP (Rocha Segundo *et al.*, 2016). In the United States, the most recycled material is RAP, with more than 80 million tons per year, representing of about twice the other fourth most recycled wastes: paper, glass, plastic, and aluminum (Brosseau, 2011). When discarded improperly, it can cause damages to the environment. With its use as a recycled material, it is possible to save money with the transport of virgin materials to the worksite, since RAP can be found on the roads to be paved around the urban perimeter, where quarries are often not located.

For the aged asphalt binder presented in RAP, its incorporation can provide more rigidity to the asphalt mixtures. On one hand, this can improve permanent deformation resistance, on the other hand, its use can decrease fatigue cracking resistance (Hussain and Yanjun, 2013).

Figure 57: First page of the research work published in Wastes [51]

9.1. Introduction

Currently, it is undeniable to say that there is an increasing concern about natural resources depletion and environmental damages. In Paving Industry, most used raw materials, generally, come from non-renewable sources, i.e. aggregates and oil products, which are used as binders. On the other hand, there has been growing motivation for recycling wastes by incorporating them into asphalt mixtures. With this it is possible to obtain more ecological pavements, guaranteeing greater sustainability. In this context, the potential of some wastes has been studied: Steel Slags (SS), Construction and Demolition (C&D) waste, tire rubber and some types of recycled polymers.

The main recycled waste incorporated in asphalt mixtures refers to the milled material from deteriorated asphalt pavement, which is called Reclaimed Asphalt Pavement (RAP). This material has already been studied in several replacement ratios in asphalt mixtures, and under different techniques of production, such as hot, warm and cold asphalt mixtures with or without additives. Its incorporation presents results which are even better than the ones found for conventional asphalt mixtures, while offering some benefits, for example, economical due to the use of aggregates and binder from RAP [218]. In the United States, the most recycled material is RAP, with more than 80 million tons per year, representing of about twice the other fourth most recycled wastes: paper, glass, plastic, and aluminum [219]. When discarded improperly, it can cause damages to the environment. With its use as a recycled material, it is possible to save money with the transport of virgin materials to the worksite, since RAP can be found on the roads to be paved around the urban perimeter, where quarries are often not located.

For the aged asphalt binder presented in RAP, its incorporation can provide more stiffness to the asphalt mixtures. On one hand, this can improve permanent deformation resistance, on the other hand, its use can decrease fatigue cracking resistance [220].

Other wastes from different sources have already been incorporated in the Paving Industry. It is worth mentioning the use of slags, the by-product of the Steel Industry. This residue has already been incorporated into asphalt mixtures, from base courses to surface layers. Generally, there are two types of slags produced by the industry: i) blast furnace: obtained directly from blast furnace; (ii) steel: resulting from the production of steel, obtained in electric furnaces and in oxygen converters.

Some of its limitations are associated with its high density, causing higher transport costs, its high water absorption, which can increase the binder content, and its high expansion, requiring a curing period before the incorporation [221].

Due to its metallic material content, mainly iron oxide (Fe_2O_3), the SS present high electrical and thermal conductivity. Thus, asphalt pavements composed of this material, when irradiated by microwaves, can melt easier snow on its surface during the winter when compared to conventional asphalt pavements. Therefore, it can be portrayed as a new function of asphalt mixture, since this property is not considered as an essential one [116].

The literature points out that most of the researches are about the mechanical characterization of recycled asphalt mixtures, but not the functional (superficial) characterization (mainly taking into account the use of SS). Thus, this chapter aims to analyze the technical viability of the use of RAP and SS for the composition of asphalt mixtures for the surface layer of road pavements.

9.2. Materials

9.2.1. Aggregates and Bitumen

In order to design the asphalt mixtures, two granite aggregates (fine aggregate 0/4 mm and course aggregate 4/10 mm), filler, RAP 0/6 mm and SS 0/10 were used. Their main properties are presented in Table 14.

Table 14: Main properties of the natural and recycled aggregates

Aggregate	Particles density (g/cm ³)	Water absorption (%)	Micro-deval abrasion loss (%)	Los angeles abrasion (%)	Binder (%)
4/10	2.63	0.9	15	30	-
0/4	2.67	0.5	-	-	-
Filler	2.71	-	-	-	-
RAP 0/6	2.55	1.0	-	-	6.7
SS 0/10	3.38	2.4	11	25	-

The Form 2D, Sphericity, Angularity, and Surface Texture were characterized by Digital Image Processing (DIP) technique using Aggregate Image Measurement System (AIMS) (Table 15) [222,223]. By Their Form 2D, the aggregates 4/10, 0/4 and RAP were classified as elongated, while SS and filler were characterized as semicircular and semi-elongated respectively. All the coarse aggregates were

characterized as moderate sphericity by the parameter sphericity. Considering the angularity, all the aggregates were sub-rounded. The surface texture of the materials was smooth for 4/10 and RAP and low rough for SS. Regarding all these parameters, it is possible to mark that the best aggregate characteristics is for SS.

The binder used was a commercial one named Elaster 13/60 provided by Cepsa®. The modified bitumen was classified as 35/50 by penetration grade. The bitumen was characterized by (i) penetration of 50×10^{-1} mm (EN 1426/2015); (ii) Brookfield viscosity of 349 cP at 180 °C (EN 13302/2010); (iii) Softening Point of 64 °C (EN 1427/2015).

Table 15: Form, sphericity, angularity and texture characterization.

Property	Aggregate	Average	Classification
Form 2D (fine)	4/10	8.0	Elongated
	0/4	8.4	Elongated
	RAP	8.1	Elongated
	SS	7.9	Semi-circular
	Filler	8.3	Semi-elongated
Sphericity (coarse)	4/10	0.764	Moderate sphericity
	RAP	0.737	Moderate sphericity
	SS	0.771	Moderate sphericity
Angularity (fine and coarse)	4/10	3619.0	Sub-rounded
	0/4	3911.4	Sub-rounded
	RAP	3825.5	Sub-rounded
	SS	3554.1	Sub-rounded
	Filler	2466.3	Sub-rounded
Surface Texture (coarse)	4/10	175.3	Smooth
	RAP	202.7	Smooth
	SS	345.4	Low roughness

9.2.2. Asphalt Mixtures

Three asphalt mixtures were designed by Marshall design method: i) R: reference mixture, ii) F: recycled mixture with 30% of RAP, iii) A: recycled mixture with 30% of SS. The asphalt mixtures have the same gradation and almost the same content of binder, of about 5.5%. Table 16: shows the composition

of the asphalt mixtures, binder contents, Bulk Density (BD), Maximum Bulk Density (MBD) and Void Content (VC).

Table 16: Asphalt mix composition and volumetric properties

Asphalt Mix	% 4/10	% 0/4	% Filler	% RAP 0/6	% SS 0/10	% binder	% virgin binder	MBD (g/cm ³)	BD (g/cm ³)	VC (%)
R	68	28	4	-	-	5.5	5.5	2.428	2.305	5.1
F	67	-	3	30	-	5.4	3.5	2.446	2.334	4.6
A	42	25	3	-	30	5.4	5.5	2.676	2.569	4.0

9.3. Methods

9.3.1. Mechanical Characterization

In order to characterize the asphalt mixture from a mechanical point of view, water sensitivity, permanent deformation, stiffness modulus, and fatigue resistance were assessed. The water sensitivity was evaluated by Indirect Tensile Strength Ratio (ITSR) test (EN 12697-12). The ratio between the wet samples (ITSw) and the dry samples (ITS) was calculated and defined as ITSR. The permanent deformation resistance of the asphalt mixtures was assessed by the Wheel Tracking Test (WTT) (EN 12697-22). The deformation curve versus cycle and the maximum rutting of the asphalt mixtures will be compared. For the stiffness modulus, the asphalt mixtures were assessed by the four-point bending test configuration (EN 12697-26) for different frequencies and temperatures. The master curve stiffness versus frequency (Hz) will be compared at 20 °C. Considering the fatigue resistance (EN 12697-24), the samples at 20 °C are submitted to sinusoidal loading at 10 Hz, in strain control mode of loading. The relationship between the strain level versus the number of cycles will be presented.

9.3.2. Superficial Characterization

In order to characterize superficial properties of the asphalt mixtures, Mean Profile Depth (MPD), British Pendulum, sound absorption, and mechanical impedance tests were carried out. The same samples of WTT were used to characterize superficial properties. The macrotexture was assessed by MPD. Profiles of 25×25 cm² surface were acquired by a device equipped with a laser, and the MPD was calculated (ISO 13473-1:2019). The device can acquire profiles every 0.2 mm with a vertical resolution up to 0.01 mm. The baseline of the profiles is divided by half of the length, and the average of their two

peak heights is used to calculate the MPD. To access the friction, British Pendulum test was carried out (EN 13036-4).

Related to tire-road noise, for sound absorption, a self-made impedance tube with 80 mm of diameter utilizing the two-microphone arrangement was used [224]. A graph of absorption versus frequency (between 500 and 2000 Hz) will be presented. For mechanical impedance, damping is a measure for determining the capacity of the structure to dissipate energy. An accelerometer was bonded to the specimen and it was submitted to a hammer impact in the opposite side. The Graph damping versus frequency (Hz) will be presented. The configuration for the last two tests of noise indicators can be seen on Freitas et al. (2014).

9.4. Results

The asphalt mixtures were mechanically characterized by water sensitivity, permanent deformation and fatigue resistance tests. The results of the water sensitivity test are shown in Table 17. On the one hand, the ITS of the recycled asphalt mixtures increased by 44% and 34% for those ones composed of RAP (F) and SS (A), respectively. The ITSw also increased, 37% and 35% for the same mixtures, respectively. On the other hand, the ITSR (water sensitivity) maintained for A but decreased 5% for F. All the asphalt mixtures respected the minimum value of ITSR (80%) required for Portuguese asphalt mixtures for the top layer of road pavements.

For the permanent deformation (Figure 58a), at the end of the test, R, F, and A mixtures respected the maximum value considering the Portuguese requirements (20 mm) and deformed 1.86, 1.93 and 2.00 mm. The recycled asphalt mixtures had similar behavior. F and R mixtures, respectively, deformed 4% and 8% more than the conventional AC 10. It can be concluded that the asphalt mixtures had a similar behavior considering the permanent deformation.

Regarding the results of the master curve of stiffness modulus at 20 °C (Figure 58b), R (reference mixture), F (composed of 30% of RAP) and A (composed of 30% of SS) had values between 201 and 10,192 MPa, 858 and 14,504 MPa, 251 and 12,143 MPa, respectively. Thus, considering the low frequencies, on the one hand, A mixture had similar moduli when compared to R. On the other hand, F mixture had stiffness modulus of about 4 times higher than R for the lowest frequency. At high frequencies, the stiffness moduli of R and A were similar and the difference between the results of F and R was lower than that one found at low frequencies. F had stiffness modulus about 1.4 times higher than R for the highest frequency. In general, A and R had similar results, and F had higher values. Probably

this resulted from the aged binder of the RAP that composed F. Its content was 1.9%. For the fatigue resistance (Figure 58c), the strain for $N = 10^6$ cycles was 339×10^{-6} , 262×10^{-6} and 317×10^{-6} for R, F, and A, respectively. A and R had similar curves and F presented lower results. It can be concluded by the mechanical results that the asphalt mixture that used SS as aggregate (A) presented superior mechanical results. Probably, this fact is related to the use of the aged binder from RAP provided higher stiffness for the mixture, contributing to lower fatigue resistance and higher stiffness modulus.

Table 17: Water sensitivity results

Asphalt Mix	% RAP 0/6	% SS 0/10	VC (%)	ITS (MPa)	ITSw (MPa)	ITSR (%)
R	-	-	5.1	1.47	1.35	92
F	30	-	4.6	2.12	1.84	87
A	-	30	4.0	1.97	1.82	92

Also, the asphalt mixtures were superficially characterized by sound absorption and mechanical impedance, macrotexture and friction. Considering the assessments related to tire-road noise, mechanical impedance, and sound absorption, the results are presented in Figure 58d. For sound absorption, the average value was 0.18, 0.16 and 0.20 for R, F, and A, respectively. Although the asphalt mixtures did not have a peak of maximum sound absorption within the interest frequencies, the best absorption was for A and the worst was for F. For damping, the investigated asphalt mixtures had 2 peaks. The first one was between 418 and 550 Hz and the second one was from 1,770 to 2,125 Hz. The same trend for sound absorption was reported. The best damping was found for A and the worst one for F.

For the macrotexture characterization, MPD was carried out and for friction characterization, the British Pendulum Test was used (Table 18). Analyzing the macrotexture, the mixture A had a macrotexture of about 17% smoother than the other mixtures.

Regarding friction, A had 7% lower PTV and F had a similar PTV when compared to that of the R. Considering the superficial analysis, the best results for macrotexture and friction of the recycled asphalt mixtures is for F (30% RAP), but, considering the noise indicators, sound absorption and mechanical impedance, mixture A (30% SS) presented the best results.

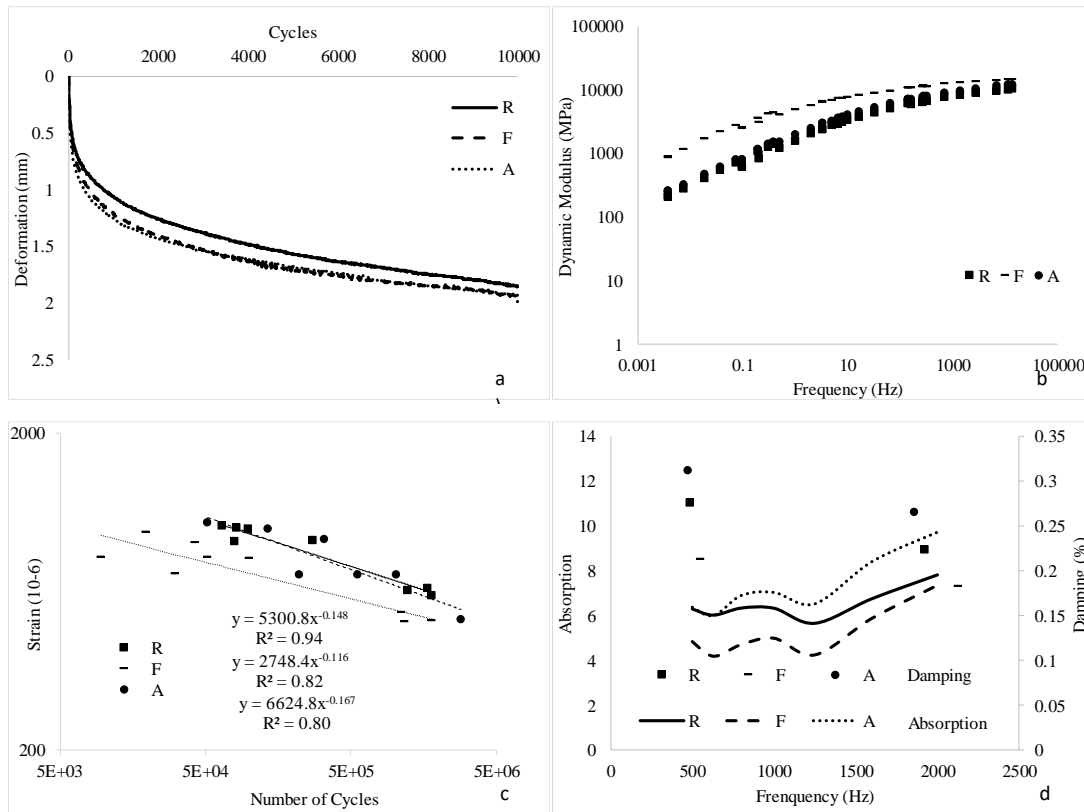


Figure 58: a) Permanent Deformation, b) Dynamic Modulus, c) Fatigue and d) Absorption and Damping

Table 18: Macrotexture and friction results

Asphalt Mix	MPD (mm)	British Pendulum Value (PTV)
R	1.3	61
F	1.3	60
A	1.1	57

9.5. Conclusions

This research aimed to analyze the viability of the use of RAP and SS in the composition of asphalt mixtures for surface layers. Three asphalt mixtures were designed, and mechanically and superficially characterized: without wastes (R), with 30% of RAP (F) and with 30 % of SS (A). Based on the results of this research, the following conclusions can be drawn:

- ITS and ITS_w of the recycled asphalt mixtures increased when compared to the conventional mixture, R. The water sensitivity of the asphalt mixtures was similar. All the asphalt mixtures had similar permanent deformation as well. In general, A and R had similar results of stiffness modulus, and F was stiffer. A and R had a similar fatigue curve and F had lower fatigue resistance. Probably,

these results were due to the aged binder of RAP that composes F. Stiffer binder conducted to a stiffer asphalt mixture and to lower fatigue resistance.

- Regarding the surface characterization, the best absorption and mechanical impedance found was for A and the worst was for F. F and R had the same value of MPD (macrotexture). The mixture A had smoother macrotexture if compared to R and F. Regarding the friction results, the asphalt mixtures had similar PTV values.

Considering mechanical results, the best asphalt mixture was A (30% SS). Regarding the superficial analysis, the best macrotexture and friction results of the recycled asphalt mixtures was for F (30% RAP), but, considering the noise indicators, sound absorption and mechanical impedance, the best one was A. Thus, probably, mix A tends to be more resistant and quieter than F, but F tends to be safer than A. The aggregate characteristics of SS contributed to better mechanical results comparing to those ones observed for F. The use of SS did not impact the asphalt mixture properties significantly, differently of the use of RAP that conducted to lower fatigue resistance. Some superficial benefits were observed with the use of SS considering the noise indicators. By the fact that the recycled asphalt mixtures respected the characterization requirements, it can be concluded that SS and RAP can be used in asphalt mixtures for surface layers.

CHAPTER 10 – ECOLOGICAL, PHOTOCATALYTIC, SUPERHYDROPHOBIC AND SELF-CLEANING ASPHALT MIXTURES

10.1. Introduction

The main objective of this chapter was to improve the photocatalytic, superhydrophobic and self-cleaning capabilities of the functionalized asphalt mixtures with better results of immobilization (fixation of the particles). To achieve it, different types of solutions were set to enhance the efficiency and keep them working as long as possible by an improved immobilization process. Also, the effect of the type of asphalt mixture (conventional or recycled with reclaimed asphalt pavement or steel slags) is analyzed.

In the previous chapters of functionalization and evaluation of new capabilities, a simple method of an aqueous solution was carried out. A solution was prepared with water and semiconductor particles (TiO_2 and ZnO) and was sprayed over the asphalt mixture samples. Other methods were evaluated, namely the volume incorporation and the asphalt binder modification, however it was concluded that the initial photocatalytic results are much better when the spraying coating is applied. In Chapter 6, it was detailed that: “The photocatalytic efficiency was much higher for the spraying coating than the functionalization by bulk incorporation before abrasion. The low efficiency by bulk incorporation was probably due to the low content of TiO_2 over the surface of samples”. This application method needs improvements considering the immobilization process. Also, in order to guarantee better results of superhydrophobicity, other particles need to be added to the solution. This fact was explained in Chapter 5: “Therefore, the combination of TiO_2 and ZnO was important to achieve the superhydrophobic property”. Thus, it is important the combination of particles to guarantee the superhydrophobicity.

The asphalt mixture AC 10 was selected to continue this process since it is a mixture between the AC 6 and the AC 14. The first one is more adequate for top layers with good functional characteristics, but it does not present good mechanical behavior. AC 14 is a mixture with higher structural capacity, but it is not the most adequate mixture to top layers due to the high nominal size of aggregates. This fact was explained in chapter 5. Also, the best photocatalytic results were achieved for AC 14 (92% for the TiO_2 ZnO) when compared to the AC 6 (81% for AC 6 TiO_2 ZnO) after 24 h of irradiation. Also, the superhydrophobicity was achieved for AC 14 TiO_2 , AC 14 TiO_2 ZnO and AC 6 TiO_2 ZnO .

Reported in the Chapter 9, the AC 10 was designed, and recycled (Steel Slags - SS - and Reclaimed Asphalt Pavement - RAP) materials were introduced into it. RAP is the most common recycled material

applied into asphalt mixtures. With the introduction of RAP, it is possible to mitigate the use of virgin material (aggregates and asphalt binder). Regarding the use of SS, it was used in order to analyze the introduction of iron from their composition on the photocatalytic capability. Iron is commonly used in order to improve the photocatalysis [33,43]. Also, it was notice in the Chapter 4 that the introduction of this recycled material, besides the ecological component, it is possible to provide new capabilities to the asphalt mixtures by the increase in the electrical conductivity, namely deicing/anti-icing and self-healing. Certainly, it is necessary the submission of induction heating or even microwaves in order to activate this new functionality. Thus, with the use of both recycled materials, the asphalt mixtures are ecological from the begging of the process (mixture and paving), during the service time with the photodegradation of air pollutants when the semiconductors are applied and to the end of lifetime with less impact to the environment.

10.2. Materials and Methods

In this Chapter, the recycled asphalt mixtures from the last chapter (Chapter 9) were functionalized using TiO₂ nanoparticles and/or PTFE microparticles. For this, two steps were carried out: i) selection of the best solutions and ii) analysis of an immobilization process of the particles. First, some solutions were prepared using these particles and different types of solvents with different concentrations. They were applied over the surface of the reference mixture, which was analyzed under photocatalytic efficiency and water contact angle to select the best solution (BS) to spray. To improve the immobilization process, two consecutive spraying coatings were carried out. The first one was performed with an epoxy resin diluted using butyl acetate and the second one with the BS previously selected. For this, tests of Rhodamine B degradation and water contact angle were carried out in order to analyze the photocatalysis and the wettability (to check the superhydrophobicity), respectively.

10.2.1. Materials

The asphalt mixtures submitted to functionalization were already described in Chapter 9: R (reference), F (with 30% RAP), and A (with 30% steel slags). The particles used were nano-TiO₂ and micro-PTFE with a particle size of 1 μm. An epoxy resin with two components was selected: i) epoxy resin composed of Bisphenol A and ii) Cycloaliphatic polyamine Adduct. According to the supplier, for pavement applications, the best mixing proportion is 2/1 in mass. Its main properties are density of 1.10 g/cm³; ideal temperature application between 10 and 30 °C; and adhesion > 3 N/mm²; curing period of 24h. Epoxy resins are commonly used in road pavements and it was already tested as binder for the application

method spreading [39,39]. Also, a similar approach was carried out by Arabzadeh et al. [225] using a diluted epoxy resin but only for superhydrophobic purposes.

10.2.3. Sample Preparation for the first step (selection of best solution)

The method of application of the particles was by spraying solutions over the surface of the asphalt mixture R (reference). First, different types of solutions were prepared with nano-TiO₂ and micro-PTFE with water, ethyl alcohol, and dimethyl ketone using different concentrations. It was impossible to prepare aqueous solutions with PTFE since the particles cannot be dispersed into this medium. The solutions were sprayed over the cut asphalt mixture R (reference) with 25 x 25 x 15 mm³ dimensions to identify the best solution. The spraying process was the same as explained in Chapter 6, with a spraying ratio of 8 mL/cm² at Room Temperature. The (functionalized) asphalt mixture samples were named by an alphanumeric string, which starts by AC 10 to indicate reference asphalt concrete, the particle used (TiO₂ and/or PTFE), and then the solvent used (W – water, ETH – ethyl alcohol, and CET – dimethyl ketone), respectively (Table 19). When both particles, nano-TiO₂ and micro-PTFE, were combined, at the end of the string, the concentration of the solution was inserted, for example, AC 10 TiO₂PTFE-ETH-8g/L. In this case, 4g/L (2 g/L of nano-TiO₂ and 2 g/L of micro-PTFE) or 8g/L (4 g/L of nano-TiO₂ and 4 g/L of micro-PTFE) was included. In the case of solutions with just one type of particles, the concentration was 4 g/L. The concentrations selected were according to the previous works carried out in this thesis (Chapter 5, 6 and 7) and also to the literature [7].

Table 19: Mixture AC 10 (R) sprayed with different solutions.

Mixture	TiO ₂ (g/L)	PTFE (g/L)	Solvent
AC 10	-	-	-
AC 10 TiO ₂ -W	4	-	Water
AC 10 TiO ₂ -ETH	4	-	ethyl alcohol
AC 10 TiO ₂ -CET	4	-	dimethyl ketone
AC 10 PTFE-ETH	-	4	ethyl alcohol
AC 10 PTFE-CET	-	4	dimethyl ketone
AC 10 TiO ₂ PTFE-ETH-4g/L	2	2	ethyl alcohol
AC 10 TiO ₂ PTFE-ETH-8g/L	4	4	ethyl alcohol
AC 10 TiO ₂ PTFE-CET-4g/L	2	2	dimethyl ketone
AC 10 TiO ₂ PTFE-CET-8g/L	4	4	dimethyl ketone

10.2.4. Sample Preparation for the second step (immobilization of the particles)

After the selection of the best solution, all the (recycled and conventional) asphalt mixtures were functionalized through two successive spraying coatings: first, spraying of a diluted resin epoxy and then spraying of the BS. Table 20 describes all the samples prepared in this step.

Table 20: Name of the samples for the immobilization of BS.

Sample	Mixture	Diluted Resin (mg/cm ²)	BS (mL/cm ²)
R 0.25g	Reference	0.10	-
R 0.25g-BS	Reference	0.10	8
R 0.5g	Reference	0.20	-
R 0.5g-BS	Reference	0.20	8
R 1g	Reference	0.40	-
R 1g-BS	Reference	0.40	8
R 2g	Reference	0.80	-
R 2g-BS	Reference	0.80	8
F 0.25g	with RAP	0.10	-
F 0.25g-BS	with RAP	0.10	8
F 0.5g	with RAP	0.20	-
F 0.5g-BS	with RAP	0.20	8
F 1g	with RAP	0.40	-
F 1g-BS	with RAP	0.40	8
F 2g	with RAP	0.80	-
F 2g-BS	with RAP	0.80	8
A 0.25g	with SS	0.10	-
A 0.25g-BS	with SS	0.10	8
A 0.5g	with SS	0.20	-
A 0.5g-BS	with SS	0.20	8
A 1g	with SS	0.40	-
A 1g-BS	with SS	0.40	8
A 2g	with SS	0.80	-
A 2g-BS	with SS	0.80	8

The epoxy resin was diluted using butyl acetate with a proportion of 1:1 in mass. The cut asphalt mixtures were sprayed with 0.25, 0.50, 1, and 2 g of the diluted resin, resulting in a covering ratio of 0.1, 0.2, 0.4, and 0.8 mg/cm². This very low covering ratio is explained by the fact that a high covering ratio could lead to the sinking of the particles. This process was similar to that one used by Arabzadeh et

al. [225]. In both steps, the selection of the BS and immobilization process of the particles was based on the photocatalytic efficiency and the water contact angle. For all tests carried out here, 2 asphalt mixture samples were functionalized and evaluated.

10.2.5. Photocatalytic Efficiency Test

The photocatalytic efficiency test was carried out using the same protocol and equipment exposed in Chapter 5. Nevertheless, in this case, it was carried out with 3 hours of dark condition (adsorption period) and 8 hours of irradiation (photocatalytic evaluation). With this change, tests are now faster than that one from the Chapter 5. In this chapter, it was noticed that the adsorption was stable after 3 hours of dark solution, being enough to split both phenomena. Moreover, 8 hours is enough to analyze the photocatalytic efficiency with details (as carried out in Chapter 6).

10.2.6. Water Contact Angle Test

The water contact angle test was carried out using the same protocol and equipment described in Chapter 5. The only difference was the total time of the test; in this case, it was only 2 minutes. The most important angles are the initial ones as explained in Chapter 5 “The initial WCA is the most important angle because the water drains in a very short time to the roadside”; thus 2 minutes is enough to analyze with details.

10.3. Results and Discussions

10.3.1. Selection of Best Solution

All photocatalytic results concerning the selection of the best solution are presented in Figure 59. To assist the analysis, they were split according to a) particles with ketone; b) particles with ethyl alcohol; c) solvents with TiO_2 ; d) solvents with TiO_2 and PTFE, as shown in Figure 60.

A global examination of the results reveals that samples only with PTFE (AC 10 PTFE-ETH and AC 10 PTFE-CET) presented a photocatalytic efficiency 21% higher than AC 10. The samples with TiO_2 showed a photocatalytic efficiency at least 38% higher than the AC 10 at the end of the test, with the worst performing results for the sample AC 10 TiO_2 PTFE-CET-4g/L, which increased the efficiency from 34% to 47% (38% increase), when at least TiO_2 is used.

When ketone was used (Figure 60a), the highest efficiencies achieved were related to the used of only TiO_2 . When the ethyl alcohol was used (Figure 60b), the best treatment was AC 10 $\text{TiO}_2\text{PTFE-ETH-8g/L}$, then AC 10 $\text{TiO}_2\text{-ETH}$ and AC 10 $\text{TiO}_2\text{PTFE-ETH-4g/L}$. The effect of the solvent on efficiency of samples with TiO_2 in decreasing order of performance were ketone followed by ethyl alcohol and water, with almost the same results. For the combination of the particles, the increase of the photocatalytic efficiency was 5% for the ethyl alcohol and 15% for the ketone, when the concentration increases from 4g/L and 8 g/L.

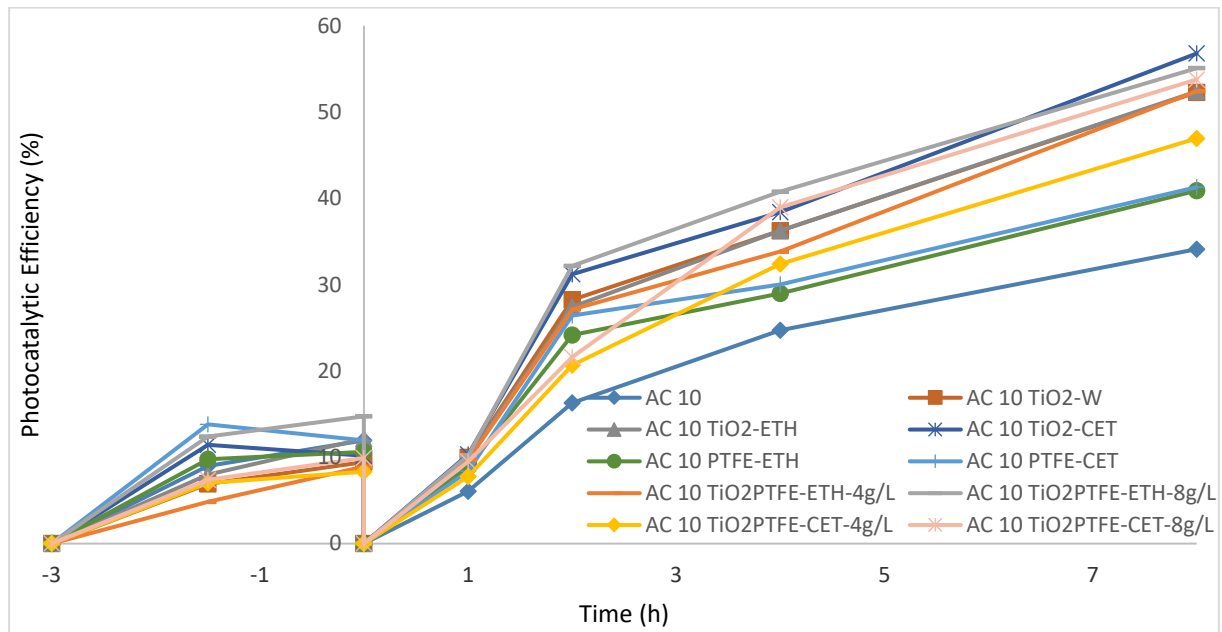


Figure 59: a) Photocatalytic Efficiency of all the samples from the first step (selection of best solution)

It can be seen that the best solutions achieved were $\text{TiO}_2\text{-CET}$ and $\text{TiO}_2\text{-PTFE}$ under an ethyl alcohol medium with a concentration of 8 g/L (AC 10 $\text{TiO}_2\text{PTFE-ETH-8g/L}$).

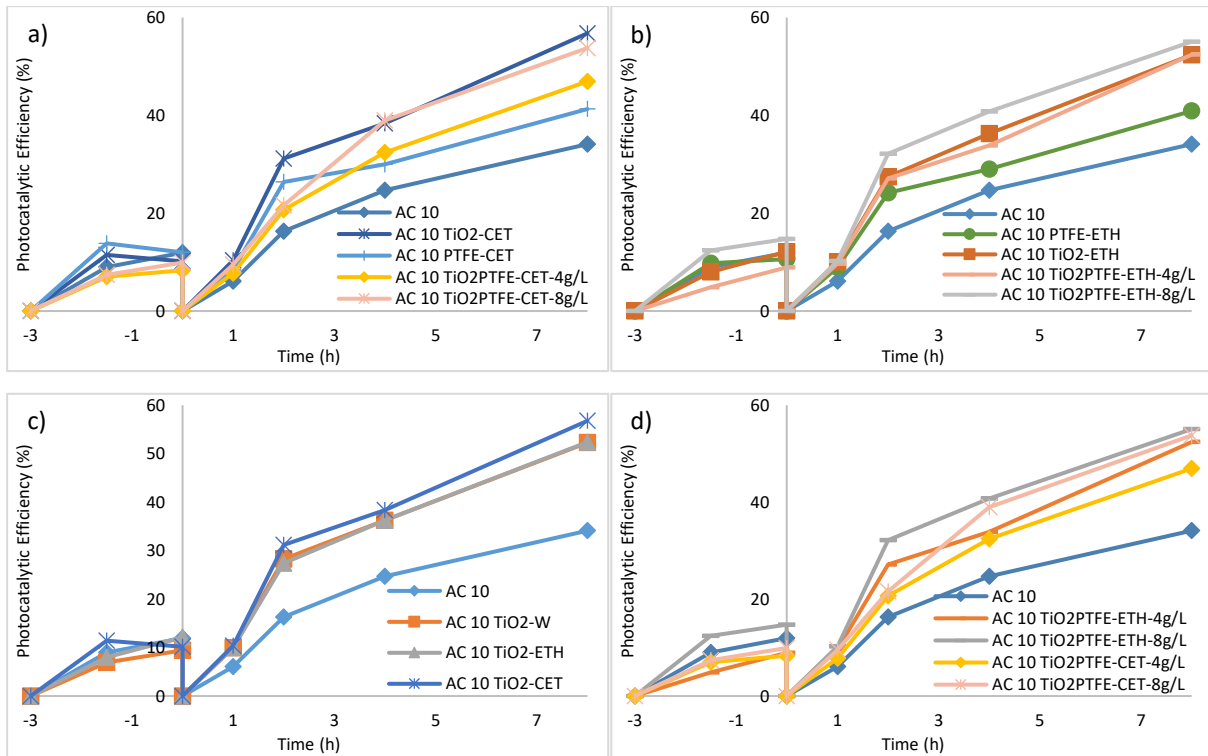


Figure 60: Photocatalytic Efficiency of the samples comparing the: a) particles with ketone; b) particles with ethyl alcohol; c) solvent with TiO₂; d) solvent with TiO₂ and PTFE from the first step (selection of best solution)

The water contact angle results are presented in Figure 61. Again, to help the results analysis, they were split and presented in Figure 62 to better compare the solvents with a) TiO₂; b) PTFE; c) TiO₂ and PTFE. Similarly, to compare the particles performance with different mean: a) ketone, and b) ethyl alcohol, the results are rearranged in Figure 63.

The reference asphalt mixture AC 10 presented an initial WCA of 117°. All the treated samples increased WCA when compared to AC 10. The increase was at least 11% concerning the AC 10 TiO₂-CET sample. All functionalized asphalt mixtures presented a superhydrophobic capability (WCA > 150°), except those with TiO₂-W (145°) and TiO₂-CET (130°), which are overhydrophobic surfaces (120° < WCA < 150°). Thus, the treatments TiO₂-ETH, PTFE-ETH, PTFE-CET, TiO₂PTFE-ETH and TiO₂PTFE-CET provided superhydrophobic capability.

Regarding the effect of the solvents with TiO₂ (Figure 62a), ethyl alcohol lead to the best WCA (153°), followed by water (145°). The worst of them was with ketone (130°), as already mentioned before. For the PTFE (Figure 62b), both treatments with ketone and ethyl alcohol presented similar initial results, but with time the best of them was with ketone.

The increase in the concentration of TiO₂-PTFE (Figure 62c and Figure 63) was more effective on the ethyl alcohol. For the whole testing, doubling the concentration leads to an increase of the WCA of 13% and 2% for ETH and CET, respectively.

When the particles were combined, the initial WCA was similar (155°), except for AC 10 TiO₂-PTFE-CET-4g/L, that was slightly less (151°). Nevertheless, taking into account the whole testing duration, it is clear that samples with higher WCA were the AC 10 TiO₂PTFE-ETH-8g/L. The average of WCA from 0 to 120s increase 36% when compared to the reference sample. This functionalized asphalt mixture showed a WCA at 20 s, and a better performance than all the other samples, that dropped the WCA to at least 131°, along this testing time. As explained before, the best results are represented by the highest initial WCAs,

For the same solvent (Figure 63), solutions with TiO₂ and PTFE and a concentration of 8 g/L delivered the highest WCA. While the results for the solutions with ketone were similar except for TiO₂-CET (the worst of them), for ethyl alcohol, the results were dispersed over time.

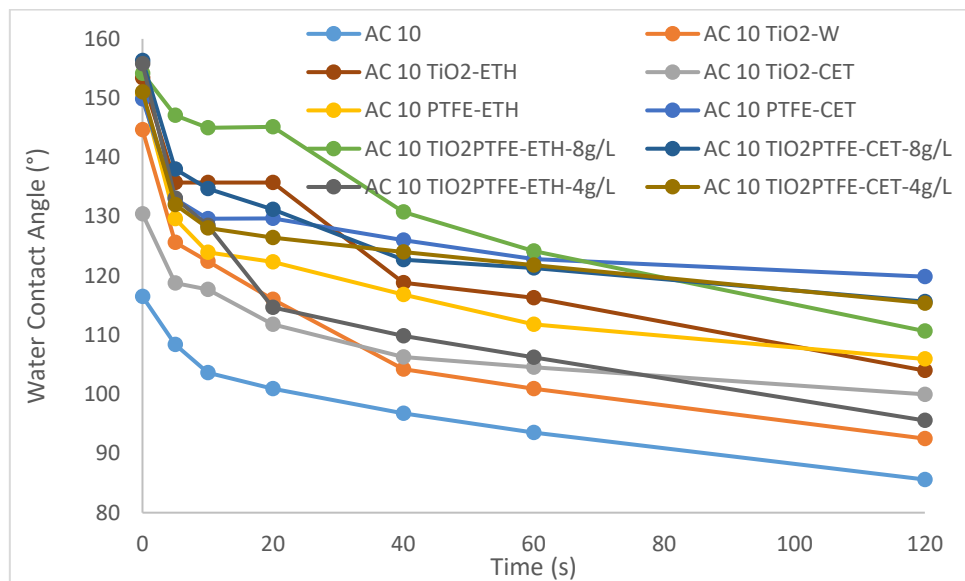


Figure 61: Results of Water Contact Angle of all the samples from the first step (selection of best solution)

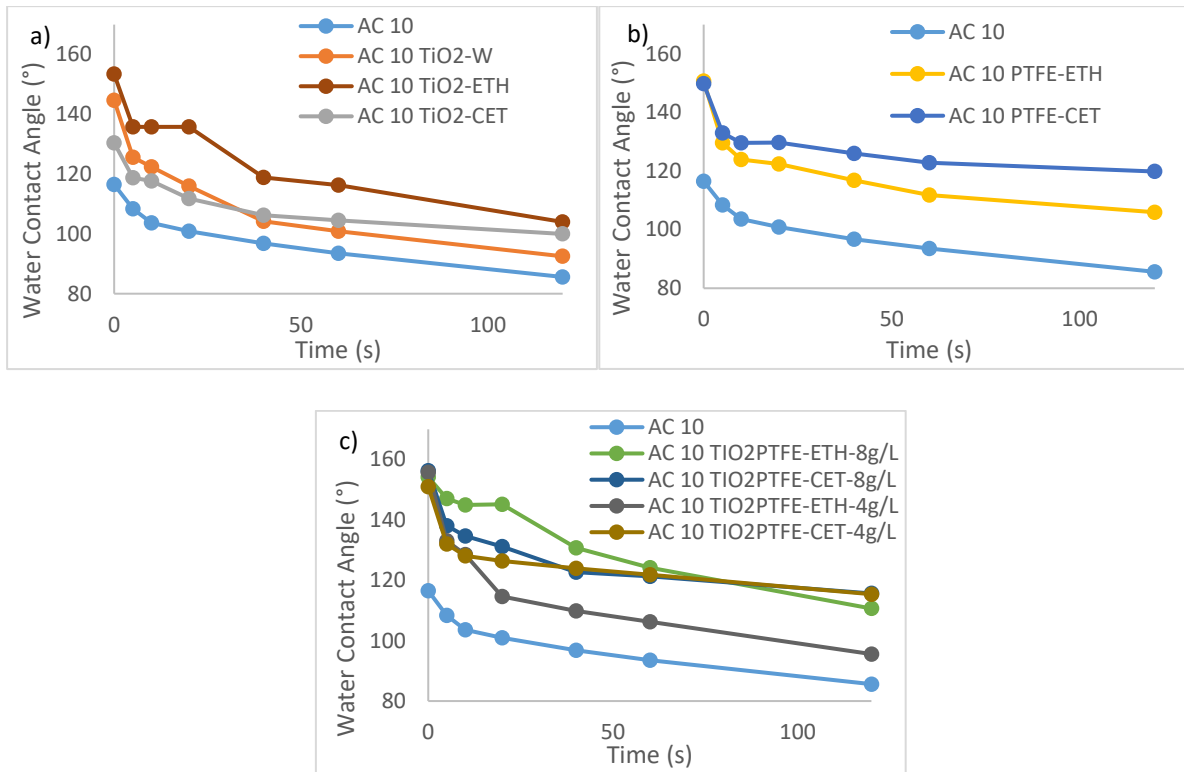


Figure 62: Results of Water Contact Angle comparing the: a) best solvent with TiO₂; b) best solvent with PTFE; c) best solvent with TiO₂ and PTFE

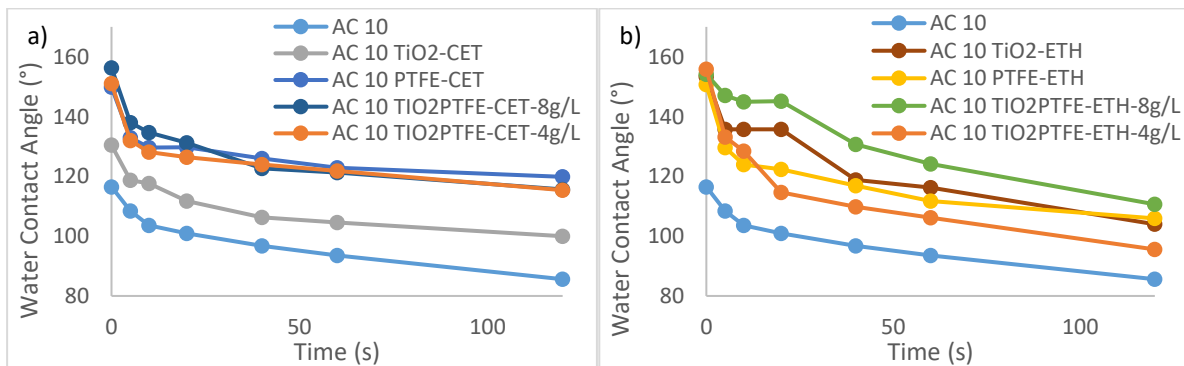


Figure 63: Results of Water Contact Angle (analysis of the particles) comparing the: a) best particles with cetone, and b) best particles with ethyl alcohol.

Thus, since the treatment TIO2PTFE-ETH-8g/L was the best considering the WCA and the second one regarding photocatalysis, it was decided to adopt this treatment as the BS to proceed with the functionalization process aiming the immobilization process. The best one regarding the photocatalytic efficiency (AC TiO₂-CET) presented the worst WCA for the treated samples. While the second best considering the WCA (AC 10 TiO₂PTFE-ETH-4g/L) was the fifth performance concerning the photocatalysis.

10.3.2. Immobilization of BS on Recycled and Conventional Asphalt Mixtures

In this section, the (recycled and conventional) asphalt mixtures were sprayed with 2 consecutive spraying coatings. Figure 64 to 64 show the results of the photocatalytic efficiency of the recycled and conventional asphalt mixtures with the spraying of the Best Solution (BS), $\text{TiO}_2\text{PTFE-ETH-8g/L}$, after the application of a diluted resin also by spraying. In general, it can be seen that the spraying of the diluted resin decreased the photocatalytic efficiency. The samples with the highest photocatalytic efficiency are those with the least amount of resin, namely with 0.25 g and 0.5 g for all the mixtures (R-0.25g-BS and R-0.50g-BS for the mixture R, F-0.25g-BS and F-0.25g for the mixture F, and A-0.25g-BS and A-0.50g for the mixture A).

The samples with 1 g and 2 g had the poorest photocatalytic performance. This fact can be explained by the adsorption of the pollutant (in this specific case, RhB) to the surface of the asphalt mixtures. The adsorption after 3 hours for all the samples with resin (and or without BS) was 7% in average. When compared to the previous ones without resin, a reduction of 3% was found. When the photocatalytic efficiency is compared with the samples without resin, there is a reduction from 49% to 28% in average. The highest results were with 0.25g-BS for all the asphalt mixtures. Another reason could be the fact that the particles can sink into the resin. These assumptions must be further investigated.

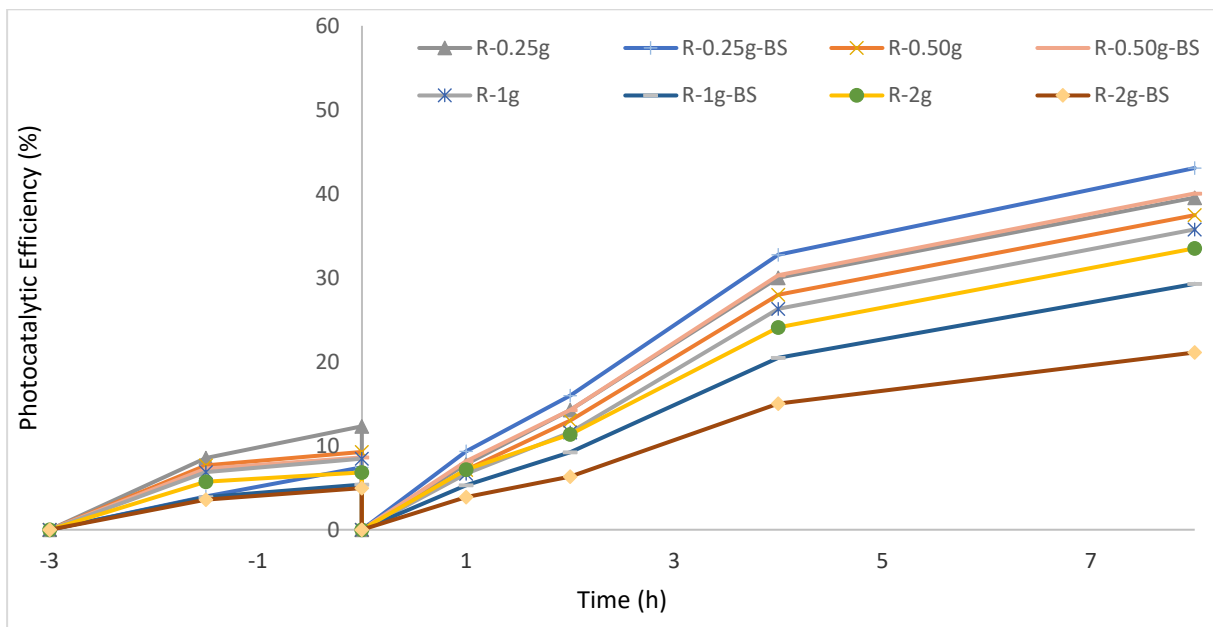


Figure 64: Results of Photocatalytic Efficiency of the mixture R with resin and BS

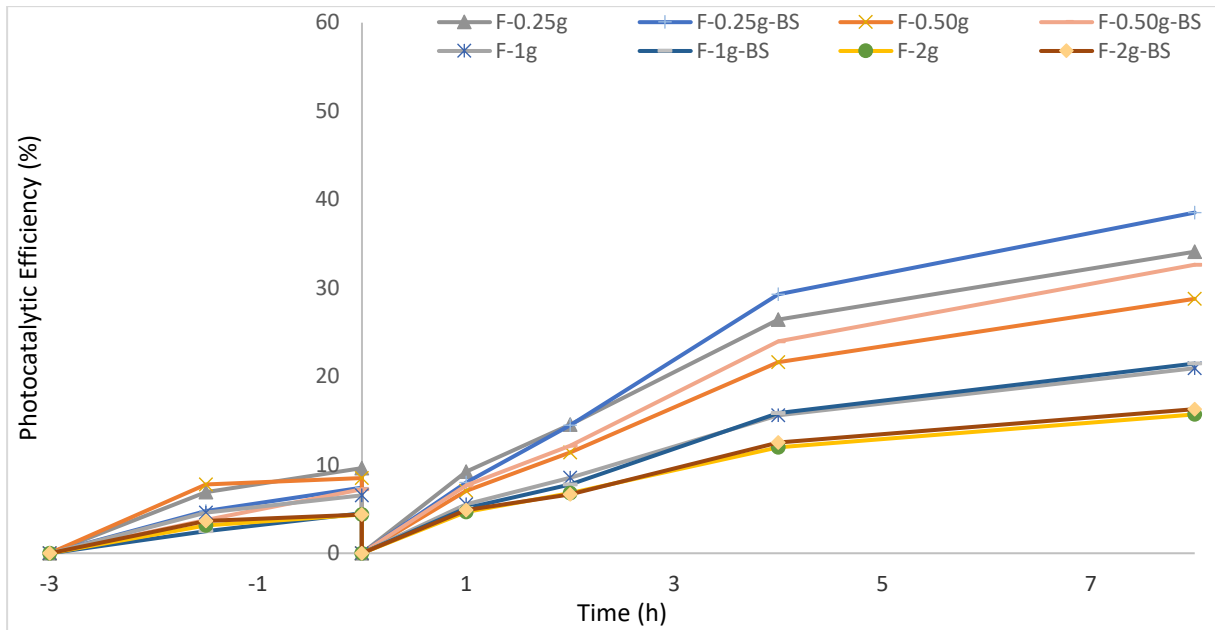


Figure 65: Results of Photocatalytic Efficiency of the mixture F with resin and BS

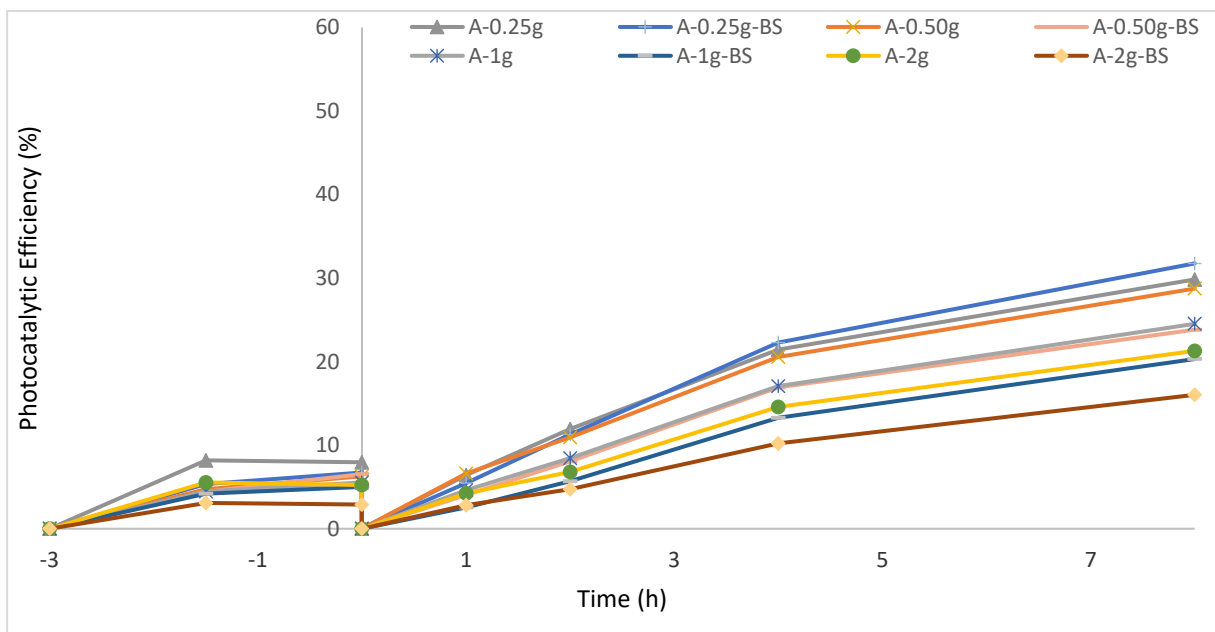


Figure 66: Results of Photocatalytic Efficiency of the mixture A with resin and BS

Figure 67 shows the comparison of the wettability of the asphalt mixtures R (reference), F (with 30% of RAP), and A (with 30% of SS). It can be seen that the wettability of mixtures F and R are similar, and mixture A is much more hydrophobic than these, with a difference of 16°.

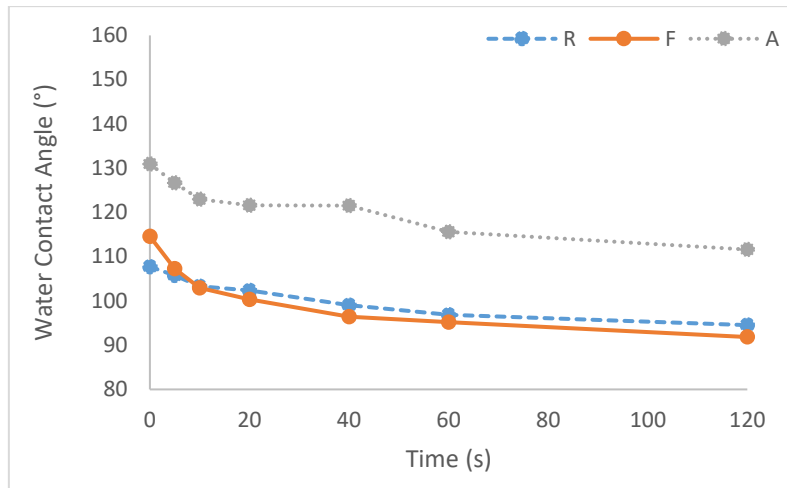


Figure 67: Results of Water Contact Angle for the mixtures without treatment (R – Reference, F – with 30% of RAP, and A – with 30% of SS)

Figure 68 shows the results of mixture R with resin only (Figure 68a) and with resin and BS (Figure 68b). The spraying of the resin decreases the WCA. The worst WCA was with 2 g, while the best one was with 0.25 g. When the mixture was functionalized with BS, the WCA increased for the samples with 0.25, 0.50, and 2 g. The superhydrophobic capability was achieved for the samples with 0.25 and 0.50 g of resin.

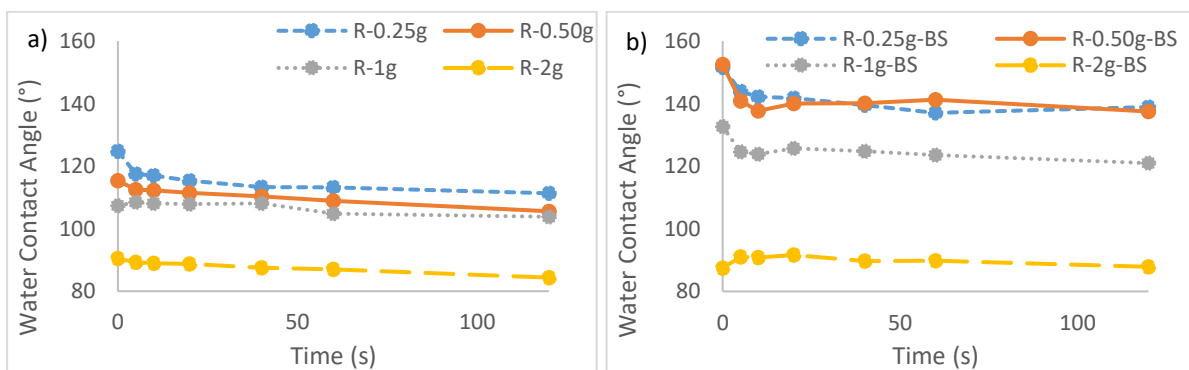


Figure 68: Results of Water Contact Angle for mixture R: a) with resin, and b) resin+BS

Figure 69 shows the results of mixture F with resin only (Figure 69a), and with resin and BS (Figure 69b). Also, for this mixture, the spraying of the resin decreased the WCA with the resin quantity. When the mixture was functionalized with BS, the WCA increased for the samples with 0.25, 0.50, and 2 g similarly to mixture R. The superhydrophobic capability was achieved for the samples with 0.25 and 0.50 g.

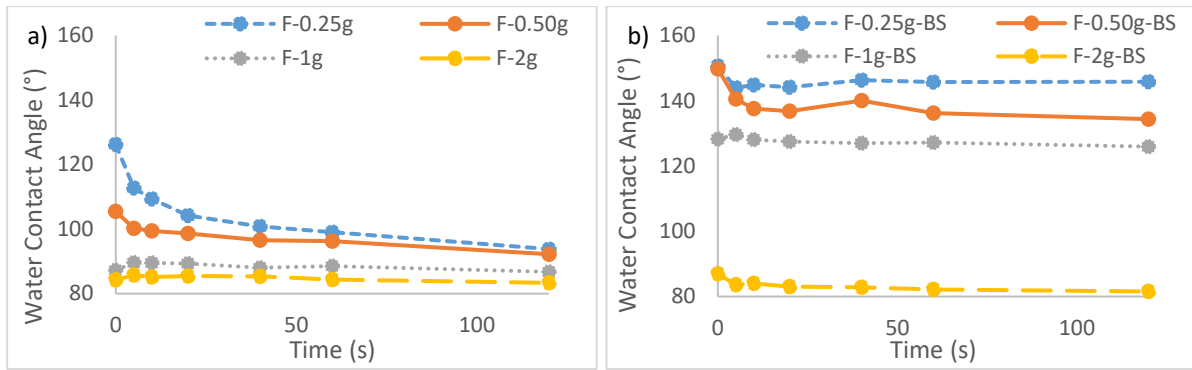


Figure 69: Results of Water Contact Angle for mixture F: a) with resin, and b) resin+BS

The results of wettability of the mixture A with resin only and with BS are presented in Figure 70. The pattern was similar to the previous mixtures (R and F). The main difference was in the only mixture that presented a superhydrophobic capability was the one treated with 0.25 g of resin.

Regarding the effect of the asphalt mixture (conventional or recycled), both situations can be used in order to have a superhydrophobic surface. The asphalt mixture with RAP (F) was more effective than the mixture with SS (A) after the functionalization by the diluted resin and the BS. As seen, before this process, the mixture with SS was better than those ones without recycled materials and also with RAP. For the photocatalysis, also the mixture A was less effective than these ones. The conventional mixture R presented the best photocatalytic results.

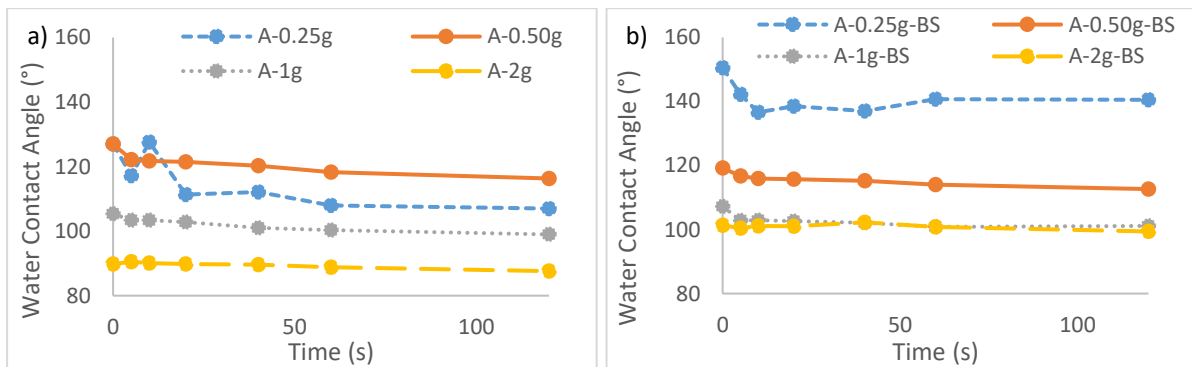


Figure 70: Results of Water Contact Angle for mixture A: a) with resin, and b) resin+BS

10.4. Conclusions

In this chapter, solutions composed of different solutes (particles) and solvents were used to select the best solution (BS) regarding photocatalytic efficiency and superhydrophobicity. Also, recycled and

conventional asphalt mixtures were functionalized using a method that consisted of two consecutive spraying coatings: i) the first one with a diluted resin and ii) the second one with the BS. This second step was aimed at improving the immobilization process of the particles over the surface of the asphalt mixtures. From the results, the following conclusions are drawn:

- The samples with TiO₂ presented a photocatalytic efficiency at least 38% higher than the AC 10 at the end of the test. The best solutions achieved were TiO₂-CET and TiO₂-PTFE under an ethyl alcohol medium with a concentration of 8 g/L (AC 10 TiO₂PTFE-ETH-8g/L). The treatments TiO₂-ETH, PTFE-ETH, PTFE-CET, TiO₂PTFE-ETH, and TiO₂PTFE-CET provided superhydrophobic capability.
- Concerning both capabilities, the treatment TIO2PTFE-ETH-8g/L was the best considering the WCA and the second one regarding the photocatalysis, therefore it was selected as BS.
- The spraying of the diluted resin decreased the photocatalytic efficiency. The highest results were with 0.25g-BS for all the asphalt mixtures. The spraying of the resin decreases the WCA. The wettability of mixtures F and R are similar (115°), but mixture A is much more hydrophobic mixture (131°). F presented an initial WCA of 115° while A showed 131°. The superhydrophobic capability was achieved for the samples with 0.25 and 0.50 g with BS for R and F mixtures. The mixture A achieved the superhydrophobic capability only for 0.25 g of resin.
- Recycled and conventional asphalt mixtures were functionalized with superhydrophobic capability. The asphalt mixture with reclaimed asphalt pavement was more effective than the mixture with steel slags after the functionalization by the diluted resin and the BS. For the photocatalysis, also the mixture A was less effective than these ones. The conventional mixture R presented the best photocatalytic results.

In general, it can be concluded that using successive spraying of a diluted resin and spraying with particles can provide the superhydrophobic capability for low amounts of resin (less than 0.50 g). The photocatalytic capability decreased with the use of the resin. The highest the use of resin, the lowest the photocatalytic efficiency. The best results were for 0.25 g of resin with BS. However, more studies are essential to explain the results and consequently to improve them. One hypothesis is that the particles can sink in the thick layers of resin losing their effectiveness for the new capabilities. Another is related to the adsorption period.

The next step of this result is to analyze better the thickness of the resin and the particles coverage over the surface by SEM. It is essential the analysis of both perspectives (photocatalytic and superhydrophobic capabilities) after a wearing process. Moreover, the analysis of friction under different conditions (dry, wet and icy) will be carried out.

CHAPTER 11 – CONCLUSIONS AND PARALLEL AND FUTURE WORKS

11.1. Conclusions

The main objective of this thesis was to develop an ecological, photocatalytic, superhydrophobic and self-cleaning asphalt pavement surface. The specific objectives were related to the revision of the new capabilities applied to asphalt mixtures, use different nano/microparticles, analysis of the essential characteristics (mechanical and functional) after functionalization, assessment of new potentialities of the use of TiO₂ by asphalt binder modification, design of recycled asphalt mixture to functionalize them with new capabilities, and evaluation of the immobilization processes. All these relevant specific objectives were accomplished and contributed to achieve the main goal of this thesis, which was also reached regarding the development of an ecological asphalt mixture with multifunctional capabilities.

Therefore, this research work presented many results (from literature reviews and laboratory work) considering the application of new capabilities to asphalt mixtures and provides several conclusions and recommendations (for future works) that will be discussed in this chapter.

The work developed in the scope of smart and multifunctional road pavements can be included in the domain of clean technology (e.g., photocatalytic pavements that promote the environmental depollution of NO_x-type gases emitted as vehicle exhaust gases). In this context, it contributes to materializing the transition to a novel socio-economic model known as “Green Recovery” that is environmentally friendly, sustainable, and inclusive. This model is a very important path toward economic and employment recovery, a vision to which many countries are strongly committed.

To fulfill the objectives of this doctoral thesis, an extensive literature review was carried out considering the application of new capabilities (functionalization) to the asphalt mixtures. Then, different types of asphalt mixtures (conventional AC 6 and AC 14, and conventional and recycled AC 10 with steel slags and reclaimed asphalt pavement) were functionalized to provide them with photocatalytic, superhydrophobic and self-cleaning capabilities by using micro/nanoparticles of TiO₂, ZnO, and PTFE. Also, it was aimed to improve the anti-aging effects of asphalt binder by using TiO₂ nanoparticles.

In general, according to the literature review, multifunctional road pavements can deliver a very positive contribution to the citizens who utilize those roads, bringing benefits to the environment and to the road performance. Several types of new capabilities have been applied to asphalt mixtures, namely photocatalytic, superhydrophobic, self-cleaning, deicing/anti-ice, self-healing, thermochromic, and Latent

Heat Thermal Energy Storage (LHTS).

The development of photocatalytic road pavements is relevant since they can degrade pollutants where there are high traffic emissions, contributing to the air cleaning and improving the health conditions of populations that live in urban centers. This new capability is mainly provided by semiconductor materials, mostly TiO_2 , usually at the nanometer scale (anatase phase or P-25) and applied by using four significant methods: spraying coating, bitumen modification, volume incorporation, and spreading.

Regarding the superhydrophobic capability, the most used materials to functionalize asphalt mixtures are PTFE, TiO_2 , TiO_2 and ZnO, SiO_2 , Mg-Al LDHs, and fluorine polymer with nano-CaO nano/microparticles. With this application, the road pavements can be safer during periods of rain and cold weather.

Considering the application of nano/micromaterials, their use on a real scale is still a challenge for the Paving Industry. This thesis showed some use opportunities, which do not require expensive technological improvements. In fact, it is reasonable to state that, very soon, one of the potential destinations for the large-scale application of nanomaterials is the road sector, as it can act as a great lever to promote the dynamism and economic growth of industries related to the production of nanomaterials and nanotechnology use.

Next are presented the main conclusions achieved in the scope the laboratory work carried out to achieve the specific objectives of this doctoral thesis.

The superhydrophobic capability (WCA higher or equal to 150°) was achieved using TiO_2 , TiO_2 ZnO, PTFE, and TiO_2 PTFE. The combination of particles improves this parameter and can also provide other capabilities, for example, photocatalytic capability and self-cleaning effects.

For the photocatalytic efficiency, the use of TiO_2 aqueous solution sprayed onto the surface of the asphalt mixtures was able to promote the photodegradation of an organic pollutant (Rhodamine B dye). After 24 hours of light irradiation, the maximum photocatalytic efficiency (92%) was obtained for samples functionalized with TiO_2 and ZnO.

Considering mechanical impacts, the semiconductors TiO_2 ZnO applied by aqueous solution have no mechanical impact, assessed by Indirect Tensile Strength after water immersion. The mechanical impact of the bulk incorporation of nano- TiO_2 was mostly reflected on the increase of moisture sensitivity

(lower Indirect Tensile Strength values after water conditioning). On the one hand, the higher content of TiO₂ (6%) improved the permanent deformation, did not affect stiffness modulus, and reduced the fatigue resistance under very low strain when compared with the conventional mixture. On the other hand, the lower content of nano-TiO₂ (3%) had a slightly higher permanent deformation, conducted to a lower stiffness, and kept the fatigue resistance when compared with a conventional mixture.

The photocatalytic efficiency was much higher for the spraying coating technique than for the functionalization by bulk incorporation, before abrasion. The low efficiency by bulk incorporation was probably due to the low content of TiO₂ over the surface of samples. After abrasion, the photocatalytic efficiency of sprayed samples was highly reduced, while for bulk incorporation samples, it increased with the level of abrasion. The rain simulation in combination with abrasion washes the surface, removing the nanoparticles which were not immobilized.

Concerning the functional characteristics, bulk incorporation of TiO₂ may have slightly smoothed the surface. The functionalization by spraying and bulk incorporation presents a maximum absolute difference of PTV of 7%, corresponding to a decrease of 4 PTV. The treatments did not affect the amplitude parameters of microtexture. Thereby, the functionalization had a low impact on skid resistance and texture, allowing the application of the semiconductors by bulk incorporation and spraying. Road safety is in this way assured for the study conditions.

In this thesis, nano-TiO₂ was used to modify Elaster and transparent asphalt binders. Taking into account the effect on Elaster modification, it is beneficial at short term as it revealed anti-aging capability. This can mitigate problems caused by increased stiffness. The increase of the percentage of TiO₂ led to a gradual decrease of mass loss. Regarding the viscosity, low content of TiO₂ of 0.25% conducted to anti-aging effect for Elaster. The next phase of this investigation will address aging in the UV chamber to assess the anti-aging effects under this perspective and consolidate this study. For both asphalt binders, in general, the incorporation of nano-TiO₂ gradually increased the softening point and decreased the penetration depending on the asphalt binder type. For the transparent asphalt binder, the use of nano-TiO₂ did not lead to substantial changes in the Complex Modulus. In addition, nano-TiO₂ would reduce the fatigue life but increase the rutting resistance for high contents.

Considering the mechanical and functional behavior of the recycled asphalt mixtures, the asphalt mixture with 30% of steel slags performed generally better. Regarding the surface characteristics, the best macrotexture and friction results of the recycled asphalt mixtures was for that one with 30% of reclaimed

asphalt pavement, but, considering the noise indicators, sound absorption, and mechanical impedance, the best one was with 30% of steel slags. Thus, mix with steel slags tends to be more resistant and quieter than with reclaimed asphalt pavement, but this one tends to be safer than that one.

Regarding the functionalization method of a successive spraying coating, the use of a diluted resin can be used to immobilize the nano/microparticles. Still, it must be used in a very low mass/volume of spraying (less than 0.50 g). Using 0.25 g of diluted resin and a solution with TiO_2 and PTFE under an ethyl alcohol medium, it was possible to achieve the superhydrophobic capability and the highest results of photocatalytic efficiency. Nevertheless, the use of resin decreased the photocatalytic efficiency, and some aspects of adsorption, particles sinking, among others, must be evaluated.

The best asphalt mixture analysed was the functionalized AC 10 without recycled materials. However, considering sustainable gains the incorporation of these materials and the new capabilities of photocatalysis and superhydrophobicity, the asphalt mixture with reclaimed asphalt pavement is one alternative. Moreover, and if new potentialities (self-healing and anti-ice/de-icing) are desired, the mixture with steel slags can be used.


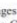

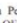
11.2. Parallel Works

During the Ph.D. course, some parallel works were carried out at the Centre for Territory, Environment and Construction (CTAC) from the Civil Engineering Department, the Center of Physics, and with the collaboration of both research centers from the University of Minho. Several scientific articles were published, and others are still under evaluation. In this section, the main contributions by the author of this thesis are detailed.

Figure 71a shows the first article written by the author. The work carried out aimed at studying the physicochemical and rheological impacts of the asphalt binder modified with nano/micro TiO_2 and micro-ZnO. This article motivated the author to further research the modification of asphalt binders with semiconductor particles (results in Chapter 8).

Figure 71b shows the research work published in Applied Acoustics. In this specific case, the author of this thesis contributed to perform the noise tests in the road pavements. This knowledge transposed to Chapter 9 where noise tests (sound absorption and mechanical impedance) were used to assess the environment contribution of the surfaces studied.

Photocatalytic asphalt pavement: the physicochemical and rheological impact of TiO₂ nano/microparticles and ZnO microparticles onto the bitumen

Iran Gomes da Rocha Segundo ^a, Elisa Alexandra Lages Dias^a, Filipa Daniela Pereira Fernandes^b, Elisabete Fraga de Freitas ^{a†}, Manuel Filipe Costa ^a and Joaquim Oliveira Carneiro ^a

^aCivil Engineering Department, University of Minho, Azurém Campus, Guimarães, Portugal; ^bPhysics Department, University of Minho, Azurém Campus, Guimarães, Portugal; ^cPhysics Department, University of Minho, Guislar Campus, Braga, Portugal

(Received 14 August 2017; accepted 3 March 2018)

A cost-effective solution to provide asphalt pavements with the photocatalytic property was addressed for the first time, based on the combination of low percentages of two semi-conductors, TiO₂ and ZnO. Two photocatalytic techniques – spray deposition and bitumen modification – were used. With the former, the chemical properties were evaluated by FTIR after spraying the bitumen samples with two aqueous solutions, one with acid pH and another alkaline, of nano-TiO₂. The solution with less chemical impact was the alkaline one. With the latter, Penetration, Softening Point, Mass Loss, Dynamic Viscosity, Complex modulus and Performance Grade, after the modification by TiO₂ nano/microparticles and ZnO microparticles, were analysed with two levels of ageing produced by the RTFOT. TiO₂ nano/microparticles and ZnO microparticles conducted to softer bitumens and better results of short-term ageing resistance and did not cause any deterioration to the bitumen before or after either short- or long-term ageing.

Keywords: functionalisation; photocatalysis; bitumen modification; nanomaterials; TiO₂; ZnO

Introduction

NO_x (NO and NO₂) and volatile organic compounds (VOC) are the main harmful gases to human health, emitted by vehicles (de Melo & Trichês, 2012; de Melo & Trichês, 2017; Dylla, Asadi, Hassan, & Mohammad, 2013; Hassan, Dylla, Asadi, Mohammad, & Cooper, 2012; Tang, Liu, Huang, & Cao, 2017). Some semiconductor materials, such as zinc oxide (ZnO), tungsten oxide (WO₃), titanium dioxide (TiO₂) and cerium oxide (CeO₂), act as catalysts in redox reactions that promote the photodegradation of pollutants, i.e. when these materials, in the presence of water (moisture) and oxygen, are irradiated with ultraviolet (UV) light emitted by the sun, reactive-free radicals have the ability to degrade organic pollutants transforming them into CO₂ and water, SO₂ into H₂SO₄ and NO_x into HNO₃, etc. (Agiros & Pichat, 2005; Fujishima & Honda, 1972; Hassan et al., 2012; Hassan, Dylla, Mohammad, & Rupnow, 2010; Liu, Wang, Zhang, & Fan, 2015; Zhao & Yang, 2003).

The road pavements, due to their large area and closeness to pollutants' sources, are potentially a good solution to help cleaning the atmosphere by the photocatalytic oxidation of pollutant

a)

†Corresponding author. Email: efreitas@civil.uminho.pt

© 2018 Informa UK Limited, trading as Taylor & Francis Group



Traffic noise and pavement distresses: Modelling and assessment of input parameters influence through data mining techniques

Elisabete F. Freitas^{a,*}, Francisco F. Martins^a, Ana Oliveira^a, Iran Rocha Segundo^a, Hélder Torres^b

^aCEAC, School of Engineering, Department of Civil Engineering, University of Minho, Portugal

^bADGE, School of Engineering, Department of Civil Engineering, University of Minho, Portugal

ARTICLE INFO

Keywords:
Type pavement noise
Acoustic and psychoacoustic indicators
Pavement distresses
Data mining
Support vector machines
Artificial neural networks

ABSTRACT

Traffic noise affects greatly health and well-being of people, consequently the knowledge and control of the factors affecting it is very important. In this study models to predict type-pavement noise acoustic and psychoacoustic indicators based on type of pavement, texture, pavement distresses and speed were developed and used to assess the importance of each factor. By applying data mining techniques, in particular artificial neural networks and support vector machines, models with good predictive capacity of both acoustic and psychoacoustic noise indicators were obtained, constituting a practical tool to reduce the type-pavement noise. Moreover, the proposed models allowed for the assessment of the influence of the input parameters controlling noise such as type of pavement, texture, speed and pavement distresses for the first time. It was found that pavement distresses and, as expected, speed influence strongly type-pavement noise. In this way it is clearly shown that preventive maintenance of road pavements by autoroutes, which eliminates distresses, can have an important effect on type-road noise, promoting the well-being of the population.

1. Introduction

The high population growth rate in urban and metropolitan areas has led to an exponential increase in car traffic in these areas leading to a substantial increase in noise. This noise is a major concern for populations given its negative impact on their health. Traffic noise may affect the mental health and sleep quality [1–3]. In addition, it is a risk factor for hearing, cardiovascular diseases and diabetes [4–7]. Taking into account these concerns of the population the car manufacturers have been reducing the noise of the motors to very low levels, becoming more significant the noise caused by the tyre. Therefore, it is very important to study the type-pavement noise.

The type-pavement noise is influenced by a number of factors, namely driver behaviour, tyre characteristics, pavement surface characteristics and climate [8]. The speed of the vehicle has a strong influence on annoyance regardless the type of pavement, as well as the traffic composition, where higher densities correspond to higher annoyance rates [9]. However, with successive vehicle push-ups and climatic variations, after a certain period of time, road pavements start to develop different types of distresses or pathologies, such as cracks and alligator cracking, rutting, potholes, raveling, among others [10].

In the period of use up to the development of the first distresses, the tyre/road noise increases with different rates depending on the

pavement type. Some studies report very important increases of noise levels in the first years of use [11,12] caused by the wearing of the tyre that removes the asphalt film from the aggregates, changes in texture, clogging and stiffening.

Although the surface characteristics are considered one of the influential factors in type-pavement noise, there are no studies relating the existing pathologies on the surface with type-pavement noise.

The existing pathological conditions on the surface of the pavement, besides causing discomfort to the drivers and increasing accident risk, appear to influence road traffic noise due to the perceptible intensification of tyre vibrations, which is expected to increase the auditive discomfort of road users, in order to demonstrate what is currently perceived by road users, a detailed acoustic study of distressed pavements is essential, therefore psychoacoustic indicators should be considered. There are three key factors associated with this type of studies: type of pavement, traffic speed and level of pavement distress. In this context, the aim of this study was to develop a type-pavement noise prediction model, with the traffic speed, the type of pavement and the existing pathological conditions on the pavement surface as inputs and as outputs the equivalent sound pressure level in decibels (dB) (L_{eq}), A-weighted equivalent mean sound pressure level (L_{eq,A}) and the A-weighted maximum sound pressure level (L_{max,A}) and also the psychoacoustic indicators such as Loudness, Roughness and Sharpness. In

* Corresponding author.
E-mail address: efreitas@civil.uminho.pt (E.F. Freitas).

<https://doi.org/10.1016/j.apacoust.2018.03.018>
Received 12 August 2017; Received in revised form 3 December 2017; Accepted 19 March 2018
0950-0682/© 2018 Elsevier Ltd. All rights reserved.

b)

Figure 71: The first page of the research work published in: a) Road Materials and Pavement Design [80], and b) Applied Acoustics [226]

Another research work was published in Construction and Building Materials: Surface rehabilitation of Portland cement concrete (PCC) pavements using single or double surface dressings with soft bitumen, conventional or modified emulsions (doi.org/10.1016/j.conbuildmat.2021.122611) (Figure 72). It aimed to develop different surface dressings using several asphalt binders (emulsions or bitumen). The author of this thesis contributed to the design of the research, laboratory testing, and writing. It contributed to a deeper knowledge on asphalt emulsions, their evaluation and application on road pavements.

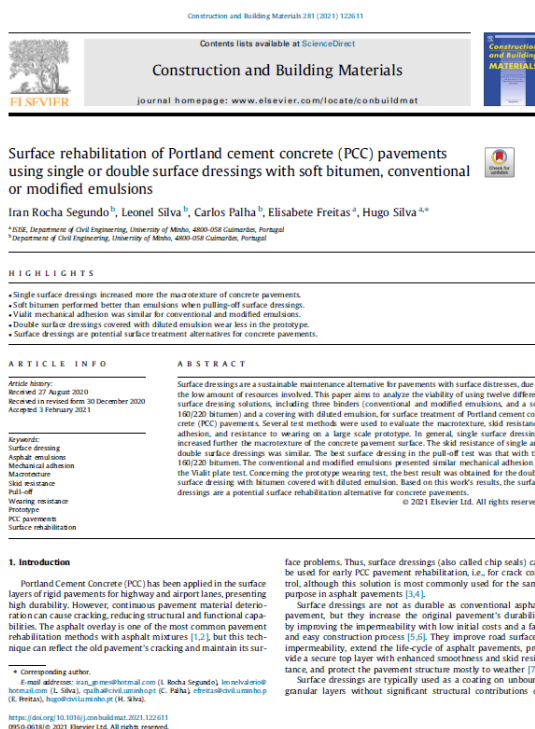


Figure 72: First page of the research work published in Construction and Building Materials [227]

Other scientific articles were prepared mainly at the Physics Department, however they were not already published, such as i) The step-by-step to obtain the Kubelka-Munk function and its use for the calculation of band gap (S. Landi Jr., I. Rocha Segundo, E. Freitas, J. Carneiro); ii) Photocatalytic performance of different textiles coated with TiO₂-RGO system for degradation of crude petroleum under similar simulation of solar irradiation (S. Landi Jr, D. Silva, F. Fernandes, E. S. Nunes, V. Teixeira, J. A. Moreto, I. Rocha Segundo, J. O. Carneiro). Also, combining both knowledges (Civil Engineering and Physics), a new collaboration was started aiming at applying TiO₂ nanoparticles over 3D printed mortars to obtain a multifunctional material. The author of this thesis has transferred his knowledge about the functionalization process and its evaluation to develop these innovative smart mortars, not yet presented in the literature. The resulting manuscript "Preliminary Study on the Photocatalytic Efficiency of 3D Segmented Printed Cementitious Mortars" (B. Zahabizadeh, I. Rocha Segundo, J. Pereira, E. Freitas, A. Camões, C. Tavares, V. Teixeira, M. Costa, V. Cunha, and J. Carneiro) is under assessment.

From another knowledge level (high school), with the assistance of the author of this thesis, three students from Maia High School developed the project Greenway. With this collaboration, two awards were obtained: i) honorable mention in the 16th Edition of the Ilídio Pinho Foundation Award and ii) second

place in the FCT NOVA Challenge Award. This small project aimed to develop an asphalt pavement layer that contributes to reduction of several current environmental problems, incorporating recycled materials such as tire rubber, recycled polymers (namely, SBS and High-density Polyethylene), and glass spheres. In addition, the surface of the layer was optimized in terms of texture to reflect light, enhancing the reduction of public electricity.

During the academic exchange mobility to the University of Antwerp, a project proposal was approved: Photocatalytic Asphalt Pavements for the Port of Antwerp (PAPPoA): a feasibility study. It aims to investigate the effects of traffic on photocatalytic efficiency, determine possible effects on traffic safety (skid resistance) and develop an in-situ test setup to measure the NO_x reduction. Different types of doped TiO₂ will be used to decrease its band gap, which improves the photocatalytic efficiency. Then, a real-life test case will be built in the Port of Antwerp if the results will be feasible. This project presents a budget of 108 K€ funded by the Industrial Research Fund (IOF) - technology concept exploration, and the name of the author of this thesis and his advisors are project members.

Under the IC&DT Projects in all Scientific Domains from FCT, the project NanoAir – Nanomaterials Applied on Innovative Road Pavements for Air-Cleaning was approved and started in March 2021. It presents a budget of 250 K€, and main researchers are the advisors of this thesis. The main objective of this project is to develop a durable and efficient photocatalytic coating over an asphalt pavement, using a cheap and validated method to assess its environmental performance and determine the actual impacts in terms of society, environment and economy. It seeks to fill the literature gaps: evaluation of efficiency and durability of photocatalytic asphalt mixtures, considering whether positive benefits exist at the end of the pavement's service life in global terms of economic, environmental, and social gains using a simple and low-cost analysis method. In this case, the author of this thesis contributed to the written part of this project proposal and expects to participate as a researcher.

Also, under IC&DT Projects in all Scientific Domains from FCT, the author of this thesis has more recently contributed to the writing of the project proposal MicroCoolPav – Coaxial Microfibers incorporated within Phase Change Materials for Cool Pavements. It is an exploratory project and presents a budget of 50 K€. Three different research centers are involved, Center of Physics, Institute for Sustainability and Innovation in Structural Engineering (ISISE from Department of Civil Engineering of UMinho), and Centre for Textile Science and Technology (2C2T - from Textile Department of UMinho). The supervisors of this proposal and the author of this thesis are involved. The main objective of this proposal is to produce

coaxial fibers containing PCMs, via the wet-spinning method to be subsequently incorporated into asphalt mixtures to provide them with LHTS (Latent Heat Thermal Energy Storage) capability. It is expected that the asphalt mixtures produced to have a thermoregulation ability superior to non-functionalized samples to mitigate UHI effects.

11.3. Future Works

To continue the activities developed under the scope of the research projects already mentioned and new projects, next research needs are listed:

- i) Doping of TiO_2 : since the TiO_2 activates under UV light, it becomes essential for outdoor applications because the light source (sunlight) is mostly composed of visible and infrared photons. Different light wavelengths should be used: visible, UV, and solar simulation to evaluate the doping of the semiconductor material;
- ii) Immobilization analysis of TiO_2 spray coating by using different application methods: the particles should be fixed (immobilized) as much as possible to keep their high photocatalytic efficiency. Different binders and application methods considering the spraying coating can be studied, as the use of asphalt emulsion and electrostatic painting. Also, reliable abrasion tests must be applied on the treated samples to evaluate the fixation/immobilization of the particles;
- iii) Analysis of gas degradation in laboratory-scale: probably this is the most important future work. Different gases (NO_2 , NO_x , SO_2 , and even VOCs) can be used in order to analyze the photocatalytic performance considering the gas degradation;
- iv) Evaluation of influencing parameters of the gas degradation: it is suggested to evaluate the following ones: application rate, the intensity of UV light, relative humidity of the air, flow of pollutants, among others;
- v) Analysis of gas degradation on a real scale: another question to be solved is how to evaluate the photocatalytic efficiency under real scale. Active and passive methods of the analysis of air quality can be used;
- vi) Real scale application of photocatalytic asphalt mixture: In order to evaluate the technical feasibility of the photocatalytic asphalt pavements, the construction of a real scale section becomes essential;
- vii) Global impacts of photocatalysis: all the impacts of the photocatalytic asphalt pavements must be evaluated, for example, their leachate, the economic, life cycle, and health aspects;
- viii) Degradation of oils and greases and analysis of the friction: Photocatalytic and self-cleaning asphalt mixtures have the ability to degrade organic compounds such as oils and fats adsorbed on their

- surface. Thus, in order to assess whether there is improvement in this matter, it is important to check the self-cleaning capacity of the materials through the degradation of oils and to analyze the friction of the asphalt mixtures before and after the contamination by these materials;
- ix) Mechanical characterization of superhydrophobic asphalt mixtures under ice and thawing and/or wetting only the surface: since the water is repelled from the surface of the pavements, maybe the mechanical properties will be improved;
 - x) Analysis of the UV light aging of photocatalytic asphalt mixtures: since the UV light is absorbed and reflected during the photocatalysis, the asphalt binder will be protected, decreasing the aging process;
 - xi) Application of different types of nano/micromaterials to asphalt pavements: regarding the fact that the use of nanomaterials is a promising subject in different areas, the use of different nano/micromaterials to asphalt mixtures is also relevant;
 - xii) Application of different smartness to asphalt pavements: several researchers have carried out a significant number of works about different capabilities about the multifunctional effects of asphalt mixtures, but most of them focused on the application of just a single new function. For this reason, the combination of different techniques and/or capabilities can result in the development of a better final product. A multifunctional asphalt mixture is desired since asphalt pavements represent an enormous area and they are built where people live including new capabilities, such as deicing and self-ice-melting, self-healing, thermochromic, latent heat thermal energy storage (LHTS);
 - xiii) Potentialities of the steel slags should be studied considering the new capabilities (de-icing/anti-ice and self-healing);
 - xiv) Cost analysis of the application of different types of functionalization processes: as it is essential to prove their economic feasibility;
 - xv) Conditioning of asphalt binders modified with TiO_2 using UV aging to consolidate the modification of asphalt binder using nano- TiO_2 for anti-aging effects;
 - xvi) The asphalt mixtures functionalized with diluted resin and particles solution will be evaluated by SEM in order to analyze the thickness of the resin and the particles coverage. The photocatalytic and wettability tests will be repeated after a wearing process. Furthermore, they will be assessed under different conditions (dry, wet and icy).

REFERENCES

- [1] I. Rocha Segundo, E. Freitas, S. Landi Jr, M. F. M. Costa, and J. O. Carneiro, *Smart, Photocatalytic and Self-Cleaning Asphalt Mixtures: A Literature Review*, *Coatings* **9**, (2019).
- [2] O. Carp, C. L. Huisman, and A. Reller, *Photoinduced Reactivity of Titanium Dioxide*, **32**, 33 (2004).
- [3] M. Gagliardi, *Photocatalysts: Technologies and Global Markets*, 2015.
- [4] K. Hashimoto, H. Irie, and A. Fujishima, *TiO₂ Photocatalysis: A Historical Overview and Future Prospects*, *Jpn. J. Appl. Phys.* **44**, (2005).
- [5] B. Han, L. Zhang, and J. Ou, *Smart and Multifunctional Concrete Toward Sustainable Infrastructures* (Springer, Heidelberg, 2017).
- [6] B. Han, Y. Wang, S. Dong, L. Zhang, and S. Ding, *Smart Concretes and Structures: A Review*, (2015).
- [7] J. O. O. Carneiro, S. Azevedo, V. Teixeira, F. Fernandes, E. Freitas, H. Silva, and J. Oliveira, *Development of Photocatalytic Asphalt Mixtures by the Deposition and Volumetric Incorporation of TiO₂ Nanoparticles*, *Constr. Build. Mater.* **38**, 594 (2013).
- [8] I. Rocha Segundo, C. Ferreira, E. F. Freitas, J. O. Carneiro, F. Fernandes, S. L. Júnior, M. F. Costa, S. Landi Júnior, and M. F. Costa, *Assessment of Photocatalytic, Superhydrophobic and Self-Cleaning Properties on Hot Mix Asphalts Coated with TiO₂ and/or ZnO Aqueous Solutions*, *Constr. Build. Mater.* **166**, 36 (2018).
- [9] I. Rocha Segundo, S. Landi Jr., S. M. B. Oliveira, E. F. de Freitas, and J. A. O. Carneiro, *Photocatalytic Asphalt Mixtures: Mechanical Performance and Impacts of Traffic and Weathering Abrasion on Photocatalytic Efficiency*, *Catal. Today* (2018).
- [10] M. Hassan, L. N. Mohammad, S. Asadi, H. Dylla, and S. Cooper, *Sustainable Photocatalytic Asphalt Pavements for Mitigation of Nitrogen Oxide and Sulfur Dioxide Vehicle Emissions*, *J. Mater. Civ. Eng.* **25**, (2012).
- [11] A. Fujishima, T. N. Rao, and D. A. Tryk, *Titanium Dioxide Photocatalysis*, *J. Photochem. Photobiol. C Photochem. Rev.* **1**, 1 (2000).
- [12] S. Bogutyn, C. Arboleda, A. Bordelon, and P. Tikalsky, *Rejuvenation Techniques for Mortar Containing Photocatalytic TiO₂ Material*, *Constr. Build. Mater.* **96**, 96 (2015).
- [13] M. Smits, T. Tytgat, B. Craeye, N. Costarramone, S. Lacombe, and S. Lenaerts, *Photocatalytic Degradation of Soot Deposition: Self-Cleaning Effect on Titanium Dioxide Coated Cementitious Materials*, *Chem. Eng. J.* **222**, 411 (2013).
- [14] M. Van Hal, S. W. Verbruggen, X. Yang, S. Lenaerts, and T. Tytgat, *Image Analysis and in Situ FTIR as Complementary Detection Tools for Photocatalytic Soot Oxidation*, *Chem. Eng. J.* **367**, 269 (2019).
- [15] K. Nakata and A. Fujishima, *TiO₂ Photocatalysis: Design and Applications*, *J. Photochem. Photobiol. C Photochem. Rev.* **13**, 169 (2012).
- [16] J. Emsley and N. B. B. Niobium, *An AZ Guide to the Elements*, Nature's Build. Blocks 141 (2001).
- [17] P. Westerhoff, G. Song, K. Hristovski, and M. A. Kiser, *Occurrence and Removal of Titanium at*

- Full Scale Wastewater Treatment Plants: Implications for TiO₂ Nanomaterials*, J. Environ. Monit. **13**, 1195 (2011).
- [18] X. Chen and A. Selloni, *Introduction: Titanium Dioxide (TiO₂) Nanomaterials*, Chem. Rev. **114**, 9281 (2014).
- [19] Y. Paz, *Application of TiO₂ Photocatalysis for Air Treatment: Patents' Overview*, Appl. Catal. B Environ. **99**, 448 (2010).
- [20] C. L. Bianchi, C. Pirola, M. Stucchi, B. Sacchi, G. Cerrato, S. Morandi, A. Di Michele, A. Carletti, and V. Capucci, *A New Frontier of Photocatalysis Employing Micro-Sized TiO₂: Air/Water Pollution Abatement and Self-Cleaning/Antibacterial Applications*, Semicond. Photocatal. - Mater. Mech. Appl. Not (2016).
- [21] X. Jiang, M. Manawan, T. Feng, R. Qian, T. Zhao, and G. Zhou, *Anatase and Rutile in Evonik Aeroxide P25: Heterojunctioned or Individual Nanoparticles?*, Catal. Today **300**, 12 (2018).
- [22] A. O. Ibhaddon and P. Fitzpatrick, *Heterogeneous Photocatalysis: Recent Advances and Applications*, 189 (2013).
- [23] R. Nakamura and Y. Nakato, *Primary Intermediates of Oxygen Photoevolution Reaction on TiO₂ (Rutile) Particles, Revealed by in Situ FTIR Absorption and Photoluminescence Measurement*, J. Am. Chem. Soc. **126**, 1290 (2004).
- [24] J. O. Carneiro, V. Teixeira, P. Carvalho, and S. Azevedo, *Self-Cleaning Smart Nanocoatings*, in *Nanocoatings and Ultra-Thin Films* (Woodhead Publishing, 2011), pp. 397–413.
- [25] A. Fujishima, X. Zhang, and D. A. Tryk, *TiO₂ Photocatalysis and Related Surface Phenomena*, Surf. Sci. Rep. **63**, 515 (2008).
- [26] M. Hernández-Alonso, F. Fresno, S. Suárez, and J. Coronado, *Development of Alternative Photocatalysts to TiO₂: Challenges and Opportunities*, Energy Environ. Sci. **2**, 1231 (2009).
- [27] J. Schneider, M. Matsuoka, M. Takeuchi, J. Zhang, Y. Horiuchi, M. Anpo, and D. W. Bahnemann, *Understanding TiO₂ Photocatalysis: Mechanisms and Materials*, Chem. Rev. **114**, 9919 (2014).
- [28] S. Riyapan, Y. Boonyongmaneerat, O. Mekasuwandumrong, P. Praserthdam, and J. Panpranot, *Effect of Surface Trapped Electrons on the Sol-Gel Derived TiO₂ in the Selective Acetylene Hydrogenation on Pd/TiO₂ Catalysts*, Catal. Today **245**, 134 (2015).
- [29] *Reactivity of Trapped and Accumulated Electrons in Titanium Dioxide Photocatalysis*, Catalysts **7**, (2017).
- [30] P. Mohammadyari and A. Nezamzadeh-ejhieh, *RSC Advances Supporting of Mixed ZnS – NiS Semiconductors onto Clinoptilolite Nano-Particles to Improve Its Activity in Photodegradation of 2-Nitrotoluene*, RSC Adv. **5**, 75300 (2015).
- [31] J. Esmaili-Hafshejani and A. Nezamzadeh-Ejhieh, *Increased Photocatalytic Activity of Zn(II)/Cu(II) Oxides and Sulfides by Coupling and Supporting Them onto Clinoptilolite Nanoparticles in the Degradation of Benzophenone Aqueous Solution*, J. Hazard. Mater. **316**, 194 (2016).
- [32] A. Nezamzadeh-Ejhieh and M. Bahrami, *Investigation of the Photocatalytic Activity of Supported ZnO–TiO₂ on Clinoptilolite Nano-Particles towards Photodegradation of Wastewater-Contained Phenol*, Desalin. Water Treat. **55**, 1096 (2015).

- [33] J. O. Carneiro, V. Teixeira, A. Portinha, L. Dupák, A. Magalhães, and P. Coutinho, *Study of the Deposition Parameters and Fe-Dopant Effect in the Photocatalytic Activity of TiO₂ Films Prepared by Dc Reactive Magnetron Sputtering*, *Vacuum* **78**, 37 (2005).
- [34] A. L. Linsebigler, G. Lu, and J. T. Yates, *Photocatalysis on TiO₂ Surfaces: Principles, Mechanisms, and Selected Results*, *Chem. Rev.* 735 (1995).
- [35] L. Spanhel, M. Haase, H. Weller, and A. Henglein, *Photochemistry of Colloidal Semiconductors. 20. Surface Modification and Stability of Strong Luminescing CdS Particles*, *J. Am. Chem. Soc.* 5649 (1987).
- [36] J. Zhao and X. Yang, *Photocatalytic Oxidation for Indoor Air Purification: A Literature Review*, *Build. Environ.* **38**, 645 (2003).
- [37] J. S. Dalton, P. A. Janes, N. G. Jones, J. A. Nicholson, K. R. Hallam, and G. C. Allen, *Photocatalytic Oxidation of NO_x Gases Using TiO₂: A Surface Spectroscopic Approach*, *Environ. Pollut.* **120**, 415 (2002).
- [38] J. Chen and C. sun Poon, *Photocatalytic Construction and Building Materials: From Fundamentals to Applications*, *Build. Environ.* **44**, 1899 (2009).
- [39] D. Wang, Z. Leng, M. Hüben, M. Oeser, and B. Steinauer, *Photocatalytic Pavements with Epoxy-Bonded TiO₂-Containing Spreading Material*, *Constr. Build. Mater.* **107**, 44 (2016).
- [40] L. Venturini and I. Bacchi, *Research , Design and Development of a Photocatalytic Asphalt Pavement*, in *Proceedings of the 2nd International Conference on Environmentally Friendly Roads: ENVIROAD* (2009), pp. 1–16.
- [41] M. Bocci, G. Cerni, and S. Colagrande, *Experimental Investigation of the Dynamic Behaviour of Asphalt Concrete Treated with Photocatalytic Mortars* (2014).
- [42] S. Banerjee, J. Gopal, P. Muraleedharan, A. K. Tyagi, and B. Raj, *Physics and Chemistry of Photocatalytic Titanium Dioxide : Visualization of Bactericidal Activity Using Atomic Force Microscopy* *Physics and Chemistry of Photocatalytic Titanium Dioxide : Visualization of Bactericidal Activity Using Atomic Force Microscopy*, *Curr. Sci.* **90**, (2006).
- [43] J. O. Carneiro, S. Azevedo, F. Fernandes, E. Freitas, M. Pereira, C. J. Tavares, S. Lanceros-Méndez, and V. Teixeira, *Synthesis of Iron-Doped TiO₂ Nanoparticles by Ball-Milling Process: The Influence of Process Parameters on the Structural, Optical, Magnetic, and Photocatalytic Properties*, *J. Mater. Sci.* **49**, 7476 (2014).
- [44] A. Truppi, M. L. Id, F. P. Id, A. Falcicchio, C. G. Id, R. Comparelli, and M. J. Mosquera, *Photocatalytic Activity of TiO₂/AuNRs–SiO₂ Nanocomposites Applied to Building Materials*, *Coatings* **1** (2018).
- [45] H. Zong, J. Schneider, G. Zhou, T. Zhao, Y. Li, J. Yang, W. Detlef, and J. H. Pan, *Charge Carrier Trapping, Recombination and Transfer during TiO₂ Photocatalysis: An Overview*, *Catal. Today* (2018).
- [46] B. Tang, X. Liu, W. Huang, and X. Cao, *Preparation of La-Doped Nanometer TiO₂ and Its Application for NO Removal on Asphalt Concrete*, *Road Mater. Pavement Des.* **18**, 43 (2017).
- [47] A. Zaleska, *Doped-TiO₂: A Review*, *Recent Patents Eng.* (2008).
- [48] S. Landi Jr., J. Carneiro, O. S. G. P. Soares, M. F. R. Pereira, A. C. Gomes, A. Ribeiro, A. M.

- Fonseca, P. Parpot, and I. C. Neves, *Photocatalytic Performance of N-Doped over Cotton Fabrics*, **8**, 1933 (2019).
- [49] R. Paolini, D. Borroni, M. Pedferri, M. Vittoria, and M. V. Diamanti, *Self-Cleaning Building Materials: The Multifaceted Effects of Titanium Dioxide*, *Constr. Build. Mater.* **182**, 126 (2018).
- [50] K. Rahla, R. Mateus, and L. Bragança, *Comparative Sustainability Assessment of Binary Blended Concretes Using Supplementary Cementitious Materials (SCMs) and Ordinary Portland Cement (OPC)*, *J. Clean. Prod.* **220**, 445 (2019).
- [51] I. Rocha Segundo, E. Freitas, M. F. Costa, and J. Carneiro, *Incorporation of Steel Slag and Reclaimed Asphalt into Pavement Surface Layers*, in *5th International Conference WASTES: Solutions, Treatments and Opportunities* (Lisbon, 2019).
- [52] Y. Ohama and D. Van Gemert, *Application of Titanium Dioxide Photocatalysis to Construction Materials* (2011).
- [53] H. Sommer, *Health Costs Due to Road Traffic-Related Air Pollution - An Impact Assessment Project of Austria, France and Switzerland*, 1999.
- [54] E. Boonen and A. Beeldens, *Recent Photocatalytic Applications for Air Purification in Belgium*, 553 (2014).
- [55] A. Rosales, A. Maury-Ramírez, R. M.-D. Gutiérrez, C. G. ID, and K. Esquivel, *SiO₂@TiO₂ Coating: Synthesis, Physical Characterization and Photocatalytic Evaluation*, *Coatings* **8**, 1 (2018).
- [56] R. Benedix, F. Dehn, J. Quaas, and M. Orgass, *Application of Titanium Dioxide Photocatalysis to Create Self-Cleaning Building Materials*, *Lacer* **5**, 157 (2000).
- [57] A. Jerónimo, A. Camões, B. Aguiar, and N. Lima, *Applied Surface Science Hydraulic Lime Mortars with Antifungal Properties*, *Appl. Surf. Sci.* **483**, 1192 (2019).
- [58] A. Syafiq, B. Vengadaesvaran, A. K. Pandey, and N. A. Rahim, *Superhydrophilic Smart Coating for Self-Cleaning Application on Glass Substrate*, *J. Nanomater.* (2018).
- [59] R. Blossey and C. Scientifique, *Self-Cleaning Surfaces – Virtual Realities*, 301 (2003).
- [60] C. Toro, B. T. Jobson, L. Haselbach, S. Shen, and S. H. Chung, *Photoactive Roadways: Determination of CO, NO and VOC Uptake Coefficients and Photolabile Side Product Yields on TiO₂ Treated Asphalt and Concrete*, *Atmos. Environ.* **139**, 37 (2016).
- [61] D. Osborn, M. Hassan, S. Asadi, and R. White John, *Durability Quantification of TiO₂ Surface Coating on Concrete and Asphalt Pavements*, *Journal of Materials in Civil Engineering*.
- [62] W. Fan, K. Y. Chan, C. Zhang, K. Zhang, Z. Ning, and M. K. H. Leung, *Solar Photocatalytic Asphalt for Removal of Vehicular NO_x: A Feasibility Study*, *Appl. Energy* **225**, 535 (2018).
- [63] X. Yang, X. Cao, and B. Tang, *Preparation of Visible Light Photocatalytic Asphalt Pavement Using Fe Doped G-C₃N₄ for Removal of Vehicular NO_x: Feasibility Study*, (2019).
- [64] X. Cao, X. Yang, D. Ph, T. Wu, B. Tang, and P. Guo, *G-C₃N₄/TiO₂ Photocatalyst and Its Performance of NO Degradation in Emulsified Asphalt*, **31**, 1 (2019).
- [65] S. Ilcan, Y. Caglar, M. Caglar, and B. Demirci, *Polycrystalline Indium-Doped ZnO Thin Films: Preparation and Characterization*, *J. Optoelectron. Adv. Mater.* **10**, 2592 (2008).

- [66] M. Laurenti and V. Cauda, *Porous Zinc Oxide Thin Films: Synthesis Approaches and Applications*, Coatings (2018).
- [67] J. Veyan, J. Chabal, and T. Thonhauser, *Structural Band-Gap Tuning in $g\text{-C}_3\text{N}_4$* , 957 (2015).
- [68] X. Cao, X. Yang, H. Li, W. Huang, and X. Liu, *Investigation of Ce-TiO₂ Photocatalyst and Its Application in Asphalt- Based Specimens for NO Degradation*, Constr. Build. Mater. **148**, 824 (2017).
- [69] W. Liu, S. Wang, J. Zhang, and J. Fan, *Photocatalytic Degradation of Vehicle Exhausts on Asphalt Pavement by TiO₂/Rubber Composite Structure*, Constr. Build. Mater. **81**, 224 (2015).
- [70] M. Chen and Y. Liu, *NO Removal from Vehicle Emissions by Functionality Surface of Asphalt Road*, J. Hazard. Mater. **174**, 375 (2010).
- [71] M. M. Hassan, H. Dylla, S. Asadi, L. N. Mohammad, and S. Cooper, *Laboratory Evaluation of Environmental Performance of Photocatalytic Titanium Dioxide Warm-Mix Asphalt Pavements*, J. Mater. Civ. Eng. **24**, 599 (2012).
- [72] S. Asadi, M. Hassan, A. Nadiri, and H. Dylla, *Artificial Intelligence Modeling to Evaluate Field Performance of Photocatalytic Asphalt Pavement for Ambient Air Purification*, Environ. Sci. Pollut. Res. **21**, 8847 (2014).
- [73] N. Tio, Q. Xiao, X. Chen, Y. Yang, and J. Zhao, *Experimental Study on NO₂ Photocatalytic Degradation on Sand Fog Seal*, in *2019 International Conference on Energy, Power, Environment and Computer Application* (2019), pp. 163–169.
- [74] E. Bocci, L. Riderelli, G. Fava, and M. Bocci, *Durability of NO Oxidation Effectiveness of Pavement Surfaces Treated with Photocatalytic Titanium Dioxide*, Arab. J. Sci. Eng. **1** (2016).
- [75] H. Dylla, S. Asadi, M. Hassan, and L. N. Mohammad, *Evaluating Photocatalytic Asphalt Pavement Effectiveness in Real-World Environments through Developing Models: A Statistical and Kinetic Study*, Road Mater. Pavement Des. **14**, 92 (2013).
- [76] J. Kruschwitz, M. Lind, and A. Muntean, *Modelling, Simulation And Parameter Identification Of Active Pollution Reduction With Photocatalytic Asphalt*, Acta Polytech. **59**, 51 (2019).
- [77] W. Zhang, Y. X. Zhang, Z. Jia, F. Wang, and L. Ding, *Test Method and Material Design of Asphalt Mixture with the Function of Photocatalytic Decomposition of Automobile Exhaust*, Constr. Build. Mater. **215**, 298 (2019).
- [78] D. Wang, Z. Leng, H. Yu, M. Hüben, J. Kollmann, and M. Oeser, *Durability of Epoxy-Bonded TiO₂-Modified Aggregate as a Photocatalytic Coating Layer for Asphalt Pavement under Vehicle Tire Polishing*, Wear **382**, 1 (2017).
- [79] H. Wang, K. Jin, X. Dong, S. Zhan, and C. Liu, *Preparation Technique and Properties of Nano-TiO₂ Photocatalytic Coatings for Asphalt Pavement*, Appl. Sci. **8**, (2018).
- [80] I. G. da I. G. D. Rocha Segundo, E. A. L. E. A. L. Dias, F. D. P. F. D. P. Fernandes, E. F. de E. F. D. Freitas, M. F. M. F. Costa, and J. O. J. O. J. O. Carneiro, *Photocatalytic Asphalt Pavement: The Physicochemical and Rheological Impact of TiO₂ Nano/Microparticles and ZnO Microparticles onto the Bitumen*, Road Mater. Pavement Des. (2018).
- [81] H. Nazari, K. Naderi, and F. Moghadas Nejad, *Improving Aging Resistance and Fatigue Performance of Asphalt Binders Using Inorganic Nanoparticles*, Constr. Build. Mater. **170**, 591

- (2018).
- [82] S. S. Sun, Y. M. Wang, and A. Q. Zhang, *Study on Anti-Ultraviolet Radiation Aging Property of TiO₂ Modified Asphalt*, *Adv. Mater. Res.* **306–307**, 951 (2011).
- [83] A. Azarhoosh, F. Moghaddas Nejad, and A. Khodaii, *Evaluation of the Effect of Nano-TiO₂ on the Adhesion between Aggregate and Asphalt Binder in Hot Mix Asphalt*, *Eur. J. Environ. Civ. Eng.* **1** (2016).
- [84] Z. Leng and H. Yu, *Novel Method of Coating Titanium Dioxide on to Asphalt Mixture Based on the Breath Figure Process for Air-Purifying Purpose*, *J. Mater. Civ. Eng.* **28**, 1 (2016).
- [85] J. Jin, B. Chen, L. Liu, R. Liu, G. Qian, H. Wei, and J. Zheng, *A Study on Modified Bitumen with Metal Doped Nano-TiO₂ Pillared Montmorillonite*, *Materials (Basel)*. **12**, (2019).
- [86] M. Chen, D. Baglee, J. W. Chu, D. Du, and X. Guo, *Photocatalytic Oxidation of NO_x under Visible Light on Asphalt-Pavement Surface*, *J. Mater. Civ. Eng.* **29**, 04017133 (2017).
- [87] M. M. Hassan, H. Dylla, L. N. Mohammad, and T. Rupnow, *Evaluation of the Durability of Titanium Dioxide Photocatalyst Coating for Concrete Pavement*, *Constr. Build. Mater.* **24**, 1456 (2010).
- [88] S. Landi, J. Carneiro, S. Ferdov, A. M. Fonseca, I. C. Neves, M. Ferreira, P. Parpot, O. S. G. P. Soares, and M. F. R. Pereira, *Photocatalytic Degradation of Rhodamine B Dye by Cotton Textile Coated with SiO₂-TiO₂ and SiO₂-TiO₂-HY Composites*, *J. Photochem. Photobiol. A Chem.* **346**, 60 (2017).
- [89] E. Carnielo and M. Zinzi, *Optical and Thermal Characterisation of Cool Asphalts to Mitigate Urban Temperatures and Building Cooling Demand*, *Build. Environ.* **60**, 56 (2013).
- [90] I. Rocha Segundo, S. Landi Jr, S. Oliveira, E. Freitas, M. F. Costa, and J. Carneiro, *Photocatalytic Asphalt Mixtures: Semiconductors' Impact in Skid Resistance and Texture*, *Road Mater. Pavement Des.* **20**, (2019).
- [91] E. Luévano-Hipólito and A. M. la Cruz, *Enhanced Photocatalytic Activity of TiO₂ Rutile by Coupling with Fly Ashes for the Removal of NO Gases*, *Ind. Eng. Chem. Res.* **55**, 11512 (2016).
- [92] I. Rocha Segundo, S. Landi, E. Freitas, V. Castelo Branco, M. F. M. Costa, and J. Carneiro, *Superhydrophobic Asphalt Pavements: Surface Improvement*, *EPJ Web Conf.* **238**, 12012 (2020).
- [93] A. Arabzadeh, H. Ceylan, S. Kim, K. Gopalakrishnan, and A. Sassani, *Superhydrophobic Coatings on Asphalt Concrete Surfaces*, *Transp. Res. Rec. J. Transp. Res. Board* **2551**, 10 (2016).
- [94] C. Peng, H. Zhang, Z. You, F. Xu, G. Jiang, S. Lv, and R. Zhang, *Preparation and Anti-Icing Properties of a Superhydrophobic Silicone Coating on Asphalt Mixture*, *Constr. Build. Mater.* **189**, 227 (2018).
- [95] J. H. O. Nascimento, P. Pereira, E. Freitas, and F. Fernandes, *Development and Characterization of a Superhydrophobic and Anti-Ice Asphaltic Nanostructured Material for Road Pavements*, in *7th International Conference on Maintenance and Rehabilitation of Pavements and Technological Control* (At Auckland, New Zealand, 2012).
- [96] H. Zhu, Z. Guo, and W. Liu, *Adhesion Behaviors on Superhydrophobic Surfaces*, *Chem. Commun.* **50**, 3900 (2014).
- [97] S. Heinonen, E. Huttunen-Saarivirta, J. P. Nikkanen, M. Raulio, O. Priha, J. Laakso, E. Storgårds,

- and E. Levänen, *Antibacterial Properties and Chemical Stability of Superhydrophobic Silver-Containing Surface Produced by Sol-Gel Route*, *Colloids Surfaces A Physicochem. Eng. Asp.* **453**, 149 (2014).
- [98] Y. Gao, L. Qu, B. He, K. Dai, Z. Fang, and R. Zhu, *Study on Effectiveness of Anti-Icing and Deicing Performance of Super-Hydrophobic Asphalt Concrete*, *Constr. Build. Mater.* **191**, 270 (2018).
- [99] J. Lee and R. S. Fearing, *Wet Self-Cleaning of Superhydrophobic Microfiber Adhesives Formed from High Density Polyethylene*, *Langmuir* **28**, 15372 (2012).
- [100] E. Eriskin, S. Karahancer, S. Terzi, and M. Saltan, *Examination of the Effect of Superhydrophobic Coated Pavement under Wet Conditions*, *Procedia Eng.* **187**, 532 (2017).
- [101] M. Zheng, J. Zhou, S. Wu, H. Yuan, and J. Meng, *Evaluation of Long-Term Performance of Anti-Icing Asphalt Pavement*, *Constr. Build. Mater.* **84**, 277 (2015).
- [102] A. Tabakovic and E. Schlangen, *Self-Healing Technology for Asphalt Pavements*, *Adv Polym Sci* (2015).
- [103] M. . de Rooij, K. Van Tittelboom, N. De Belie, and E. Schlangen, *Self-Healing Phenomena in Cement-Based Materials* (2013).
- [104] J. Nazarko, P. Radziszewski, K. Dębowska, J. Ejdys, A. Gudanowska, K. Halicka, J. Kilon, A. Kononiuk, K. J. Kowalski, J. B. Król, Ł. Nazarko, M. Sarnowski, and T. Vilutiene, *Foresight Study of Road Pavement Technologies*, *Procedia Eng.* **122**, 129 (2015).
- [105] A. N. FARUK;, D. H. CHEN;, C. MUSHOTA;, M. MUYA;, and L. F. WALUBITA, *Application of Nano-Technology in Pavement Engineering: A Literature Review*, in *Application of Nanotechnology in Pavements, Geological Disasters, and Foundation Settlement Control Technology* (2014), pp. 9–16.
- [106] W. J. Steyn, *Applications of Nanotechnology in Road Pavement Engineering*, *Nanotechnol. Civ. Infrastruct.* **49** (2011).
- [107] W. J. Steyn, *Potential Applications of Nanotechnology*, *J. Transp. Eng.* **135**, 764 (2009).
- [108] W. J. Steyn, *Research and Application of Nanotechnology in Transportation*, in *25th Annual Transportation Conference* (Pretoria, 2008), pp. 345–353.
- [109] C. Peng, J. Yu, Z. Zhao, J. Fu, M. Zhao, W. Wang, and J. Dai, *Preparation and Properties of a Layered Double Hydroxide Deicing Additive for Asphalt Mixture*, *Cold Reg. Sci. Technol.* **110**, 70 (2015).
- [110] Z. Liu, M. Xing, S. Chen, R. He, and P. Cong, *Influence of the Chloride-Based Anti-Freeze Filler on the Properties of Asphalt Mixtures*, *Constr. Build. Mater.* **51**, 133 (2014).
- [111] D. Aydin, R. Kizilel, R. O. Caniaz, and S. Kizilel, *Gelation-Stabilized Functional Composite-Modified Bitumen for Anti-Icing Purposes*, (2015).
- [112] S. Luo and X. Yang, *Performance Evaluation of High-Elastic Asphalt Mixture Containing Deicing Agent Mafilon*, *Constr. Build. Mater.* **94**, 494 (2015).
- [113] T. Ma, L. Geng, X. Ding, D. Zhang, and X. Huang, *Experimental Study of Deicing Asphalt Mixture with Anti-Icing Additives*, *Constr. Build. Mater.* **127**, 653 (2016).
- [114] P. K. Dehdezi and I. Widyatmoko, *De-Icing/Anti-Icing Agents and Their Effects on Airfield Asphalt*

- Pavements*, Asph. Prof. **February**, 28 (2015).
- [115] P. Pan, S. Wu, F. Xiao, L. Pang, and Y. Xiao, *Conductive Asphalt Concrete: A Review on Structure Design, Performance, and Practical Applications*, J. Intell. Mater. Syst. Struct. **26**, 755 (2015).
- [116] J. Gao, A. Sha, Z. Wang, Z. Tong, and Z. Liu, *Utilization of Steel Slag as Aggregate in Asphalt Mixtures for Microwave Deicing*, J. Clean. Prod. **152**, 429 (2017).
- [117] N. Tang, C. J. Sun, S. X. Huang, and S. P. Wu, *Damage and Corrosion of Conductive Asphalt Concrete Subjected to Freeze–Thaw Cycles and Salt*, Mater. Res. Innov. **17**, 240 (2014).
- [118] Y. Sun, S. Wu, Q. Liu, J. Hu, Y. Yuan, and Q. Ye, *Snow and Ice Melting Properties of Self-Healing Asphalt Mixtures with Induction Heating and Microwave Heating*, Appl. Therm. Eng. (2017).
- [119] H. Fischer, *Self-Repairing Material Systems - a Dream or a Reality?*, Nat. Sci. **2**, 873 (2010).
- [120] S. Xu, A. García, J. Su, Q. Liu, A. Tabaković, and E. Schlangen, *Self-Healing Asphalt Review: From Idea to Practice*, Adv. Mater. Interfaces **1800536**, 1800536 (2018).
- [121] B. Bhushan, *Biomimetics: Lessons from Nature - an Overview*, Philos. Trans. R. Soc. A Math. Phys. Eng. Sci. **367**, 1445 (2009).
- [122] C. E. Diesendruck, N. R. Sottos, J. S. Moore, and S. R. White, *Biomimetic Self-Healing*, Angew. Chemie - Int. Ed. **54**, 10428 (2015).
- [123] C. S. Miranda, A. R. M. Ribeiro, N. C. Homem, and H. P. Felgueiras, *Spun Biotextiles in Tissue Engineering and Biomolecules Delivery Systems*, Antibiotics **9**, (2020).
- [124] Y. Agzenai, J. Pozuelo, J. Sanz, I. Perez, and J. Baselga, *Advanced Self-Healing Asphalt Composites in the Pavement Performance Field: Mechanisms at the Nano Level and New Repairing Methodologies.*, Recent Pat. Nanotechnol. **9**, 43 (2015).
- [125] Y. Hou, L. Wang, T. Pauli, and W. Sun, *Investigation of the Asphalt Self-Healing Mechanism Using a Phase-Field Model*, J. Mater. Civ. Eng. **27**, 04014118 (2015).
- [126] J. Norambuena-Contreras and A. Garcia, *Self-Healing of Asphalt Mixture by Microwave and Induction Heating*, Mater. Des. **106**, 404 (2016).
- [127] Q. Liu, Á. García, E. Schlangen, and M. Van De Ven, *Induction Healing of Asphalt Mastic and Porous Asphalt Concrete*, Constr. Build. Mater. **25**, 3746 (2011).
- [128] S. Fan, H. Zhu, and H. Wang, *Influential Factors of Self-Healing Performance of Asphalt Concrete in Fracture Behavior*, Mater. Sci. Eng. (2017).
- [129] J. F. Su, Y. Y. Wang, N. X. Han, P. Yang, and S. Han, *Experimental Investigation and Mechanism Analysis of Novel Multi-Self-Healing Behaviors of Bitumen Using Microcapsules Containing Rejuvenator*, Constr. Build. Mater. **106**, 317 (2016).
- [130] K. Chung, S. Lee, M. Park, P. Yoo, and Y. Hong, *Preparation and Characterization of Microcapsule-Containing Self-Healing Asphalt*, J. Ind. Eng. Chem. **29**, 330 (2015).
- [131] A. Garcia, J. Jelfs, and C. J. Austin, *Internal Asphalt Mixture Rejuvenation Using Capsules*, Constr. Build. Mater. **101**, 309 (2015).
- [132] J. Qiu, M. F. C. van de Ven, A. A. A. Molenaar, J. Qiu, S. Wu, and J. Yu, *Investigating the Self Healing Capability of Bituminous Binders*, Road Mater. Pavement Des. **10**, 81 (2009).

- [133] B. Liang, F. Lan, K. Shi, G. Qian, Z. Liu, and J. Zheng, *Review on the Self-Healing of Asphalt Materials: Mechanism, Affecting Factors, Assessments and Improvements*, *Constr. Build. Mater.* **266**, 120453 (2021).
- [134] Y. Shi, *High Temperature Shape Memory Polymers & Ionomer Modified Asphalts*, The University of Akron, 2013.
- [135] Y. Chen, M. Gong, Z. Yao, X. Dong, and K. Song, *Investigation on the Self-Healing Abilities of Base and Ionomer-Modified Asphalt Binders with a T-Peel Test*, *New Front. Road Airpt. Eng. - Sel. Pap. from 2015 Int. Symp. Front. Road Airpt. Eng. IFRAE 2015* 64 (2015).
- [136] G. H. Shafabakhsh and O. J. Ani, *Experimental Investigation of Effect of Nano TiO_2/SiO_2 Modified Bitumen on the Rutting and Fatigue Performance of Asphalt Mixtures Containing Steel Slag Aggregates*, *Constr. Build. Mater.* **98**, 692 (2015).
- [137] N. I. M. Yusoff, A. A. S. Breem, H. N. M. Alattug, A. Hamim, and J. Ahmad, *The Effects of Moisture Susceptibility and Ageing Conditions on Nano-Silica/Polymer-Modified Asphalt Mixtures*, *Constr. Build. Mater.* **72**, 139 (2014).
- [138] G. M. Amin and A. Esmail, *Application of Nano Silica to Improve Self-Healing of Asphalt Mixes*, *J. Cent. South Univ.* **24**, 1019 (2017).
- [139] Á. García, E. Schlangen, M. Van De Ven, and G. Van Bochove, *Optimization of Composition and Mixing Process of a Self-Healing Porous Asphalt*, *Constr. Build. Mater.* **30**, 59 (2012).
- [140] H. Kim, K. Yoo, Y. Kim, and S. Y. Yoon, *Thermochromic Behaviors of Boron–Magnesium Co-Doped $BiVO_4$ Powders Prepared by a Hydrothermal Method*, *Dye. Pigment.* **149**, 373 (2018).
- [141] S. Wang, M. Liu, L. Kong, Y. Long, X. Jiang, and A. Yu, *Recent Progress in VO_2 Smart Coatings: Strategies to Improve the Thermochromic Properties*, *Prog. Mater. Sci.* **81**, 1 (2016).
- [142] J. Hu, Q. Gao, and X. Yu, *Characterization of the Optical and Mechanical Properties of Innovative Multifunctional Thermochromic Asphalt Binders*, *J. Mater. Civ. Eng.* **27**, 1239 (2013).
- [143] J. Hu and X. (Bill) Yu, *Innovative Thermochromic Asphalt Coating: Characterisation and Thermal Performance*, *Road Mater. Pavement Des.* **17**, 187 (2016).
- [144] H. Zhang, Z. Chen, L. Li, and C. Zhu, *Evaluation of Aging Behaviors of Asphalt with Different Thermochromic Powders*, *Constr. Build. Mater.* **155**, 1198 (2017).
- [145] H. Zhang, Z. Chen, G. Xu, and C. Shi, *Physical, Rheological and Chemical Characterization of Aging Behaviors of Thermochromic Asphalt Binder*, *Fuel* **211**, 850 (2018).
- [146] J. Hu, S. M. Asce, X. B. Yu, and M. Asce, *Reflectance Spectra of Thermochromic Asphalt Binder: Characterization and Optical Mixing Model*, *J. Mater. Civ. Eng.* **28**, 1 (2015).
- [147] S. E. Kalnæs and B. P. Jelle, *Phase Change Materials and Products for Building Applications: A State-of-the-Art Review and Future Research Opportunities*, *Energy Build.* **94**, 150 (2015).
- [148] C. MeiZhu, H. Jing, S. Wu, W. Lu, and G. Xu, *Optimization of Phase Change Materials Used in Asphalt Pavement to Prevent Rutting*, *Adv. Mater. Res.* **219–220**, 1375 (2011).
- [149] L. H. He, J. R. Li, and H. Z. Zhu, *Analysis on Application Prospect of Shape-Stabilized Phase Change Materials in Asphalt Pavement*, *Appl. Mech. Mater.* **357**, 1277 (2013).
- [150] B. Guan, *Application of Asphalt Pavement with Phase Change Materials to Mitigate Urban Heat*

- Island Effect*, 2011 Int. Symp. Water Resour. Environ. Prot. 2389 (2011).
- [151] A. Sharma, V. V. Tyagi, C. R. Chen, and D. Buddhi, *Review on Thermal Energy Storage with Phase Change Materials and Applications*, *Renew. Sustain. Energy Rev.* **13**, 318 (2009).
- [152] M. K. Rathod and J. Banerjee, *Thermal Stability of Phase Change Materials Used in Latent Heat Energy Storage Systems: A Review*, *Renew. Sustain. Energy Rev.* **18**, 246 (2013).
- [153] D. J. H. Dieckmann, *Latent Heat Storage in Concrete*, University of Kaiserslautern.
- [154] B. Ma, W. Si, J. Ren, H. N. Wang, F. W. Liu, and J. Li, *Exploration of Road Temperature-Adjustment Material in Asphalt Mixture*, *Road Mater. Pavement Des.* **15**, 659 (2014).
- [155] J. Ren, B. Ma, W. Si, X. Zhou, and C. Li, *Preparation and Analysis of Composite Phase Change Material Used in Asphalt Mixture by Sol-Gel Method*, *Constr. Build. Mater.* **71**, 53 (2014).
- [156] B. J. Manning, P. R. Bender, S. A. Cote, R. A. Lewis, A. R. Sakulich, and R. B. Mallick, *Assessing the Feasibility of Incorporating Phase Change Material in Hot Mix Asphalt*, *Sustain. Cities Soc.* **19**, 11 (2015).
- [157] B. Ma, S. S. Wang, and J. Li, *Study on Application of PCM in Asphalt Mixture*, *Adv. Mater. Res.* **168–170**, 2625 (2010).
- [158] B. Ma, J. Li, R. W. Liu, and J. Ma, *Study on Road Performance of Phase-Change Temperature-Adjusting Asphalt Mixture*, *Adv. Mater. Res.* **287–290**, 978 (2011).
- [159] L. F. Cabeza, A. Castell, C. Barreneche, A. De Gracia, and A. I. Fernández, *Materials Used as PCM in Thermal Energy Storage in Buildings: A Review*, *Renew. Sustain. Energy Rev.* **15**, 1675 (2011).
- [160] F. Fernandes, E. Freitas, J. O. Carneiro, V. Pires, M. Pastor, and E. A. Luís, *Smart Road Paint and Road Signs with the Ability to Change Colour at Low Temperature*, in *1st European Road Infrastructure Congress* (Leed, UK, 2016), pp. 2–7.
- [161] V. Džimbeg-malčić, Ž. Barbarić-mikočević, and K. Itrić, *Kubelka-Munk Theory in Describing Optical Properties of Paper (I)*, *Teh. Vjesn.* **18**, 117 (2011).
- [162] H. G. Hecht, *The Interpretation of Diffuse Reflectance Spectra*, *J. Res. Natl. Bur. Stand. Phys. Chem.* **80a**, 567 (1976).
- [163] A. Jager, R. Lackner, C. Eisenmenger-Sittner, and R. Blab, *Identification of Microstructural Components of Bitumen by Means of Atomic Force Microscopy (AFM)*, *Proc. Appl. Math. Mech.* **4**, 400 (2004).
- [164] A. T. Pauli, J. F. Branthaver, C. M. Eggleston, R. E. Robertson, and W. Grimes, *Atomic Force Microscopy Investigation of Shrp Asphalts*, in *Symposium on the Compatibility and Stability of Heavy Oils and Residua* (San Diego, California, 2001), pp. 1–11.
- [165] H. L. ZHANG, H. C. WANG, and J. Y. YU, *Effect of Aging on Morphology of Organo-Montmorillonite Modified Bitumen by Atomic Force Microscopy*, *J. Microsc.* **92**, 1 (2010).
- [166] W. Zhang, X. Xiao, X. Zeng, Y. Li, L. Zheng, and C. Wan, *Enhanced Photocatalytic Activity of TiO₂ Nanoparticles Using SnS₂/RGO Hybrid as Co-Catalyst: DFT Study and Photocatalytic Mechanism*, *J. Alloys Compd.* **685**, 774 (2016).
- [167] B. Madhukar, J. Wiener, J. Militky, S. Rwawiire, R. Mishra, K. I. Jacob, Y. Wang, B. M. Kale, J. Wiener, J. Militky, S. Rwawiire, R. Mishra, K. I. Jacob, and Y. Wang, *Coating of Cellulose-TiO₂*

- Nanoparticles on Cotton Fabric for Durable Photocatalytic Self-Cleaning and Stiffness*, Carbohydr. Polym. **150**, 107 (2016).
- [168] N. E. Altun, *Incidental Release of Bitumen during Oil Shale Grinding and Impacts on Oil Shale Beneficiation*, Oil Shale **26**, 382 (2009).
- [169] I. M. Asi, *Evaluating Skid Resistance of Different Asphalt Concrete Mixes*, Build. Environ. **42**, 325 (2007).
- [170] M. F. M. Costa, *Optical Triangulation-Based Microtopographic Inspection of Surfaces*, Sensors **12**, 4399 (2012).
- [171] M. F. M. Costa, E. F. Freitas, H. Torres, and V. Cerezo, *Optical Microtopographic Inspection of Asphalt Pavement Surfaces*, Proc. SPIE - Int. Soc. Opt. Eng. **10453**, (2017).
- [172] M. F. M. Costa, *Microtopographical Characterization of Microcavities on X-Rays Sensor Array*, in *AIP Conference Proceedings* (2008), pp. 507–512.
- [173] W. Wang, X. Yan, H. Huang, X. Chu, and M. Abdel-Aty, *Design and Verification of a Laser Based Device for Pavement Macrotexure Measurement*, Transp. Res. Part C Emerg. Technol. **19**, 682 (2011).
- [174] S. M. Bazlamit and F. Reza, *Changes in Asphalt Pavement Friction Components and Adjustment of Skid Number for Temperature*, J. Transp. Eng. **131**, 470 (2005).
- [175] M. Bocci, A. Grilli, F. Cardone, and A. Virgili, *Clear Asphalt Mixture for Wearing Course in Tunnels: Experimental Application in the Province of Bolzano*, in *SIIV - 5th International Congress - Sustainability of Road Infrastructures*, Vol. 53 (Elsevier B.V., 2012), pp. 115–124.
- [176] Z. Chen, H. Zhang, C. Zhu, and B. Zhao, *Rheological Examination of Aging in Bitumen with Inorganic Nanoparticles and Organic Expanded Vermiculite*, Constr. Build. Mater. **101**, 884 (2015).
- [177] B. Sengoz, L. Bagayogo, J. Oner, and A. Topal, *Investigation of Rheological Properties of Transparent Bitumen*, Constr. Build. Mater. **154**, 1105 (2017).
- [178] E. Bocci and M. Bocci, *Clear Asphalt Concrete for Energy Saving in Road Tunnels Clear Asphalt Concrete for Energy Saving in Road Tunnels*, in *12th International Society for Asphalt Pavements* (2014).
- [179] M. Bocci, Projekt INTERREG IV Innovative Beläge Und Beleuchtung Für Tunnel IBBT (ID 5273), 2012.
- [180] F. M. Nejad, R. Tanzadeh, J. Tanzadeh, and G. H. Hamed, *Investigating the Effect of Nanoparticles on the Rutting Behaviour of Hot-Mix Asphalt*, Int. J. Pavement Eng. **17**, 353 (2016).
- [181] L. Sun, X. Xin, and J. Ren, *Asphalt Modification Using Nano-Materials and Polymers Composite Considering High and Low Temperature Performance*, Constr. Build. Mater. **133**, 358 (2017).
- [182] FHWA, Superpave Fundamentals Reference Manual, 2005.
- [183] M. I. Khan, M. H. Sutanto, S. Sunarjono, and S. Room, *Effect of Crumb Rubber, Epolene (EE-2), and Date Palm Ash as Modifiers on the Performance of Binders and Mixtures: A Sustainable Approach*, Sustainability **11**, 1 (2019).
- [184] RHEA, *Rheology Analysis Software, Version 1.2. 1*, Abatech, Inc., Bloom. Glen, PA (2011).

- [185] G. V Gordon and M. T. Shaw, *Computer Programs Für Rheologists* (Hanser, 1994).
- [186] G. D. Airey, *Use of Black Diagrams to Identify Inconsistencies in Rheological Data*, Road Mater. Pavement Des. **3**, 37 (2002).
- [187] C. Hintz, R. Velasquez, C. Johnson, and H. Bahia, *Modification and Validation of Linear Amplitude Sweep Test for Binder Fatigue Specification*, Transp. Res. Rec. J. Transp. Res. Board **2207**, 99 (2011).
- [188] E. Masad, N. Somadevan, H. U. Bahia, and S. Kose, *Modeling and Experimental Measurements of Strain Distribution in Asphalt Mixes*, J. Transp. Eng. **127**, 477 (2001).
- [189] R. Kleiziene, M. Panasenkienė, and A. Vaitkus, *Effect of Aging on Chemical Composition and Rheological Properties of Neat and Modified Bitumen*, Materials (Basel). **12**, (2019).
- [190] L. Z. Feng, H. Bian, X. Li, and J. Yu, *FTIR Analysis of UV Aging on Bitumen and Its Fractions*, Mater. Struct. **49**, 1381 (2016).
- [191] I. Yut and A. Zofka, *Attenuated Total Reflection (ATR) Fourier Transform Infrared (FT-IR) Spectroscopy of Oxidized Polymer-Modified Bitumens*, Appl. Spectrosc. **65**, 765 (2011).
- [192] P. Marsac, N. Piérard, L. Porot, W. Van den bergh, J. Grenfell, V. Mouillet, S. Pouget, J. Besamusca, F. Farcas, T. Gabet, and M. Hugener, *Potential and Limits of FTIR Methods for Reclaimed Asphalt Characterisation*, Mater. Struct. (2014).
- [193] A. Dony, L. Ziyani, I. Drouadaine, S. Pouget, S. Faucon-Dumont, D. Simard, V. Mouillet, J. E. Poirier, T. Gabet, L. Boulange, A. Nicolai, and C. Gueit, *MURE National Project: FTIR Spectroscopy Study to Assess Ageing of Asphalt Mixtures*, in *Proceedings of the E&E Congress* (2016).
- [194] Z. Zhang, N. Kang, J. Zhou, X. Li, and L. He, *Novel Synthesis of Choline-Based Amino Acid Ionic Liquids and Their Applications for Separating Asphalt from Carbonate Rocks*, Nanomaterials **9**, 5 (2019).
- [195] J. Lamontagne, P. Dumas, V. Mouillet, and J. Kister, *Comparison by Fourier Transform Infrared (FTIR) Spectroscopy of Different Ageing Techniques: Application to Road Bitumens*, Fuel **80**, 483 (2001).
- [196] G. Rajakumar, A. A. Rahuman, S. M. Roopan, V. G. Khanna, G. Elango, C. Kamaraj, A. A. Zahir, and K. Velayutham, *Molecular and Biomolecular Spectroscopy Fungus-Mediated Biosynthesis and Characterization of TiO₂ Nanoparticles and Their Activity against Pathogenic Bacteria*, Spectrochim. Acta Part A **91**, 23 (2012).
- [197] K. B. Jaimy, S. Ghosh, S. Sankar, and K. G. K. Warriar, *An Aqueous Sol – Gel Synthesis of Chromium (III) Doped Mesoporous Titanium Dioxide for Visible Light Photocatalysis*, Mater. Res. Bull. **46**, 914 (2011).
- [198] J. Wei, L. Zhao, S. Peng, J. Shi, Z. Liu, and W. Wen, *Wettability of Urea-Doped TiO₂ Nanoparticles and Their High Electrorheological Effects*, J. Sol-Gel Sci. Technol. **311** (2008).
- [199] N. C. Homem, N. de C. Beluci, S. Amorim, R. Reis, A. M. Vieira, M. F. Vieira, R. Bergamasco, and M. T. P. Amorim, *Applied Surface Science Surface Modification of a Polyethersulfone Micro Filtration Membrane with Graphene Oxide for Reactive Dyes Removal*, Appl. Surf. Sci. **486**, 499 (2019).
- [200] A. V Kataware and D. Singh, *Dynamic Mechanical Analysis of Crumb Rubber Modified Asphalt*

- Binder Containing Warm Mix Additives*, Int. J. Pavement Eng. **8436**, 0 (2017).
- [201] G. D. Airey, *Rheological Properties of Styrene Butadiene Styrene Polymer Modified Road Bitumens*, Fuel **82**, 1709 (2003).
- [202] H. Soenen, J. De Visscher, A. Vanelstraete, and P. Redelius, *Influence of Thermal History on Rheological Properties of Various Bitumen*, Rheol. Acta **45**, 729 (2006).
- [203] Z. Hossain and D. Ghosh, *Use of the Multiple Stress Creep Recovery (MSCR) Test Method to Characterize Polymer - Modified Asphalt Binders*, J. Test. Eval. **44**, (2016).
- [204] Z. Ren, Y. Zhu, Q. Wu, M. Zhu, F. Guo, and H. Yu, *Enhanced Storage Stability of Different Polymer Modified Asphalt Binders through Nano-Montmorillonite Modification*, Nanomaterials **10**, 641 (2020).
- [205] N. C. Homem, N. U. Yamaguchi, M. F. Vieira, M. T. S. P. Amorim, and R. Bergamasco, *Surface Modification of Microfiltration Membrane with GO Nanosheets for Dyes Removal from Aqueous Solutions*, Chem. Eng. Trans. **60**, 259 (2017).
- [206] J. F. Masson, L. Pelletier, and P. Collins, *Rapid FTIR Method for Quantification of Styrene-Butadiene Type Copolymers in Bitumen*, J. Appl. Polym. Sci. **79**, 1034 (2001).
- [207] H. Zhang, M. Su, S. Zhao, Y. Zhang, and Z. Zhang, *High and Low Temperature Properties of Nano-Particles/Polymer Modified Asphalt*, Constr. Build. Mater. **114**, 323 (2016).
- [208] H. Yao, Z. You, M. Asce, L. Li, C. H. Lee, D. Wingard, M. Asce, Y. K. Yap, X. Shi, M. Asce, and S. W. Goh, *Rheological Properties and Chemical Bonding of Asphalt Modified with Nanosilica*, J. Mater. Civ. Eng. 1619 (2013).
- [209] J. Mirwald, S. Werkovits, I. Camargo, D. Maschauer, B. Hofko, and H. Grothe, *Understanding Bitumen Ageing by Investigation of Its Polarity Fractions*, Constr. Build. Mater. **250**, 118809 (2020).
- [210] X. Zhao, L. Wei, S. Cheng, Y. Huang, Y. Yu, and J. Julson, *Catalytic Cracking of Camelina Oil for Hydrocarbon Biofuel over ZSM-5-Zn Catalyst*, Fuel Process. Technol. **139**, 117 (2015).
- [211] S. Cheng, L. Wei, X. Zhao, E. Kadis, and J. Julson, *Conversion of Prairie Cordgrass to Hydrocarbon Biofuel over Co-Mo/HZSM-5 Using a Two-Stage Reactor System*, Energy Technol. **4**, 706 (2016).
- [212] L. Zajíčková, V. Buršíková, Z. Kučerová, J. Franclová, P. Šťáhel, V. Peřina, and A. Macková, *Organosilicon Thin Films Deposited by Plasma Enhanced CVD: Thermal Changes of Chemical Structure and Mechanical Properties*, J. Phys. Chem. Solids **68**, 1255 (2007).
- [213] A. Urda, I. Popescu, I. C. Marcu, G. Carja, N. Apostolescu, and I. Sandulescu, *Methane and Propane Total Oxidation on Catalysts from FeLDH Precursors*, Rev. Chim. **61**, 267 (2010).
- [214] M. Yaseen, Z. Shah, R. C. Veses, S. L. P. Dias, E. C. Lima, G. S dos Reis, J. C. P. Vaggetti, W. S. D. Alencar, and K. Mehmood, *Photocatalytic Studies of TiO₂/SiO₂ Nanocomposite Xerogels*, J. Anal. Bioanal. Tech. **08**, 8 (2017).
- [215] Y. Jiang, X. Gu, Z. Zhou, F. Ni, and Q. Dong, *Laboratory Observation and Evaluation of Asphalt Blends of Reclaimed Asphalt Pavement Binder with Virgin Binder Using SEM / EDS*, Transp. Res. Rec. 1 (2018).
- [216] E. Rinaldini, P. Schuetz, M. N. Partl, G. Tebaldi, and L. D. Poulikakos, *Investigating the Blending*

- of Reclaimed Asphalt with Virgin Materials Using Rheology, Electron Microscopy and Computer Tomography*, Compos. PART B (2014).
- [217] W. Zhang, J. Shi, and Z. Jia, *The UV Anti-Aging Performance of TPS Modified Bitumen*, Pet. Sci. Technol. **36**, 1 (2018).
- [218] I. G. da Rocha Segundo, V. T. F. Castelo Branco, K. L. Vasconcelos, and Á. S. de Holanda, *Hot Mix Recycled Asphalt with the Incorporation of a High Percentage of Reclaimed Asphalt Pavement as an Alternative to High Modulus Layer (in Portuguese Language)*, Transportes **24**, 85 (2016).
- [219] Y. Brosseaud, *Recycling of Asphalt Mixtures: Evolution After 20 Years and the Current Situation of France (In Portuguese Language)*, in *Congresso Brasileiro de Rodovias e Concessões* (Foz Do Iguçu, 2011).
- [220] A. Hussain and Q. Yanjun, *Effect of Reclaimed Asphalt Pavement on the Properties of Asphalt Binders*, Procedia Eng. **54**, 840 (2013).
- [221] M. Fakhri and A. Ahmadi, *Recycling of RAP and Steel Slag Aggregates into the Warm Mix Asphalt: A Performance Evaluation*, Constr. Build. Mater. **147**, 630 (2017).
- [222] V. M. C. Araujo, I. S. Bessa, and V. T. F. Castelo Branco, *Measuring Skid Resistance of Hot Mix Asphalt Using the Aggregate Image Measurement System (AIMS)*, Constr. Build. Mater. **98**, 476 (2015).
- [223] T. M. Al Rousan, *Characterization of Aggregate Shape Properties Using a Computer Automated System*, Texas A&M University, 2004.
- [224] E. F. Freitas, J. D. Rodrigues, J. de A. Rocha, and H. M. R. D. da Silva, *Innovative Low Noise Surfaces: Comparison of Damping and Absorption*, Inter.Noise 2014 - 43rd Int. Congr. Noise Control Eng. 1 (2014).
- [225] A. Arabzadeh, H. Ceylan, S. Kim, K. Gopalakrishnan, and A. Sassani, *Superhydrophobic Coatings on Asphalt Concrete Surfaces: Toward Smart Solutions for Winter Pavement Maintenance*, Transp. Res. Rec. **2551**, 10 (2016).
- [226] E. F. Freitas, F. F. Martins, A. Oliveira, I. R. Segundo, and H. Torres, *Traffic Noise and Pavement Distresses: Modelling and Assessment of Input Parameters Influence through Data Mining Techniques*, Appl. Acoust. **138**, (2018).
- [227] I. Rocha Segundo, L. Silva, C. Palha, E. Freitas, and H. Silva, *Surface Rehabilitation of Portland Cement Concrete (PCC) Pavements Using Single or Double Surface Dressings with Soft Bitumen, Conventional or Modified Emulsions*, Constr. Build. Mater. **281**, 122611 (2021).